

**THERMAL AND MICROBIAL GAS GENERATION,
ACCUMULATION AND DISSIPATION IN COAL BASINS:**

ROLE OF SORPTIVE STORAGE CAPACITY EVOLUTION

Von der Fakultät für Georessourcen und Materialtechnik der Rheinisch-
Westfälischen Technischen Hochschule Aachen

zur Erlangung des akademischen Grades eines

Doktors der Naturwissenschaften

genehmigte Dissertation

vorgelegt von

Dipl.-Geol. Philipp Weniger

aus Osterode am Harz

Berichter: **Univ.-Prof. Dr. Ralf Littke**

Prof. Dr. Bernhard Cramer

Tag der mündlichen Prüfung: 4. Juni 2012

Diese Dissertation ist auf den Internetseiten der Hochschulbibliothek online verfügbar.

Acknowledgements

The present study received financial support from the German Research Funding Organisation (DFG) under grant KR1783/5-1, which is gratefully acknowledged.

First of all I would like to thank Univ.-Prof. Dr. Ralf Littke for giving me the opportunity to carry out my PhD studies at the Institute of Geology and Geochemistry of Petroleum and Coal and for his support throughout my studies. Furthermore I thank Prof. Dr. Bernhard Cramer for taking the time to review and supervise my thesis, even at a difficult time of change and transition.

I am especially grateful to Dr. Bernhard M. Krooss for sharing his passion for science and reason that inspired me throughout the past five years. Without his tireless support and countless scientific and non-scientific discussions as well as his friendship, I would not have been able to write this thesis.

A significant part of this PhD work was only possible by contribution and support from colleagues in Czech Republic and Brazil. I thank Drs. Juraj and Eva Francu of the Czech Geological Survey in Brno, who invited us to Czech Republic, organized field trips and sampling campaigns and always supported us throughout the project. I also thank Frantisek Buzek of the CGS in Prague for isotope analyses and for helpful discussion on isotope geochemistry. Dr. Petr Hemza and co-workers at GreenGas DPB are thanked for providing sample material and for their support in analytical and geological questions.

I thank Prof. Dr. Wolfgang Kalkreuth and his colleagues at the Universidade Federal do Rio Grande do Sul in Porto Alegre for their support and the fruitful research cooperation on coal and CBM in Brazil. I am also indebted for the invitation to Brazil and the financial support that allowed us to visit the UFRGS in 2011.

The present work was only possible with the help and assistance of numerous colleagues and fellow PhD students at the LEK. I thank Dr. Andreas Busch, Yves Gensterblum and Dr. Alexandra Amann for introducing me to the exciting world of sorption measurements and supercritical CO₂, as well as for their support during laboratory work. I thank Pieter Bertier for long and inspiring discussions on clay minerals and surface processes, as well as for reminding me to see things from a different angle. I thank Dr. Sabine Heim for her invaluable help with pyrolysis experiments and her support and friendship since my first day at the institute. I thank Dongyong Li, Fengshuang Han, Reinhard Fink, Matus Gasparik, Alexej Merkel and Amin Ghanizadeh for their assistance with laboratory measurements and many interesting discussions. Furthermore I am grateful to Rolf Mildenerger and Donka Macherey for their assistance in sample preparation and organic petrography and to Jens Köster and Kerstin Windeck for numerous TOC analyses. I thank Anette Schneiderwind and Stefan Schnorr for technical support. I thank Dr. Patrick Riefer for the joyful times when we shared an office and for being a friend, even at times when it seemed like we belong to two entirely different worlds. I am also grateful to many fellow students whose company made work at the lab and institute a pleasure. I thank Nadja Al-Sandouk, Roschni Kalathoor and Susan Giffin for being a wonderful distraction from the sometimes frustrating work of writing and editing. I also thank Dorit Kanellis, Dorothee Degen and Olga Scheffler for guiding me through the jungle of administration and accounting.

I am also grateful to all the friends for reminding me that there is a world outside of the lab. I thank Patrick, Seongje, Män, Anja, Tim, Reinhard and Sandra for their company during many exciting and unforgettable rock climbing trips. I especially thank Jens, Cinzia and the Berrittella family for inviting me to Sicily and their kind hospitality. It was that beautiful place in Valguanera where I found the time and peace to finalize the last parts of this thesis.

Most importantly I thank my parents Wolfgang and Ingrid Weniger, my brother Sascha and grandma Elfriede to whom I dedicate this thesis. Their endless support, encouragement and love provided me with the necessary strength to write this thesis.

Summary

The regional variation of chemical and isotopic composition of coal gases has been investigated in the Upper Silesian Coal Basin (USCB), Czech Republic, and the Paraná Basin, Brazil.

The field studies were complemented by laboratory experiments on selected samples to elucidate the effects of sorption/desorption processes on the chemical and isotopic composition of coal gases. Non-isothermal open system pyrolysis (Py-GC) was used to assess the gas generation potential and kinetics for the reconstruction of gas generation history in the study areas. The experimental results were integrated into a conceptual dynamic model of gas generation and storage in coal seams during structural and thermal basin evolution.

Coal gases in the southern part of the USCB have a thermogenic isotope signature, while gases in the northern part have isotope signatures typical for microbial CO₂ reduction and mixed thermogenic/microbial origin. Chemical and isotopic compositions of gas samples from canister desorption of coal cores showed larger variations, but were generally in agreement with those of samples taken from cross-measure boreholes. Canister desorption did not cause any systematic isotope fractionation effects. Trends in geochemical composition of thermogenic gases suggest a contribution of gas from deeper parts underlying the Carpathian overthrust.

Coals from the two principal coal-bearing sequences of the USCB (paralic Ostrava Fm. and limnic Karviná Fm.) are vitrinite-rich, of high- to low-volatile bituminous rank and have mostly reached the stage of gas generation and expulsion. Using mass balance calculations the volumes of gas generated up to this coalification stage were estimated at 201 m³ per ton of Total Organic Carbon (TOC) for methane and 138 m³/t TOC for carbon dioxide. Cumulative pyrolytic methane yields ranged between 52 and 79 m³/t TOC. Based on the reaction-kinetic parameters obtained from these tests thermogenic gas generation at a geologic heating rate of 10⁻¹¹ K/min was predicted to reach a maximum between 208 and 246°C. A 1D basin model of the subsidence and thermal history of the study area indicated that major gas generation occurred at maximum burial between 319 and 285 Ma b.p. and that no significant methane generation was associated with reburial in the Miocene.

Excess sorption isotherms (up to 27 MPa) for methane and carbon dioxide under different experimental conditions showed that gas sorption capacity is mainly controlled by pressure, moisture content and temperature, whereas organic matter content and maturity have a lesser impact. The average methane sorption capacity of USCB coals of 15 m³/t was significantly higher than the present-day gas contents in the study area (< 2 - 10 m³/t). Correlations between sorption capacity, coal rank and temperature were derived from sorption experiments and used in combination with geological pressure and temperature data.

A static model assuming present-day pressure and temperature gradients predicts an increase in sorption capacity with increasing depth towards a maximum value between 600 and 1000 m, followed by a decrease due to increasing temperature.

Results from 1D burial history and temperature history modeling were integrated with experimental results to reconstruct the dynamic evolution of sorption capacity during basin history in relation to thermal gas generation. These computations revealed that the sorption capacity of the coals at maximum burial depth was significantly lower than estimated based on present-day pressure and temperature gradients. At the time of maximum gas generation, the amount of generated gas exceeded the sorption capacity of coals and the excess gas was expelled. Uplift started at the Carboniferous/Permian transition and the concomitant temperature decrease resulted in the presently observed under-saturation of the coal seams. From the end of the Permian uplift phase until present, coal seams of the Karviná formation were at temperatures below 80°C and thus amenable to microbial methane generation. In contrast, temperatures of coal seams of the Ostrava formation were significantly higher in the post-uplift phase and microbial methane generation from these coals was unlikely.

Coal from the Santa Terezinha coalfield in the southern Paraná Basin, Brazil had a significantly lower residual gas generation potential than USCB coals. Gas contents and average gas sorption capacities were also lower. Methane and carbon dioxide sorption capacities of coals and shales correlated with the TOC. For CO₂ the linear regression showed a non-zero intercept, indicating a significant sorption capacity of the mineral matter. The present-day gas content of coals from the Santa Terezinha coalfield amounts to 13 – 38% of the methane sorption capacity. Assuming sorption capacities at reservoir conditions theoretically an amount of up to 15.4 Gt CO₂ could be stored in the Santa Terezinha coal seams, if all methane were produced prior to CO₂ injection.

Zusammenfassung

Regionale Unterschiede in der chemischen und isotopischen Zusammensetzung von Flözgasen wurden im Oberschlesischen Becken (USCB) in Tschechien und im Santa Terezinha Kohlefeld (STC) des Paraná Beckens in Brasilien untersucht.

Geländestudien wurden durch Laborexperimente an ausgewählten Proben ergänzt um den Einfluss von Sorptions- und Desorptionsprozessen auf die chemische und isotopische Zusammensetzung von Flözgas zu untersuchen. Unter Einsatz von nicht-isothermer, offener Pyrolyse (Py-GC) wurden Gasbildungspotenzial und Kinetik zur Rekonstruktion der Gasbildungsgeschichte ermittelt. Experimentelle Ergebnisse wurden in ein konzeptionelles dynamisches Modell zur Bildung und Speicherung von Gas in Kohlenflözen während der strukturellen und thermischen Beckenentwicklung integriert.

Flözgas aus dem südlichen USCB weist eine thermogene Isotopensignatur auf, während die Signatur im nördlichen Bereich auf mikrobielle CO₂ Reduktion und eine Mischung von Gasen thermogenen und mikrobiellen Ursprungs hindeutet. Die chemische und isotopische Zusammensetzung von Gasen die während der Kanisterdesorption beprobt wurden, war stark Variabel aber grundsätzlich ähnlich der Zusammenstzung von Gasen aus Flözentgasungsbohrungen. Während der Kanisterdesorption wurden keine eindeutigen Isotopenfraktionierungseffekte beobachtet. Trends in der geochemischen Zusammensetzung thermogener Gase im USCB lassen einen Beitrag von Gas aus tieferen Bereichen unterhalb der Karpathenüberschiebung vermuten.

Kohlen der zwei hauptflözführenden Formationen im USCB (paralische Ostrava Fm. und limnische Karviná Fm.) sind Vitrinit-reiche Gasflamm- bis Esskohlen die überwiegend das Stadium der Gasbildung und Gasfreisetzung erreicht haben. Aus Massenbilanzrechnungen konnte ein während der Inkohlung gebildetes Methanvolumen von 201 m³/t organischen Kohlenstoffs (TOC) und ein CO₂-Volumen von 138 m³/t TOC abgeschätzt werden. Die kumulative im Pyrolyseexperiment freigesetzte Methanmenge lag zwischen 52 und 79 m³/t TOC. Aus experimentell bestimmten reaktionskinetischen Parametern wurde ermittelt dass die thermogene Gasbildung bei einer geologischen Aufheizrate von 10⁻¹¹ K/min in einem Temperaturbereich zwischen 208 und 246°C ihr Maximum findet. Ein 1D Beckenmodell der Subsidenz- und Temperaturgeschichte des USCB deutet darauf hin dass die Hauptgasbildung während der maximalen Versenkung zwischen 319 und 285 Ma b.p. stattfand und es zu keiner signifikante Gasbildung im Zusammenhang mit der Wiederversenkung im Miozän kam.

Exzess Sorptionsisothermen (bis zu 27 MPa) für Methan und CO₂ unter verschiedenen experimentellen Bedingungen zeigten dass die sorptive Speicherkapazität hauptsächlich von Druck, Wassergehalt und Temperatur abhängt und in geringerem Maße von TOC und Reife beeinflusst wird. Die mittlere Sorptionskapazität im USCB (15 m³/t) liegt deutlich über dem heutigen Gasgehalt der Kohlen (<2 – 10 m³/t). Korrelationen zwischen Sorptionskapazität, Inkohlungsgrad und Temperatur wurden experimentell ermittelt und mit geologischen Druck- und Temperaturdaten kombiniert. Bei Annahme heutiger Druck- und Temperaturgradienten ergibt ein statisches Modell dass die Sorptionskapazität mit zunehmender Teufe bis zu einem Maximum zwischen 600 und 1000 m ansteigt und anschließend aufgrund steigender Temperaturen wieder absinkt.

Resultate einer 1D Modellierung der Versenkungs- und Temperaturgeschichte wurden mit experimentellen Ergebnissen integriert um die Entwicklung der Sorptionskapazität zusammen mit der thermischen Gasbildung während der Beckengeschichte zu rekonstruieren. Diese Berechnungen zeigten dass die Sorptionskapazität der Kohlen bei maximaler Versenkungstiefe deutlich niedriger lag, als die mit heutigen Druck- und Temperaturgradienten berechnete. Während der maximalen Gasbildung überstieg die gebildete Gasmenge die Speicherkapazität der Kohlen und überschüssiges Gas entwich. Die am Karbon-Perm Übergang einsetzende Hebung und die daraus resultierende Abkühlung bewirkte die heutige Gas-Untersättigung der Flöze. Seit dem Ende der Permischen Hebungsphase lagen Flöze der Karviná Fm. in einem

Temperaturbereich der mikrobielle Gasbildung ermöglichte ($<80^{\circ}\text{C}$). Im Gegensatz hierzu lagen die Temperaturen der Ostrava Fm. nach der Hebungsphase deutlich höher und mikrobielle Gasbildung war unwahrscheinlich.

Kohlen aus dem Santa Terezinha Kohlefeld weisen ein deutlich niedrigeres Gasbildungspotenzial auf als Kohlen aus dem USCB. Gasgehalt und Sorptionskapazität sind ebenfalls niedriger. Die Korrelation der Methan und CO_2 Sorptionskapazität brasilianischer Kohlen und Brandschiefer mit dem TOC-Gehalt deutet auf eine signifikante CO_2 Sorptionskapazität der Mineralsubstanz hin. Heutige Gasgehalte im STC liegen zwischen 13 und 38% der Methan Sorptionskapazität. Bei Annahme der Sorptionskapazität unter Reservoirbedingungen lässt sich eine theoretische Menge von bis zu 15.4 Gt CO_2 in Flözen des STC speichern, wenn vor der CO_2 Injektion das gesamte Flözgas gefördert wird.

Symbols and Abbreviations

A	pre-exponential factor
A	area (chapter 5)
α_{a-b}	isotopic fractionation factor <i>e.g.</i> $((\delta^{13}\text{C}_a + 10^3) / (\delta^{13}\text{C}_b + 10^3))$
AMM	abandoned mine methane
ASTM	American Society for Testing and Materials
BI	bitumen index [mg HC/g TOC]
b.p.	before present
C ₂₊	gaseous hydrocarbons with more than two carbon atoms
C	concentration
C	completion factor (chapter 5)
CBM	coalbed methane
CCS	carbon capture and storage
CHP	combined heat and power
CMM	coal mine methane
CSG	coal seam gas
δD	stable hydrogen isotopic composition (‰)
$\delta^{13}\text{C}$	stable carbon isotopic composition (‰)
Δ	isotopic difference, isotopic separation (<i>e.g.</i> $\delta^{13}\text{C}_a - \delta^{13}\text{C}_b$) (‰)
daf	dry, ash-free
DIN	Deutsche Industrie Norm
E _a	activation energy
ECBM	enhanced coalbed methane production
EOS	equation of state
ER	exchange ratio
ESG	enhanced shale gas production
FID	flame ionization detector
GC	gas content
GIP	gas in place
HC	hydrocarbons

HI	hydrogen index [mg HC/g TOC]
ICCP	International Committee for Coal and Organic Petrology
IGIP	initial gas in place
IUPAC	International Union of Pure and Applied Chemistry
k	reaction rate constant
mBtu	million British thermal units
n	molar amount
n_{ads}	molar amount of adsorbed gas
n_{max}	maximum measured sorption
n_L	Langmuir sorption capacity
OI	oxygen index [mg HC/g TOC]
OKC	Ostrava – Karviná Coalfield
P	pressure
P_L	Langmuir pressure
PGIP	producible gas in place
ppm	parts per million
Py-GC	pyrolysis coupled to gas chromatography
QI	quality index [mg HC/g TOC]
q_{st}	isosteric heat of adsorption
R	universal gas constant = $8.3145 \text{ m}^3 \cdot \text{Pa} / (\text{mol} \cdot \text{K})$
RF	recovery factor
RS	Rio Grande do Sul
$\rho_{adsorbed}$	density of adsorbed phase
ρ_{gas}	gas density
scf	standard cubic feet
SCO ₂	storage capacity for CO ₂
T	temperature
T_{max}	temperature of maximum hydrocarbon generation rate
t	time
$\tau_{1/2}$	half-life

TCD	thermal conductivity detector
TCF	trillion cubic feet
TFRR	thermal oxidation by flow reversal reactor
TH	thickness (m)
TIC	total inorganic carbon (wt. %)
TOC	total organic carbon (wt. %)
TST	transition state theory
TVD	true vertical depth (m)
TR	transformation ratio
USCB	Upper Silesian Coal Basin
V _{CH4}	volume of methane
VM	volatile matter yield (wt. %)
VMM	ventilation mine methane
VPDB	Vienna Pee Dee Belemnite (stable carbon isotope standard)
VR	vitronite reflectance (%)
VRc	calculated vitronite reflectance (%)
VRr	vitronite reflectance measured in random mode (%)

Units and Conversions

J	Joule ; 1 kJ = 4.184 kcal
°C	degrees Celsius
K	Kelvin ; 0°C = 273.15 K
ft ³	cubic foot ; 1 ft ³ = 0.028 m ³
Pa	Pascal ; 100kPa = 1 bar
psi	pound per square inch ; 1 psi = 6.894 kPa
t	metric ton ; 1 t = 10 ⁶ g
scf/t	standard cubic feet per ton

IUPAC standard conditions T = 273.15 K (0 °C); P= 100000 Pa

1 mmol/g = 22.71 std. m³/t = 802.03 scf/t (using IUPAC standard conditions)

1 mmol/g = 23.69 std. m³/t (using T = 15.56°C = 60°F and P = 101.325 kPa)

1mmol/g = 922.16 scf/t_s

(using T = 15.56°C = 60°F; P = 101325 Pa and short ton (t_s), 1 t_s = 907185 g)

Contents

Acknowledgements.....	iii
Summary.....	v
Zusammenfassung.....	vii
Symbols and Abbreviations.....	ix
Units and Conversions.....	xii
Contents.....	xiii
Figures.....	xviii
Tables.....	xxiii
1. Introduction.....	1
1.1. Coal related gas.....	1
1.2. Upper Silesian Coal Basin (USCB).....	2
1.3. Chapter 2: Geochemical and stable carbon isotopic composition of coal related gases from the SW Upper Silesian Coal Basin, Czech Republic.....	2
1.4. Chapter 3: Gas generation from bituminous coals of the Upper Silesian Coal Basin, Czech Republic and the Paraná Basin, Brazil.....	3
1.5. Chapters 4 and 5: Investigations on the methane and carbon dioxide sorption capacity of coals from the SW Upper Silesian Coal Basin, Czech Republic and the Paraná Basin, Brazil.....	3
2. Geochemical and stable carbon isotopic composition of coal related gases from the SW Upper Silesian Coal Basin, Czech Republic.....	5
2.1. Abstract.....	6
2.2. Introduction.....	6
2.2.1. Study area.....	7
2.2.2. Coal-related methane in the OKC.....	9
2.2.3. Previous studies on the origin of hydrocarbon gases in the OKC.....	10
2.3. Samples.....	11
2.4. Methods and experimental procedures.....	11
2.5. Results.....	11
2.5.1. Gas from cross-measure safety degassing.....	11

2.5.1.1.	Molecular gas composition	11
2.5.1.2.	Stable carbon isotopic composition	12
2.5.2.	Canister desorption experiments.....	13
2.5.2.1.	Gas contents	13
2.5.2.2.	Molecular gas composition	14
2.5.2.3.	Stable carbon isotopic composition.....	16
2.6.	Discussion	17
2.6.1.	Origin of CO ₂	17
2.6.2.	Origin of methane and higher hydrocarbons	17
2.6.3.	Influence of thermal maturity on the carbon isotopic composition of thermogenic methane	19
2.6.4.	Occurrence and genetic origin of coal-related gas.....	20
2.7.	Conclusions	23
2.8.	Acknowledgements	24
3.	Gas generation from bituminous coals of the Upper Silesian Coal Basin, Czech Republic and the Paraná Basin, Brazil.....	25
3.1.	Introduction.....	26
3.2.	Estimation of gas generation from volatile matter yield.....	26
3.3.	Mass balance calculation	26
3.4.	Rock-Eval pyrolysis	30
3.4.1.	Method	30
3.4.2.	Results and discussion	30
3.5.	Open system non-isothermal pyrolysis.....	32
3.5.1.	Method of Pyrolysis Experiments	32
3.5.2.	Results and discussion	33
3.5.3.	Evaluation of the kinetic parameters of methane generation	37
3.6.	Conclusions	47

4.	Investigations on the methane and carbon dioxide sorption capacity of coals from the SW Upper Silesian Coal Basin, Czech Republic.....	49
4.1.	Abstract.....	50
4.2.	Introduction.....	50
4.3.	Study area and previous work	51
4.3.1.	Geological setting	51
4.3.2.	Thermal maturity of coal from the Ostrava-Karviná Coalfield	53
4.4.	Samples.....	54
4.5.	Methods and experimental procedures.....	56
4.5.1.	Proximate analysis	56
4.5.2.	Determination of equilibrium moisture content	56
4.5.3.	Coal petrography.....	56
4.5.4.	TOC analysis.....	56
4.5.5.	High-pressure sorption experiments.....	56
4.5.5.1.	Experimental set-up.....	56
4.5.5.2.	Determination of multiple isotherms	57
4.5.5.3.	Parameterization of experimental sorption isotherms.....	57
4.6.	Results	58
4.6.1.	Coal Petrography.....	58
4.6.2.	Maceral composition.....	58
4.6.3.	Vitrinite Reflectance.....	58
4.6.4.	Proximate analysis and moisture equilibration.....	59
4.6.5.	Hygroscopic moisture and equilibrium moisture.....	59
4.6.6.	Equilibrium moisture.....	59
4.6.7.	Volatile matter yield.....	60
4.6.8.	Total Organic Carbon (TOC)	60
4.6.9.	High-pressure gas sorption	60
4.6.9.1.	Methane sorption isotherms	61

4.6.9.2.	Carbon dioxide sorption isotherms	63
4.7.	Discussion	65
4.7.1.	Correlations between maturity parameters	65
4.7.2.	Influence of coal properties and reservoir parameter on sorption capacity.....	66
4.7.3.	Influence of moisture content on sorption capacity.....	66
4.7.4.	Effect of temperature on sorption capacity.....	67
4.7.5.	Effect of thermal maturity	70
4.7.6.	Effect of mineral matter content (ash yield)	71
4.7.7.	Effect of maceral composition	72
4.7.8.	Comparison of CH ₄ and CO ₂ sorption – implications for CO ₂ enhanced methane recovery (CO ₂ -ECBM).....	73
4.7.9.	Calculated variation of sorption capacity with depth	74
4.8.	Conclusions	79
4.9.	Acknowledgements	80
5.	High-pressure methane and carbon dioxide sorption on coal and shale samples from the Paraná Basin, Brazil	81
5.1.	Abstract.....	82
5.2.	Introduction.....	82
5.3.	Geological setting	84
5.3.1.	Irati Formation	85
5.3.2.	Rio Bonito Formation.....	85
5.3.3.	Ponta Grossa Formation	86
5.4.	Samples	87
5.4.1.	Sample preparation.....	87
5.5.	Methods and experimental procedures.....	87
5.5.1.	Coal characterisation	87
5.5.2.	High-pressure sorption isotherms.....	88
5.5.2.1.	Experimental setup and conduction of sorption experiments	88

5.5.2.2.	Parameterization of experimental sorption isotherms.....	89
5.5.2.3.	Evaluation of sorption experiments	90
5.6.	Results and discussion	90
5.6.1.	Proximate analysis	90
5.6.2.	TOC contents.....	91
5.6.3.	Coal petrography	91
5.6.3.1.	Vitrinite reflectance.....	91
5.6.3.2.	Maceral group analysis	92
5.6.4.	Gas contents.....	92
5.6.5.	Results of gas sorption experiments.....	92
5.6.5.1.	Methane sorption isotherms	92
5.6.5.2.	Carbon dioxide sorption isotherms	93
5.6.6.	Effect of mineral matter content (ash yield) on gas sorption	93
5.6.7.	Effect of moisture on sorption isotherms.....	97
5.6.8.	Effect of coal maceral composition on sorption isotherms.....	98
5.6.1.	Effect of maturity on sorption isotherms	99
5.6.2.	Evaluation of potential for carbon dioxide sequestration and enhanced coalbed methane (CO ₂ -ECBM) and shale gas recovery (CO ₂ -ESG).....	100
5.7.	Conclusions	104
5.8.	Acknowledgements	106
6.	Final Discussion and Outlook	107
6.1.	Origin and composition of coal-related gas.....	107
6.2.	Gas generation	109
6.3.	Gas storage capacity.....	109
6.4.	Comparison of sorption capacity of coals from the Upper Silesian Coal Basin and the Paraná Basin	111
6.5.	Outlook and Recommendation.....	112
6.6.	Gas composition and generation.....	113

6.7.	Microbial gas.....	113
6.8.	Basin history of the USCB	113
6.9.	Influence of coal rank on sorptive gas storage capacity.....	113
6.10.	Comparison of European coals and Gondwana coals.....	114
6.11.	Shale gas.....	114
6.12.	Environmental impact of coalbed methane and shale gas exploration	114
7.	References.....	116
Appendix I Geochemical and stable carbon isotopic composition of coal related gases from the SW Upper Silesian Coal Basin, Czech Republic.....		132
Appendix II Pyrolytic gas generation from bituminous coals of the Upper Silesian Coal Basin, Czech Republic and the Paraná Basin, Brazil.....		135
Appendix III Investigations on the methane and carbon dioxide sorption capacity of coals from the SW Upper Silesian Coal Basin, Czech Republic		156
Appendix IV High-pressure methane and carbon dioxide sorption on coal and shale samples from the Paraná Basin, Brazil.....		172

Figures

Figures Chapter 2: Geochemical and stable carbon isotopic composition of coal related gases from the SW Upper Silesian Coal Basin, Czech Republic

<i>Fig. 2.1 Location of the study area in the SW Upper Silesian Basin, Czech Republic (adapted from Sivek et al., 2003) and PP' section (adapted from Menčík et al. 1983).....</i>	8
<i>Fig. 2.2 Stratigraphic overview of the Ostrava Karviná Coalfield (modified from Sivek et al., 2003).</i>	9
<i>Fig. 2.3 Variation of stable isotope composition of CH₄ (top) and CO₂ (bottom) of gas extracted from cross-measure degassing boreholes.....</i>	13
<i>Fig. 2.4 Gas content determined by canister desorption of coals from Paskov, Lazy and ČSM mine on "as-received" basis.....</i>	14
<i>Fig. 2.5 Variation of helium and argon concentrations during canister desorption of samples from different depth of ČSM well 1.</i>	15
<i>Fig. 2.6 Variation of stable carbon isotope composition of methane (top) and CO₂ (bottom) during canister desorption of coals from Paskov, Lazy and ČSM mine.</i>	16

Fig. 2.7 Bernard plot combining molecular and isotopic composition of coal related gas from cross-measure boreholes and canister desorption (after Bernard et al., 1976 with interpretations after Whiticar, 1999). 18

Fig. 2.8 Variation of $\delta^{13}\text{C}$ of CH_4 and CO_2 in gas from cross-measure boreholes and canister desorption. Diagram after Jenden and Kaplan (1986) with diagnostic fields from Smith and Palasser (1996) and Whiticar (1999). Isotope fractionation lines according to $\alpha = (\delta^{13}\text{C}_{\text{CH}_4} + 10^3)/(\delta^{13}\text{C}_{\text{CO}_2} + 10^3)$ 19

Fig. 2.9 Variation of $\delta^{13}\text{C}$ - CH_4 with coal rank for desorbed gases from different mines. For comparison, maturity $\delta^{13}\text{C}$ trends for thermogenic methane, calculated after relationships reported by Stahl 1977 and Berner and Faber, 1996, were added. 20

Fig. 2.10 Distribution of coal-related gas in the Czech USCB below impermeable cover (Carpathian nappes) (A) and below permeable cover (B). Redrawn after Sivek et al. (2003). 22

Fig. 2.11 Reconstructed temperature history of coal-bearing formations in the OKC, based on a 1-D basin model. 23

Figures Chapter 3: Gas generation from bituminous coals of the Upper Silesian Coal Basin, Czech Republic and the Paraná Basin, Brazil

Fig. 3.1 Influence of removal of methane, carbon dioxide and water during thermal decomposition on the elemental composition of organic matter. For comparison, the composition of glucose and the end members CH_4 and CO_2 are plotted. The shaded area represents the range of elemental composition of sedimentary organic matter. 27

Fig. 3.2 Comparison of cumulative methane and carbon dioxide generation from mass balance calculations for coals from the German Ruhr Basin (RB) and Upper Silesian Coal Basin (USCB) for a maturity range between 0.6 and 2.6 VRc %. Data for RB calculations from Gaschnitz (2001). 29

Fig. 3.3 Bitumen Index (BI) and Quality Index (QI) versus maturity (T_{max}) for coal samples from the USCB including interpretation according to Sykes and Snowdon (2002). 32

Fig. 3.4 Methane generation rates during temperature-programmed (0.5 K/min) open system pyrolysis. 34

Fig. 3.5 Cumulative methane yield from temperature-programmed (0.5 K/min) open system pyrolysis. (166 = Coal sample from Brazil) 34

Fig. 3.6 Maximum measured generation rate (top) and cumulative generation (bottom) versus maturity. For comparison, estimated hydrocarbon generation fields for type III kerogen modified from Schimmelmann et al. (2006) have been added (not to scale with pyrolysis methane generation). 35

<i>Fig. 3.7 Nitrogen generation rates during temperature-programmed (0.5 K/min) open system pyrolysis</i>	36
<i>Fig. 3.8 Cumulative nitrogen yield from temperature-programmed (0.5 K/min) open system pyrolysis</i>	36
<i>Fig. 3.9 Comparison of methane generation of sample 8 before and after solvent extraction.</i>	37
<i>Fig. 3.10 Half-life values calculated using activation energies between 10 and 100 kcal/mol and a pre-exponential factor of 10^{16} s^{-1} (solid lines) and 10^{12} s^{-1} (dashed lines). The time and temperature range of laboratory experiments is represented by the red area, the blue area represents conditions during 'natural' coalification.</i>	39
<i>Fig. 3.11 Comparison of methane generation at different heating rates for sample 8.</i>	40
<i>Fig. 3.12 Calculation of the pre-exponential factor (A) from the shift of the temperature of maximum methane generation (T_{max}) between pyrolysis experiments on sample 8 using three different heating rates.</i>	40
<i>Fig. 3.13 Approximations of experimental pyrolysis data for two coal samples using different kinetic sets. Sample 8 shows significant methane generation at high temperatures (top) while sample 30 generates only small amounts of methane at high temperatures (bottom).</i>	42
<i>Fig. 3.14 Comparison of activation energy distributions obtained from least-square fits of experimental data using different frequency factors.</i>	43
<i>Fig. 3.15 Comparison of activation energy distribution obtained for coal from the Ruhr Basin (D) (Krooss et al., 1993) and for coal (sample 19) from the Upper Silesian Coal Basin (CR). Both kinetic parameter sets use a single pre-exponential factor ($A= 4.33^{13} \text{ s}^{-1}$).</i>	44
<i>Fig. 3.16 Experimental methane generation curve measured at a laboratory heating rate of 0.5 K/min (red), and extrapolation to a constant geologic heating rate of 10^{-11} K/min (black).</i>	44
<i>Fig. 3.17 Gas generation during basin history of the USCB for coal from the principal coal bearing formations, showing that major gas generation was complete by the Carboniferous – Permian transition (290 Ma b.p.).</i>	46
<i>Fig. 3.18 Gas generation during the basin history of the USCB for coal samples from the principle coal-bearing formations on a logarithmic scale showing the influence of the Carpathian overthrust during Miocene.</i>	47
Figures Chapter 4: Investigations on the methane and carbon dioxide sorption capacity of coals from the SW Upper Silesian Coal Basin, Czech Republic	
<i>Fig. 4.1 Location of the study area in the Southern Upper Silesian Coal Basin, Czech Republic (adapted from Sivek et al., 2003).</i>	52
<i>Fig. 4.2 Stratigraphic overview of the Ostrava Karviná Coalfield (modified from Sivek et al., 2003).</i>	53

<i>Fig. 4.3 Maceral group composition of the coals from the three sampling locations.</i>	58
<i>Fig. 4.4 Maturity vs. depth plot showing different trends for coals from Paskov and Lazy mine.</i>	59
<i>Fig. 4.5 Methane sorption isotherms for “as-received” (open symbols) and moisture-equilibrated (solid symbols) coal from Paskov mine (squares) and ČSM mine (circles).</i>	62
<i>Fig. 4.6 Methane isotherms for three “as received” coals from Paskov mine measured at 20°C and 45°C.</i>	63
<i>Fig. 4.7 CO₂ sorption isotherms for “as-received” (open symbols) and moisture-equilibrated (solid symbols) coal from Paskov mine (squares) and ČSM mine (circles).</i>	64
<i>Fig. 4.8 Relationship between the estimated density of the adsorbed CO₂ phase and ash yield of coal samples.</i>	65
<i>Fig. 4.9 Relationship between vitrinite reflectance (VRr%) volatile matter yield and the Rock-Eval T_{max} value for coal samples from Paskov mine.</i>	66
<i>Fig. 4.10 Relationship between methane sorption capacity and experimental temperature for moisture equilibrated coal sample 8. n_{max} = maximum excess sorption, n_L = Langmuir sorption capacity.</i>	68
<i>Fig. 4.11 Isothermic heat of adsorption for different sorbate loadings determined from methane isotherms measured on moisture-equilibrated sample 8.</i>	69
<i>Fig. 4.12 CO₂ isotherms for “as received” coals from the Paskov mine measured at 20°C (open symbols) and 45°C (solid symbols).</i>	69
<i>Fig. 4.13 Relationship between methane sorption capacity and coal rank (“as-received”, 45°C). ...</i>	71
<i>Fig. 4.14 Relationship between rank and sorption capacities measured for CH₄ and CO₂ on “as received” and moisture equilibrated coal from Paskov mine.</i>	71
<i>Fig. 4.15 Correlation between methane sorption capacity and TOC content for samples from Lazy cores (“as- received”, 45°C).</i>	72
<i>Fig. 4.16 Rank dependence of the preferential sorption capacity between CO₂ and CH₄ at 5MPa....</i>	73
<i>Fig. 4.17 Influence of different parameters on calculated sorption capacity depth trends.</i>	76
<i>Fig. 4.18 Simplified burial history and 1-D model calibrated on data from Lazy 76 well.</i>	77
<i>Fig. 4.19 Comparison of calculated sorption capacity depth trends for different stratigraphic units using depth data from burial history (top) data and pore pressure and temperature information from a 1-D model (Petromod). Black lines represent calculated trends using linear pressure (10.1 MPa/km) and temperature (35K/km) trends and depth information from the burial history. Red lines represent trajectories of sorption capacity during basin evolution (uplift).</i>	78
<i>Fig. 4.20 Comparison of linear present-day pressure (p) (10.1 MPa/km) and temperature (T) (35K/km) gradients with paleo- pressure and temperature data from 1-D basin model.</i>	79

Figures Chapter 5: High-pressure methane and carbon dioxide sorption on coal and shale samples from the Paraná Basin, Brazil

<i>Fig. 5.1 Location of the Santa Terezinha coal field, state of Rio Grande do Sul, Brazil (Kalkreuth et al., 2008b).</i>	84
<i>Fig. 5.2 Stratigraphic profile of the CBM-001-ST-RS well and position of canister samples analysed by Kalkreuth et al. (2008b). Sorption experiments of the present study were carried out on samples from canisters 2, 3, 7, 11, 20, 22 and 24.</i>	88
<i>Fig. 5.3 Schematic flow diagram for the manometric method for gas sorption measurements: (1) evacuation of the whole system (2) filling of the reference cell (3) closure of valve 1 and thermal equilibration, (4) valve 2 is opened and gas transferred into the sample cell; start of the sorption process (5) after pressure equilibration, closure of valve 2 and refilling of the reference cell. Steps 3 to 5 are repeated until the maximum system pressure is reached (after Siemons and Busch, 2007).</i>	89
<i>Fig. 5.4 Comparison of moisture content determined after sample acquisition in Brazil (UFRGS) and later before sorption tests in Germany (RWTH) indicating drying of powdered coal samples.</i> 91	
<i>Fig. 5.5 Correlation of excess sorption capacity with gas content of coal and carbonaceous shale from CBM-001-ST-RS well.</i>	91
<i>Fig. 5.6 Methane sorption isotherms (45 °C) with Langmuir approximations (solid lines) for coal and carbonaceous shale samples from the Permian Rio Bonito Formation of CBM well 001-ST-RS on a raw basis (top) and dry, ash-free basis (bottom).</i>	94
<i>Fig. 5.7 Methane sorption isotherms (35 °C) with Langmuir approximations (solid lines) for coal and carbonaceous shale samples from the Permian Rio Bonito Formation of CBM-001- ST-RS well on a raw basis (top) and dry, ash-free basis (bottom).</i>	96
<i>Fig. 5.8 Methane sorption isotherms with Langmuir approximations (solid lines) for Permian (Irati) and Devonian (Ponta Grossa) shale samples on a raw basis (top) and TOC basis (bottom, sample 08_101 with TOC<1% not included).</i>	98
<i>Fig. 5.9 Carbon dioxide sorption isotherms for coal and carbonaceous shale samples from well CBM-001-ST-RS on a raw basis (top) and dry, ash-free basis (bottom), measured at 45 °C.</i>	100
<i>Fig. 5.10 Carbon dioxide sorption isotherms for coal and carbonaceous shale samples from CBM well 001-ST-RS on a raw basis (top) and dry, ash-free basis (bottom), measured at 35 °C. Solid lines represent Langmuir fit.</i>	101
<i>Fig. 5.11 Carbon dioxide sorption isotherms for Permian (Irati) and Devonian (Ponta Grossa) shale samples on a raw basis (top) and TOC basis (bottom), measured at 45 °C.</i>	102
<i>Fig. 5.12 Maximum excess sorption capacities (45 °C) of methane and carbon dioxide as a function of ash yield for coals and carbonaceous shales from CBM well 001-ST-RS.</i>	103

<i>Fig. 5.13 Maximum excess sorption capacities for methane and carbon dioxide (8–12 MPa pressure range, 45 °C) vs. TOC contents of coal and shale samples from CBM-001-ST-RS well and Permian (Irati) and Devonian (Ponta Grossa) shale samples.</i>	<i>103</i>
<i>Fig. 5.14 Effect of moisture on methane sorption for coal sample 07_166. At equilibrium moisture (2.44%) the sorption capacity is 45% lower as compared to the “as received” coal (moisture content: 0.93%). Solid lines represent Langmuir fit.</i>	<i>104</i>
<i>Fig. 5.15 Effect of moisture on carbon dioxide sorption for coal sample 07_166 from CBM well ST-RS-001. At equilibrium moisture (2.44%) the sorption capacity is 56% lower as compared to the “as received” coal (moisture content: 0.93%). Solid lines represent 3-parameter fit.....</i>	<i>105</i>
<i>Fig. 5.16 Maximum excess sorption of capacity of methane and carbon dioxide vs. vitrinite content for coal samples from well CBM-001-ST-RS.</i>	<i>105</i>
<i>Fig. 5.17 Maximum excess sorption of capacity of methane and carbon dioxide vs. vitrinite reflectance for coals from well CBM-001-ST-RS.</i>	<i>106</i>

Figures Chapter 6: Final discussion and outlook

<i>Fig. 6.1 Composition of gas from canister desorption of samples from the CBM well, drilled in the Santa Terezinha coalfield, Brazil (from Kalkreuth et al., 2011 (submitted); modified from Schoell, 1983). To = gas associated with oil, Tc = condensate, TT = dry gas.</i>	<i>107</i>
<i>Fig. 6.2 Temperature history of coal-bearing formations in the USCB showing that temperature conditions in the Ostrava Formations were less favourable for microbial methanogenesis than for sediments of the Karviná Foramtion.</i>	<i>108</i>
<i>Fig. 6.3 Relationship between methane sorption capacity (n_L) and coal rank for Carboniferous coals from different Europea basins (blue squares represent samples from the USCB analysed in the present study).....</i>	<i>110</i>
<i>Fig. 6.4 Variation of “as-received” (hygroscopic) moisture (left) and equilibrium moisture (right) with coal rank for Carboniferous coals from different Europea basins (blue squares represent samples from the USCB analysed in the present study).</i>	<i>111</i>
<i>Fig. 6.5 Comparison of the influence of coal rank (vitrinite reflectance) on methane sorption capacity for coal from the Upper Silesian Coal Basin with coal from the Paraná Basin.</i>	<i>112</i>

Tables

<i>Table 3.1 Comparison of mass balance calculations for methane generation from coals</i>	<i>29</i>
<i>Table 3.2 Results of temperature-programmed open system pyrolysis (heating rate = 0.5K/min) .</i>	<i>37</i>
<i>Table 3.3 Results of kinetic modelling for coal samples from the USCB</i>	<i>41</i>

Table 3.4 Gas generation calculated for a linear geologic heating rate (10^{-11} K/min) and for the temperature history obtained from 1D basin modelling. These values are derived from mature coals and do not reflect the entire gas generation during the basin history. 45

Table 4.1 Overview of samples from the Ostrava-Karviná coalfield 55

Table 4.2 Parameter for 'static' estimation of sorption capacity (n_L) vs. depth trends..... 75

Table 5.1 Sample list and results of proximate and petrographic analyses. For stratigraphic position of canister samples, see Fig. 5.2. 86

1. Introduction

The past two decades have seen significant changes in the global energy supply from fossil fuels. While many, if not all, oil producing countries passed peak production rates, oil and gas prices have increased drastically. This led to increased exploration and production activities for unconventional resources, such as coalbed methane (CBM) and more recently, shale gas. On the one hand, technological improvements enabled production of these resources, which often occur in deep and low-permeable reservoirs, *e.g.* by reservoir stimulation techniques, such as hydraulic fracturing. On the other hand, these unconventional resources are characterized by a more evenly global distribution as compared to conventional oil and gas reserves, of which more than 50% are located in the Middle East alone. Increased production of unconventional gas has led to significant changes in gas supply for some countries. For the United States, proven CBM resources of 19 trillion cubic feet (TCF) and estimated resources of 158 TCF (EIA, 2007) and even larger shale gas resources (687 TCF, OPEC, 2011) are reported. Production of these unconventional gas resources increased significantly during the last 10 years and now accounts for 30% of US gas production, resulting in a decrease in gas price from 13\$/ million British thermal units (mBtu) in 2006 to less than 4\$/mBtu in 2011 (OPEC, 2011). These developments and an increasing global energy demand led to predictions that the role of gas (conventional and unconventional) for the global primary energy supply will see a steady increase within the next decades (BP, 2011; OPEC, 2011). Some organizations even predict that the world might face a "golden era for gas" (IEA, 2010). However, unconventional gas resources are associated with significant geologic and technical uncertainty regarding their reserve assessment. Production of coalbed methane has been successful in the US, Canada, Australia and China and other countries, whereas in European coal basins, economic production of CBM has not been possible until now. Low or highly variable gas contents, low permeability of coal seams and also compositional variation of the coal related gas are some of the reasons why CBM exploration and production was problematic and less successful in Europe and other countries. This led to an increasing scientific interest in methane and its role in geologic and biologic processes influencing generation, migration and accumulation of coal related gas. Scientific interest is also driven by environmental concerns, raised by increasing greenhouse gas emissions that are associated with coal basins and coal mining. Methane (CH₄), water vapour and carbon dioxide (CO₂) are the most abundant greenhouse gases and affect the global climate change. Several case studies have proven that methane and CO₂ are often genetically linked in the subsurface due to microbial activity, which modifies the chemical and isotopic signature of the natural gases. Differentiation among the various sources of emissions related to coal seam gas, oil and gas fields, microbial CO₂ reduction, and methane oxidation requires additional research (Thielemann et al., 2000, 2001, 2004; IPCC, 2005). Comprehension of geochemical and microbiological processes involved in natural gas habitats and compositions within the geosphere provides the key to understanding atmospheric CH₄ change (Whiticar 1990).

The present work presents results of a bilateral research project that was aimed to improve the understanding of generation, migration and dissipation of coal-related gas in the course of the geological history of sedimentary basins, with special consideration of the influence of sorption and desorption processes on the compositional and isotopic signature. The main study area of this project was the SW Upper Silesian Basin in Czech Republic, which was chosen as a 'natural laboratory'. In this basin the occurrence of gases of both, thermal and microbial origin has been documented in previous studies (Buzek et al. 1999a, b; Franců et al., 2007). Additionally, a coal field from the Paraná Basin, Brazil was studied, where CBM and shale gas resources and potential carbon dioxide sequestration in unminable coal seams are currently under evaluation.

1.1. Coal related gas

Methane is formed either during thermal maturation of coals and kerogen in deeper zones of sedimentary basins or due to microbial activity in soils and at depth up to several hundred meters and temperature up to 75-85 °C (Schoell, 1980; Tissot and Welte 1984; Schoell, 1983, 1988 and Whiticar, 1990, 1996). About 6% of global methane emissions originate from coal mining activities (USEPA, 2006). Additionally, considerable methane flux to the atmosphere occurs from agriculture, mainly flooded rice fields and ruminant manure (Thielemann, 2004; IPCC, 2005). Different genetic types of methane are distinguished from one another by isotopic composition of carbon and hydrogen in combination with the molecular composition (Schoell, 1988; Whiticar, 1990, 1996). In general, thermogenic gas is isotopically heavy and wet (rich in C₂₊ hydrocarbons), when associated with oil, or dry, i.e. poor in C₂₊ hydrocarbons, when generated from highly mature coals. Bacterial gas is isotopically very light and contains almost no C₂₊ hydrocarbons. The deuterium content (δD) is used to distinguish between methane formed by acetate fermentation, *e.g.* in liquid manure, and by bacterial CO₂ reduction.

Coal related gases are classified into:

1. *Coalbed methane* (CBM) (termed coal seam gas (CSG) in Australia), produced from boreholes in unworked and hydrodynamically fractured coal beds
2. *Coal mine methane* (CMM) released in active collieries
3. *Abandoned mine methane* (AMM) which escapes or is extracted from abandoned mines.

Coalbed methane

Coalbed methane is often found in significant quantities, either within coal seams itself, but also in the surrounding rock formations. CBM is trapped underground as free gas in the pore space and as adsorbed gas on the micropore surface of coal, which is rank dependant and often in the range of several hundred square meters per gram. The amount of adsorbed gas in coal is approximately 28 times the volume of coal at standard pressure and temperature (Cervik, 1969). Coalbed methane is generally not released into the atmosphere until it is liberated, *e.g.* by mining activities. Depending on the depth of the seams and the petrophysical properties of the coal (porosity, permeability, water-saturation) this gas can be produced economically, however, production often requires reservoir stimulation, such as hydraulic fracturing, to improve permeability.

Coalmine methane

Historically, coal mine methane has been considered as a nuisance rather than a resource. During coal mining activities, methane contained in coal seams is released into the coalmine itself. This poses a potential safety hazard because methane concentrations between ca. 4 and 16% in air form explosive mixtures and above 16% the oxygen-deficient atmosphere may cause suffocation. While modern coal mines are equipped with ventilation systems ensuring that methane concentrations in the workings are kept below 1%, firedamp explosions during underground coal mining activities remain a major hazard causing significant casualties, especially in China but also in other countries. In coal mines where gas-rich coal is produced, additional pre-mining gas extraction is used to reduce the methane concentration. Methane concentrations from such a mineface extraction are often high enough for energy production, *e.g.* by gas power plants or smaller combined heat and power (CHP) units. The ventilation mine methane (VMM) is mostly vented into the atmosphere, but recent technologies emerged, such as thermal oxidation using a flow-reversal reactor (TFRR), which enable conversion of methane to CO₂ in order to reduce greenhouse gas emissions (Somers and Schulz, 2008). By integrating CMM capture into the mining strategy it is now possible to utilize >90% of the coalmine methane for energy production (Stöttner, 2003)

Abandoned mine methane

The decline in coal-mining activities in Western and Central Europe during the past decades has resulted in a large number of abandoned mines. From these mines considerable amounts of methane may leak to the atmosphere over extended periods of time. The intensity and duration of this leakage process depends on the rate at which the mines are flooded by inflowing groundwater. One example of hazardous AMM leakage occurred in Czech Republic in the early 1990s. During a period of mine closure in the Ostrava-Karviná Coalfield (Upper Silesian Coal Basin) that followed the collapse of the communist regime in former Czechoslovakia, uncontrollable methane emissions to the surface occurred, caused by the termination of mine ventilation and water pumping (Martinec and Schejbalova, 2004). Where methane emissions penetrated buildings in the Ostrava area, gas explosions took place, causing fatal injuries. Currently, AMM is utilized in several European countries for thermal or electrical energy production, partly under emission-reduction schemes.

1.2. Upper Silesian Coal Basin (USCB)

An overview of geology, structural evolution, and coal resources of the study area has been given by Dopita et al. (1997). Methane is reported to occur in three major structural zones: 1) primary source zone, 2) degassed zone in the upper part of the Carboniferous, and 3) secondary accumulations of methane gas in the weathered crust of the Carboniferous and in overlying Miocene reservoirs (Martinec, 1999).

In previous geochemical studies a substantial amount of analytical data has been compiled on the chemical and isotopic composition of coal-related gases in the study area (Buzek et al. 1999a, b; Franců et al., 2007).

It is evident from these previous studies that both, microbial and thermal gas is encountered in the Czech part of the Upper Silesian Basin. While methane with microbial isotope signature occurs mainly in the northern section of the study area, the southern area is characterised by thermogenic methane. The distribution of the methane types follows neither stratigraphy, nor the thermal maturity of the coal seams. More systematic research is necessary to elucidate the influence of hydrology, isolation by impermeable seals in the overburden, human activities such as coal mining, and mine ventilation on the microbial coal oxidation, CO₂ reduction, and methane oxidation.

1.3. Chapter 2: Geochemical and stable carbon isotopic composition of coal related gases from the SW Upper Silesian Coal Basin, Czech Republic

Chapter 2 presents results of gas analyses carried out to investigate composition and origin of coal related gas in the Czech part of the Upper Silesian Coal Basin. In the course of these studies, a range of gas samples from mine face extraction in different underground coal mines were analyzed. Additionally, gas samples obtained during canister desorption experiments, which are routinely performed by coal mines in the OKC to determine gas contents, were analyzed. Most of these gas analyses were performed by the Czech Geological Survey. Results of chapter 2 were presented at the international meeting on organic geochemistry (IMOG 2011) and are published in *Organic Geochemistry* by Weniger et al. (2012).

1.4. Chapter 3: Gas generation from bituminous coals of the Upper Silesian Coal Basin, Czech Republic and the Paraná Basin, Brazil

Chapter 3 presents results of non-isothermal open system pyrolysis experiments that were performed to evaluate the hydrocarbon generation potential of coals from the USCB. Analysis comprised Rock-Eval pyrolysis measurements for 30 coal samples from coal seams of different stratigraphic units in the USCB. Additionally, temperature-programmed open system pyrolysis coupled to gas chromatography (Py-GC) was carried out on 6 selected coal samples from the USCB and one coal sample from the Paraná Basin, Brazil. These pyrolysis experiments were performed to determine reaction kinetic parameters, which were used to extrapolate laboratory gas generation to geologic conditions in order to estimate the thermogenic gas generation during basin evolution of the USCB. Results of Rock-Eval pyrolyses presented in chapter 3 were published in proceedings to the annual meeting of the German Society for Petroleum and Coal Science and Technology (DGMK) (Weniger et al., 2011a). Results of pyrolysis experiments of the Brazilian coal are part of a publication submitted to AAPG Bulletin (Kalkreuth et al., submitted). Parts of the results of Py-GC of coal from USCB are published in the International Journal of Coal Geology by Heim et al. (2012).

1.5. Chapters 4 and 5: Investigations on the methane and carbon dioxide sorption capacity of coals from the SW Upper Silesian Coal Basin, Czech Republic and the Paraná Basin, Brazil

Chapter 4 and 5 presents results of high-pressure methane sorption experiments carried out to determine the sorptive storage capacity of coal samples from the Upper Silesian Coal Basin (Czech Republic) and the Paraná Basin (Brazil). Additional sorption experiments were performed using carbon dioxide to evaluate the potential for carbon dioxide sequestration in unmined coal seams (CCS) and CO₂ enhanced coalbed methane production (CO₂-CBM). The aim of these sorption studies was to evaluate influence and controls of different reservoir parameters (pressure, temperature, water saturation) and coal properties (coal rank, petrographic composition, amount and composition of mineral matter) on the gas storage capacity.

Upper Silesian Coal Basin, Czech Republic

Chapter 4 presents results from extensive sorption tests on 30 coal samples from different coal mines in the Ostrava-Karviná Coal District, covering almost the entire stratigraphic range of Carboniferous coal seams in the Czech part of the USCB. Samples from one mine (ČSM) were selected because they are of similar rank but differed in age and maceral composition and thus allowed evaluation of these factors. Other samples covered a wide range in coal rank and were used to evaluate rank dependence of gas sorption.

This chapter represents a manuscript by Weniger et al. (2012), published in the International Journal of Coal Geology in 2012.

Paraná Basin, Brazil

Chapter 5 presents results from methane and carbon dioxide sorption experiments carried out on coal samples from the Santa Terezinha coalfield, located in the SW Paraná Basin, Brazil. This work was performed to analyse the influence of different controlling factors on sorption capacities and to evaluate the methane and carbon dioxide storage capacity of coals from the Santa Terezinha coalfield. One aim of this study was to evaluate controls on sorption capacity for coals of different geologic age, formed under significantly different paleoenvironmental conditions as compared to coals from the USCB. This study also includes an evaluation of CO₂ storage in the Santa Terezinha coalfield, which is currently under investigation by different research groups and petroleum companies in Brazil.

Work of this chapter is published in the International Journal of Coal Geology by Weniger et al. (2010).

2. Geochemical and stable carbon isotopic composition of coal related gases from the SW Upper Silesian Coal Basin, Czech Republic

Geochemical and stable carbon isotopic composition of coal-related gases from the SW Upper Silesian Coal Basin, Czech Republic

Philipp Weniger^{a*}, Juraj Franců^b, Bernhard M. Krooss^a, František Bůžek^c, Petr Hemza^d, Ralf Littke^a

^aEnergy & Mineral Resources Group, Institute of Geology and Geochemistry of Petroleum and Coal, RWTH Aachen University, Lochnerstr. 4-20, 52056 Aachen, Germany

^bCzech Geological Survey, Leitnerova 22, 65869 Brno, Czech Republic

^cCzech Geological Survey, Geologická 6, 15200 Prague, Czech Republic

^dGreenGas DPB a.s., Rudé armády 637, 73921 Paskov, Czech Republic

2.1. Abstract

Gas associated with Carboniferous coal seams and younger Miocene sediments in the SW Upper Silesian Basin in Czech Republic shows wide compositional variation. Coal-related gas extracted from cross-measure degassing boreholes, as well as gas released during canister desorption of coal samples from three different mines was analyzed to evaluate the genetic origin and the influence of sorption / desorption processes on the gas composition. Analyses comprised the compositional and stable carbon and isotope composition of coal-related gases. The isotopic composition of gas from cross-measure boreholes indicates thermogenic origin in the southern part of the basin and microbial CO₂ reduction and mixed type origin in the northern part. Gas from canister desorption shows similar origins, but larger compositional and isotopic variation. No consistent isotopic fractionation due to desorption could be observed. Differences in geochemical composition of thermogenic gases could indicate a contribution of gas migrated from deeper parts below the Carpathian overthrust.

2.2. Introduction

Worldwide coal deposits are associated with the occurrence of gas, which is most commonly composed of variable amounts of methane, carbon dioxide and nitrogen. Methane is primarily generated during coalification, but also through anaerobic microbial activity in coal seams (Rice, 1993). Microbial coalbed methane has been found in major coal basins in the U.S., Europe, Asia and Australia (Strapoc et al., 2006, 2011). Especially in underground mines methane represents a major safety hazard and its concentration has to be controlled by ventilation. Coal mine methane (CMM) is released during underground and surface mining operations as well as during post-mining activities and from abandoned mines. It can also migrate from unmined coal seams to the surface by diffusion or transport through natural faults. When released to the atmosphere, methane acts as a potent greenhouse gas. About 6% of global methane emissions originate from coal mining activities (USEPA, 2006). Methane represents an important energy source when extracted during coal mining as mine gas or gob gas, as well as during post-mining activities from abandoned mines. Coalbed methane (CBM) from unmined coal seams also represents an unconventional hydrocarbon source, if efficient extraction is possible. Carbon dioxide, which also acts as a greenhouse gas in the atmosphere, has been observed in certain coal seams. It can be of magmatic origin but may also be produced by chemical or microbial oxidation in active and abandoned coal mines, where oxygen is

present. Knowledge of the genetic origin of coal-related gas is important for the correlation of surface emissions with potential gas sources and the understanding of gas migration pathways.

2.2.1. Study area

The Upper Silesian Coal Basin (USCB) is one of Europe's major hard coal basins. It is located at the eastern edge of the Variscan Bohemian Massif, representing the eastern extension of the Moravo-Silesian Basin (*Fig. 2.1*). The NW part of the USCB is covered by the Miocene Carpathian Foredeep. The SE part is buried below nappes of the Carpathian overthrust belt (Silesian and Subsilesian units). The USCB occupies a known area of more than 7000 km², of which more than two thirds are located in Poland, whereas the southern part of the basin, the Ostrava-Karviná coalfield (OKC), with a known area of 1550 km², is situated in NE Czech Republic (Sivek et al., 2003). In this region coal mining has been carried out for more than 200 years. Economically important coal reserves occur within Upper Carboniferous siliciclastic, molasse-type sediments of the Ostrava Formation (Namurian A, paralic facies) and Karviná Formation (Namurian B, C and Westphalian, limnic facies). Most coal bearing strata of the OKC are of Namurian A-C age (*Fig. 2.2*). More than 250 coal seams with a cumulative thickness of 150 m were identified at depth between 480 and 1200 m. Thermogenic gas generation from these coal seams took place during and after Late Carboniferous burial. Laboratory pyrolysis of Carboniferous coals of the German Ruhr Basin yielded methane volumes in excess of 38 m³ per ton of coal (Jüntgen and Karweil, 1966; Krooss et al., 1995). Mass balance approaches predict even larger volumes (180-200 m³/t coal). Similar results were obtained for coals of the OKC (Weniger et al., unpublished results). Present day gas contents of coals in the OKC indicate that during the post-Carboniferous period of erosion and the lack of an effective seal, a significant part of the thermogenic gas was lost due to migration to the surface. The emplacement of Carpathian nappes in the southern OKC as well as deposition of sediments of the outer Carpathian foredeep 12-15 million years ago and deposition of Quarternary sediments formed a seal, below which hydrocarbon gases accumulated (Martinec and Schejbalová, 2004). Low maturities of coal seams, found Below the Carpathian nappes, render a new onset of the coalification process and associated secondary thermogenic gas generation unlikely (Kotarba, 2001). A simplified map of Carboniferous geology of the OKC is given in *Fig. 2.1* and a stratigraphic overview is shown in *Fig. 2.2*.

Ostrava-Karviná Coalfield

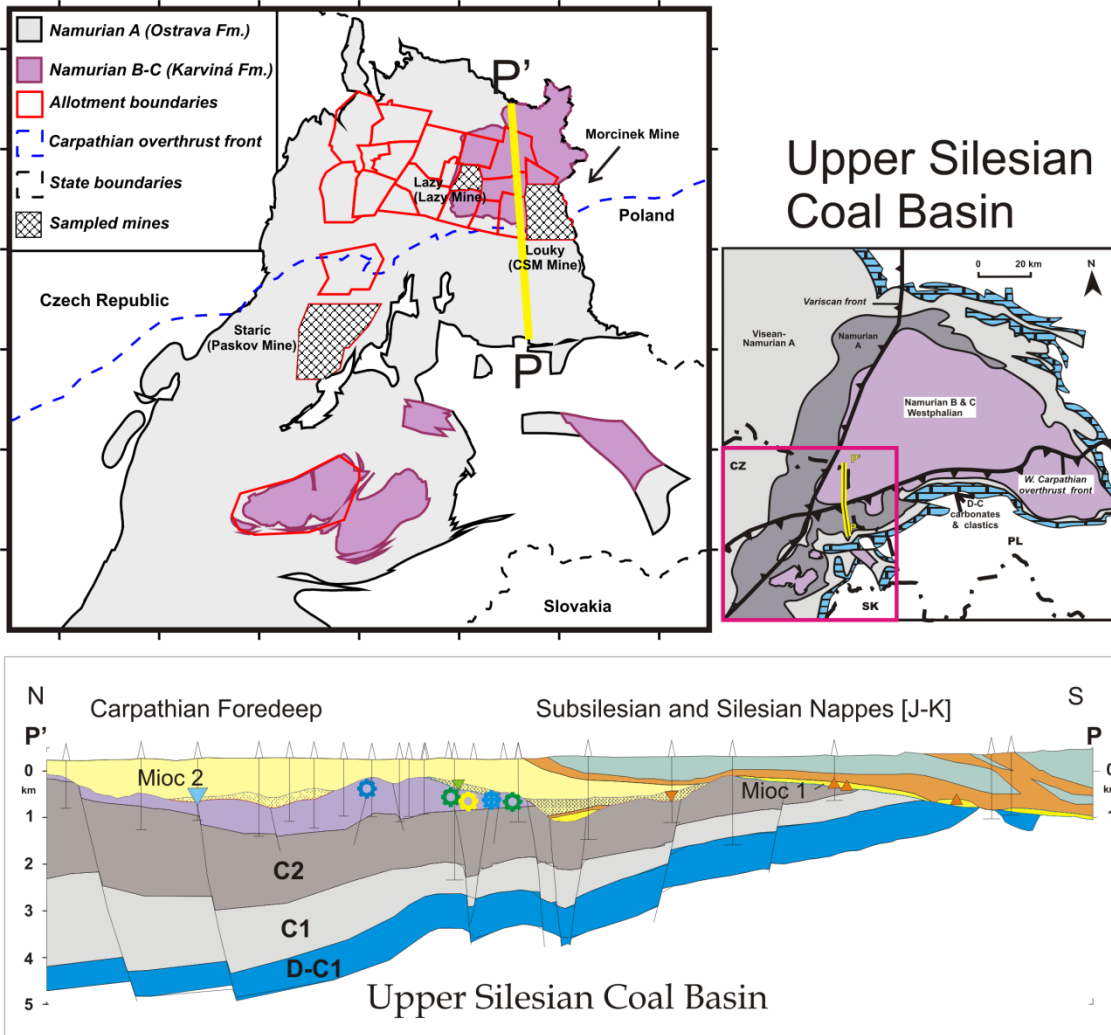


Fig. 2.1 Location of the study area in the SW Upper Silesian Basin, Czech Republic (adapted from Sivek et al., 2003) and PP' section (adapted from Menčík et al. 1983).

		Czech Republic				Samples		
Pennsylvanian	Bashkirian	311.7 Ma	B	Eroded		mineface ⊖ desorbed ⊕		
		316.5 Ma	A	Upper	Doubrava Member Seam 962	⊖ ⊕ ⊕ ⊕ ⊕		
			C		G		Lower	Suchá Member Seam 702 Seam 686
				B				R
		318.1 Ma	H	Hiatus			⊖	
Mississippian	Serpukhovian	326.5 Ma	A	Upper	Poruba Member Seam 499		⊕	
					E ₂	Jaklovec Member Seam 403 Seam 385		
						E ₁	Lower	Upper Hrušov Member Seam 255 Seam 201 Seam 169
					Petřkovice Member Seam 102 Seam 099 Seam 009			⊖ ⊕

Fig. 2.2 Stratigraphic overview of the Ostrava Karviná Coalfield (modified from Sivek et al., 2003).

2.2.2. Coal-related methane in the OKC

The gas content of coal-bearing sequences in the Czech part of the USCB mostly ranges between 2 m³/t and 10 m³/t and shows an overall decline with increasing depth (Hemza et al., 2009). The occurrence of methane in the OKC is related to the Carboniferous paleotopography, coal rank and permeability of overlying sediments as well as zones of intense faulting (Martinec and Schejbalová, 2004). To reduce the hazard of explosive methane-air mixtures in coal mines the methane is emitted by controlled mine ventilation and also extracted by controlled gas drainage for methane utilization. Between 1965 and 1997, 20 x 10⁹ m³ have been produced

during coal mining. More than two thirds of this gas was emitted through mine air systems (Martinec and Schejbalová, 2004). During the last decade utilization of coal-related methane has been intensified and today extracted coal mine methane (CMM) from five active mines supplies combined heat and power (CHP) units. Abandoned mine methane (AMM) is produced from abandoned shafts and wells. During the 1990s the potential for coalbed methane production (CBM) from virgin coal seams has been evaluated. CBM resources from coal seams deeper than 1200 m were estimated to range between $50\text{-}370 \times 10^9 \text{ m}^3$ (USEPA, 2005). However, CBM production tests in the OKC did not prove to be economic.

2.2.3. Previous studies on the origin of hydrocarbon gases in the OKC

Possible source for gases in the OKC include humic, type III organic matter of the Ostrava and Karviná Formations, but also the Menilite Formation of the deeper Carpathian Flysch Belt, which is also the main source rock for oil in the NE Czech Republic and in Poland (Franců et al., 1996; Krejčí et al., 1996; Köster et al., 1998). Miocene sediments of the Carpathian Foredeep are immature and did not generate hydrocarbons in significant amounts. Oil and gas reservoirs are located at different stratigraphic levels.

Several studies have been carried out by the Czech Geological Survey (CGS) to evaluate the origin of hydrocarbon gases in the OKC. These studies comprised analyses of gas samples from numerous boreholes, *e.g.* in Miocene sediments of the Carpathian Foredeep (Badenian, Karpatian), Devonian and Carboniferous sediments (Culm and Devonian to Carboniferous carbonates), sediments of the Carpathian overthrust, as well as the crystalline basement. Additionally, gas from active and abandoned coal mines was analyzed (Bůzek et al., 1999; Franců et al., 2007).

Based on the results of these studies the USCB was divided into the following gas-geochemical systems: (1) Upper Carboniferous coal-bearing strata in front of and below the Carpathian overthrust, (2) abandoned workings in coal mines of the OKC and (3) Lower and Middle Miocene sediments and Carpathian overthrust. Geochemical and stable isotope analyses showed evidence of the co-occurrence of several different gases in the OKC. Microbial gas (^{13}C depleted, dry gas ($\delta^{13}\text{C}\text{-CH}_4$ from -80‰ to -50‰) is associated with coal seams of the Karviná Formation, where infiltration of freshwater occurred as deep as 500 m. Microbial gas also occurs in Middle Miocene sediments (Badenian), where it is probably related to CO_2 reduction.

Thermogenic gas (less ^{13}C depleted, wet gas ($\delta^{13}\text{C}\text{-CH}_4$ -49‰ to -33‰) occurs in coal beds of the Ostrava Formation and Lower Miocene sediments (Karpatian) sealed by Silesian and Subsilesian nappes. Oxidized microbial and thermogenic gases occur in the abandoned and active mine workings.

The absence of a relationship between gas composition and stratigraphy or thermal maturity of associated coal beds suggests that the gases do not represent the original coalification pattern in the USCB and that the coal seams are rather reservoirs than source rocks. Kotarba (2001) made similar observations in the Polish part of the USCB. Kandarachevová et al. (2009) report that the occurrence of gas accumulations found in Carboniferous rocks and overburden strata in the OKC is spatially related to zones of elevated thermal maturity.

Thermal modelling suggests that the recent hydrocarbon generation and migration from below the deeper parts of the Carpathian Flysch Belt is possible. Miocene thrusting, burial and heating may have affected the coal sorption properties and induced local sorbed gas redistribution (Krejčí et al., 1996; Franců et al., 1999, 2002).

2.3. Samples

For this study gas samples were collected by GreenGas DPB from three different coal mines (ČSM, Lazy and Paskov-Staříč) in the SW USCB in Czech Republic between 2006 and 2008. From each coal mine, coal-related gas was sampled from cross-measure boreholes, as well as during canister desorption of coal samples from exploration wells.

Gas samples were collected from three subhorizontal cross-measure degassing boreholes drilled for safety reasons prior and during coal extraction. Six samples were collected during 28 days of gas extraction at Paskov mine, three in 12 days at ČSM South, and seven samples in 25 days at ČSM North (*Appendix I, Table 1*).

During exploration drilling operations by GreenGas DPB in areas of active mines in the Ostrava-Karviná coal district, the gas content of coal cores was evaluated by canister desorption. Desorbed gas was collected for periods of up to 35 days. For each canister between 1 and 4 gas samples (average of 3) were obtained at different intervals. A total of 49 gas samples from individual desorption experiments of coals from 15 different wells were analyzed. A list of all analyzed desorbed gas samples is given in *Appendix I, Table 2*.

2.4. Methods and experimental procedures

Canister desorption experiments were performed by GreenGas DPB, Paskov following recommended procedures of the US Bureau of Mines (USBM) (Kiessell et al., 1973) and Gas Research Institute (GRI) (McLennan et al., 1995). Lost gas was estimated using the USBM “straight line” method. Desorbed gas was measured after placing coal samples into desorption canisters at reservoir temperature and atmospheric pressure. Residual gas contents were measured after crushing of coal samples in an air-tight ball mill. The total gas content was calculated as the sum of lost gas, desorbed gas and residual gas. Gas contents were converted to volumes at standard conditions (273 K, 101.325 kPa) and reported as m³/t “as-received” coal in this study.

The molecular composition of desorbed and extracted gas was determined at CGS, Brno by conventional gas chromatography (GC). The detection limits were 0.2 ppm for hydrocarbon gases, 10 ppm for helium, 20 ppm for hydrogen and 100 ppm for CO, CO₂, N₂ and O₂. The chemical gas composition is given in volume % or ppm on an air-free basis.

The stable carbon isotopic composition of CH₄ and CO₂ was determined at the CGS laboratory in Prague using a Finnigan MAT 251 mass spectrometer following on-line combustion. Carbon isotope data are given relative to the VPDB standard as $\delta^{13}\text{C} = (R_{\text{sample}}/R_{\text{standard}} - 1000)$. Reproducibility of $\delta^{13}\text{C}$ determinations was better than $\pm 0.3\%$. The isotopic difference is given as $\Delta = \delta^{13}\text{C}_e - \delta^{13}\text{C}_s$, with e = end of desorption and s = start of desorption. Carbon isotopic fractionation factors are given as $\alpha_{a-b} = (\delta^{13}\text{C}_a + 10^3)/(\delta^{13}\text{C}_b + 10^3)$, with a = CH₄ and b = CO₂.

2.5. Results

2.5.1. Gas from cross-measure safety degassing

2.5.1.1. Molecular gas composition

Gas sampled from boreholes during cross-measure degassing contained significant amounts of air. Since it is very unlikely that coal gases contain large amounts of free oxygen, the gas composition was calculated to the air-free basis by setting the oxygen content to zero and

subtracting the amount of nitrogen (atmospheric N_2/O_2 ratio = 3.72). For some samples this correction yielded negative N_2 values most likely due to measurement uncertainties (*Appendix I, Table 1*). These samples were excluded from further evaluations with regard to chemical and isotopic composition. Methane contents showed large variation of 7-92%. At ČSM South, the methane content gradually increased during degassing, whereas it showed no systematic variation at Paskov and ČSM North. Gas extracted at Paskov mine contained significantly larger amounts of higher molecular mass hydrocarbon gases (C_{2+}) than ČSM gases. The amount of CO_2 was generally higher in ČSM gases (1-8%) than in Paskov gases (0.4-3%). Argon concentrations were higher at ČSM North (1.2-3.6%), than at ČSM South (0.6-0.7%) and showed large variation at Paskov mine (0.7-2.9%). Since argon was not taken into account when normalizing to the air-free basis, the high concentrations can also reflect contamination. Helium and hydrogen were below the detection limits (10 ppm and 20 ppm respectively) for ČSM gases, while some Paskov gases contained up to 45 ppm helium and up to 101 ppm hydrogen (H_2).

2.5.1.2. Stable carbon isotopic composition

Stable carbon isotopic composition of methane in cross-measure borehole gas from Paskov mine ranged from -24‰ to -39‰ (average -34‰), whereas gases from the ČSM mine showed significantly lower abundance of the ^{13}C carbon isotope ($\delta^{13}C-CH_4$ from -60‰ to -68‰; average -64‰). The variation of $\delta^{13}C-CH_4$ values was higher for Paskov gas than for ČSM gas. No significant difference in methane $\delta^{13}C$ values was observed between gas from ČSM North and ČSM South. During gas extraction at ČSM South, $\delta^{13}C-CH_4$ showed a slight increase, whereas no systematic variation was observed for gas extracted from Paskov and ČSM North mine (*Fig. 2.3*).

Carbon dioxide of gas collected from cross-measure boreholes at ČSM South was depleted in ^{13}C ($\delta^{13}C-CO_2$ from -22‰ to -24‰), whereas CO_2 of cross-measure gas from ČSM North and Paskov mine was less depleted in ^{13}C ($\delta^{13}C-CO_2$ from -9‰ to -16‰ and +3‰ to -14‰, respectively). At ČSM North, $\delta^{13}C$ of CO_2 decreased during gas extraction (*Fig. 2.3*). The isotopic fractionation (α) between $\delta^{13}C-CO_2$ and $\delta^{13}C-CH_4$ of gas collected from cross-measure boreholes ranged from 0.96-0.99 for samples from Paskov mine and from 0.94-0.96 for gas from ČSM mine. Results of geochemical and stable carbon isotope analysis of cross-measure degassing samples are listed in *Appendix I Table 1*.

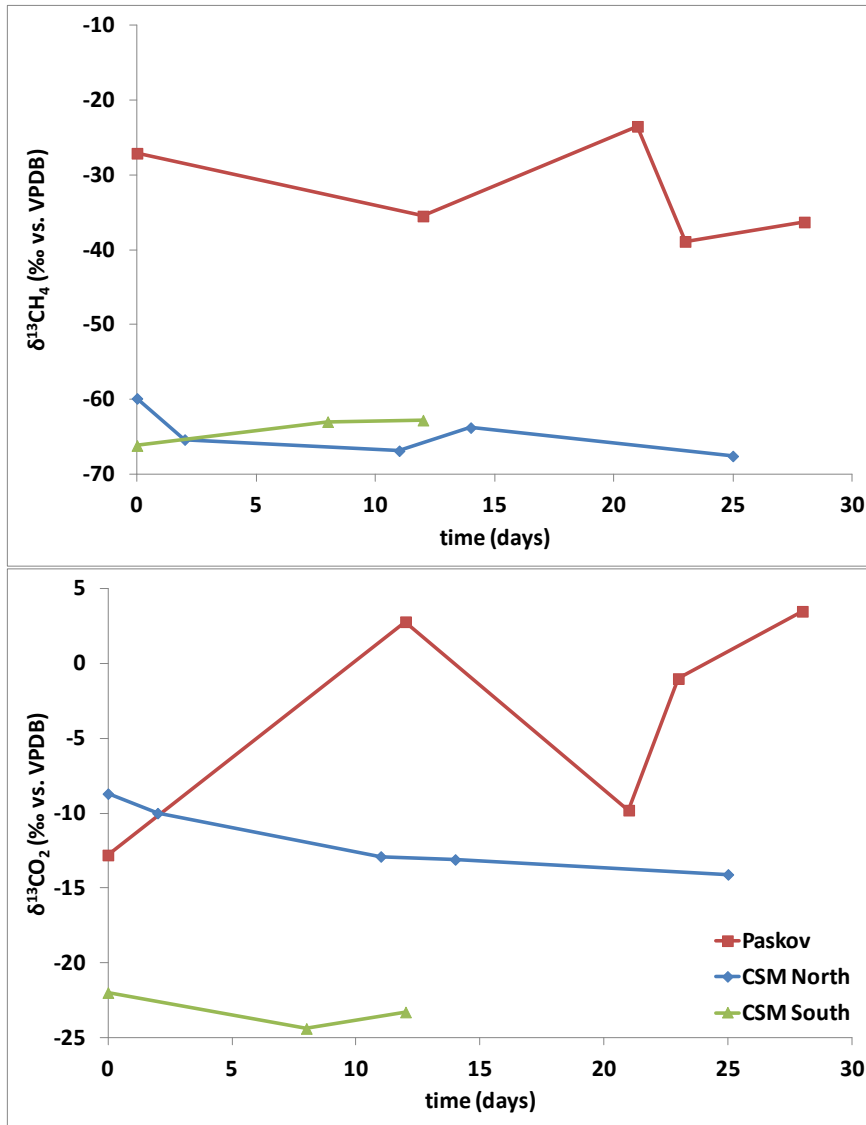


Fig. 2.3 Variation of stable isotope composition of CH₄ (top) and CO₂ (bottom) of gas extracted from cross-measure degassing boreholes.

2.5.2. Canister desorption experiments

2.5.2.1. Gas contents

Gas contents determined in 15 canister desorption experiments were generally low (<5 m³/t). Lowest gas contents were measured for ČSM coals, ranging from 0.4-2.3 m³/t (average 1.3 m³/t). Higher gas contents were measured for the four samples from Paskov mine (1.9 to 3.9 m³/t) and the five Lazy coal samples (0.9- 4.8 m³/t). The total gas content was made up of 0.2-4% of lost gas (average 1.3%), 45-88% desorbed gas (average 71%) and 10-54% of residual gas (average 27%). Gas contents ČSM coals from different seams decrease with increasing well depth, whereas they increase with depth at the Paskov and Lazy mines. However, since only well depth data were available, no systematic change of gas contents with true vertical depth (TVD) could be evaluated. Results of gas content measurements are shown in Fig. 2.4.

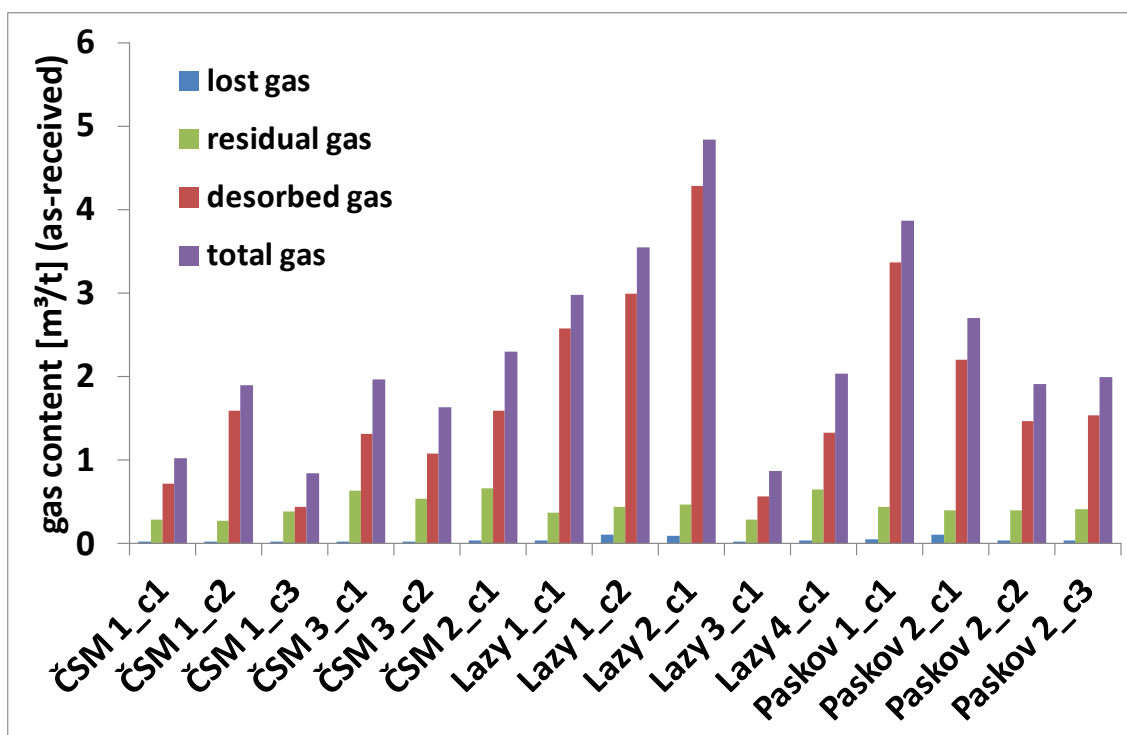


Fig. 2.4 Gas content determined by canister desorption of coals from Paskov, Lazy and ČSM mine on "as-received" basis.

2.5.2.2. Molecular gas composition

Multiple analyses were performed to determine the chemical composition of the gases collected during the 15 canister desorption tests. Results of the geochemical analyses (49 gas samples) are listed in *Appendix I Table 2*.

Desorption canisters were not filled with water or inert gas before they were sealed and therefore the first gas samples in each desorption test contained significant amounts of oxygen (1.8-17.8%). In most cases the amount of oxygen and nitrogen decreased in the course of desorption. In some instances desorbed gases with significantly elevated oxygen concentrations were observed, which might indicate contamination by atmospheric air during gas sampling or leaking desorption containers. Similar to cross-measure degassing samples, the desorbed gas values were normalized to an air-free basis. Samples yielding negative nitrogen values upon this correction were excluded from further evaluations with respect to molecular and isotopic composition.

Desorbed gases were dominated by nitrogen and methane. Both gases show a large variation between 0 and 91% (nitrogen) and <1% to >99% for methane. Highest amounts of nitrogen were measured in desorbed gases from ČSM North well 1. C₂₊ hydrocarbon gases were generally less abundant in ČSM wells (C₂H₆ < 800 ppm), variable in Lazy wells (C₂H₆ ranging from 4-7870 ppm) and highest in Paskov wells (C₂H₆ up to 4.4%). Besides a general increase in ethane contents between the first two desorption steps, no significant change was observed.

CO₂ contents were generally <10%, ranging from 0.03-8.9%. Highest CO₂ contents were measured in desorbed gas from ČSM well 1.

Argon contents ranged from 0-3.1% and again, highest amounts were measured in gases from ČSM well 1, where they generally decreased with increasing desorption time.

Most desorbed gases did not contain any helium, with the exception of three canisters from well 1 at ČSM North. These gases contained up to 1225 ppm of helium and showed a

general increase with increasing well depth and decrease with increasing desorption time (Fig. 2.5). Only three desorbed gas samples contained significant amounts of hydrogen, ranging from 300-580 ppm. This amount of molecular hydrogen could be the product of fermentation processes in the desorption canister. In the presence of oxygen the molecular hydrogen can not be utilized by microbial methenogenesis.

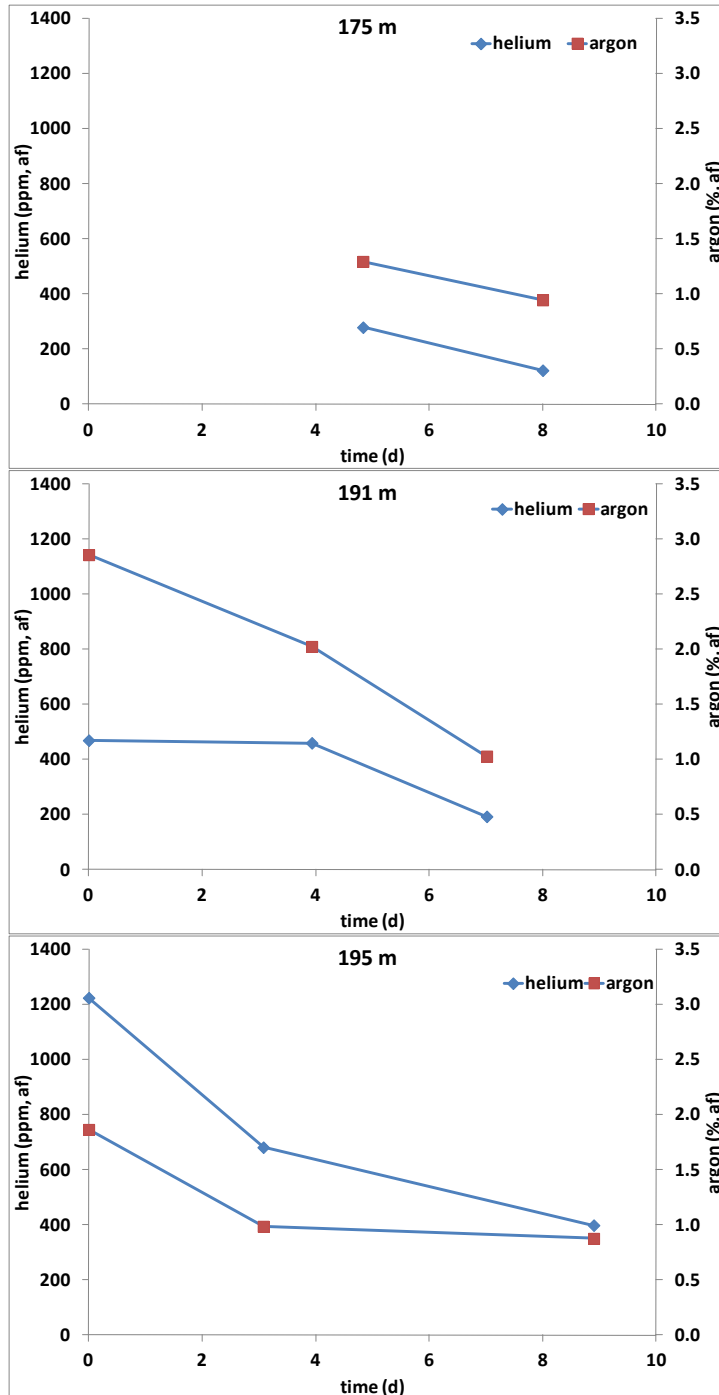


Fig. 2.5 Variation of helium and argon concentrations during canister desorption of samples from different depth of ČSM well 1.

2.5.2.3. Stable carbon isotopic composition

The isotopic composition of methane and CO₂ collected during canister desorption tests from all three mines is highly variable. Methane $\delta^{13}\text{C}$ values range from -72‰ to -35‰ with an average of -54‰. Strong depletion in ¹³C is observed for methane desorbed from coal at ČSM North mine (average $\delta^{13}\text{C-CH}_4$ -71.6‰) with little variation, whereas the $\delta^{13}\text{C-CH}_4$ from ČSM South and Lazy range from -44‰ to -71‰ (average -58‰). Methane desorbed from coals from the Paskov mine are significantly less depleted in ¹³C, ranging from -46‰ to -35‰ (average -42‰). The carbon isotopic composition of methane and CO₂ measured at different times during canister desorption was also highly variable (Fig. 2.6). The isotopic difference between methane desorbed at the start and at the end of desorption ($\Delta\text{CH}_4 = \delta^{13}\text{C}_{\text{CH}_4\text{e}} - \delta^{13}\text{C}_{\text{CH}_4\text{s}}$) varies from +3‰ to -2‰ with an average of -0.6‰. For carbon dioxide the isotopic difference shows even larger variation, ranging from +8‰ to -9‰ (average of -0.7‰).

The isotopic fractionation factor α between CO₂ and CH₄ ($\alpha = \delta^{13}\text{C-CH}_4 + 10^3 / \delta^{13}\text{C-CO}_2 + 10^3$) ranged from 0.94-1.01 (average of 0.96). The largest fractionation was observed for gases from ČSM and Lazy mine.

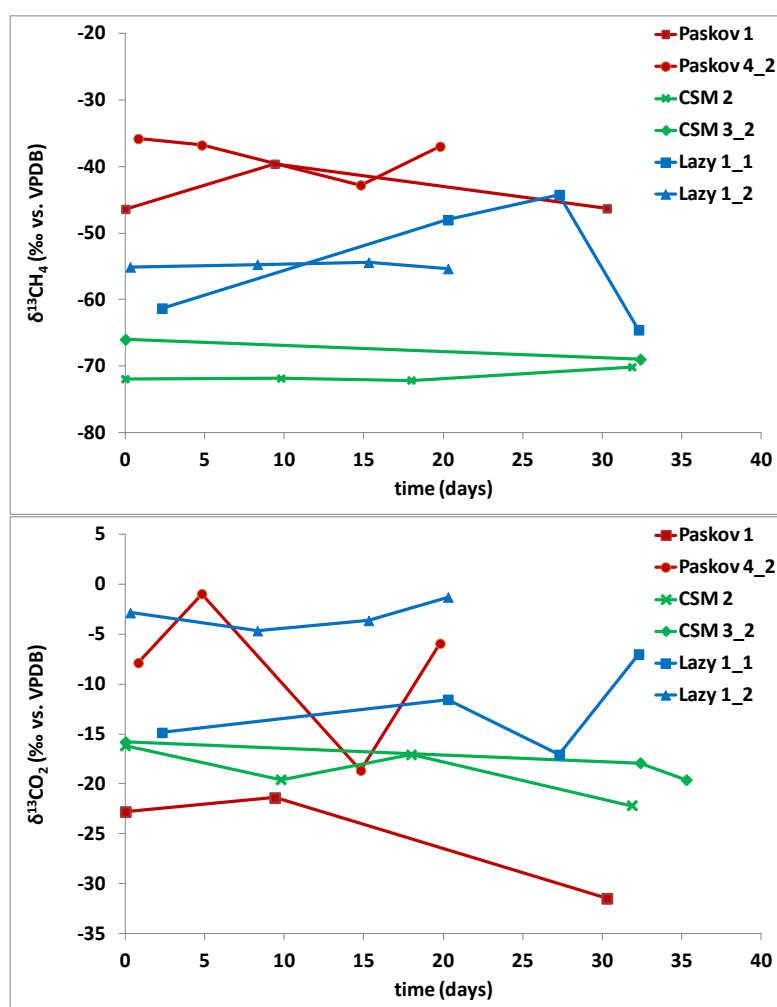


Fig. 2.6 Variation of stable carbon isotope composition of methane (top) and CO₂ (bottom) during canister desorption of coals from Paskov, Lazy and ČSM mine.

2.6. Discussion

2.6.1. Origin of CO₂

The carbon dioxide encountered in natural gases may be of organic origin (*e.g.* acetate fermentation or decarboxylation) or of inorganic origin. CO₂ of organic origin has usually low $\delta^{13}\text{C}$ values ($< -10\%$) and concentrations are mostly $< 10\%$, while CO₂ of inorganic origin is enriched in ^{13}C (0% to $+10\%$) often forms CO₂ rich reservoirs ($> 15\%$; Wycherley et al., 1999 and references therein). However, the isotopic signatures of CO₂ of different origins are highly variable and overlap. Thus, $\delta^{13}\text{C}$ values of CO₂ from biogenic decay can range from $+15\%$ to -30% (Schoell, 1983; Whiticar, 1994) and therefore the origin of CO₂ cannot be deduced from $\delta^{13}\text{C}$ alone. A combination of stable carbon isotope data from CO₂ with the stable isotope composition from associated noble gases (Ar, He, Ne) could significantly improve the identification of CO₂ sources (Sherwood-Lollar et al., 1997).

Generally, gas samples from the SW USCB have low CO₂ concentrations with stable carbon isotopic signature mostly $< -15\%$, indicating a purely organic origin. The large variation in isotopic composition most likely reflects different degrees of organic decomposition or oxidation of organic matter. The coals from Paskov well 3 contain low concentrations ($< 2\%$) of isotopically heavy CO₂ (average $\delta^{13}\text{C}$ -7%), which is probably related to oxidation of the isotopically heavy methane or coal components, rather than derived from a mantle source or metamorphism.

2.6.2. Origin of methane and higher hydrocarbons

Methane generated by thermal cracking during coalification is characterized by high $\delta^{13}\text{C}$ values ($> -55\%$) (Cramer et al., 1998; Gaschnitz et al., 2001). This thermogenic gas usually contains significant amounts of higher molecular weight hydrocarbons (C₂ – C₅). For some coals, thermogenic methane with $\delta^{13}\text{C}$ values as low as -61% has been reported (Whiticar, 1996). The isotopic composition of thermogenic methane depends on the type of the source organic matter. Gas generated from vitrinite rich coal, where cracking of aromatic structures is the dominant process, is isotopically heavier than gas generated from liptinite rich coals, where cracking of aliphatic hydrocarbons is dominant (Galimov, 1988). Similarly, gas generated from bitumen cracking will be more depleted in ^{13}C than gas from kerogen cracking. The isotopic fractionation during thermogenic gas generation also depends on the degree of depletion of molecular structures that can easily be cracked to form hydrocarbon gases (Galimov, 2006).

Microbial methane can be generated during diagenesis or during late stage secondary processes and involves groups of fermentive bacteria that are syntrophically associated with methanogenic archaea (Thauer, 1990; Strapoc et al., 2011). Microbial methane is more depleted in ^{13}C than thermogenic methane (Rice, 1993). The two most common processes of microbial methanogenesis are the reduction of CO₂, occurring predominantly in marine environments, and the fermentation of acetate, prevailing in young terrigenous freshwater environments. Microbial CO₂ reduction is associated with methane $\delta^{13}\text{C}$ values between -55% and -110% (carbon isotopic fractionation factors $\alpha_{\text{CH}_4\text{-CO}_2}$ between 0.94 and 0.92) (Jenden and Kaplan, 1986).

The hydrogen isotopic composition of methane generated by CO₂ reduction depends on the hydrogen source. If hydrogen is derived from direct utilization of water hydrogen, it shows a close relationship to the isotopic composition of formation waters $\delta\text{D}_{\text{CH}_4} = \delta\text{D}_{\text{water}} - 180\%$ (Whiticar, 1999; Galimov, 2006).

Methane generated during acetate fermentation is characterized by $\delta^{13}\text{C}$ values between -40% and -70% (carbon isotopic fractionation factors $\alpha_{\text{CH}_4\text{-CO}_2}$ between 0.96 and 0.94) (Jenden

and Kaplan, 1986) and δD values closer to the isotopic composition of the precursor acetate ($\delta D_{CH_4} = 0.4 \cdot \delta D_{water} - 323\text{‰}$) (Whiticar, 1999; Galimov, 2006).

Bernard et al. (1976) used a combination of the stable carbon isotopic composition and the molecular gas composition ($C_1/(C_2+C_3)$) to discriminate between thermogenic and microbial gas. A plot of gas data from cross-measure degassing and desorbed gases analyzed in the present study classifies gas in coals from Paskov mine (paralic Ostrava Formation) as thermogenic, whereas cross-measure gas from the ČSM mine shows a microbial signature (Fig. 2.7). Gas samples collected during canister desorption show a similar microbial signature for ČSM and Lazy mine gas and a thermogenic signature for Paskov mine gas. Additionally, desorbed gases show larger variation in isotopic and molecular composition and exhibit significant influence of oxidation or mixing of thermogenic and microbial gas. These results are in good agreement with those previously obtained by Kotarba (2001) who analyzed coal gases from the USCB in Poland and also one sample from Paskov mine. The purely thermogenic signature of gas from Paskov coals indicates that in mature coals below impermeable layers of the Carpathian overthrust, no secondary biogenic gas generation took place. It is also possible that gas generated from organic-rich sediments in deeper parts below the Carpathian overthrust, e.g. the Oligocene Menilite Formation, migrated upwards and was adsorbed by Carboniferous coals. The Menilite kerogen slightly depleted in ^{13}C ($\delta^{13}C-CH_4 = -26\text{‰}$ to -28‰) compared to the one of coal ($\delta^{13}C-CH_4 = -24\text{‰}$). A contribution of migrated gas is difficult to identify based on carbon isotopes alone and would rather lead to increased ^{13}C depletion of methane (Köster et al., 1998; Kotarba, 2001; Cornford, 2011).

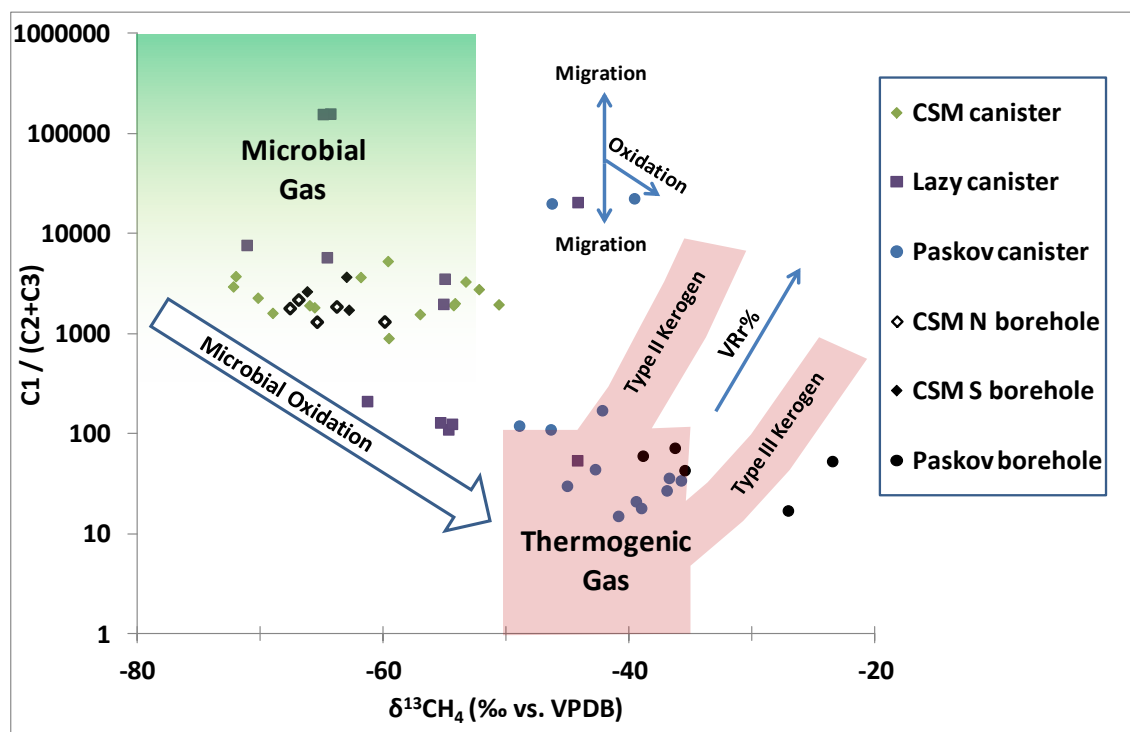


Fig. 2.7 Bernard plot combining molecular and isotopic composition of coal related gas from cross-measure boreholes and canister desorption (after Bernard et al., 1976 with interpretations after Whiticar, 1999).

Fig. 2.8 shows a plot of $\delta^{13}C-CH_4$ versus $\delta^{13}C-CO_2$ for coal-related gas analyzed in the present study. The interpretational fields indicate the range for acetate fermentation between $\alpha = 0.96$ and $\alpha = 0.94$ and the range for CO_2 reduction between $\alpha = 0.94$ and $\alpha = 0.92$ (Jenden and Kaplan, 1986). Additionally, diagnostic fields for microbial gas and methane oxidation by Whiticar et al. (1986) and for thermogenic gases by Smith and Palasser (1996) are plotted.

Dashed lines represent lines of equal carbon isotopic fractionation $\alpha_{\text{CH}_4\text{-CO}_2}$. This plot confirms a thermogenic origin of gases from Paskov mine and also indicates influence of methane oxidation. Coals from ČSM and Lazy mine (limnic Karviná Formation) show a microbial origin from CO_2 reduction and acetate fermentation and also a possible alteration by migration or oxidation of methane. More detailed differentiation between these methanogenic processes requires combining δD and $\delta^{13}\text{C}$ of methane (Whiticar, 1986, 1999; Schimmelmann et al., 2006).

Preliminary hydrogen isotopic composition of methane from a cross-measure degassing borehole in the ČSM mine (Franců et al., unpublished results) indicate that these gases result from microbial CO_2 reduction, rather than acetate fermentation. This is in good agreement with results of stable carbon and hydrogen isotope analyses by Kotarba (2001) and Kotarba and Pluta (2009) of gas from coals in the Morzinek mine, which is located in the Polish part of the USCBA, a few kilometers NE from the ČSM mine (Fig. 2.1). Analysis of formation waters in the SW USCBA provide evidence of infiltration of meteoric waters between late Permian and the Miocene transgression (Kotarba and Pluta, 2009 and references therein). These meteoric waters could have introduced methanogenic microbes and nutrients into coal-bearing Carboniferous strata. The isotopic information from $\delta^{13}\text{C}\text{-CO}_2$ and $\delta^{13}\text{C}\text{-CH}_4$ of the majority of gas samples from canister desorption is most likely the result of a mixture of thermogenic gas with gas from CO_2 reduction or of alteration during canister desorption, rather than the result from different microbial methanogenic pathways.

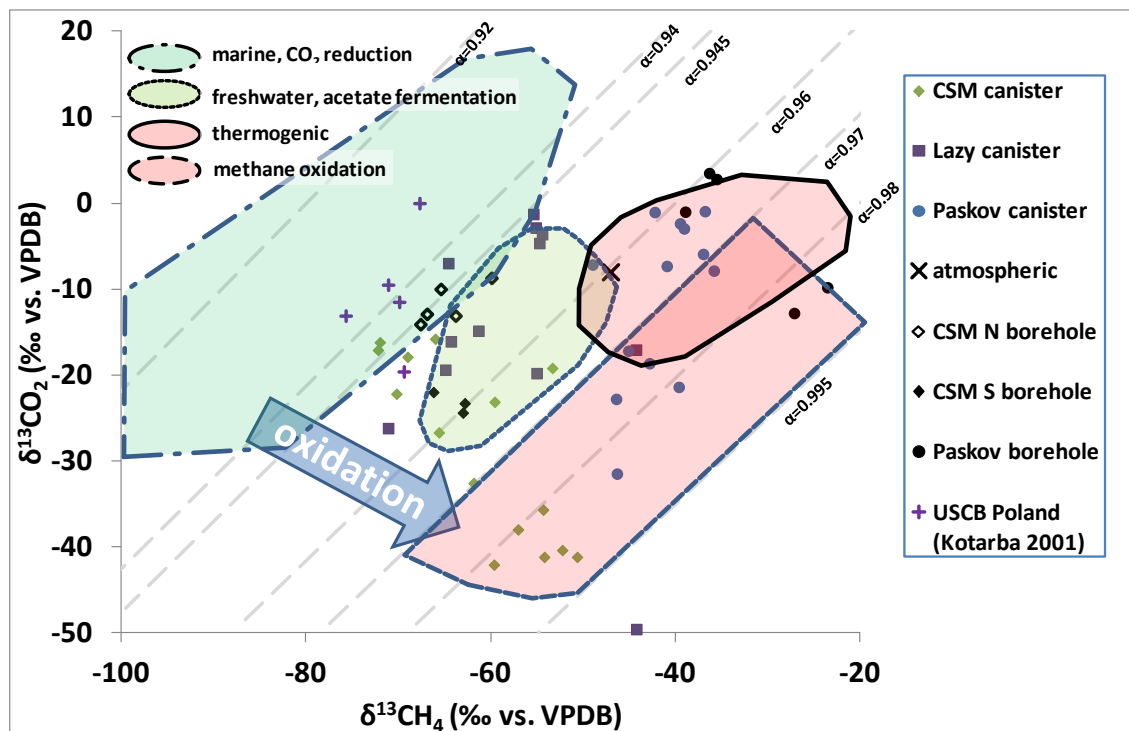


Fig. 2.8 Variation of $\delta^{13}\text{C}$ of CH_4 and CO_2 in gas from cross-measure boreholes and canister desorption. Diagram after Jenden and Kaplan (1986) with diagnostic fields from Smith and Palasser (1996) and Whiticar (1999). Isotope fractionation lines according to $\alpha = (\delta^{13}\text{C}_{\text{CH}_4} + 10^3)/(\delta^{13}\text{C}_{\text{CO}_2} + 10^3)$.

2.6.3. Influence of thermal maturity on the carbon isotopic composition of thermogenic methane

Differences in binding energies of carbon-carbon bonds for ^{13}C and ^{12}C result in kinetic isotope fractionation during thermal maturation. During the early stage of thermal maturation,

methane depleted in the ^{13}C isotope will be generated, whereas methane generated from high rank coals will be enriched in ^{13}C . This relationship between the maturity of type III kerogens (e.g. humic coals) and the stable carbon isotopic composition of generated methane has been studied by Stahl (1977) and later Faber (1987) for Carboniferous coals from Germany. The relationship has been described by the following functions:

$$\delta^{13}\text{C}-\text{CH}_4 = 8.6 \log \text{VR} - 28 (\text{‰}) \text{ (Stahl, 1977)}$$

$$\delta^{13}\text{C}-\text{CH}_4 = 13.4 \log \text{VR} - 27.7 (\text{‰}) \text{ (Faber, 1987)}$$

VR is the vitrinite reflectance of the coal in %.

Later Berner and Faber (1996) calculated a linear relationship between kerogen maturity and methane isotopic composition from pyrolysis experiments:

$$\delta^{13}\text{C}-\text{CH}_4 = 3.6848\text{VR} - 31.292 \text{ (Berner and Faber, 1996)}.$$

A comparison of $\delta^{13}\text{C}-\text{CH}_4$ values measured for the USCB gases with these maturity $\delta^{13}\text{C}$ relationships indicates that thermogenic gas from Paskov mine is significantly more depleted in ^{13}C than predicted based on coal rank (Fig. 2.9). This could indicate that coal gas from Paskov coals represents a mixture of primary thermogenic gas ^{13}C depleted methane, either from secondary microbial generation or methane generated from a different source that migrated into the coal seams. One potential source could be kerogen of the Oligocene Menilite Formation, which is more depleted in ^{13}C than the carboniferous coals (Köster et al., 1998). Molecular partitioning during migration could explain the 'dry' character of such migrated gas.

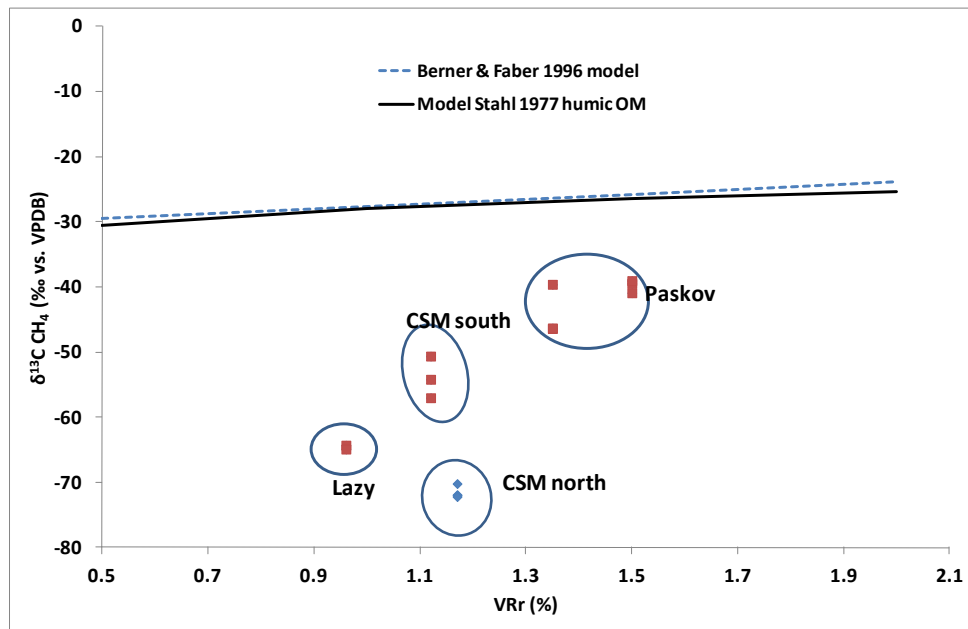


Fig. 2.9 Variation of $\delta^{13}\text{C}-\text{CH}_4$ with coal rank for desorbed gases from different mines. For comparison, maturity $\delta^{13}\text{C}$ trends for thermogenic methane, calculated after relationships reported by Stahl 1977 and Berner and Faber, 1996, were added.

2.6.4. Occurrence and genetic origin of coal-related gas

Coal-related methane in Carboniferous basins has long been known to exhibit a wide variation in $\delta^{13}\text{C}$ (Colombo et al., 1966; Teichmüller et al., 1970). These studies report $\delta^{13}\text{C}-\text{CH}_4$ values ranging from $>-20\text{‰}$ to $<-70\text{‰}$. It was found that ^{13}C depleted methane ($<-40\text{‰}$) is associated with shallow coal seams and that $\delta^{13}\text{C}-\text{CH}_4$ significantly increases (-30‰ to $>-20\text{‰}$) for gases below a certain depth (desorption zone). The depth of this desorption zone can be highly variable and is controlled by regional tectonics, permeability and the position of seals. It

ranges from -300 m to -800 m in German coal basins. From these early studies Colombo et al. (1966) and Teichmüller et al. (1970) concluded that indigenous methane from the desorption zone was lost to the atmosphere due to a lack of sealing formations after coalification was completed. Furthermore they propose that gas currently present in the coals migrated from deeper coal seams into the desorption zone and, due to fractionation during desorption and migration, became depleted in ^{13}C and lost most of the heavier hydrocarbons on the way. Gas in the primary zone below this desorption zone represents the indigenous methane that is enriched in ^{13}C and heavier hydrocarbons. Later studies on coal-related gas found evidence that the process of secondary microbial gas generation can play a significant role in coal basins and that kinetic isotope effects associated with microbial processes have a much larger impact on gas isotopic composition than isotope effects associated with thermogenic gas generation (Stahl, 1977; Rice and Claypool, 1981; Whiticar et al., 1986; Schoell, 1988; Rice, 1993; Smith and Pallasser, 1996). Additionally, early field studies and experimental results showed that the isotopic fractionation associated with diffusion in a CH_4 -water-solution system is only small (0.3‰) (Zhang and Krooss, 2001; Galimov, 2006 and references therein).

Accumulations of coal related gas in the USCB show variations in methane concentrations with depth, which mainly depend on the depth of the Carboniferous paleosurface and on the permeability of overlying sediments. Sivek et al. (2003) distinguished three different zones of methane accumulations (*Fig. 2.10*). Zone I represents accumulations of indigenous thermogenic methane. This zone occurs at depth >1250 m if an impermeable cover is present and below ~ 1050 m if covering sediments are of higher permeability. Zone II is characterized by significantly lower methane concentrations ($<10^{-3} \text{ m}^3/\text{t}$). This zone is located near the top of the Carboniferous paleorelief, where most of the methane is desorbed and lost. Zone III represents secondary methane accumulations at the top of the Carboniferous paleorelief, where impermeable sediments *e.g.* shales of the Carpathian overthrust represent an effective seal. This zone occurs between ~ 750 m and 1000 m depth. Similar observations are also reported from the Polish USCB, *e.g.* by Kotarba and Pluta (2009) and Kedzior (2009). The large variability of gas content at similar depth (*Fig. 2.10*) indicates that depth is not the primary control of gas content.

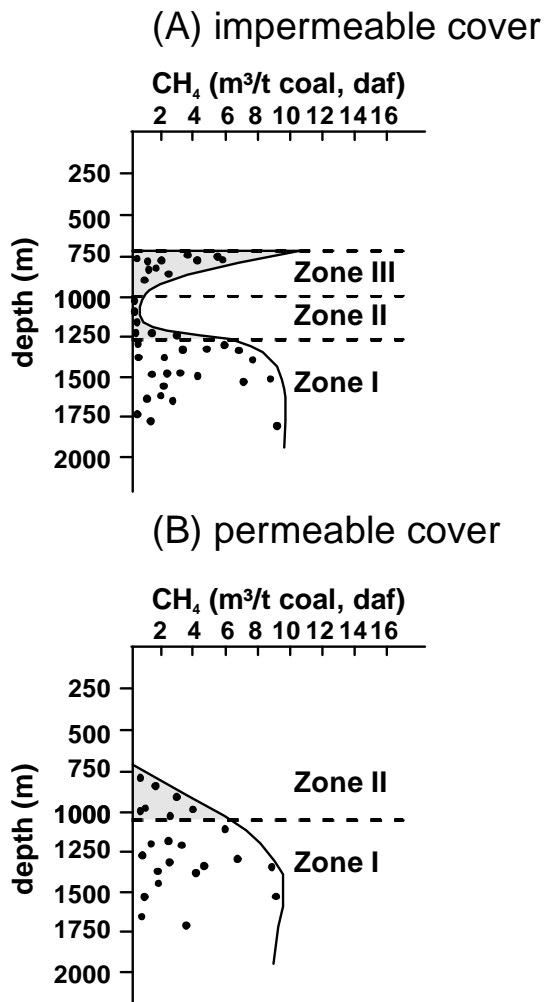


Fig. 2.10 Distribution of coal-related gas in the Czech USCB below impermeable cover (Carpathian nappes) (A) and below permeable cover (B). Redrawn after Sivek et al. (2003).

A direct correlation of gas contents determined in the present study with the zones of gas occurrence described by Sivek et al. (2003) is not possible because no information on the true vertical depth of the samples was available. Gas samples collected from coal seams at the Paskov mine, which is located in an area covered by low permeable sediments of the Carpathian overthrust, are more likely to represent primary thermogenic gas. A reconstruction of the thermogenic gas generation history of coal seams in the OKC indicates that gas generation was completed in the early Permian and that no significant thermogenic gas generation resulted from re-burial upon the overthrust of Carpathian nappes (see chapter 6). The temperature history of coal-bearing formations of the OKC indicates that reservoir temperatures of coal seams of the Ostrava Formation were not favourable for microbial gas generation (>80°C) for most of the basin history, whereas conditions were much more favourable for coal seams of the younger Karviná Formation (Fig. 2.11). A reconstruction of the evolution of the sorptive gas storage capacity of coal seams during basin history in the OKC showed that the uplift of coal-bearing formations was associated with an increase in storage capacity (Weniger et al., 2012; see also chapter 5). This increase can explain the gas undersaturation (present day gas content smaller than sorptive gas storage capacity) that is observed for coal seams in the OKC. On the other hand, the "free" sorptive storage capacity could accommodate gas from migration or secondary microbial generation. The average isotope fractionation of <1‰ observed during desorption and the evaluation of the basin history suggest that the large variation of the chemical and isotopic composition observed in coal-related gases of the OKC is related to

differences in the geologic history and different gas origin, rather than bein a result of fractionation processes associated with sorption and migration.

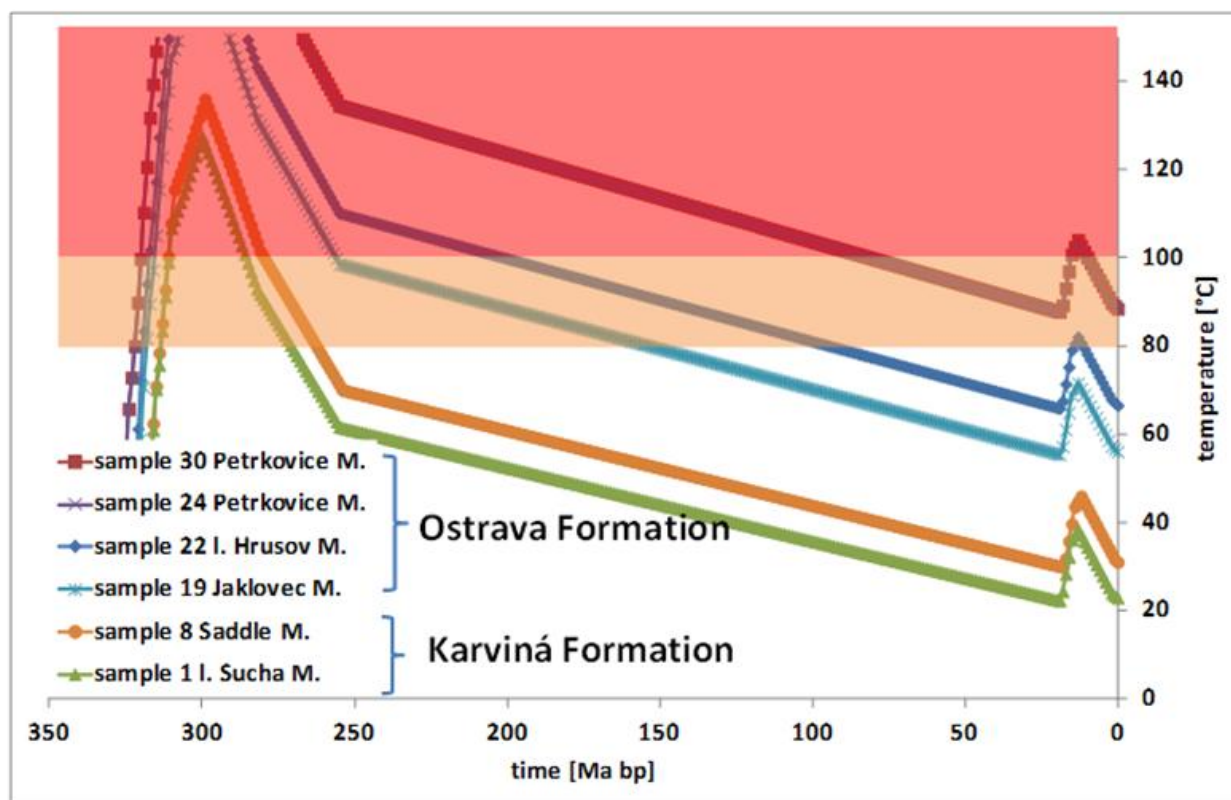


Fig. 2.11 Reconstructed temperature history of coal-bearing formations in the OKC, based on a 1-D basin model.

2.7. Conclusions

Experimental results of the geochemical and stable carbon isotopic composition of coal-related gas in the Czech part of the Upper Silesian Basin revealed a wide range of $\delta^{13}\text{C}$ of methane, indicating multiple genetic origins.

Gas of thermogenic origin is associated with coal seams in the southern part of the basin, where Carboniferous and Miocene sediments are covered by impermeable nappes of the Carpathian Flysch Belt. Composition of gas from coal seams in the NE part of the basin, where permeable Miocene molasse sediments overlie Carboniferous formations and infiltration of meteoric waters occurred, indicate a microbial and mixed type origin.

These compositions of coal gases are similar to results of gases from overlying Miocene sediments, analyzed in previous studies.

Coal-related gas from cross-measure extraction shows a similar composition as gas released from coal samples during canister desorption.

Stable carbon isotope composition of methane and carbon dioxide indicates in some cases microbial oxidation of methane during canister desorption, resulting in a coeval shift in the isotopic values.

No consistent isotopic fractionation related to desorption is observed. Low abundance of higher molecular mass hydrocarbons (C_{2+}) in some of the thermogenic gases indicates possible C_{2+} loss during migration. Thus mixture of coal gases and migrated gas, *e.g.* from source rocks below the Carpathian overthrust is conceivable.

Conditions for secondary microbial gas generation were more favourable in coal seams of the Karviná Formation, where temperatures after maximum burial were lower than in the Ostrava Formation and no impermeable cover of Carpathian overthrust nappes exists.

Microbial methane could be stored in the free storage capacity of coal seams that resulted from the uplift of these sediments.

Further studies are required to evaluate the influence of migrated gas and associated fractionation processes.

2.8. Acknowledgements

This study received financial support from the German Research Funding Organisation (DFG) under Grant KR1783/5-1, Czech Ministry of Education under project NPV II 2B06010, and from the Czech Science Foundation (GA_CR) under grant 205/07/J061.

The editors and two anonymous reviewers are thanked for their helpful comments and contributions that allowed us to improve the manuscript.

3. Gas generation from bituminous coals of the Upper Silesian Coal Basin, Czech Republic and the Paraná Basin, Brazil

3.1. Introduction

Thermal maturation of coal is associated with the generation of methane and carbon dioxide. Gas generation results from thermal decomposition of complex kerogen molecular structures during geologic times. For type III kerogen, such as humic coals, effective gas generation is believed to begin at a rank of >0.8% VR and reaches a maximum around 1.1% VR (Schimmelmann, 2006).

Several approaches have been proposed to estimate the amount of gas that can be generated from coal. Correlations based upon the volatile matter yield of coals were used in several studies to evaluate potential gas generation (Karweil, 1969; Meissner, 1984; Ryan, 1992).

Mass balance calculations based upon the intrinsic changes of the elemental composition of coal during generation of methane, carbon dioxide and water were used in early studies, *e.g.* by Jüntgen and Karweil (1966) and have been applied in numerous following studies.

Early observations of products generated in coal pyrolysis experiments showed that the composition of gas generated in the laboratory is remarkably similar to the gas present in coal seams (Hanbaba and Jüntgen, 1969). These observations led to the assumption that thermogenic gas generation that occurs during coalification can be simulated by open system pyrolysis experiments. While it is not possible to simulate gas generation under geological conditions, pyrolysis experiments with coal have been used to estimate the amount of gas generated during coalification by extrapolation of experimentally derived reaction kinetic parameters to geological heating rates (Hanbaba and Jüntgen, 1969; Ungerer and Pelet, 1997; Schenk et al., 1997 and references therein) and also to estimate the stable isotope composition of generated gas (Tang et al., 2000; Cramer et al., 2001; Gaschnitz et al., 2001).

3.2. Estimation of gas generation from volatile matter yield

An early approach to evaluate gas generation from coal based upon the change of volatile matter yield between high volatile bituminous and anthracite rank was introduced by Karweil to estimate gas generation from German coals with volatile matter yield less than 37.8% (ca. 0.8% VR). His equation was later used by Meissner (1984) and Ryan (1992) to evaluate gas generation from US coals and Canadian coals respectively:

$$VCH_4 = -325.6 \cdot \log (VM/37.8) \text{ (Ryan, 1992 and references therein)}$$

Here VCH_4 is the volume of generated methane and VM is the volatile matter yield in wt. % (daf).

Applying this approach to coals from the USCB analyzed in the present study a maximum volume of 120 m³ of methane per ton of dry, ash-free coal, can potentially be generated. This indicates that the amount of gas that can be generated from coal is significantly higher than the amount of gas that can be stored in coal by sorption processes. However, this equation does not take into account any gas that has been generated during early catagenesis (<0.8% VR) and it is also not based upon correlations for coal from the USCB.

3.3. Mass balance calculation

The amount of gas that theoretically can be generated through thermal decomposition of organic matter can be estimated by mass balance calculations, based upon intrinsic changes of the elemental composition during gas generation (van Krevelen, 1961). Jüntgen and Karweil (1966) used this stoichiometric mass balance approach to estimate the amount of gas generated from coal seams of the German Ruhr Basin. It was subsequently applied in several other studies (Littke et al., 1989, 1995; Krooss et al., 1995; Thielemann, 2000 and Gaschnitz, 2001).

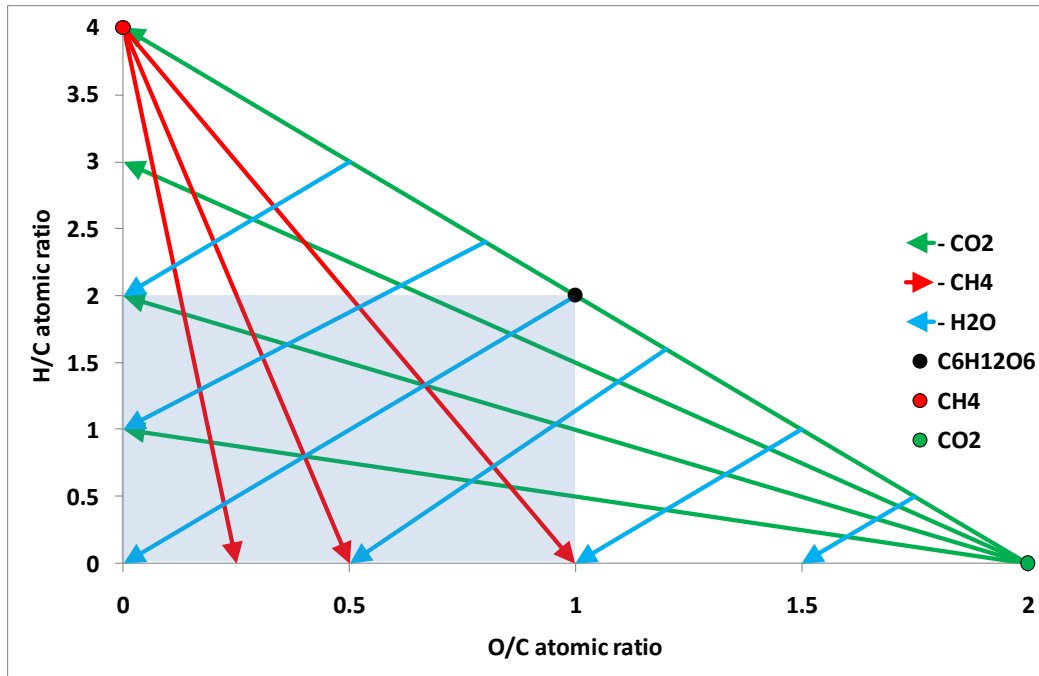


Fig. 3.1 Influence of removal of methane, carbon dioxide and water during thermal decomposition on the elemental composition of organic matter. For comparison, the composition of glucose and the end members CH_4 and CO_2 are plotted. The shaded area represents the range of elemental composition of sedimentary organic matter.

Mass balance calculation based upon changes of the atomic H/C and O/C ratios can be used to estimate the amount of gas (CO_2 and CH_4) generated during coalification (Fig. 3.1).

For these calculations, the relationship between elemental composition (CHNO) and coal rank, derived from numerous elemental analyses of coals is used. Martinec et al. (2005) report the following correlations for coals from the Upper Silesian Coal Basin:

$$C = -0.0004 \cdot VM^3 + 0.0169 \cdot VM^2 - 0.395 \cdot VM + 94 \quad (1)$$

$$H = 0.001 \cdot VM^2 + 0.0927 \cdot VM + 3.3 \quad (2)$$

$$N = 0.0035 \cdot VM + 1.3241 \quad (3)$$

VM = volatile matter yield (wt. %, dry, ash-free)

The amount of oxygen was calculated by difference:

$$O = 100 - (C + H + N) \quad (4)$$

Volatile matter yield was converted to vitrinite reflectance (VRc) using the following relationship reported by Martinec et al. (2005):

$$VRc = 3.04 - 0.1 \cdot VM + 0.001 \cdot VM^2 \quad (5)$$

The mass balance calculation was performed using the following assumptions:

- only the two primary products methane (CH_4) and carbon dioxide (CO_2) are generated during coalification
- the generation of H_2O during coalification is not taken into account. Jüntgen and Karweil (1966) estimated from mass balance calculations that below a carbon content of 94% (anthracite rank) no significant generation of water occurs during coalification. Loss of water during coalification would decrease the H/C and O/C ratios and reduce the generation of CO_2

and CH₄. Thus, the present mass balance calculation represents an estimation of the maximum amount of generated gases.

For the mass balance the molar elemental composition was used. The initial molar amounts are defined as: $n_C^0; n_H^0; n_O^0$

The molar amounts of the product are defined as: $n_C^1; n_H^1; n_O^1$

The initial molar ratios are: $R_{O/C}^0 = \frac{n_O^0}{n_C^0}; R_{H/C}^0 = \frac{n_H^0}{n_C^0}$

The molar ratios of the product are: $R_{O/C}^1 = \frac{n_O^1}{n_C^1}; R_{H/C}^1 = \frac{n_H^1}{n_C^1}$

The molar amounts of produced gases are: $\Delta nCO_2; \Delta nCH_4$

Changes of the initial molar composition of carbon, oxygen and hydrogen during coalification can be described by the following mass balance equations:

$$n_C^1 = n_C^0 - \Delta nCO_2 - \Delta nCH_4 \quad (6)$$

$$n_O^1 = n_O^0 - 2\Delta nCO_2 \quad (7)$$

$$n_H^1 = n_H^0 - 4\Delta nCH_4 \quad (8)$$

Substitution of molar ratios and rearrangement yields an expression for the amount of substance of carbon dioxide formed:

$$\Delta nCO_2 \cdot \left(\frac{2}{R_{O/C}^1} - \frac{R_{H/C}^1}{2R_{O/C}^1} - 1 \right) = \left(\frac{R_{O/C}^0}{R_{O/C}^1} n_C^0 \right) \cdot \left(1 - \frac{R_{H/C}^1}{4} \right) - n_C^0 \cdot \left(1 - \frac{R_{H/C}^0}{4} \right) \quad (9)$$

$$\frac{\Delta nCO_2}{n_C^0} \cdot \left(2 - \frac{R_{H/C}^1}{2} - R_{O/C}^1 \right) = R_{O/C}^0 \cdot \left(1 - \frac{R_{H/C}^1}{4} \right) - R_{O/C}^0 \cdot \left(1 - \frac{R_{H/C}^0}{4} \right) \quad (10)$$

$$\frac{\Delta nCO_2}{n_C^0} = \frac{R_{O/C}^0 \cdot \left(1 - \frac{R_{H/C}^1}{4} \right) - R_{O/C}^0 \cdot \left(1 - \frac{R_{H/C}^0}{4} \right)}{\left(2 - \frac{R_{H/C}^1}{2} - R_{O/C}^1 \right)} \quad (11)$$

This equation allows for the calculation of generated CO₂ relative to the initial amount of carbon from the initial and final molar ratios. The calculation of generated methane can be performed in a similar way:

$$R_{O/C}^1 \cdot n_C^1 = R_{O/C}^0 \cdot n_C^0 - 4\Delta nCO_2 \quad (12)$$

$$\Delta nCO_2 = \frac{R_{O/C}^0 \cdot n_C^0 - R_{O/C}^1 \cdot n_C^1}{2} \quad (13)$$

$$R_{H/C}^1 \cdot n_C^1 = R_{H/C}^0 \cdot n_C^0 - 4\Delta nCH_4 \quad (14)$$

$$n_C^1 = \frac{R_{H/C}^0 \cdot n_C^0 - 4\Delta nCH_4}{R_{H/C}^1} \quad (15)$$

$$n_C^1 = n_C^0 - \frac{(R_{O/C}^0 \cdot n_C^0 - R_{O/C}^1 \cdot n_C^1)}{2} - \Delta nCH_4 \quad (16)$$

$$\left(\frac{R_{H/C}^0 \cdot n_C^0 - 4\Delta nCH_4}{R_{H/C}^1} \right) \cdot \left(1 - \frac{R_{O/C}^1}{2} \right) = n_C^0 - \frac{(R_{O/C}^0 \cdot n_C^0)}{2} - \Delta nCH_4 \quad (17)$$

$$\left(\frac{R_{H/C}^0 \cdot n_C^0 - 4\Delta nCH_4}{n_C^0} \right) \cdot \left(1 - \frac{R_{O/C}^1}{2} \right) = R_{H/C}^1 - \frac{R_{H/C}^0 \cdot R_{O/C}^0}{2} - \frac{\Delta nCH_4}{n_C^0} \cdot R_{H/C}^1 \quad (18)$$

$$R_{H/C}^0 \cdot \left(1 - \frac{R_{O/C}^1}{2} \right) = R_{H/C}^1 \cdot \left(1 - \frac{R_{O/C}^0}{2} \right) + \left(\frac{\Delta nCH_4}{n_C^0} \right) \cdot (4 - 2 \cdot R_{O/C}^1 - R_{H/C}^1) \quad (19)$$

$$\frac{\Delta n_{CH_4}}{n_C^0} = \frac{R_{H/C}^1 \cdot \left(1 - \frac{R_{O/C}^1}{2}\right) - R_{H/C}^1 \cdot \left(1 - \frac{R_{O/C}^0}{2}\right)}{4 - 2 \cdot R_{O/C}^1 - R_{H/C}^1} \quad (20)$$

Equations (11) and (20) were used in the mass balance calculation to estimate the maximum amount of gas that can be generated from coal for CO₂ and methane, respectively. The calculation was performed for coals in a rank range starting at VRc = 0.57% up to a rank of VRc = 2.57%. Any gas that has been generated at an earlier maturation stage (< VRc = 0.57%) is not taken into account. Molar amounts of generated gas were converted to volumes using standard conditions (100kPa, 0°C). Results of the mass balance calculation are given in *Appendix II Table 1*. For the rank range considered here, a total cumulative volume of 201 m³ methane per ton of TOC was calculated for coal from the Upper Silesian Coal Basin. For carbon dioxide a total cumulative volume of 138 m³/t TOC was calculated. Results of the mass balance calculation for coals from the Upper Silesian Coal Basin were compared with calculations based upon elemental analysis data for coals from the German Ruhr Basin, by Gaschnitz (2001) (*Fig. 3.2*).

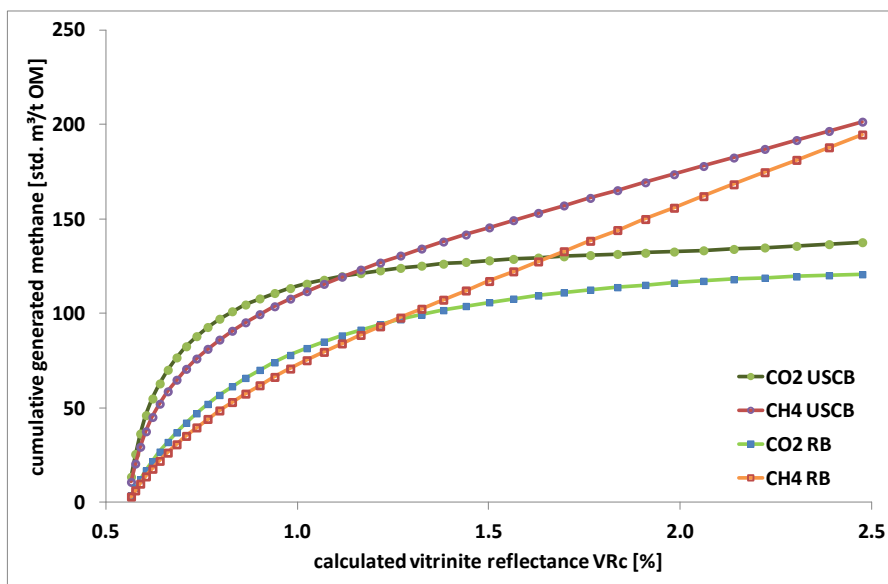


Fig. 3.2 Comparison of cumulative methane and carbon dioxide generation from mass balance calculations for coals from the German Ruhr Basin (RB) and Upper Silesian Coal Basin (USCB) for a maturity range between 0.6 and 2.6 VRc %. Data for RB calculations from Gaschnitz (2001).

The comparison shows that for both coal basins the amount of methane that theoretically can be generated from coal is slightly higher for USCB coals at low coal rank, but the total cumulative amount at semi-anthracite rank range is similar for both basins. These results are in good agreement with mass balance results from previous studies (*Table 3.1*).

Table 3.1 Comparison of mass balance calculations for methane generation from coals

	Coal basin	Rank range %VR	Generated methane m ³ /t OM
Jüntgen and Karweil (1966)	Ruhr Basin	0.75 – 3	250 (200 m ³ /t coal)
Krooss et al. (1995)	Ruhr Basin	0.75 – 3.2	181
Gaschnitz (2001)	Ruhr Basin	0.65 – 2.7	230
This study	USCB	0.57 – 2.57	201

3.4. Rock-Eval pyrolysis

Rock-Eval pyrolysis is based upon a method developed by Espitalié et al. (1977) to determine the degree of maturity of organic matter and to detect the petroleum potential of source rocks. While Rock-Eval pyrolysis can also be used to experimentally determine reaction kinetic parameters for bulk hydrocarbon generation, it was applied in the present study only as a first “screening” method to assess the maturity and hydrocarbon generation potential of coals. For detailed evaluation of the reaction kinetics of gas generation, open system non-isothermal pyrolysis coupled to gas chromatography (Py-GC) was applied (see chapter 3.5).

3.4.1. Method

Analyses were carried out on a Rock-Eval II system (Delsi-Nermag, France) in duplicate measurements. A standard was measured three times every 10 samples. To avoid the problem of coal swelling, caking and incomplete reaction of high-rank coal during Rock-Eval pyrolysis (Bostick and Daws, 1994), 9-10 mg of each coal sample were blended with 90 mg quartz sand. During pyrolysis, samples were heated under inert atmosphere (helium) using the following temperature program: Rapid heating to 300°C; holding this temperature for 3 minutes; heating to 550°C with a rate of 25°C/min. At 300°C free hydrocarbons are vaporized and detected by a flame ionization detector (FID) as S1-peak [mg HC/g coal]. Between 300°C and 600°C heavy hydrocarbons (>C40) and unextractable organic matter (kerogen) are thermally cracked and expelled. These hydrocarbons are detected by the FID as S2-peak [mg HC/g coal]. The temperature at which S2 reaches its maximum is recorded as T_{max} [°C]. After heating, trapped carbon dioxide, which was released during pyrolysis, is detected by a thermal conductivity detector (TCD) as S3-peak [mg CO₂/g coal]. From measured peaks for S1, S2 and S3 and the amount of TOC, the following indices are calculated (Tissot and Welte, 1984):

$$\text{Hydrogen Index} \quad \text{HI} = 100 \cdot \text{S2}/\text{TOC} \text{ [mg HC/g TOC]} \quad (21)$$

$$\text{Oxygen Index} \quad \text{OI} = 100 \cdot \text{S3}/\text{TOC} \text{ [mg CO}_2\text{/g TOC]} \quad (22)$$

$$\text{Transformation Ratio} \quad \text{TR} = \text{S1}/(\text{S1}+\text{S2}) \quad (23)$$

$$\text{Bitumen Index} \quad \text{BI} = \text{S1}/\text{TOC} \text{ (Killops et al., 1998) [mg HC/g TOC]} \quad (24)$$

$$\text{Quality Index} \quad \text{QI} = (\text{S1} + \text{S2})/\text{TOC} \text{ [mg HC/g TOC]} \quad (25)$$

(Pepper and Corvi, 1995)

3.4.2. Results and discussion

All coal samples studied here are within the effective oil window for type III kerogen (VR_r 0.85-1.8%) and most of them have reached the peak of thermogenic gas generation (VR_r ~1.1%) (Schimmelmann et al., 2006). For humic organic matter the end of the oil window is suggested to correspond to a vitrinite reflectance of 1.8% (Petersen, 2002).

The amount of “free” bitumen (S1 peak) in coal samples from the limnic Karviná Formation (ČSM mine) is very low (<2 mg HC/g), whereas coal samples from the paralic Ostrava Formation (Paskov and Lazy mine) released more “free” bitumen (1.5 – 11 mg HC/g) during pyrolysis. For samples from the Paskov mine, S1 values are lower than 4 mg HC/g, with one exception (approx. 10 mg HC/g). This sample has the lowest thermal maturity (highest volatile matter yield) among the Paskov samples. Coal samples from the Lazy mine show a larger variation in S1 (4.5 to 11 mg HC/g). Low amounts of “free” bitumen (S1) have previously been reported for different coals from the U.S., England and Poland (Teichmüller and Durand, 1983; Bostick and Daws, 1994; Kotarba et al., 2002).

The amounts of hydrocarbons released during thermal cracking of organic matter (S2 peak) vary between 47 and 103 mg/g for Paskov samples, between 89 and 118 mg/g for ČSM samples and between 106 and 252 mg/g for Lazy samples. The liptinite-rich sample from Prokop seam has the highest S2 yield of 252 mg/g.

The Hydrogen Index (HI) is used to assess the kerogen type as well as the hydrocarbon potential. As expected for humic coals, essentially all samples plot in the type III kerogen field ($HI < 300$). The temperatures of maximum hydrocarbon generation rate during Rock-Eval pyrolysis, T_{max} , range between 456 and 483°C for coal samples from the Paskov and ČSM mines and from 443 to 465°C for coals from the Lazy mine. Such high T_{max} values are typically found in mature and overmature type III kerogens (Taylor et al., 1998). The T_{max} values show a good correlation with vitrinite reflectance for the Paskov coals, whereas the correlation for the ČSM and Lazy coals is very weak. Kotarba et al. (2002) have previously reported a good correlation between T_{max} and VRr% for coals from the Polish part of the USCB.

Hydrogen Index (HI) decreases with increasing coal rank (VRr %, T_{max}), reflecting the loss of hydrocarbon generation potential during thermal maturation (Bertrand, 1984). Boreham et al. (1999) observed a maximum of HI at $T_{max} \sim 440^\circ\text{C}$ for Permian coals from Australia, which was followed by a continuous decrease of HI with increasing coal rank, reflecting active petroleum generation and expulsion. For coals from the USCB the decrease of HI is well expressed for samples from the Paskov mine and also for coals from the Polish part of the USB (Kotarba et al., 2002), whereas it is not obvious for coals from ČSM and Lazy mines. This is due to the narrow maturity range of ČSM coal samples and the large variation in petrographic properties of the Lazy samples. The Rock-Eval data can provide insight into the thermal maturation process of coals and the thresholds of hydrocarbon generation and expulsion. Thus, the Bitumen Index, as defined by Killops et al. (1998), may be used to identify the onset of oil and gas generation (Sykes and Snowdon, 2002). For coals from New Zealand and other regions, an increase of BI with increasing maturity around $T_{max} 430^\circ\text{C}$, followed by a peak around $T_{max} 450^\circ\text{C}$ is interpreted to represent the onset of oil generation and gas generation, respectively (Sykes and Snowdon, 2002 and references therein). A cross-plot of BI with T_{max} for coals from the USB shows that almost all coals from the Czech part have reached the stage of gas generation (Fig. 3.3). In Poland, coals from the south-eastern part of the USCB, where thermal maturity is lower ($T_{max} \sim 430^\circ\text{C}$, $VR_r < 1\%$), are at the onset of petroleum generation, whereas coals of higher maturity ($T_{max} 460\text{-}470^\circ\text{C}$, $VR_r > 1.2\%$) from the south-western part have passed the stage of gas generation (Kotarba et al., 2002). The quality index ($QI = (S1+S2)/TOC$) indicates the decrease in total generation potential per unit mass of organic carbon (Sykes and Snowdon, 2002). For New Zealand coals QI increases with increasing maturity to a maximum around $T_{max} 440^\circ\text{C}$, followed by a continuous decrease, which can be interpreted as the onset of petroleum expulsion (Sykes and Snowdon, 2002). A cross-plot of QI vs. T_{max} for coals from the USB shows that all coals are beyond this onset of petroleum expulsion. Coal samples from Paskov mine show a clear decline of QI with increasing maturity, whereas this trend is not well expressed for the other samples (Fig. 3.3). Some coals from the south-eastern part of the USB in Poland did not reach the stage of petroleum expulsion, whereas coals from the western part plot close to samples from the upper Ostrava and lower Karviná Formation (ČSM and Lazy mine) analyzed in this study. The Rock-Eval S3 values for all samples are very low, resulting in oxygen index (OI) values less than 5 for most samples. A decrease of OI with increasing rank is observed, indicating that most original organic oxygen is lost. Samples with high inertinite contents tend to show higher OI values compared to samples with low amounts of inertinite.

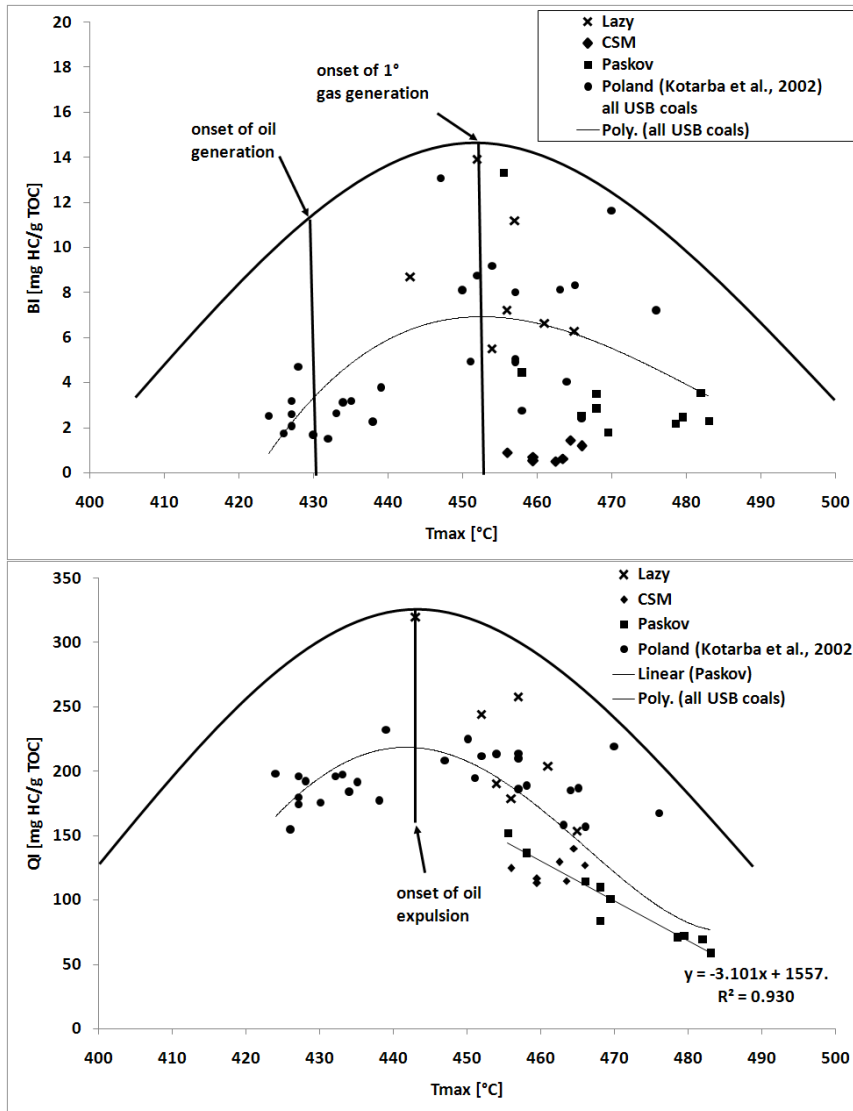


Fig. 3.3 Bitumen Index (BI) and Quality Index (QI) versus maturity (T_{max}) for coal samples from the USCB including interpretation according to Sykes and Snowdon (2002).

3.5. Open system non-isothermal pyrolysis

This approach is based on the concept that gas generation measured in laboratory experiments at high temperatures (up to 1200°C) and high heating rates (0.1 – 10 K/min) can be extrapolated to geologic conditions (<200°C, heating rates of ca. 10^{-11} K/min) to estimate gas generation during coalification (Hanbaba and Jüntgen, 1969).

3.5.1. Method of Pyrolysis Experiments

A non-isothermal open system pyrolysis unit coupled to a gas chromatograph (Py-GC) according to Krooss et al. (1995, 2005) was used to evaluate methane (CH_4) and nitrogen (N_2) generation from powdered coal samples. The pyrolytic gas generation reflects successive liberation of both components during artificial thermal maturation. The experimental set-up consists of a pyrolysis oven, a gas chromatograph (HP 5890), a flow controller for the furnace gas (He) current and an automated 6-port sampling valve (Valco). The pyrolysis gases evolving from the sample (0.14 – 0.3 g) during programmed heating are continuously flushed out of the

tubular furnace by a constant helium stream of known flow-rate (12 ml/min). Every 5 minutes, aliquots of the pyrolysis gas current are transferred to a 5 ml sample loop and injected into the carrier gas stream of the GC system by the automated sampling valve. With a programmed heating rate of 0.5 °K/min, the pyrolysis gas is analyzed at 2.5 °C temperature intervals throughout the experiment. The amounts of pyrolysis gases in these aliquots are quantified by a thermal conductivity detector (TCD).

Before each experiment, the furnace is purged with helium for several hours to remove atmospheric oxygen and nitrogen. When the background N₂ and O₂ signals have declined to an acceptable level, the heating program is started at room temperature with a constant heating rate of 0.5 K/min until the final temperature of 1200 C is reached. Before and after each pyrolysis run the GC/TCD is calibrated with a certified gas mixture containing known concentrations of CH₄.

Generation rates in terms of mass (mg) of gas per unit mass (g) of original substance and unit time (s) are computed, based on original sample mass, flow rate of helium through the furnace, sample loop volume and integrated TCD signal after conversion to mass units (mg).

A total of 6 coals from the Upper Silesian Basin (Czech Republic) and one coal from the Paraná Basin (Brazil) were pyrolysed at a heating rate of 0.5 K/min.

Additionally sample 8 from the USCB (Prokop seam) was pyrolysed at higher heating rates (1 K/min and 2 K/min), to evaluate kinetic parameters of pyrolytic gas generation. Furthermore, the bitumen of sample 8 was extracted for 48h using a Soxhlet extraction system and an azeotropic solvent mixture of chloroform, acetone and methanol (47/30/23 v/v/v). After solvent extraction, the residue was air-dried and pyrolyzed using a heating rate of 0.5 K/min.

Gas generation rates were normalized to mass of organic matter and, using the constant heating rate, converted to ((mg gas / g TOC) / K) for better comparison. Generation rates and cumulative amounts of gas generation were also converted to volumes ((m³gas / t TOC) / K) using IUPAC standard conditions (0°C, 100kPa). For better comparison with literature data, activation energies are given in kcal/mol (1 J = 2.39 · 10⁻⁴ kcal).

3.5.2. Results and discussion

During temperature-programmed open-system pyrolysis (0.5 K/min heating rate) the onset of methane generation occurred between 280 and 326°C. Generation rates increased until a maximum was reached between 467 and 503 °C was reached. At the same heating rate the temperature of maximum methane generation shifts towards higher values with increasing coal rank. Maximum measured methane generation rates ranged from 0.23 to 0.37 (mg/gTOC)/K for coals from USCB whereas a significantly lower generation rate was observed for the coal sample from Brazil (0.14 (mg/gTOC)/K). Generation rates for most coals exhibit a characteristic 'shoulder' or, in case of sample 8, even a second maximum at higher temperatures between 650 and 900°C (*Fig. 3.4*).

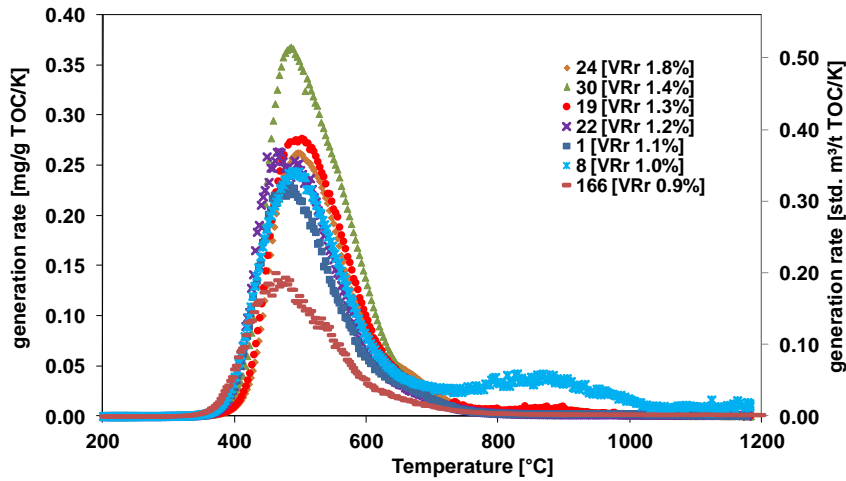


Fig. 3.4 Methane generation rates during temperature-programmed (0.5 K/min) open system pyrolysis

Similar features have been reported in previous studies for coals of different rank (Krooss et al., 2005; Heim et al., 2012). This observed methane generation at higher temperatures indicates additional late gas generation from a thermally more stable portion of the kerogen. A cumulative methane yield of up to 79 m³/tTOC was determined from pyrolysis experiments for coal from the USCB. The cumulative methane yield for the coal sample from Brazil was significantly lower (32 m³/tTOC) (Fig. 3.5).

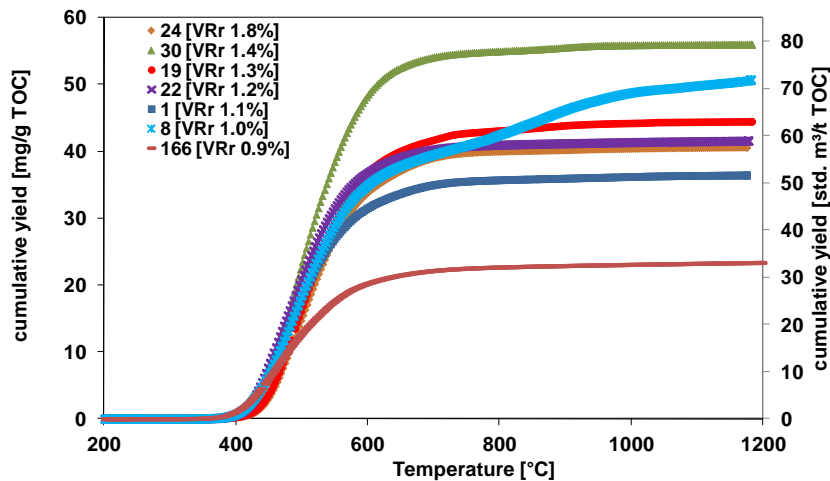


Fig. 3.5 Cumulative methane yield from temperature-programmed (0.5 K/min) open system pyrolysis. (166 = Coal sample from Brazil)

The methane generation shows a general increase with increasing coal rank towards a maximum, roughly coinciding with the peak of effective hydrocarbon generation for type III kerogen (ca. 1.35% VR) (Schimmelmann et al., 2006), followed by a decrease at higher coal ranks (Fig. 3.6).

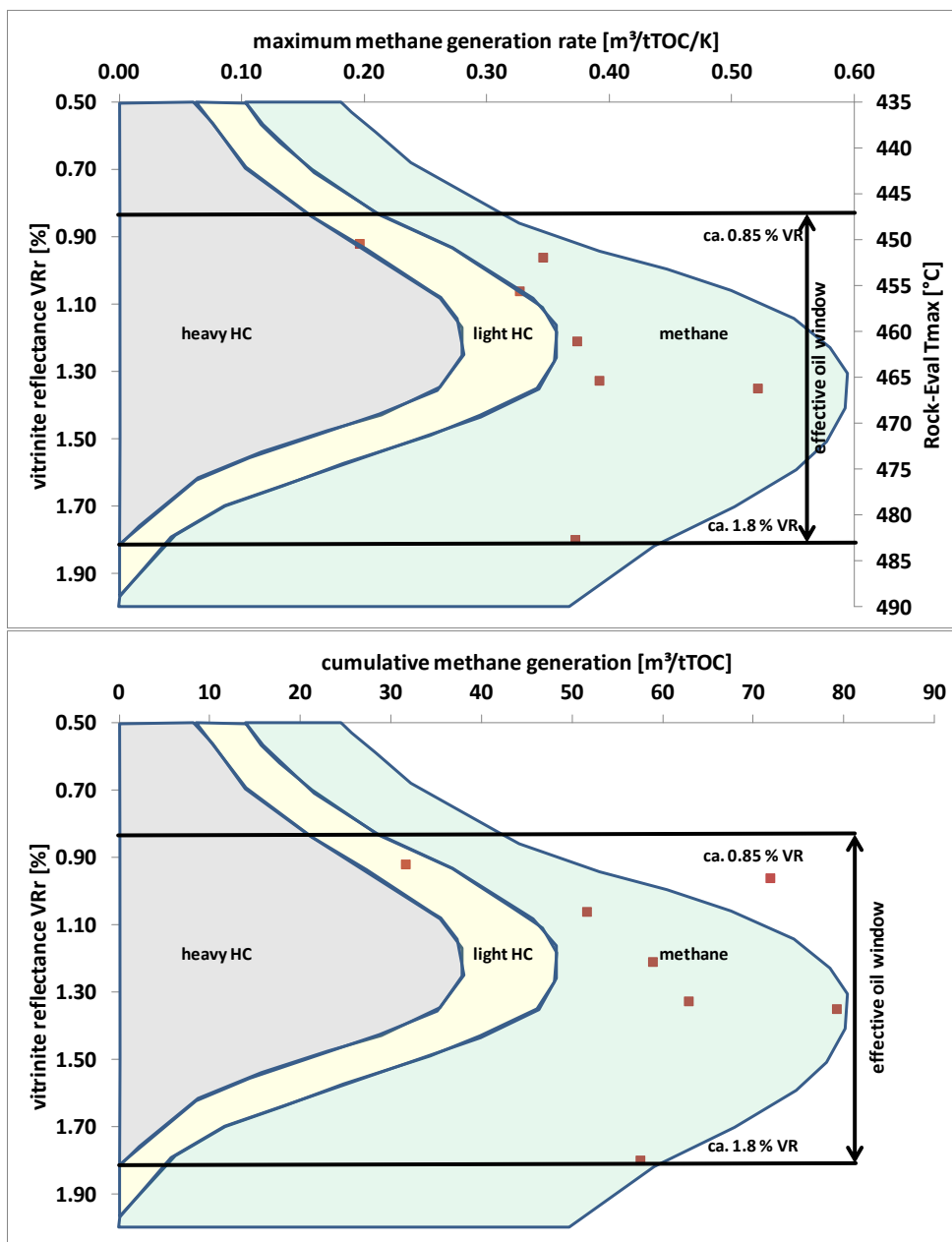


Fig. 3.6 Maximum measured generation rate (top) and cumulative generation (bottom) versus maturity. For comparison, estimated hydrocarbon generation fields for type III kerogen modified from Schimmelmann et al. (2006) have been added (not to scale with pyrolysis methane generation).

Pyrolytic release of nitrogen was significantly lower than methane and began at significantly higher temperatures (>600°C). Nitrogen generation rate curves exhibit a bimodal shape, showing a first small maximum around 700°C and a second, larger maximum at very high temperatures around 1100°C (Fig. 3.7). For coals from the USCB, the generation maxima shift towards higher temperatures with increasing coal rank. The coal from Brazil shows significantly lower nitrogen generation than coal from the USCB of similar rank. Additionally, nitrogen generation for the Brazilian coal started at higher temperatures and the second generation maximum is much less expressed. This indicates that not only maturity, but also the composition of coal plays a controlling role for nitrogen generation. The high ash yield of the

Brazilian coal also indicates that inorganic matter does not significantly contribute to the pyrolytic generation nitrogen.

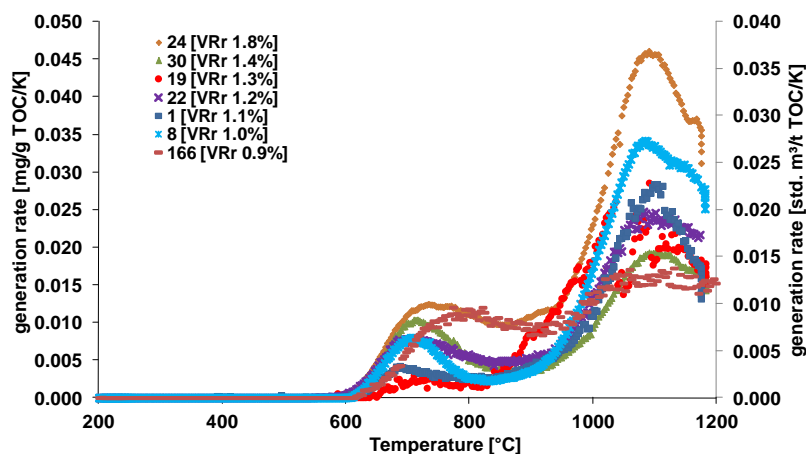


Fig. 3.7 Nitrogen generation rates during temperature-programmed (0.5 K/min) open system pyrolysis

The cumulative nitrogen yield is much smaller compared to methane, varying between 4 and 9 m³/tTOC (Fig. 3.8). The highest nitrogen yield was observed for the highest rank coal. However, no clear correlation between nitrogen generation and coal rank was observed.

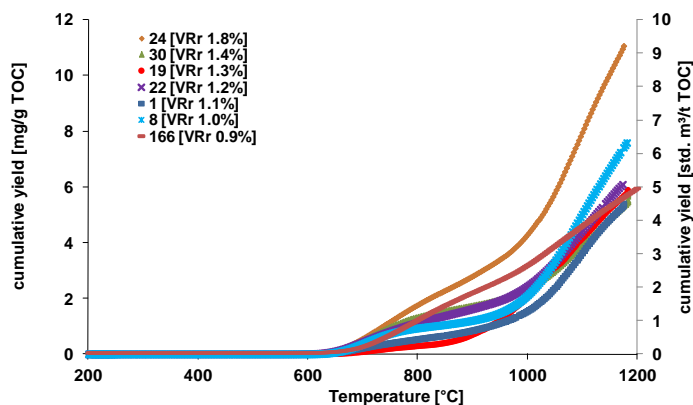


Fig. 3.8 Cumulative nitrogen yield from temperature-programmed (0.5 K/min) open system pyrolysis

Observations from pyrolysis experiments of the present study are in good agreement with results reported in previous studies, *e.g.* by Krooss et al. (1995) and Heim et al. (2012). To evaluate the influence of the bitumen fraction on the pyrolytical methane generation, one coal (sample 8) was pyrolyzed after solvent extraction. Methane generation from the extraction residue was lower than from the unextracted coal and the cumulative methane yield decreased by 28% (Fig. 3.9). Results of temperature-programmed open system pyrolyses are given in Table 3.2 and Appendix II.

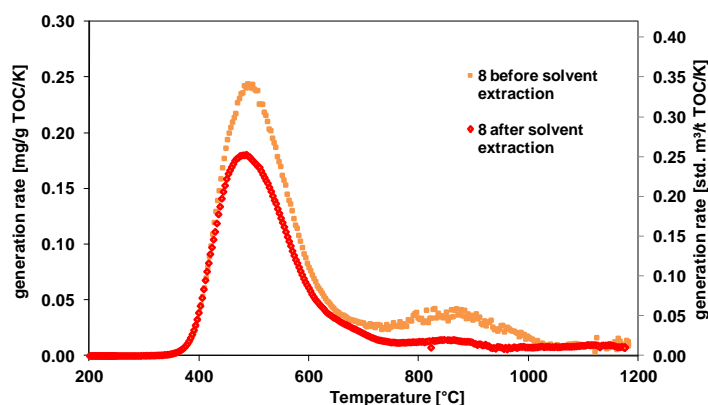


Fig. 3.9 Comparison of methane generation of sample 8 before and after solvent extraction.

Table 3.2 Results of temperature-programmed open system pyrolysis (heating rate = 0.5K/min)

sample #	max pyrolysis temp [°C]	CH ₄ onset temp. [°C]	CH ₄ max generation temp. [°C]	CH ₄ yield [mg/g coal]	CH ₄ yield [m ³ /t coal]	CH ₄ yield [mg/g TOC]	CH ₄ yield [m ³ /t TOC]	N ₂ yield [mg/g coal]	N ₂ yield [m ³ /t coal]	N ₂ yield [mg/g TOC]	N ₂ yield [m ³ /t TOC]
1	1175	302	483	31.79	45.00	36.45	51.60	4.62	3.75	5.66	4.30
8	1182	291	488	41.11	58.20	50.75	71.85	6.21	5.04	7.91	6.22
8 *	1174	272	489	35.91	50.84	44.34	62.77	5.01	4.06	6.93	4.78
8 +	1177	283	506	24.63	34.87	30.41	43.05	2.75	2.23	3.39	2.75
8 #	1175	295	486	30.91	43.75	36.36	51.47	5.43	4.40	6.38	5.17
19	1183	326	502	21.94	31.07	44.39	62.84	2.88	2.34	5.84	4.73
22	1178	294	467	29.63	41.95	41.59	58.88	4.69	3.81	1.54	5.29
24	1182	310	503	36.35	51.46	40.62	57.50	10.18	8.26	11.38	9.23
30	1183	280	485	43.84	62.06	55.94	79.19	4.31	3.49	5.50	4.46
07_166	1209	301	477	9.80	13.87	22.31	31.59	2.65	2.15	6.04	4.90

heating rate: *=(1K/min); +=(2K/min); #= after solvent extraction

3.5.3. Evaluation of the kinetic parameters of methane generation

Chemical reactions such as those involved in thermal gas generation result in changes of the concentration (C) of the involved components over time (t). These changes are described by rate equations. The most commonly used rate equation in petroleum system analysis is the first-order rate equation which relates the decay rate ($-dC_i/dt$) of a (precursor, reactant) substance i to the concentration C_i present at time t.

$$1. \text{ order reaction: } -\frac{dC}{dt} = k \cdot C; (k = \text{const.}) \rightarrow C = C_0 \cdot \exp(-k \cdot t)$$

Here k is a temperature-dependant reaction rate constant (k(T)).

For constant temperature (T) the first-order rate equation can be readily integrated and yields the remaining precursor concentration $C_i(t)$.

The temperature dependence of chemical reactions was described in earlier studies by a simplified assumption that upon a 10°C temperature increase, the reaction rate is doubled (Waples, 1980).

A more realistic approach to the temperature dependence of reaction rates is provided by the Transition State Theory (TST) or Absolute Rate Theory, which describes elemental reactions of activated complexes that require overcoming of potential barriers (activation energies) (Lasaga, 1981). The Arrhenius equation is a semi-empirical form that is widely used to describe the temperature dependence of the reaction rate of petroleum generation (Ungerer, 1990; Schenk et al., 1997 and references therein).

Integration of the rate equation allows for the calculation of the cumulative yield of generated gas:

$$k(T) = A \cdot \exp\left(-\frac{E_a}{R \cdot T}\right) \quad (26)$$

$$\frac{dC}{C} = -k(T(t)) \cdot C(t) dt \quad (27)$$

$$d \ln(C) = -k(T(t)) \cdot dt \quad (28)$$

$$\ln\left(\frac{C}{C_0}\right) = \int_0^t -k(T(t)) \cdot dt \quad (29)$$

$$C = C_0 \cdot \exp\left(-\int_0^t k(T(t)) \cdot dt\right) \quad (30)$$

$$C = C_0 \cdot \exp\left(-A \cdot \int_0^t \exp\left(-\frac{E_a}{R \cdot T}\right) \cdot dt\right) \quad (31)$$

Here A is a pre-exponential factor, E_a is the activation energy, R is the universal gas constant and T is the temperature. The pre-exponential factor has the dimension of a frequency (s^{-1}) for first order reactions. For reactions of the form $A \rightarrow B + C$ that occur during thermal decomposition of a larger molecule (A) into two smaller ones (B and C), the pre-exponential factor describes the frequency of intra-molecular vibration (Polanyi and Wigner, 1928). The vibrational frequency of molecular bonds in organic molecules lies within the range of infrared light ($\sim 10^{12}$ - 10^{14}). Consequently, the vibrational frequency to break these bonds will be higher, *e.g.* in the range of ultraviolet light ($\sim 10^{14}$ - 10^{17}). The pre-exponential factor is also temperature dependent; however, as discussed by Hanbaba and Jüntgen (1969), the influence of this temperature dependence is several magnitudes lower than the overall temperature dependence of the reaction rate constant (Hanbaba and Jüntgen, 1969). The activation energy of thermal cracking reactions depends on the kerogen composition and covers a range from <50 kcal/mol to >80 kcal/mol. For type I and II kerogens a normal (Gaussian) distribution of activation energies was found, with a maximum between 40 and 60 kcal/mol, whereas for type III kerogen a discrete (asymmetrical) distribution of activation energies with higher mean values was found (Ungerer, 1990 and references therein). Different ranges of activation energies have been used in previous studies to describe pyrolytic methane generation from coal and type III kerogen; *e.g.* 40 - 60 kcal/mol (Hanbaba and Jüntgen, 1969), 47 - 60 kcal/mol (Ungerer, 1990), 40 - 80 kcal/mol (Krooss et al., 1995), 30 - 94 kcal/mol (Schaefer et al., 1999), 40 - 80 kcal/mol (Schenk et al., 1997). The same applies for the pre-exponential factor derived from pyrolysis experiments. It ranged from low values of $3.18^9 s^{-1}$ (Krooss et al., 1995) to significantly higher values $> 10^{16} s^{-1}$ (Ungerer, 1990; Schenk et al., 1997). Detailed information on the individual cracking reactions occurring during coal pyrolysis and also during natural coalification can not be derived from laboratory bulk pyrolysis experiments. To evaluate the influence of the kinetic parameters activation energy (E_a) and the pre-exponential factor (A) on methane generation rates, especially with regard to an extrapolation to geologic conditions, half-life values ($\tau_{1/2}$) for methane generation were calculated:

$$\tau_{\frac{1}{2}} = \frac{\ln(2)}{k} \text{ [Ma]} \quad (32)$$

The half-life represents the time required to transform 50% of the substrate (coal). Half-life calculations were performed for a range of activation energies between 10 and 100 kcal/mol and pre-exponential factors of 10^{16} s^{-1} and 10^{12} s^{-1} (Fig. 3.10). The calculation shows that the half-life of reactions that require energies $>80 \text{ kcal/mol}$ is larger than 10 Ma for a frequency factor of 10^{16} s^{-1} and even higher for larger frequency factors. Contribution of these reactions to the overall methane generation under geologic conditions ($T < 250^\circ\text{C}$) will be minor compared to reactions of lower activation energy. Smaller pre-exponential factors result in a shift towards greater half-life values. Consequently, gas generation at geologic temperatures for the same time interval will be significantly lower if a smaller pre-exponential factor is used.

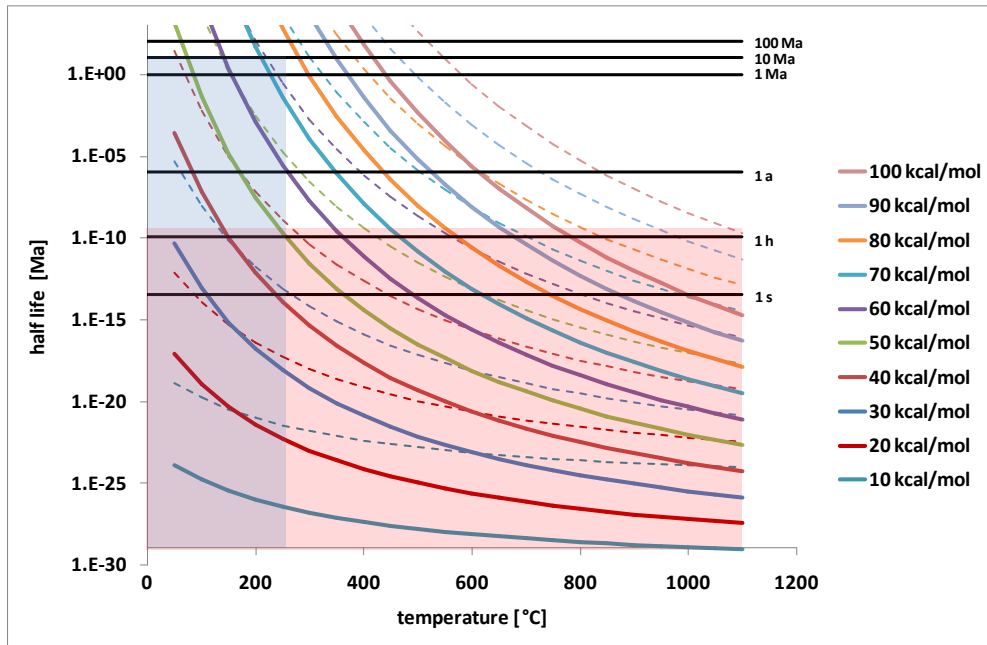


Fig. 3.10 Half-life values calculated using activation energies between 10 and 100 kcal/mol and a pre-exponential factor of 10^{16} s^{-1} (solid lines) and 10^{12} s^{-1} (dashed lines). The time and temperature range of laboratory experiments is represented by the red area, the blue area represents conditions during 'natural' coalification.

During coalification (catagenesis) the complex kerogen structure of coal is thermally decomposed by different chemical reactions that result in the formation of gaseous products (Jüntgen and Klein, 1975). The chemical reactions occurring during coal pyrolysis and also during natural coalification are very complex and not known in great detail. Thus, thermal decomposition is commonly described by a series of parallel first order reactions with different activation energies. To obtain kinetic parameters for methane generation, pyrolytically measured methane generation rates were approximated by generation rates calculated for a set of first order reactions. Experimental data were fitted with calculated reaction rates by a least squares method using the Arrhenius function and a range of activation energies from 35 to 100 kcal/mol. Similar to kinetic evaluations reported by Ungerer (1990) and Krooss et al. (1995), a single pre-exponential factor was used for reaction rate calculations in order to decrease the number of adjustable parameters. Since experimentally measured generation rate curves exhibit an asymmetric shape, a discrete distribution of activation energies was calculated, rather than assuming a Gaussian distribution. A pre-exponential factor of $8.7 \cdot 10^{16} \text{ s}^{-1}$ was derived from the shift of the generation maximum between pyrolysis measurements at three different heating rates, as described by van Heek and Jüntgen (1968), was used (Fig. 3.11, 3.12).

However, the correlation was only weak ($R^2 = 0.77$), which is attributed to uncertainties in the determination of the pyrolysis maxima. To evaluate the influence of different pre-exponential factors, additional reaction rate calculations were performed using a pre-exponential factor of 10^{15} s^{-1} . Finally, a narrower set of 10 activation energies between 46 and 78 kcal/mol and a pre-exponential factor of $4.3 \cdot 10^{13}$, similar to parameters used by Krooss et al. (1993) for coals of the German Ruhr Basin, was used for comparison. Results of these kinetic models are given in *Table 3.3*.

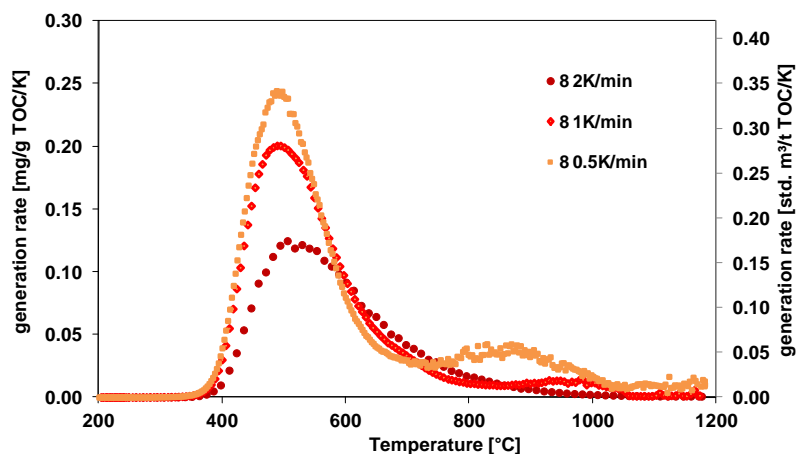


Fig. 3.11 Comparison of methane generation at different heating rates for sample 8.

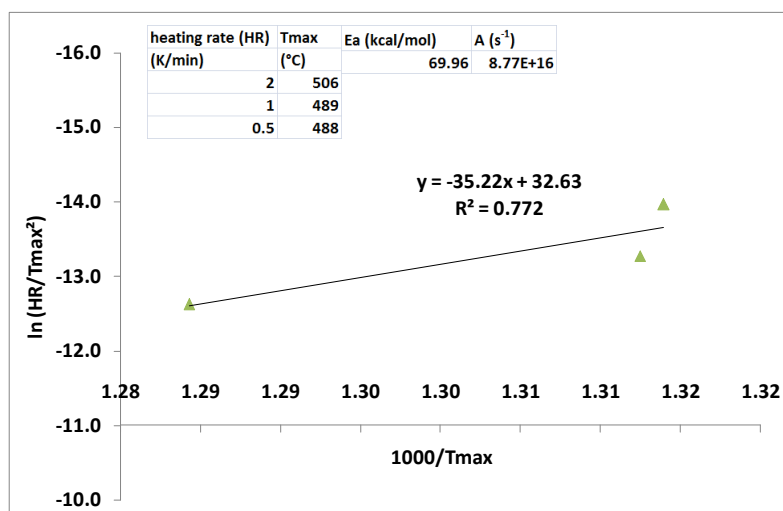


Fig. 3.12 Calculation of the pre-exponential factor (A) from the shift of the temperature of maximum methane generation (T_{max}) between pyrolysis experiments on sample 8 using three different heating rates.

The approximation of the experimental data by different kinetic parameter sets yielded similar results for samples that did not show significant methane generation at high temperatures ($>700^\circ\text{C}$) (*Fig. 3.13* bottom).

Table 3.3 Results of kinetic modelling for coal samples from the USCB
 (A = pre-exponential factor [s^{-1}])

sample #	stratigraphy	stratigraphy	[m ³ /tTOC] Pyrolysis experiment	cumulative CH ₄ yield			
				[m ³ /t TOC] A=10 ¹⁵	[m ³ /t TOC] A=8 · 10 ¹⁶	[m ³ /t TOC] A=4.3 · 10 ¹³ Krooss et al., 1993	[m ³ /t TOC] A=8 · 10 ¹⁶ geol. Rate 10 ⁻¹¹ K/min
1	L. Sucha M.		51.59	50.63	50.65	50.07	48.00
8	Saddle M.	Karviná	71.84	66.76	61.29	57.73	59.42
19	Jaklovec M.		62.86	61.20	61.04	60.17	57.73
22	L. Hrušov M.		58.85	58.04	57.35	57.94	54.96
24	Petrkovice M	Ostrava	57.46	56.81	56.66	56.10	51.62
30	Petrkovice M		79.26	78.34	77.94	77.22	73.33

In contrast, the approximation of pyrolysis data for sample 8, which showed significant methane generation above 700°C, yielded better results with a wide range of activation energies and a frequency factor of 10¹⁵ s⁻¹, whereas approximation with a higher frequency factor (8.7 · 10¹⁶ s⁻¹) could only fit 85% of the experimental data. For this sample, the approximation using a narrow range of activation energies was less satisfactory in describing gas generation at high temperatures and only 80% of experimental data were represented (*Fig. 3.13*).

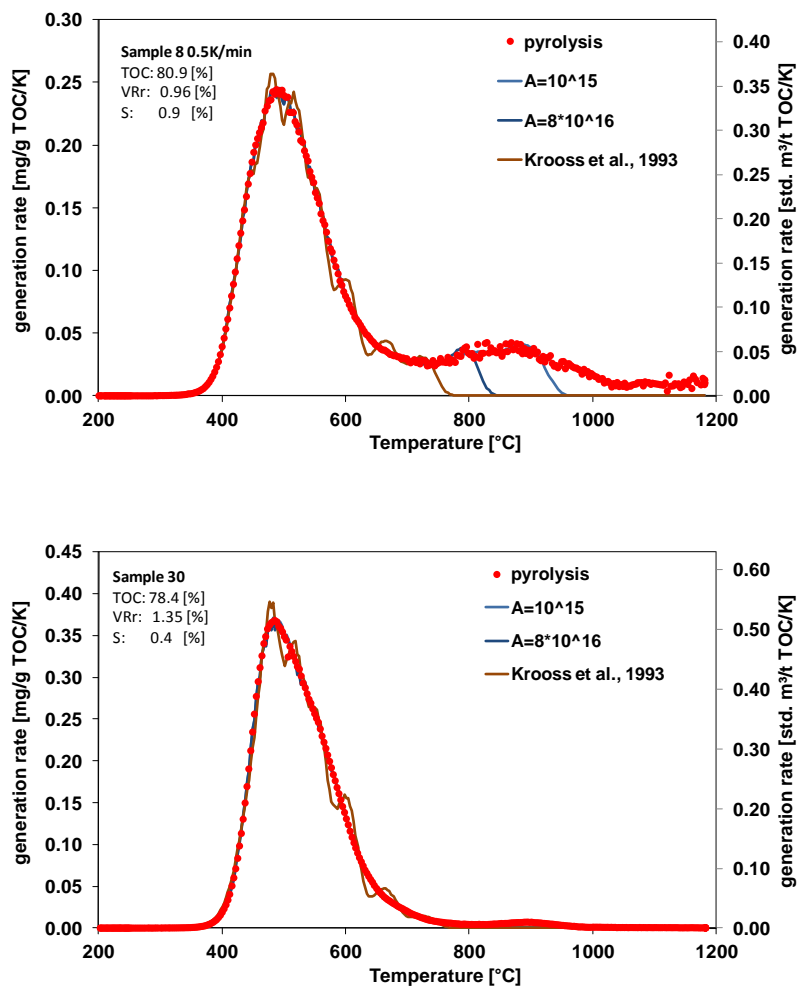


Fig. 3.13 Approximations of experimental pyrolysis data for two coal samples using different kinetic sets. Sample 8 shows significant methane generation at high temperatures (top) while sample 30 generates only small amounts of methane at high temperatures (bottom).

The activation energy distribution obtained from the different kinetic models showed no significant contribution of reactions with activation energies lower than 55 kcal/mol. The model using the experimentally derived frequency factor of $8.7 \cdot 10^{16} \text{ s}^{-1}$ resulted in an activation energy distribution with a maximum between 70 and 75 kcal/mol. Activation energies obtained from modeling using a lower frequency factor of 10^{15} s^{-1} showed a maximum between 60 and 70 kcal/mol and were generally lower than those generated using the higher frequency factor (Fig. 3.14).

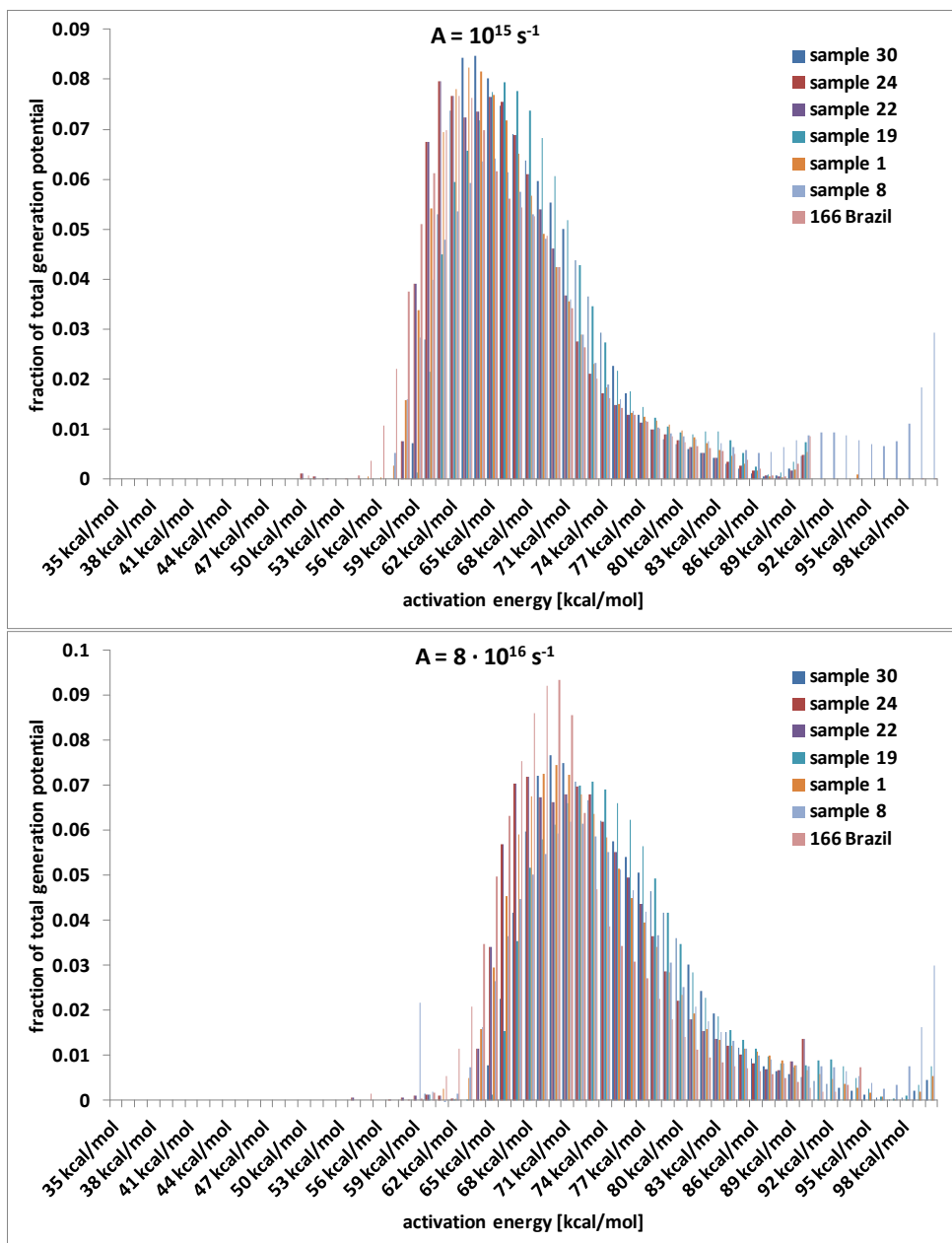


Fig. 3.14 Comparison of activation energy distributions obtained from least-square fits of experimental data using different frequency factors.

The kinetic model used by Krooss et al. (1993) to for coal from the German Ruhr Basin yields higher activation energies for coal from the Upper Silesian Coal Basin in the present study (Fig. 3.15). This indicates that the kerogen of coal samples from USCB is thermally more stable than coal from the Ruhr Basin. The differences in activation energy distributions are therefore due to the higher rank of the Czech coals (VRr 1.4%) as compared to the German coal (VRr 0.7%).

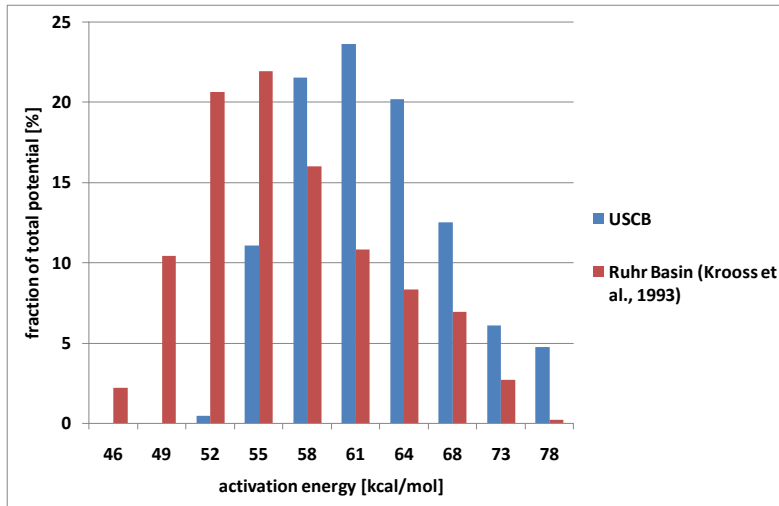


Fig. 3.15 Comparison of activation energy distribution obtained for coal from the Ruhr Basin (D) (Krooss et al., 1993) and for coal (sample 19) from the Upper Silesian Coal Basin (CR). Both kinetic parameter sets use a single pre-exponential factor ($A = 4.33^{13} \text{ s}^{-1}$).

To evaluate the methane generation during coalification on the geologic scale, a constant heating rate of 10^{-11} K/min may be assumed (Schenk et al., 1997). Extrapolation of methane generation to the geologic heating rate was performed using the same activation energy distribution obtained from approximation of experimental data using a frequency factor of $8 \cdot 10^{16} \text{ s}^{-1}$. Results of the extrapolation show a shift of methane generation rates towards lower temperature and a relative increase in generation rates (Fig. 3.16). The maximum of methane generation for the geologic conditions occurred between 208 and 246 °C.

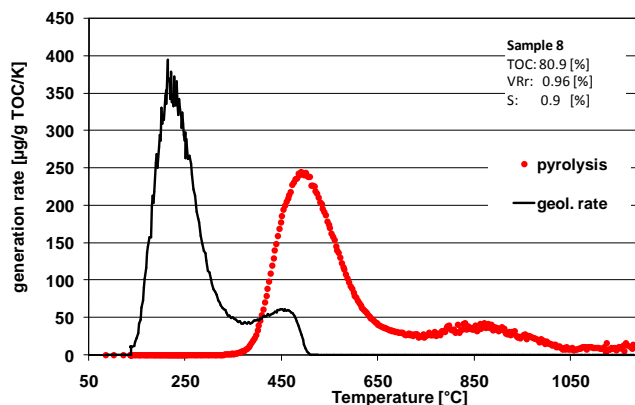


Fig. 3.16 Experimental methane generation curve measured at a laboratory heating rate of 0.5 K/min (red), and extrapolation to a constant geologic heating rate of 10^{-11} K/min (black).

Cumulative methane generation for the geologic heating rate ranged from 48 to 73 m^3/tTOC for coals from the USCB. The onset ($> 0.0001 \text{ mg/gTOC/K}$) of methane generation at geologic heating rates occurred between 93 and 136 °C.

Combining the temperature history from basin modelling with gas generation kinetics gives information on the timing of gas generation in the USCB. For these calculations the temperature history data from PetroMod were converted to 1Ma temperature steps and kinetic parameters for a constant frequency factor (10^{15} s^{-1}) were used.

Since these calculations are based upon pyrolysis data from coal samples of medium- to high rank that have already generated gas during the earlier basin history, the extrapolation of these data to geologic times can only be used to estimate the timing of gas generation during the basin evolution. However, such estimation is based upon the assumption that the activation energy distribution derived from laboratory experiments is similar to the activation energy distribution of processes occurring during natural coalification, which might not be the case. To evaluate the amount of gas generated in the geologic past from coals in the USCB, pyrolysis of low rank coals that did not generate significant amounts of gas would be required. Such low rank samples were not available for the present study. Gas generation reported here represents the residual gas generation potential of present-day coals from the USCB (Table 3.4). Maximum gas generation occurred earlier in coal seams from the Ostrava Formation, resulting in higher methane generation yields than from coal seams of the younger Karviná Formation. These Methane yields are based on experimental kinetic parameters derived from coals of a rank interval between 1.0 and 1.8% VRr and thus are significantly lower than the theoretical methane yield obtained from mass balance calculations for the rank interval from 0.6 to 2.6% VRc. Accordingly, the amount of gas that was generated during the basin history could not be assessed from coal samples available for the present study.

Results of the extrapolation of kinetic parameters to the temperature history of the USCB show that gas generation started between 319 and 306 Ma b.p. and that no significant generation took place from 285 Ma b.p. until present day (Fig. 3.17). Coal from the Hrusov Formation shows a bimodal generation rate, with a small generation phase between 319 and 316 Ma b.p. and the major gas generation between 314 and 286 Ma b.p.. Coal seams from the Ostrava Formation (Jaklovec M., Hrusov M.) showed the highest gas generation compared to coal from the Karviná Formation (Saddle M., Sucha M.). The maximum gas generation rate was reached at 310 Ma for the Ostrava Formation and 10 million years later for coals from the Karviná Formation.

Table 3.4 Gas generation calculated for a linear geologic heating rate (10^{-11} K/min) and for the temperature history obtained from 1D basin modelling. These values are derived from mature coals and do not reflect the entire gas generation during the basin history.

geologic heating rate (10^{-11} K/min)					Temperature history from 1D basin model		
sample #	stratigraphy	stratigraphy	temperature at max. generation rate [°C]	temperature at onset of gas generation (> 0.001 $\mu\text{g/gTOC/K}$) [°C]	Time of gas generation (> $1e^{-4}$ mg/gTOC/Ma) [Ma]	Gas generation rate. [$\text{m}^3/\text{t TOC Ma}$]	Cumulative CH_4 yield [$\text{m}^3/\text{t TOC}$]
1	L. Sucha M.		225	113	306 - 293	0.001	0.46
8	Saddle M.	Karviná	231	122	310 - 290	0.005	1.89
19	Jaklovec M.		246	130	312 - 286	0.019	9.78
22	L. Hrušov M.		208	93	319 - 316; 314 - 286	0.054	24.49
24	Petrkovice M	Ostrava	242	132	318 - 285	0.072	32.02
30	Petrkovice M		235	136	317 - 285	0.106	46.39

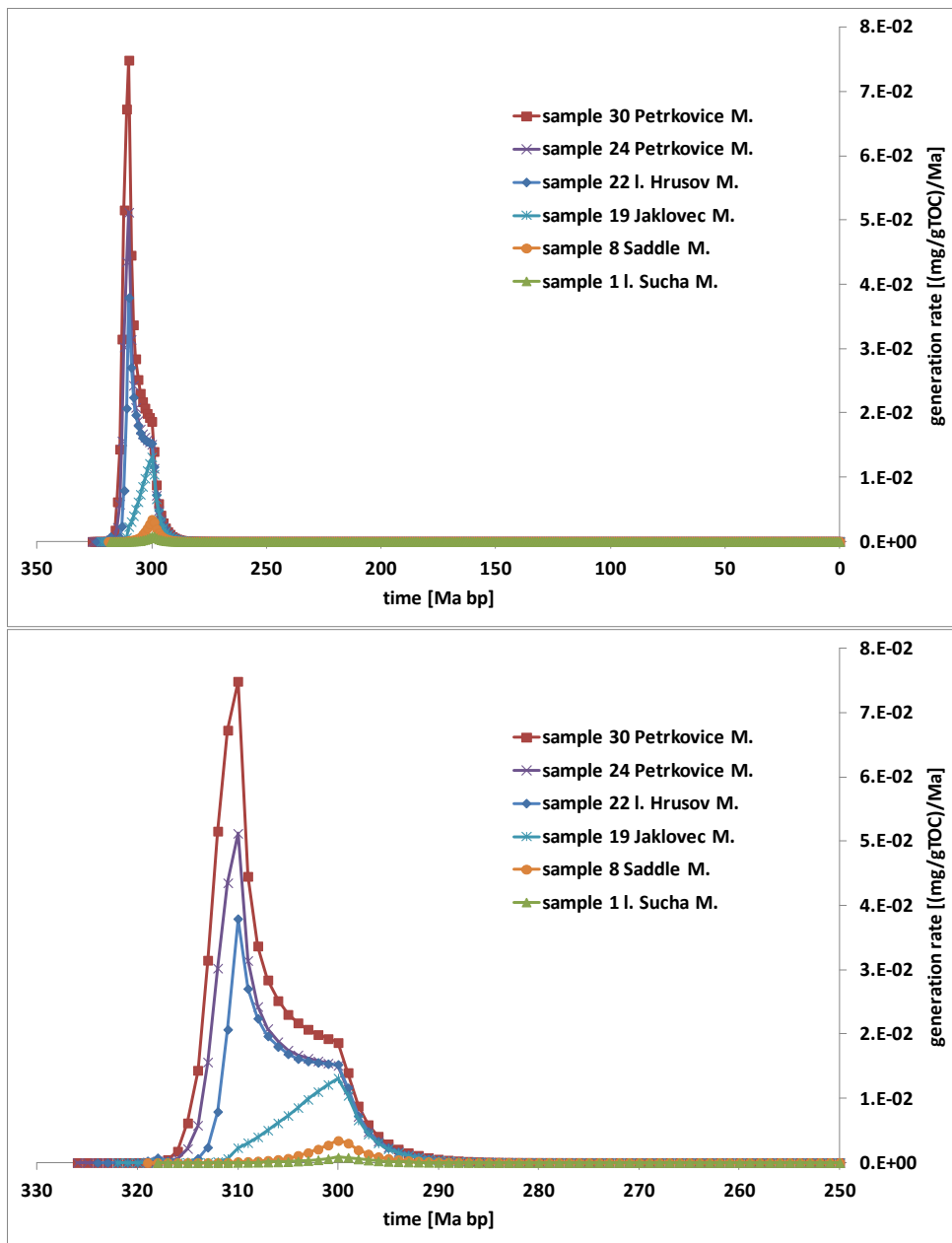


Fig. 3.17 Gas generation during basin history of the USCB for coal from the principal coal bearing formations, showing that major gas generation was complete by the Carboniferous – Permian transition (290 Ma b.p.).

The reburial of coal bearing sequences during the Carpathian overthrust in the Miocene and the associated temperature increase was too small to reinitiate significant gas generation in the study area (Fig. 3.18).

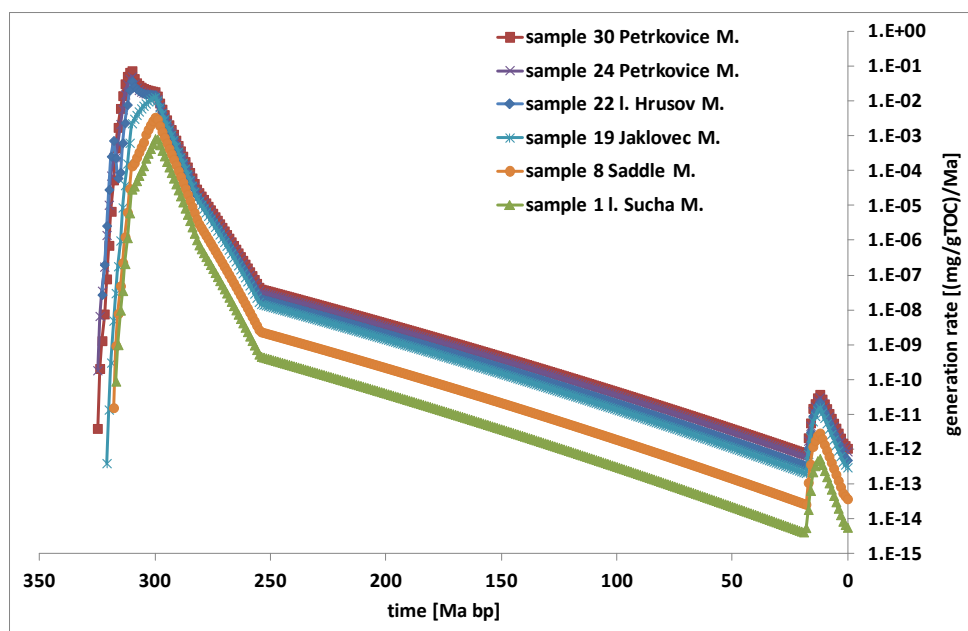


Fig. 3.18 Gas generation during the basin history of the USCBA for coal samples from the principle coal-bearing formations on a logarithmic scale showing the influence of the Carpathian overthrust during Miocene.

3.6. Conclusions

Estimation of the theoretical gas generation potential of coals from the Upper Silesian Coal Basin by mass balance calculation showed that a cumulative amount of 201 m³/tTOC of methane and 138 m³/tTOC of CO₂ could be generated during coalification from 0.6% to 2.6% vitrinite reflectance.

Maturity information from Rock-Eval pyrolysis (T_{max}) of coals from the USCBA analysed in this study showed that coals are of high-volatile bituminous A to low-volatile bituminous rank. Comparison of different maturity parameters (Rock-Eval T_{max} , VRr, VM) showed good correlations. Results of this bulk pyrolysis indicate that all of the analysed coals have reached the stage of effective thermogenic gas generation and expelled hydrocarbons during catagenesis.

During temperature-programmed open system pyrolysis experiments (Py-GC) at a constant heating rate of 0.5 K/min, gas generation from coals started around 300°C and reached maximum generation rates around 500°C. Methane generation showed a single peak for most samples; in some instances methane generation at higher temperatures (>700°C) was observed. The cumulative methane yield measured from Py-GC experiments of coals from the USCBA ranged from 52 to 79 m³/tTOC, while for a coal sample from the Brazilian Paraná Basin a significantly lower methane yield of 32 m³/tTOC was measured. Pyrolysis experiments performed on one sample at different heating rates showed a shift of the methane generation maximum towards higher temperatures with increasing heating rate. From this shift a pre-exponential factor of $8.7 \cdot 10^{16} \text{ s}^{-1}$ was derived. Furthermore, pyrolysis of a sample from the USCBA before and after solvent extraction indicated a contribution of the bitumen fraction to the overall residual methane yield of 28%.

Calculations of the half-life of gas generation for different kinetic parameters showed that activation energies >80 kcal/mol do not contribute significantly to methane generation at geologic times (pre-exponential factor = 10^{16} s^{-1}).

Approximation of experimental gas generation data by kinetic models using different combinations of activation energies and pre-exponential factor show good fits for coals with a single generation peak. Coals that exhibit additional methane generation at high temperatures (>700°C) require higher activation energies for a good approximation of experimental data.

Activation energy distributions from kinetic analysis of the experimental data showed a maximum between 70 and 75 kcal/mol for the determined pre-exponential factor of $8.7 \cdot 10^{16} \text{ s}^{-1}$, whereas calculations using a lower pre-exponential factor (10^{15} s^{-1}) result in a shift towards lower activation energies (60 – 70 kcal/mol).

Extrapolation of methane generation to geologic conditions represented by a constant heating rate of 10^{-11} K/min results in a shift of generation maxima to lower temperatures between 208 and 246°C. The residual cumulative methane yields at these geologic conditions are lower than the methane yields measured in pyrolysis experiments under laboratory conditions. Calculation of methane generation using time and temperature information from 1D basin modelling showed that major gas generation in the SW USCB took place between 319 and 285 Ma b.p.. The maximum gas generation occurred earlier in coal seams from the Ostrava Formation, resulting in higher residual methane generation potentials than for coal seams of the younger Karviná Formation. These residual methane generation potentials represent less than 25% of the theoretical methane yield that was estimated from mass balance calculations.

Methane generation associated with the Carpathian overthrust during Miocene did not yield significant amounts of gas.

4. Investigations on the methane and carbon dioxide sorption capacity of coals from the SW Upper Silesian Coal Basin, Czech Republic

Investigations on the methane and carbon dioxide sorption capacity of coals from the SW Upper Silesian Coal Basin, Czech Republic

Philipp Weniger^{1*}, Juraj Franců², Petr Hemza³, Bernhard M. Krooss¹

¹*Institute of Geology and Geochemistry of Petroleum and Coal, RWTH Aachen University, Germany*

²*Czech Geological Survey, Leitnerova 22, 65869 Brno, Czech Republic*

³*GreenGas, DPB a.s., Rudé armády 637, 73921 Paskov, Czech Republic*

4.1. Abstract

High-pressure sorption experiments with methane (CH₄) and carbon dioxide (CO₂) were performed on coals from different mines in the SW Upper Silesian Basin in Czech Republic. The coals were of high- to low-volatile bituminous rank, representing the late stage of catagenesis. The influence of different factors on the sorption capacity of these coals was evaluated by varying the experimental conditions. Excess sorption capacities of moisture equilibrated coals ranged from 0.3 to 0.8 mmol/g daf for CH₄ and from 0.8 to 1.2 mmol/g, daf for CO₂. Excess sorption capacities of as-received (air dried) coals were on average 34% higher for CH₄ and 17% higher for CO₂ as compared to the moisture equilibrated state. Sorption capacity shows a weak positive correlation with coal rank and a negative correlation with temperature. The CO₂/CH₄ sorption capacity ratio is larger for moisture-equilibrated coal, while it decreases with increasing pressure as well as increasing coal rank. From the experimental data correlations were derived between sorption capacity, and coal rank and temperature. These correlations were used to estimate the 'static' variation of sorption capacity with coal seam depth. Estimated sorption capacities increase towards a maximum value between 600 and 1000 m depth, followed by a decrease due to the predominance of the temperature effect. Temperature and pressure data derived from the reconstructed (1D) burial history were used to calculate the 'dynamic' variation of sorption capacity during basin evolution. These computations show that initial sorption capacity was significantly higher compared to the one estimated from present day pressure and temperature gradients. Uplift of coal seams resulted in under-saturation of the coal.

4.2. Introduction

Methane is the most common gas associated with bituminous coal seams worldwide (Rice, 1993). It is primarily generated during coalification, but also through anaerobic microbial activity in coal seams. Coal mine methane (CMM) is released during underground and surface mining operations as well as during post mining activities and from abandoned mines. Especially in underground mines it represents a major safety hazard and its concentration has to be controlled by ventilation. When released to the atmosphere, methane acts as a potent greenhouse gas. It is estimated that about 6% of global methane emissions originate from coal mining activities (USEPA, 2006). On the other hand methane represents an important energy source when extracted during coal mining as mine gas or gob gas. Coalbed methane (CBM) from unmined coal seams also represents an unconventional hydrocarbon source, if efficient extraction is possible.

Carbon dioxide, as a greenhouse gas in the atmosphere, has also been observed commonly in coal seams. It can be of geologic origin but may also be produced by chemical or

microbial oxidation of methane and other organic substances in active and abandoned coal mines, where oxygen is present. The sequestration of carbon dioxide in unmined coal seams has been evaluated as a means to reduce industrial CO₂ emissions (*e.g.* from power plants) and to enhance coalbed methane recovery (ECBM) (White et al., 2005). Consequently, there is growing demand for a better understanding of occurrence, transport and reactivity of coalbed methane and coalbed carbon dioxide.

To improve knowledge of the influence of adsorption/desorption processes on the amount and composition of coal-related gas, the work presented in this paper was focused on the determination of the methane and carbon dioxide sorption capacity of bituminous coals, as well as the characterization of coal maturity and composition, which can have an effect on the sorption capacity. The Upper Silesian Coal Basin (USCB) in Czech Republic was chosen as a 'natural laboratory' for this study. Samples from three different underground coal mines in the Ostrava-Karviná coalfield (OKC) in the SE USCB were analyzed. Based on the experimental results, a simple model was developed to estimate the in situ methane sorption capacity of coals as a function of inherent coal properties such as ash yield and rank as well as pressure, temperature and moisture content.

4.3. Study area and previous work

4.3.1. Geological setting

The Upper Silesian Coal Basin is one of Europe's major hard coal basins. It is located at the eastern edge of the Variscan Bohemian Massif, representing the eastern extension of the Moravo-Silesian Basin (*Fig. 4.1*). The USCB occupies a known area of more than 7000 km², of which more than two thirds are located in Poland, whereas the southern part of the basin, the Ostrava-Karvina coalfield (OKC), with a known area of 1550 km², is situated in NE Czech Republic (Sivek et al., 2003). Most coal bearing strata of the OKC are of Namurian A-C age. A simplified map of Carboniferous geology of the OKC is given in *Fig. 4.1* and a stratigraphic overview is shown in *Fig. 4.2*.

Economically important coal reserves of the OKC occur within the Upper Carboniferous Ostrava and Karviná formations.

The paralic Ostrava Formation (Upper Mississippian) contains 168 coal seams with an average thickness of 0.73 m. The most important unit is the Petrkovice Member, which contains more than 60% of the coal reserves of the Ostrava Formation (Dopita and Kumpera, 1993).

The coal content of the limnic Karviná Formation (Lower Pennsylvanian) is up to four times higher than that of the paralic Ostrava Formation. The largest coal reserves of the basin are found in the Saddle and Sucha Member of the Karvina Formation, which contains a total of 87 seams with an average thickness of 1.76 m. The most important seam is the Prokop (504) seam of the Saddle Member, which alone contains about 14% of all coal reserves. With a thickness of more than 10 m it is the thickest coal seam of the OKC (Dopita and Kumpera, 1993).

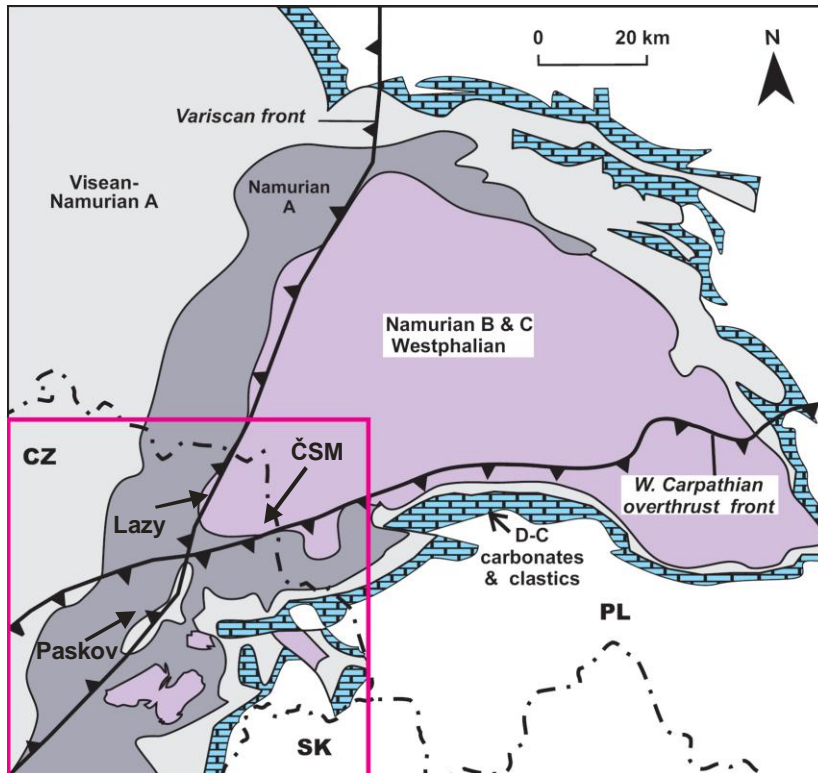


Fig. 4.1 Location of the study area in the Southern Upper Silesian Coal Basin, Czech Republic (adapted from Sivek et al., 2003).

The gas content of coal-bearing sequences in the Czech part of the USCB mostly ranges between 2 and 10 m³/t and shows an overall decline with increasing depth (Hemza et al., 2009). Geochemical and carbon isotopic investigations of coal related gas provide evidence of co-occurrence of thermogenic and microbial gas in the Ostrava-Karviná Coalfield, showing no clear relationship between gas composition and stratigraphy or thermal maturity of associated coal beds (Franců et al., 2007; Weniger et al., 2011b submitted). Similar observations were made in the Polish part of the USCB by Kotarba (2001). Kandarachevová et al. (2009) report that the occurrence of gas deposits found in Carboniferous rocks and overburden strata in the OKC is spatially related to zones of elevated thermal maturity.

		Czech Republic				Poland		
						Western Part	Eastern Part	
Pennsylvanian	Bashkirian	Westphalian	B	Eroded			Orzesze Beds	
			A	Upper	Doubrava Member	Zalęże Beds		
			C	G	Suchá Member	Ruda Beds		
			B	R	Saddle Member	Saddle/Zabrze Beds		
Mississippian	Serpukhovian	Namurian	H	Hiatus			Jejkowitz Beds	Hiatus
			E ₂	Upper	Poruba Member	Poręba Beds		Grodziec Beds
			A	Upper	Jaklovec Member	Jakłowic Beds		
			E ₁	Lower	Hrušov Member	Gruszów Beds		Flora Beds
				Petřkovic Member	Pietrkowice Beds		Sarnów Beds	

Fig. 4.2 Stratigraphic overview of the Ostrava Karviná Coalfield (modified from Sivek et al., 2003).

McCants et al. (2001) observed a zone of ‘gassy coal’ below ca. 1000 m during CBM exploration in the Polish part of the USCB. They found a link between the occurrence of gas rich coal seams and changes in the local depth/rank gradient and emphasized the importance of coal rank information for CBM exploration.

4.3.2. Thermal maturity of coal from the Ostrava-Karviná Coalfield

In the Czech part of the Upper Silesian Basin, intense exploration for coal was conducted in the course of the 20th century. During this exploration phase, maturity was primarily determined based on volatile matter yield (VM, daf). Only recently, during the final stage of exploration, vitrinite reflectance (VRr) measurements have been used for thermal maturity assessment (Sivek et al., 2003; Sivek et al., 2008; Hemza et al., 2009). Coals in the Czech part of the USB are mostly of bituminous rank and show the highest thermal maturity in the WNW part of the OKC, where Variscan orogenic processes were most intense and coals locally reach anthracite rank. The degree of coalification decreases towards the ESE and S to SSW (Kandarachevová et al., 2009; Sivek et al., 2003). Sivek et al. (2008) report a good correlation of thermal maturity (VM, daf) with increasing depth, showing slightly different trends in different parts of the basin.

4.4. Samples

A total of thirty coal, carbonaceous shale and coal-bearing rock samples, from different mines of the Ostrava-Karviná Coalfield were analyzed in this study. These samples cover almost the entire stratigraphic range of coal-bearing sequences in the study area. The set comprised ten channel samples from the Paskov mine near Staric, representing coal seams of the lower Ostrava Formation, and seven channel samples from the ČSM mine near Stonava, representing coal seams from the Karviná Formation. Additionally, thirteen samples from two exploration wells (Lazy D-75/08, Lazy D-76/08), drilled in the Karviná mine (Lazy Business Unit), representing coal seams from the upper Ostrava and Karviná Formations were analysed in this study. The Prokop seam of the Lazy D-76/08 well was split into two sub-samples (8.1 and 8.2). All seventeen channel samples, as well as nine samples from exploration wells, were subjected to high pressure sorption experiments. Locations of sampled coal mines are given in *Fig. 4.1*. A list of all analyzed samples is given in *Table 4.1*.

Table 4.1 Overview of samples from the Ostrava-Karviná coalfield

Sample #	Mine	Seam Code	Lithology	Litostratigraphy	Formation	Age	Depth (m)
1	ČSM	648	coal	l. Suchá M.	Karviná	Namurian C	714
2	ČSM	634	coal	l. Suchá M.	Karviná	Namurian C	700
3	ČSM	624	coal	l. Suchá M.	Karviná	Namurian C	700
4	ČSM	608	coal	l. Suchá M.	Karviná	Namurian C	638
5	ČSM	546	coal	Saddle M.	Karviná	Namurian B	694
6	ČSM	530	coal	Saddle M.	Karviná	Namurian B	743
7	ČSM	504	coal	Saddle M.	Karviná	Namurian B	558
8.1	Karviná (Lazy)	504	coal	Poruba M.	Karviná	Namurian B	460
8.2	Karviná (Lazy)	504	coal	Poruba M.	Karviná	Namurian B	460
9	Karviná (Lazy)		ss+coal	Poruba M.	u. Ostrava	Namurian A E2	467
10	Karviná (Lazy)	446	coal	Poruba M.	u. Ostrava	Namurian A E2	804
11	Karviná (Lazy)	440	coal	Poruba M.	u. Ostrava	Namurian A E2	831
12	Karviná (Lazy)	444	si+coal	Poruba M.	u. Ostrava	Namurian A E2	832
13	Karviná (Lazy)	436	coal	Poruba M.	u. Ostrava	Namurian A E2	866
14	Karviná (Lazy)	432	laminit	Poruba M.	u. Ostrava	Namurian A E2	862
15	Karviná (Lazy)	424	coal	Poruba M.	u. Ostrava	Namurian A E2	951
16	Karviná (Lazy)	420	ss-si	Poruba M.	u. Ostrava	Namurian A E2	948
17	Karviná (Lazy)	410	laminite	Poruba M.	u. Ostrava	Namurian A E2	1009
18	Karviná (Lazy)	409	coal	Poruba M.	u. Ostrava	Namurian A E2	1060
19	Karviná (Lazy)		volc, ss	Jaklovec M.	u. Ostrava	Namurian A E2	1142
20	Karviná (Lazy)	386	ss	Jaklovec M.	u. Ostrava	Namurian A E2	1152
21	Paskov	112	coal	l. Hrušov M.	l. Ostrava	Namurian A E1	550
22	Paskov	112	coal	l. Hrušov M.	l. Ostrava	Namurian A E1	599
23	Paskov	84	coal	Petřkovice M.	l. Ostrava	Namurian A E1	855
24	Paskov	82	coal	Petřkovice M	l. Ostrava	Namurian A E1	840
25	Paskov	82	coal	Petřkovice M	l. Ostrava	Namurian A E1	815
26	Paskov	80	coal	Petřkovice M	l. Ostrava	Namurian A E1	800
27	Paskov	76	coal	Petřkovice M	l. Ostrava	Namurian A E1	749
28	Paskov	63	coal	Petřkovice M	l. Ostrava	Namurian A E1	707
29	Paskov	63	coal	Petřkovice M	l. Ostrava	Namurian A E1	600
30	Paskov	41	coal	Petřkovice M	l. Ostrava	Namurian A E1	505

ss= sandstone; si= siltstone; volc= volcanics

4.5. Methods and experimental procedures

4.5.1. Proximate analysis

Proximate analyses of coal samples according to DIN 51700 comprised of the determination of “as received” (hygroscopic) moisture content, ash yield and volatile matter yield. All analyses were performed in triplicate on powdered sub-samples (1 g, grain size <0.2 mm).

4.5.2. Determination of equilibrium moisture content

The equilibrium moisture content was determined according to the ASTM 1412 standard method in an atmosphere of 97% relative humidity (saturated K₂SO₄ solution at 30°C). All measurements were performed in triplicate on coal samples from ČSM and Paskov mines.

4.5.3. Coal petrography

Petrographic analyses were performed following recommendations by the International Committee for Coal and Organic Petrology (ICCP) (Taylor et al., 1997). For petrographic analyses polished particulate mounts were prepared from representative subsamples. Optical petrographic characterization comprised maceral group analysis on a H-Pl-Pol microscope (Zeiss, Germany) by point counting (500 counts) and determination of vitrinite reflectance on an Axioplan microscope (Zeiss, Germany) using DISKUS Fossil software (Hilgers, Germany) in random mode (100 measurements).

4.5.4. TOC analysis

The total organic carbon (TOC) contents were determined in triplicate measurements on a multiphase carbon analyzer RC-412 (LECO, USA) using 50 mg of powdered samples (grain size <0.2 mm).

4.5.5. High-pressure sorption experiments

4.5.5.1. Experimental set-up

Methane and carbon dioxide excess sorption isotherms were determined using the manometric method described by Krooss et al. (2002), Busch et al. (2004), Siemons and Busch (2007) and Gensterblum et al. (2009, 2010). The experimental set-up consists of a stainless-steel sample cell (~14 cm³ for CH₄, ~8.5 cm³ for CO₂), a set of actuator-driven valves, and a pressure transducer (max. pressure 17 MPa for CH₄ and 25 MPa for CO₂), with a precision of 0.05% of the full-scale value. The volume of the reference cell and the void volume in the sample cell were determined by helium (He) expansion in a calibration run. The stainless-steel sample cell is equipped with a 2-μm filter to prevent coal or mineral particles from entering the valves. The entire experimental device is placed in a temperature-controlled oven to ensure constant temperature (±0.1°C) throughout the experiments. Helium density of samples was calculated from sample mass and void volume (determined by helium expansion) for each measurement / isotherm.

The procedure of sorption measurements on moisture-equilibrated coal was as follows:

- Moisture equilibration
- Transfer of moist samples to sample cell and weight measurement
- Transfer of sample cell to the sorption apparatus

- Leak test (100 bar helium for ca. 2 h until temperature, pressure equilibration)
- Evacuation (10^{-3} Pa, 15 minutes)
- Void volume measurement (helium, stepwise pressure increase until 100 bar)
- Evacuation (10^{-3} Pa, 15 minutes)
- Sorption measurement (CH_4 or CO_2)

4.5.5.2. Determination of multiple isotherms

In order to avoid moisture loss from previously moisture-equilibrated samples during depressurization and evacuation between successive sorption experiments, multiple isotherms were recorded in a single run by varying the system temperature during each pressure step. A defined quantity of gas was charged into the system through the reference cell at 45°C . After pressure equilibration, the temperature was raised to 55°C and 65°C . At each temperature the system was equilibrated for two hours and the pressures recorded. Finally, the temperature was set back to 45°C and the resulting equilibrium pressure was compared with the initial equilibrium pressure at 45°C to check for consistency and absence of leaks. This procedure was repeated at all pressure steps. Based on the known quantities of gas introduced into the system at each pressure step, the equilibrium pressures at each temperature and the equations of state of the gases the excess sorption isotherms were calculated for the three temperatures.

4.5.5.3. Parameterization of experimental sorption isotherms

The experimental methane sorption isotherms were fitted by the Langmuir function:

$$n_{ads} = n_L \cdot \frac{p}{P_L + p} \quad (1)$$

The Langmuir function is based on the implicit assumption that the adsorbed phase has a negligible volume i.e. that its density is much higher than the density of the free gas phase. This assumption is not valid any longer for CO_2 at high pressures. Therefore the density of the adsorbed phase is explicitly taken into account in the extended formulation of the Langmuir sorption capacity function for CO_2 :

$$n_{ads} = n_L \cdot \frac{p}{P_L + p} \cdot \left(1 - \frac{\rho_{free}}{\rho_{adsorbed}} \right) \quad (2)$$

Here Here the density of the adsorbed phase ($\rho_{adsorbed}$) represents an adjustable parameter, in addition to the Langmuir parameters n_L and P_L .

The equations of state (EOS) for CO_2 and CH_4 by Span and Wagner (1996) and Setzman and Wagner (1991), respectively, were used in the evaluation of the manometric sorption experiments. Helium densities used for the assessment of the void volume of the measuring cell were calculated by a van der Waals equation of state after Michels and Wouters (1941).

The total experimental error for adsorption measurements is less than 10% n_{ads} for carbon dioxide isotherms and less than 3% n_{ads} for methane isotherms at the final experimental pressure. Further information on the accuracy of the manometric sorption setup used for this

study, as well as a thorough evaluation of possible experimental errors and pitfalls has been published recently by Li et al. (2010) and Gensterblum et al. (2009, 2010).

4.6. Results

4.6.1. Coal Petrography

Results of the maceral group analysis and random vitrinite reflectance measurements are listed in *Appendix III, Table 1*. The maceral group composition is reported on a mineral matter free (mmf) basis.

4.6.2. Maceral composition

Coals from all three locations are dominated by vitrinite (*Fig. 4.3*). Coals from Paskov mine have vitrinite contents from 78 to 92%, whereas inertinite varies between 8% and 22% and liptinite is generally less abundant (<2.5%) or absent. The limnic coals from the ČSM mine have a higher abundance of liptinite group macerals (1-11%), dominated by sporinite. Vitrinite contents range from 52% to 84%, i.e. lower than those of the paralic Paskov coals, and inertinite contents vary between 5% and 39%. The maceral composition of coals from Lazy mine have a higher variability, with vitrinite ranging from 49 to 98%, inertinite between 2 and 51% and liptinite up to 23%.

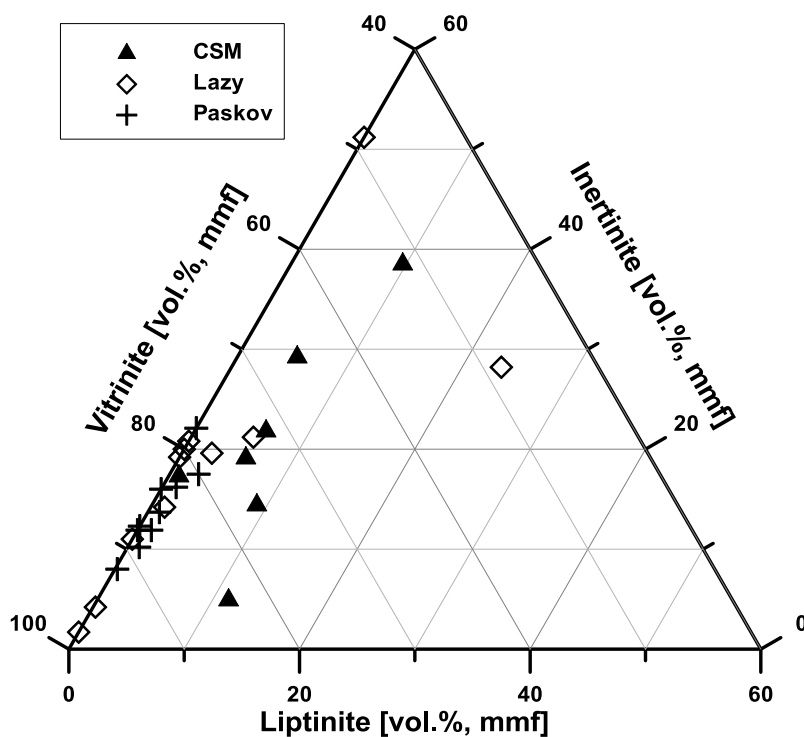
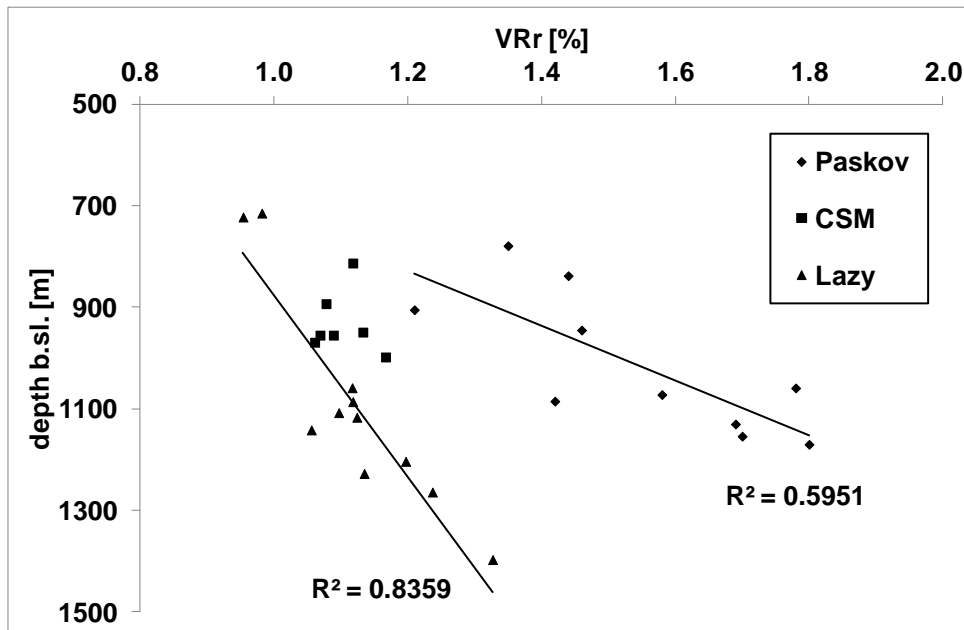


Fig. 4.3 Maceral group composition of the coals from the three sampling locations.

4.6.3. Vitrinite Reflectance

Vitrinite reflectance (VRr) values of coal samples used in this study range from 1.0 to 1.8%. Coals from Paskov mine cover a range from medium volatile to low volatile bituminous

rank, whereas coal samples from ČSM mine are of medium volatile bituminous rank (VRr 1.1 – 1.2%) and coals from Lazy mine are of high volatile bituminous A and medium volatile bituminous rank. Vitrinite reflectance values increase with depth. This rank vs. depth trend is steeper for coals from Paskov mine (0.18% VRr / 100 m) than for coals from Lazy mine (0.05% VRr / 100 m) (Fig. 4.4).



4.6.7. Volatile matter yield

The volatile matter (VM) yield has been used predominantly to classify coal rank in the Czech part of the Upper Silesian Basin. Due to the lack of vitrinite reflectance data for most of the coal deposits in the OKC, it is the main parameter for thermal maturity ranking of these coals. However, low-rank coals with volatile matter yields in excess of 31 wt.% (daf) are difficult to classify by this parameter (van Krevelen, 1993). It is also known that maceral composition as well as amount and type of mineral matter, especially carbonates and clay minerals, can affect the volatile matter yield, thus compromising the applicability of VM for rank classification (Alpern et al., 2002). Therefore, in this study VM yields were not determined for samples with ash yields higher than 80 wt.% and samples with ash yields significantly higher than 10 wt.% were not used for correlation of volatile matter with other maturity parameters (VRr, T_{max}).

For coals from the ČSM mine the volatile matter yield ranged from 23 to 26 wt.%, indicating medium volatile bituminous rank. Coal samples from Paskov mine show a larger variation in VM, ranging from 16 to 28 wt.%, corresponding to a range from medium volatile bituminous to low volatile bituminous rank. Coal samples from the Lazy mine wells cover the largest maturity range with VM yields between 22 and 35 wt.%. The highest volatile matter yield of 35 wt.% was found for a coal from the Prokop seam, which also had the highest liptinite (sporinite) content of 23%. However, the correlation between liptinite content and volatile matter yield is very weak ($r^2=0.3$).

4.6.8. Total Organic Carbon (TOC)

The amount of total organic carbon (TOC) measured for all coal samples ranged between 70% and 85%.

The amount of total inorganic carbon (TIC) ranged between 0.3% and 3.8%. TOC values are given in *Appendix III, Table 1*.

4.6.9. High-pressure gas sorption

Results of the methane and carbon dioxide sorption tests as well as sample densities calculated from sample mass and void volume (helium expansion) for each measurement are summarized in *Appendix III Tables 3 through 9*. All measured isotherms as well as all measured isotherm data are listed in *Appendix III*.

Variations in calculated density for the same sample were observed and are attributed to changes in sample volume and / or weight during sample handling (evacuation). While additional water (adsorbed or in pore space) would cause a decrease in the overall sample density, we observe slightly higher densities for moist coals. While errors in sample weight are very unlikely, one explanation could be that coal samples lost water during sample transfer or during evacuation after the leak test. Because sample weight was only determined before the leak test, the density would be overestimated if water was lost during evacuation and thus the 'real' sample mass would have been lower.

If water was lost during evacuation, this would also mean that the observed effect of moisture on sorption is underestimated.

Another factor could be alteration effects such as oxidation of coal samples during storage between the different measurements, which could cause an increase in ash yield

(Mastalerz et al., 2009). However, this would be more likely for low-rank coal and the amount of oxygen uptake required explaining the higher density would be very high.

4.6.9.1. Methane sorption isotherms

To allow for good comparison of sorption isotherms on different coal samples, all sorption measurements were carried out at 45°C. Since sorption capacity decreases with increasing temperature, sorption capacities determined at 45°C represent minimum capacities for the coal samples analyzed in this study.

Methane excess sorption isotherms were determined on all samples in the “as-received” state. Furthermore, sorption isotherms were determined at 20°C on three “as-received” samples from the Paskov mine and at 55°C and 65°C on one moisture-equilibrated coal from Lazy mine. Results of the methane sorption tests are summarized in Appendix II, Tables 4 through 10. Apart from the measured maximum value of excess sorption (n_{\max}) isotherms, these Tables list the Langmuir pressures (P_L) and the maximum sorption capacities (n_L), obtained from a least-squares fit of the Langmuir function to the experimental results. All parameters are reported on the “raw” and “dry, ash-free” basis.

Results from sorption isotherms measured at different temperatures were used to construct isosteres (plots of $\ln(P)$ vs. reciprocal temperature $1/T$) for measured constant sorbate loadings (n_m) between 0.15 - 0.3 mmol/g. From the slope of each of these isosteres, the isosteric heat of adsorption (q_{st}) was calculated using the Clausius Clapeyron equation (Sircar, 1985; Shen and Bülow, 2000):

$$q_{st} = -R[d\ln P/(1/T)]n_m \quad [\text{kJ/mol}] \quad (3)$$

It should be noted that this approach is strictly only valid for an ideal gas. Since the isosteres used for the calculation are derived from isotherms measured at pressures between 1 and 6 MPa, calculated heats of adsorption should be viewed with caution and were only used to confirm that the observed process was physisorption rather than chemisorption.

To evaluate the effect of moisture content on gas sorption, isotherms for all Paskov and ČSM samples, as well as for one sample from the Lazy mine, were also measured in the moisture equilibrated state according to ASTM 1412. Plots of methane sorption isotherms measured on “as-received” and moisture-equilibrated coal at 45°C are given in *Fig. 4.5* and *Appendix III Fig. 1*. For two of the Paskov samples isotherms were also measured after drying them in the sample cell (evacuation and heating to 105°C for approximately 1.5 h). After the end of the measurements it was found that the samples still had moisture contents of 0.2 – 0.8%.

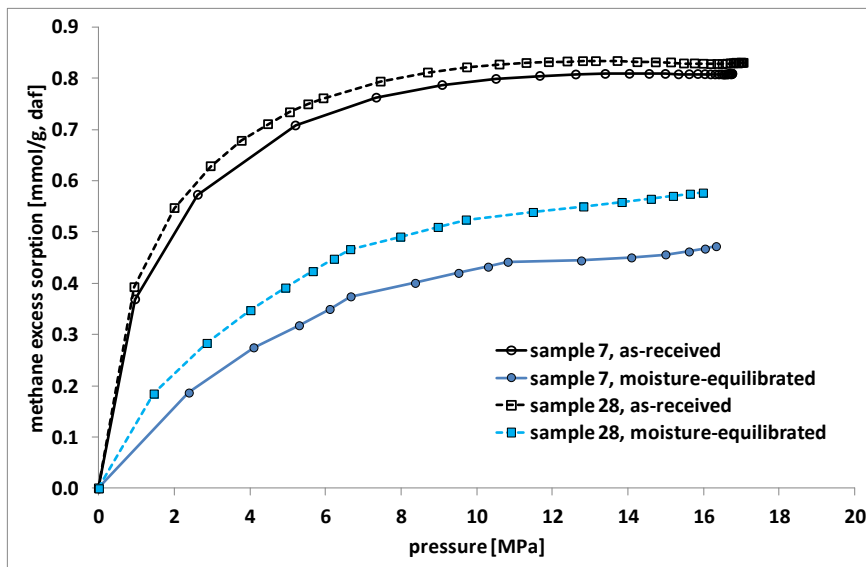


Fig. 4.5 Methane sorption isotherms for “as-received” (open symbols) and moisture-equilibrated (solid symbols) coal from Paskov mine (squares) and ČSM mine (circles).

Maximum methane excess sorption capacities measured on “as-received” coal at 45°C range from 0.49 to 0.99 mmol/g of dry ash-free coal. The calculated Langmuir sorption capacities (n_L) range from 0.57 to 1.1 mmol/g, daf. Moisture-equilibration causes a significant reduction of excess sorption capacity ranging from 0.30 to 0.78 mmol/g, daf. The corresponding Langmuir sorption capacities range from 0.40 to 1.08 mmol/g, daf, which corresponds to a reduction in sorption capacity between 4 and 47% (average 24%).

Isotherms measured at 20°C show maximum excess sorption and sorption capacities very similar to the 45°C isotherms. However, the excess sorption in the low- to intermediate-pressure region (<10MPa) is significantly higher at 20°C. In the high-pressure region above ~12MPa, methane sorption isotherms measured at 20°C converge with isotherms measured at 45°C for two of the three compared coals (Fig. 4.6). On a dry, ash-free basis, a temperature increase of 25°C, from 20°C to 45°C, is accompanied by a decrease in sorption capacity by 7 – 13% at a pressure of 3 MPa. However, in the high-pressure range (15 – 17 MPa) temperature variation does not result in a significant change in maximum excess sorption (<5%).

Maximum excess sorption measured on a moisture-equilibrated coal from the Lazy mine decreased with increasing temperature from 0.44 mmol/g, daf at 45°C to 0.39 mmol/g, daf at 65°C (n_L 0.54 – 0.45 mmol/g, daf).

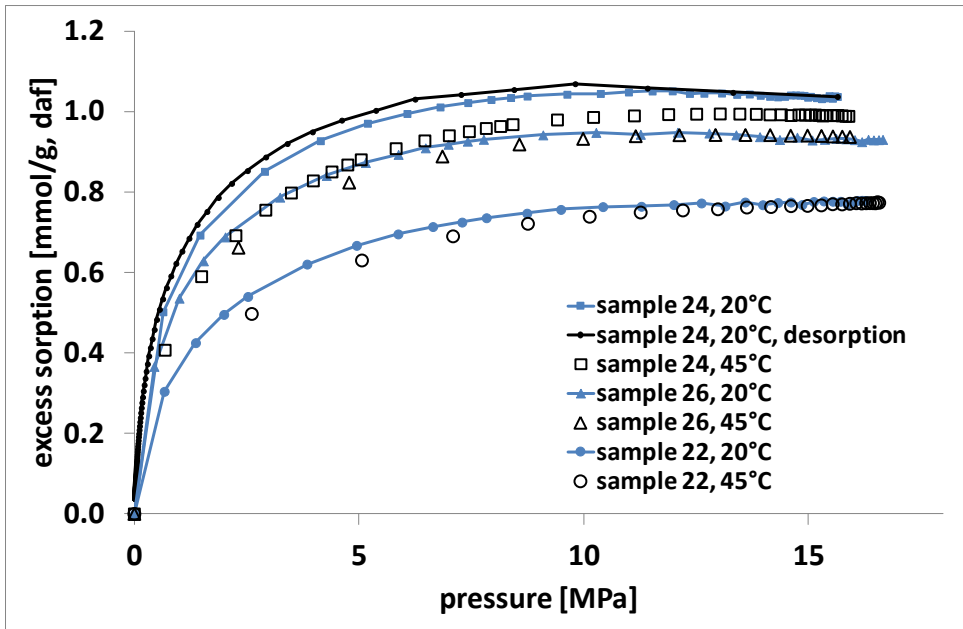


Fig. 4.6 Methane isotherms for three “as received” coals from Paskov mine measured at 20°C and 45°C.

4.6.9.2. Carbon dioxide sorption isotherms

High-pressure carbon dioxide sorption isotherms were measured at 45°C on “as-received” coal samples from the Paskov and ČSM mines, as well as on one sample from Lazy mine. In addition, carbon dioxide sorption measurements were performed after moisture equilibration on four coals from Paskov mine, one coal from ČSM mine and one coal from Lazy mine (Fig. 4.7, Appendix III Fig. 2). Analogue to methane sorption experiments, additional sorption measurements were performed at 20°C and on one sample at 55°C and 65°C. To avoid condensation of carbon dioxide in the sorption apparatus, CO₂ sorption measurements at 20°C were only performed up to 5.5 MPa. All measured CO₂ isotherms were approximated by the excess sorption function given in equation (3). Maximum excess sorption as well as the three parameters n_L , P_L and ρ_{adsorbed} , adjusted by a least-squares optimization procedure, for the individual isotherms are listed in Appendix III Tables 4 through 8.

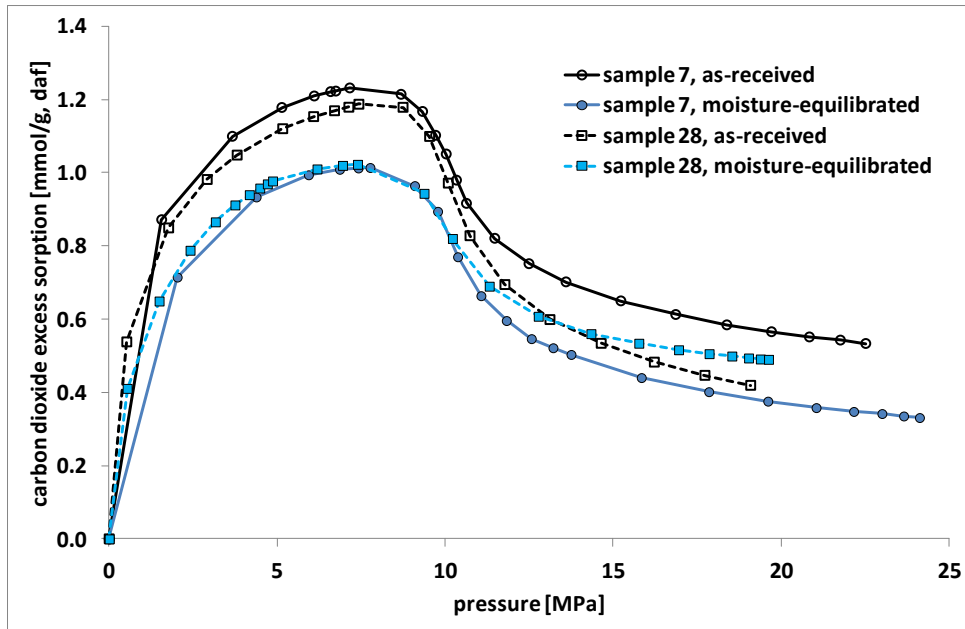


Fig. 4.7 CO₂ sorption isotherms for “as-received” (open symbols) and moisture-equilibrated (solid symbols) coal from Paskov mine (squares) and ČSM mine (circles).

All high-pressure CO₂ excess sorption isotherms measured at 45°C exhibit a maximum in the 6 to 10 MPa pressure range, followed by a continuous decline. This maximum is due to the steep increase in the specific density of supercritical CO₂ in this pressure range (cf. Gensterblum et al., 2009, Bae and Bhatia, 2006).

Maximum excess sorption (n_{\max}) values measured on “as-received” coals range from 0.96 to 1.41 mmol/g, daf. CO₂ sorption capacities (n_L) obtained from approximation of the experimental data range from 1.38 to 2.42 mmol/g, daf.

CO₂ sorption on moisture-equilibrated coals is generally lower as compared to “as-received” samples. Maximum CO₂ excess sorption values measured on moisture equilibrated coals range from 0.80 to 1.16 mmol/g, daf, which represents a reduction between 14 and 28% (average 18%) relative to “as-received” samples. CO₂ sorption capacities, derived from approximation of experimental data using equation (3), range from 1.53 to 1.96 mmol/g, daf, corresponding to a reduction between 2 and 31% (average 12%) relative to “as-received” samples.

Parameterisation of experimental data using equation (3) yields approximate values for the density of the sorbed phase. Alternatively, the density of sorbed CO₂ can be estimated by plotting the measured excess sorption data versus the density of the gas CO₂ phase. Extrapolation of the linear part of this plot in the high density (high pressure) region to the x-intercept yields the sorbed phase density (Sudibandriyo et al., 2003; Gensterblum et al., 2009). At this (extrapolated) intercept the free (supercritical) CO₂ phase and the sorbed phase have the same density so that they cannot be distinguished any more. In consequence, the excess sorption at this pressure is zero. Estimations of the sorbed phase density by both methods were compared and show good agreement (*Appendix III Table 4 – 8*). The estimated sorbed phase density differs among the analyzed samples and ranges from 940 g/cm³ to 1490 g/cm³. Comparison of CO₂ sorbed phase densities with ash yield of coal samples seems to indicate that CO₂ is more densely sorbed on organic surfaces as compared to inorganic surfaces, *e.g.* of clay minerals (*Fig. 4.8*). This is in agreement with results from CO₂ sorption experiments on shales and clay minerals performed in our laboratory. However, additional research is needed to

investigate whether the sorbed phase density is similar to the density of liquid CO₂ at the boiling point or if and how it is controlled by the adsorbent composition.

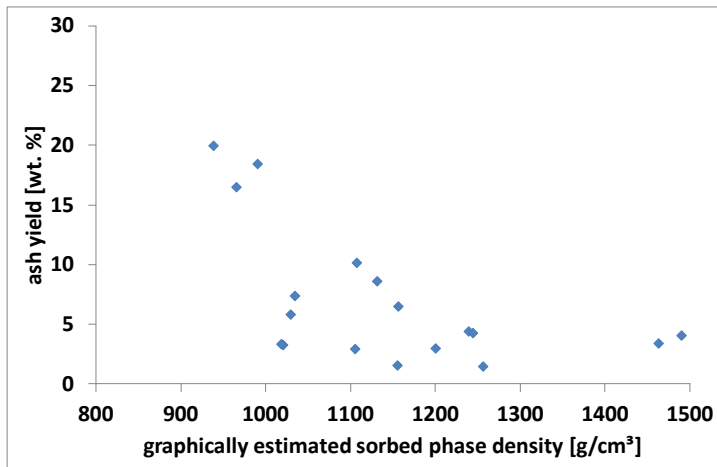


Fig. 4.8 Relationship between the estimated density of the adsorbed CO₂ phase and ash yield of coal samples.

Maximum excess sorption values measured at 20°C range from 1.07 to 1.36 mmol/g, daf. Sorption capacities derived from approximation of experimental data by the Langmuir function range from 1.99 to 2.48 mmol/g, daf. These isotherms exhibit a maximum in the 2 to 4 MPa pressure region, exceeding those of the 45°C isotherms. At higher pressures between 4 and 5 MPa the 20°C isotherms decrease until they cross the 45°C isotherms. A 25°C temperature increase results in a decrease of sorption capacity between 27 and 59% at a pressure of 3 MPa, whereas the maximum measured excess sorption is only reduced by up to 8%, which might indicate inaccuracies of the parameterization of experimental data by the extended Langmuir function.

4.7. Discussion

4.7.1. Correlations between maturity parameters

For the entire set of coal samples, the volatile matter yield shows good correlation with other maturity parameters, such as vitrinite reflectance or T_{\max} (Fig. 4.9). These correlations may thus be used to relate archived data of volatile matter yields of coals from the study area to vitrinite reflectance. The best correlations are observed for coal samples from the Paskov mine which cover a maturity range from 1.0 – 1.8 % VRr. This is in good agreement with previous results for Upper Silesian Basin coals (Kotarba et al., 2002; Martinec, 2005).

Because T_{\max} is influenced by the petrographic composition of coal (Teichmüller and Durand, 1983) and volatile matter yield is a valid rank parameter only in the mvb to semi-anthracite range (1.2 – 2.5% VRr; cf. Teichmüller and Teichmüller, 1979), we chose to use vitrinite reflectance as the parameter for rank correlation of sorption characteristics.

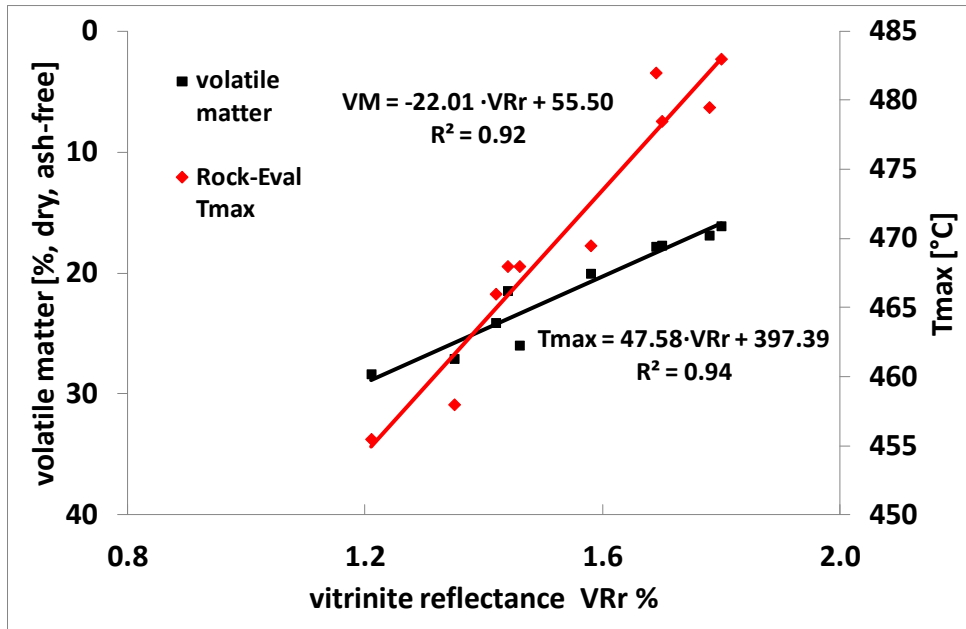


Fig. 4.9 Relationship between vitrinite reflectance (VRr%) volatile matter yield and the Rock-Eval T_{max} value for coal samples from Paskov mine.

4.7.2. Influence of coal properties and reservoir parameter on sorption capacity

The in-situ sorption capacity of coal seams is not only influenced by pressure and temperature, but also in-situ moisture content and inherent coal properties such as mineral matter content, coal rank and maceral composition. However, these parameters affect the sorption capacity to different degrees. Knowledge of the influence of each parameter is necessary to evaluate the distribution of sorption capacity of individual coal seams throughout a basin. Previous studies *e.g.* by Hildenbrand et al. (2006) have derived algorithms to evaluate the sorption capacity distribution in a certain coal basin, based upon literature data from different basins (Ruhr Basin, Campine Basin) and different sample types (lithotypes, sapropel, humic coals). In the present study the sorption capacity distribution is derived based upon experimental data for coal seams of the same basin.

4.7.3. Influence of moisture content on sorption capacity

The presence of moisture reduces the sorptive gas storage capacity of coals. In low-pressure sorption experiments on dry and moisture-equilibrated coal Ettinger et al. (1958) observed a linear decrease of sorption capacity with increasing moisture content which he described by the empirical formula:

$$V_d/V_w = C_0 \cdot m + 1 \quad (4)$$

Where V_d and V_w are the methane sorption capacity of dry and moist coal, m is the moisture content in wt. % and C_0 is a pressure-dependent constant for which Ettinger et al. (1958) found a value of 0.31 (ca. 1 bar) and later Joubert et al. found values between 0.27 (10 bar) and 0.19 (60 bar) (Joubert et al., 1973, 1974 and references therein). The negative effect of moisture on gas sorption has been studied in several subsequent studies (Smith and Williams, 1987, Yee et al., 1993; Levy et al., 1997; Bustin and Clarkson, 1998; Clarkson and Bustin, 2000;

Crosdale et al., 2008; Day et al., 2008a,b; Ozdemir and Schroeder, 2009). Beyond a critical moisture content, no further reduction in sorption capacity occurs (Joubert et al., 1973, 1974; Gaschnitz, 2001; Day et al., 2008a). Day et al. (2008a) report that this critical moisture content is slightly higher for CO₂ sorption as compared to CH₄ and that it is equivalent to equilibrium moisture achieved between 40 and 80% relative humidity.

Results from sorption isotherm measurements in this study on “as-received” and moisture-equilibrated coals show an average reduction of CH₄ sorption capacity of 23% for ČSM samples and 27% for Paskov samples, which is similar to observations reported in previous studies. For example Krooss et al. (2002) observed a reduction of 20 - 25% between dry and moisture-equilibrated Carboniferous coal from Netherlands. The sensitivity of sorption capacity to moisture decreases with increasing rank, as reported by Kim (1977) for US coals.

Experimental results from the present study indicate a higher degree of reduction of CH₄ (average 24%) sorption capacity as compared to CO₂ (average 12%), which is in agreement with results by Day et al. (2008a). These observations can be interpreted as a result of the competition between water and gas molecules for specific sorption sites, which also influences the selectivity between CO₂ and CH₄ sorption (Bustin and Clarkson, 1998; Clarkson and Bustin, 2000; Busch and Gensterblum, 2011).

To evaluate the effect of moisture on sorption, we compare the methane sorption capacity at different moisture states m (m = moisture of “as-received” or partially dried coal) relative to the moisture equilibrated state em . Taking the equilibrium moisture as reference state, the distance d of the “as-received” or partially dried moisture to the equilibrium moisture is defined as:

$$d = m/em. \tag{5}$$

For d a value of 1 represents equilibrium moisture and 0 represents dry samples. Correlations between Langmuir sorption capacity and distance from moisture equilibrium were calculated for individual samples for two different moisture states and for three samples additionally for the partially dried or dry state.

From the slope of the observed correlation for these three samples we derive the following linear equation:

$$n_{CH_4} = -0.19 \cdot d + 0.86 \tag{6}$$

For all coal samples an average correlation is derived:

$$n_{CH_4} = -0.43 \cdot d + 1.13 \tag{7}$$

However, this average correlation shows a strong variation between -0.1 and -1.5 with a standard deviation of 0.3. The y-axis intercept represents the average CH₄ sorption capacity of dry coal. This estimated sorption capacity of dry coal increases with increasing coal rank.

4.7.4. Effect of temperature on sorption capacity

Adsorption of gas molecules results in entropy reduction and thus it is an invariably exothermic process. Consequently, a negative correlation between sorption capacity of coals and temperature exists, which has been reported in previous studies for a wide temperature range (Ruppel et al., 1974; Yee et al., 1993; Levy et al., 1997; Bustin and Clarkson, 1998; Gaschnitz, 2001; Krooss et al., 2002). From CH₄ sorption experiments on moisture-equilibrated

coal Levy et al. (1997) calculated a linear reduction of sorption capacity (at 5 MPa) between 10°C and 70°C of 0.12 cm³/g per 1K temperature increase. Other studies report that sorption capacity decreases more slowly at temperatures above 30 to 60°C (Ruppel et al., 1974; Krooss et al., 2002; Crosdale et al., 2008). These authors also observed a decreasing influence of temperature in the high pressure region (above ca. 10 MPa).

Isotherms measured in this study show the expected reduction of excess sorption with higher temperature. Methane Langmuir sorption capacities for the moisture-equilibrated sample 8 decrease linearly with increasing temperature (Fig. 4.10). A 1K increase in temperature reduces the sorption capacity by 0.11 cm³/g, which is similar to the reduction calculated by Levy et al. (1997). Isothermic heats of adsorption calculated from this set of isotherms range from 10 to 21 kJ/mol and show a linear increase with increasing adsorbate loading (Fig. 4.11). At low loading, the values lie within the range of 1 – 1.5 times the heat of evaporation (8.2 kJ/mol for methane), corresponding to the range of physisorption (Ruthven, 2008). For comparison, Day et al. (2008a) report net heats of adsorption between 8 and 12 kJ/mol for methane on moist coal from Australia, showing a decrease with increasing moisture content from 0 to 7 wt.%.

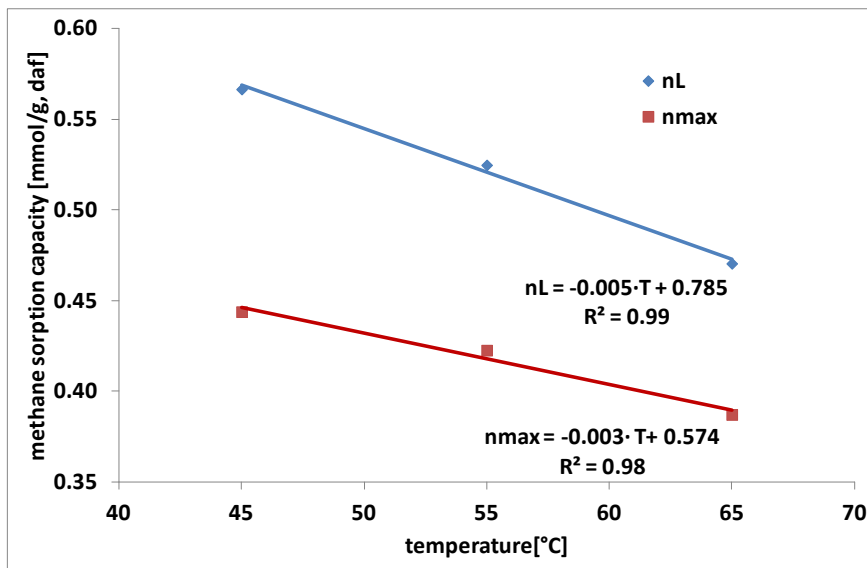


Fig. 4.10 Relationship between methane sorption capacity and experimental temperature for moisture equilibrated coal sample 8. n_{max} = maximum excess sorption, n_L = Langmuir sorption capacity.

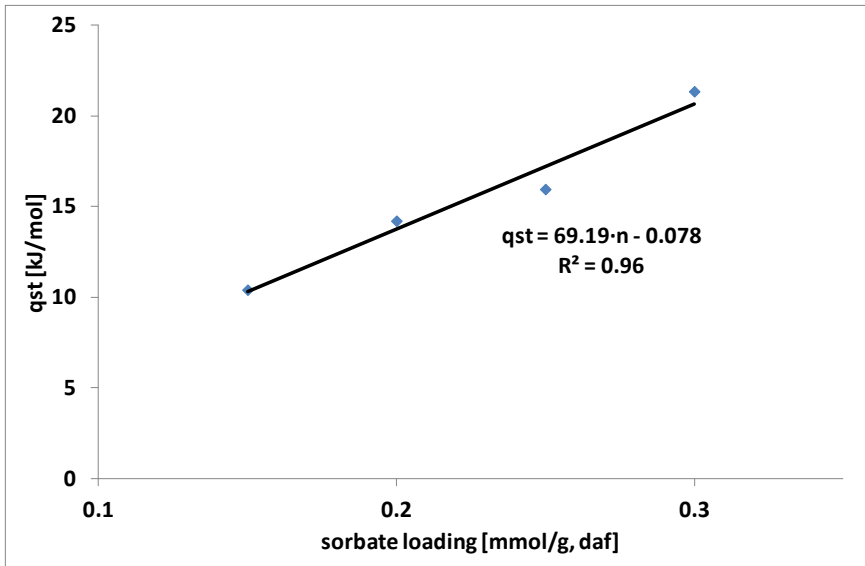


Fig. 4.11 Isosteric heat of adsorption for different sorbate loadings determined from methane isotherms measured on moisture-equilibrated sample 8.

For some methane sorption isotherms measured on “as-received” coal at 20°C and 45°C a temperature dependence is no longer observed at higher pressures (between 10 MPa and 12 MPa). Similar observations were reported by Krooss et al. (2002) for isotherms measured on moisture-equilibrated coal at 40°C and 60°C.

At 20°C CO₂ is in the subcritical state and isotherms were only measured up to a pressure of 5 MPa to avoid condensation. Comparison of the 20°C and the 45°C isotherms is difficult because for the 45°C isotherm only a few data points were recorded below 5 MPa. The 20°C excess sorption isotherms initially lie above the 45°C isotherms, but the difference decreases with increasing pressure and a cross-over occurs between 4 MPa and 5 MPa as the 20°C excess isotherms decline due to the onset of condensation (Fig. 4.12).

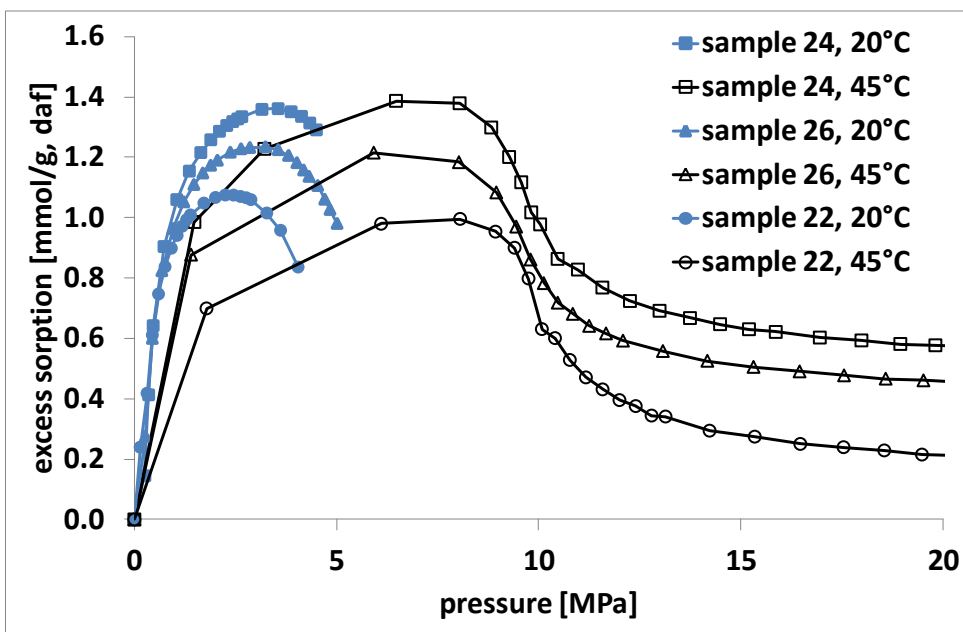


Fig. 4.12 CO₂ isotherms for “as received” coals from the Paskov mine measured at 20°C (open symbols) and 45°C (solid symbols).

Comparison of CO₂ sorption isotherms measured at 45°C and 55°C on the moisture-equilibrated sample 8 shows that in the pressure region below 8 MPa, the 45°C isotherm has higher excess sorption capacities, while at higher pressures (>8.5 MPa) the excess sorption values of the 55°C isotherm are higher. Such behaviour has also been reported by Krooss et al. (2002), but the pressure at which the crossover occurs seems to vary from sample to sample. The decline of CO₂ isotherms results from the steep increase of CO₂ gas density in the pressure region close to the critical point (8-10 MPa). At higher temperatures this density increase is less dramatic and the decline in excess sorption decreases. Thus, for carbon dioxide, the influence of temperature on gas density is larger than the direct influence on the adsorption process.

4.7.5. Effect of thermal maturity

In previous studies, no global correlation was found between coal rank and methane sorption (Bustin and Clarkson, 1998). However, for moisture-equilibrated coal from individual coal basins, methane sorption showed a linear increase of sorption capacity with increasing coal rank (Joubert et al., 1973, 1974; Kim, 1977, Ryan, 1992, Laxminarayana and Crosdale, 2002; Reeves et al., 2005; Chalmers and Bustin, 2007). This relationship could allegedly be applied to estimate the coal-bed methane potential in the US and Canada (Kim, 1977; Ryan, 1992). For methane sorption (Levy et al., 1997 (5 MPa, 30°C); Laxminarayana and Crosdale, 1999 (9 MPa, 23.5°C); Laxminarayana and Crosdale, 2002 (9 MPa, 23.5°C); Faiz et al., 2007 (5 MPa, 27°C)) and low-pressure (<0.13 MPa to 4 MPa; 0°C to 22°C) CO₂ sorption (Levy et al., 1997; Bustin and Clarkson, 1998; Prinz and Littke, 2005; Ozdemir and Schroeder, 2009) on “as received” and dry coals, a ‘U’-shaped or polynomial correlation between coal rank and sorption capacity has been reported, which exhibits a minimum similar to the correlation between moisture and sorption. For high pressure CO₂ sorption on the other hand, no or only weak correlation with coal rank was found (Krooss et al., 2002; Mastalerz et al., 2004; Reeves et al., 2005; Day et al., 2008a). Structural changes during coalification or plugging of pores by low-boiling hydrocarbons, generated during coalification are believed to cause this ‘U-shaped’ correlation (Levine, 1993; Prinz and Littke, 2005; Chalmers and Bustin, 2007).

A decrease of Langmuir pressure with increasing coal rank has also been reported and was attributed to the homogenization of the pore space during coalification (Laxminarayana and Crosdale (1999).

Methane sorption capacities measured on coal samples in the present study show a general increase with increasing coal rank (*Fig. 4.13*). For medium- to low-volatile bituminous coal from the Paskov mine, a similar correlation is observed for CH₄ and CO₂ sorption on “as-received” coal, as well as for CH₄ sorption on moist coal. CO₂ sorption capacity on moisture-equilibrated coal shows a steeper increase with coal rank and a much better correlation (*Fig. 4.14*). However, this correlation is only based on four measurements and thus has to be viewed with caution. Apart from the general correlation between sorption capacity and maturity, the influence of moisture content on sorption capacity, as well as the molar ratio of CO₂ and CH₄ sorption capacity, shows a dependence coal rank.

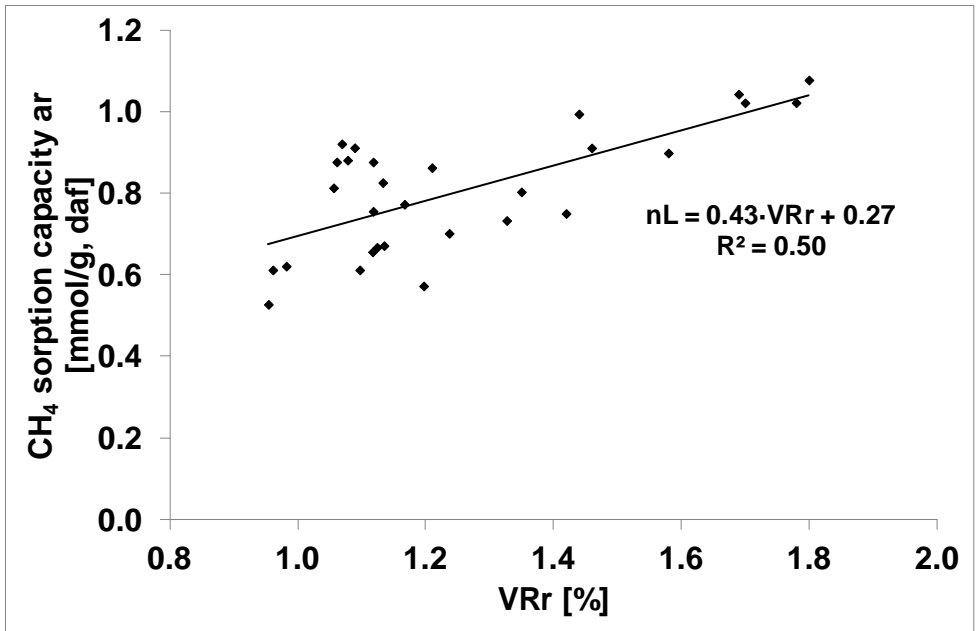


Fig. 4.13 Relationship between methane sorption capacity and coal rank (“as-received”, 45°C).

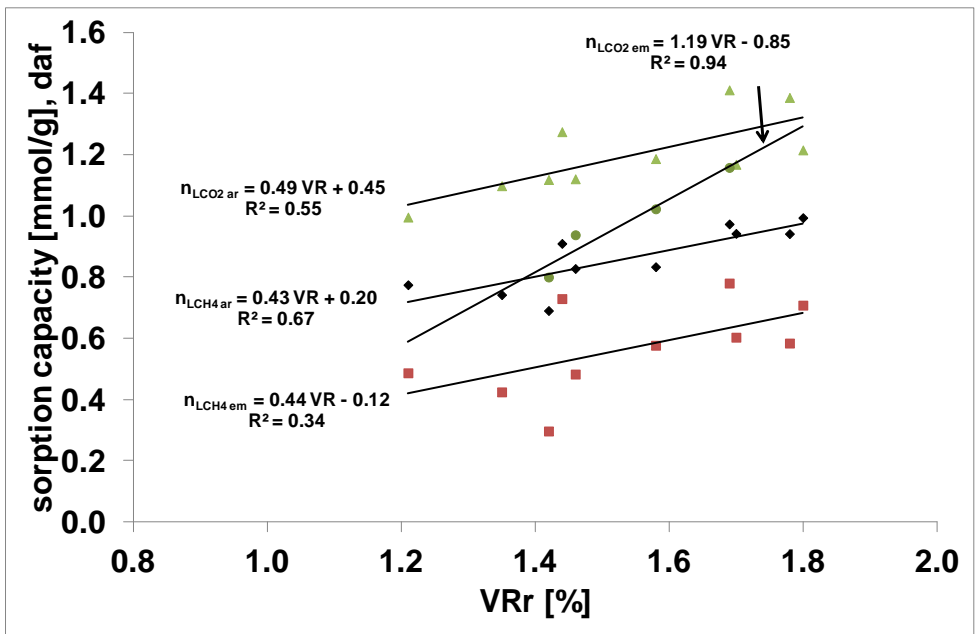


Fig. 4.14 Relationship between rank and sorption capacities measured for CH₄ and CO₂ on “as received” and moisture equilibrated coal from Paskov mine.

4.7.6. Effect of mineral matter content (ash yield)

Coal samples from the Lazy mine exploration well exhibit the largest variation in ash yield. On a ‘raw’ basis, these samples show a linear decrease in sorption capacity with increasing ash yield and decreasing TOC content (Fig. 4.15). A 1% increase in ash yield decreases the sorption capacity by 0.16 cm³/g. The observed trend is in agreement with results from previous studies reporting a linear decrease in methane sorption capacity with increasing mineral matter content (ash yield) (Barker-Read and Radchenko, 1989; Laxminarayana and Crosdale, 1999;

Clarkson and Bustin, 2000; Laxminarayana and Crosdale, 2002; Weniger et al., 2010). No correlation between ash yield and CH₄ or CO₂ sorption is observed for coal samples from Paskov mine and ČSM mine, which are dominantly high-grade coals. These results support that organic matter plays a dominant role in methane sorption in coals and carbonaceous sediments, whereas mineral matter has a diluting effect on methane sorption.

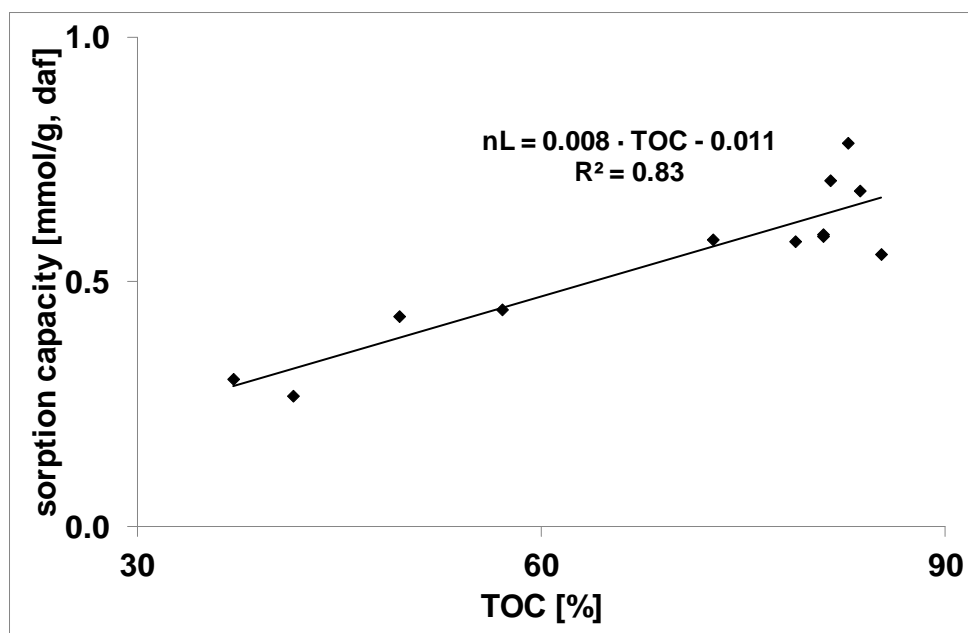


Fig. 4.15 Correlation between methane sorption capacity and TOC content for samples from Lazy cores (“as-received”, 45°C).

4.7.7. Effect of maceral composition

Petrographic composition can influence the sorption capacity of coal, but, no consistent global correlation has been reported. Some studies showed a positive correlation between vitrinite content and sorption capacity, which are attributed to higher microporosity of vitrinite (Lamberson and Bustin, 1993; Bustin and Clarkson, 1998; Laxminarayana and Crosdale, 1999; Clarkson and Bustin, 2000; Chalmers and Bustin, 2007). Other studies did not observe any correlation between sorption capacity and maceral composition (Laxminarayana and Crosdale, 2002; Mastalerz et al., 2004; Faiz et al., 2007; Weniger et al., 2010). Different sorption capacities of inertinite group macerals could explain why no consistent influences of maceral group composition on sorption is observed. For instance Faiz et al. (2007) report that Permian coals from Australia contain more inertinite, which is dominated by semi-fusinite, compared to Carboniferous coals from the northern hemisphere, which are dominated by fusinite. The higher microporosity of semi-fusinite compared to fusinite could explain why negative correlations between inertinite and sorption capacity are mostly reported for coals from the northern hemisphere. Some studies report an influence of liptinite on sorption capacity but no consistent correlation appears to exist (Mastalerz et al., 2004; Chalmers and Bustin, 2007).

Of all samples analyzed in this study, coals from the ČSM mine extend over the smallest maturity range. Therefore they are suitable for studying the dependence of sorption capacity on petrographic composition. No clear correlation between sorption capacity of “as received” or moisture equilibrated coal and maceral composition was observed. Furthermore, the liptinite-rich coal from Prokop seam (sample 8) did not show a higher sorption capacity as compared to coal samples of similar rank. Vitrinite was the dominant maceral in all coals analyzed in this

study, and for this rank range, the influence of maceral composition on sorption capacity seems to be minor.

4.7.8. Comparison of CH₄ and CO₂ sorption – implications for CO₂ enhanced methane recovery (CO₂-ECBM)

The ratio of the Langmuir sorption capacities ($n_{L,CO_2}/n_{L,CH_4}$) derived from the single-component sorption isotherms is consistently >1, reflecting the preferential sorption of CO₂ as compared to CH₄. The degree of preferential sorption of CO₂ is reduced with moisture content. Clarkson and Bustin (2000) used single gas sorption isotherms of methane and carbon dioxide measured on dry and moisture equilibrated coal to model the sorption capacity of CO₂ - CH₄ gas mixtures. They found that the selectivity for carbon dioxide sorption decreases in the presence of moisture and concluded that water competes with gas for sorption sites, especially higher energetic sites that would be occupied by CO₂ molecules in the dry state.

A decrease of the CO₂/CH₄ sorption ratio with increasing pressure has also been observed in previous studies from single gas isotherms (Krooss et al., 2002, Mastalerz et al., 2004, Reeves et al., 2005), whereas Clarkson and Bustin (2000) report increasing carbon dioxide selectivity with increasing pressure. Further, Mastalerz et al. (2004) report a slight increase of CO₂/CH₄ sorption ratio with increasing rank for sub-bituminous coals, whereas Krooss et al. (2002) and Reeves et al. (2005) report a decrease in CO₂/CH₄ ratio with increasing rank.

In the present study, CO₂/CH₄ sorption ratios were found to be lower (1.5 – 2.7) for “as-received” coals, as compared to moisture-equilibrated coals (1.3 – 4.3). For most “as-received” coals the $n_{L,CO_2}/n_{L,CH_4}$ ratio increases with increasing pressure, whereas for moisture-equilibrated coals it decreases. However, for some “as-received” coals this ratio decreased or showed little change with increasing pressure, and for one moisture-equilibrated coal it remained constant with increasing pressure. Sorption measurements on coal samples from the Paskov mine indicate a rank-dependence of the preferential sorption of CO₂, similar to the one observed by Krooss et al. (2002) and Reeves et al. (2005). For moisture-equilibrated coals, the reduction of the CO₂/CH₄ sorption ratio with increasing rank is more significant (Fig. 4.16).

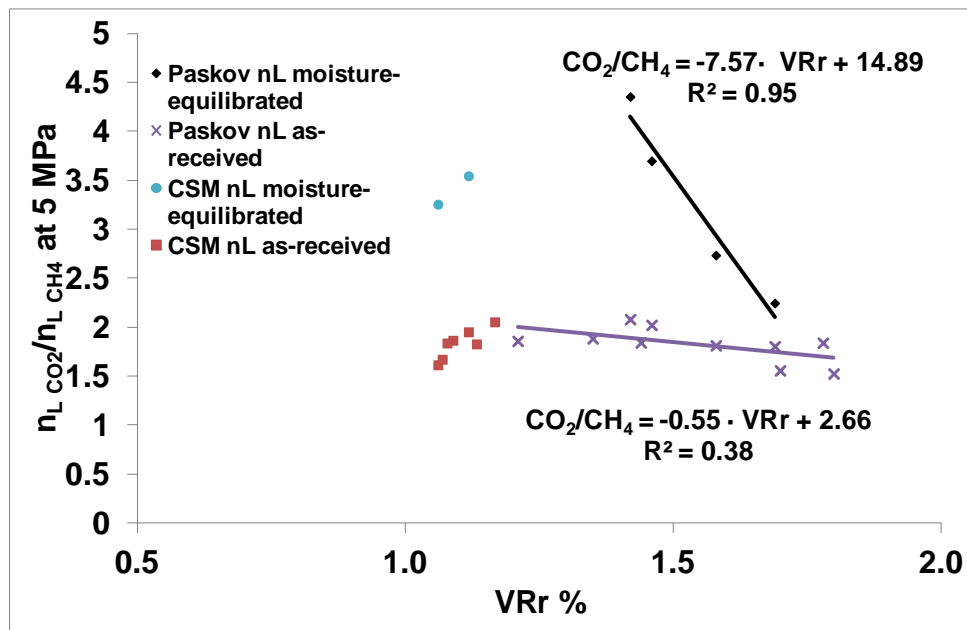


Fig. 4.16 Rank dependence of the preferential sorption capacity between CO₂ and CH₄ at 5MPa.

4.7.9. Calculated variation of sorption capacity with depth

The observed relationships between temperature, pressure and sorption capacity can be used to estimate the sorption capacity of a coal seam at a certain depth, if the local pressure and temperature gradients are known. Vertical movements of coal seams during geological basin history, such as burial and uplift, result in changes of reservoir pressure and temperature conditions, which influence the sorption capacity. During burial, the (hydrostatic) reservoir pressure increases and more gas can be stored in the coal, while the increase in temperature during burial will reduce the sorption capacity. On the other hand, uplift is accompanied by a decrease in reservoir pressure, which reduces the sorption capacity while the concomitant decrease in temperature enhances sorption capacity. The interplay of these opposing effects determines whether gas will be desorbed from coal and migrate, or if coals will gain sorption capacity and either become undersaturated or adsorb available gas, migrated from deeper seams or produced during secondary generation.

Gaschnitz (2001) measured methane sorption isotherms on dry and moist sapropelic coal and a vitrain from the Ruhr Basin in a temperature range from 35 to 150°C up to 20 MPa. He used logarithmic functions to describe the variation of the Langmuir parameters n_L and P_L with increasing temperature and estimated sorption capacities for burial depths down to 6000 m, using different pressure and temperature gradients. Hildenbrand et al. (2006) used results from sorption experiments on coals from the German Ruhr Basin (Denneberg, 1997, Gaschnitz, 2001) and the Belgian Campine Basin (Arets et al., 1962, Coppens 1967), to model the evolution of methane sorption capacity for coal seams. Bustin and Bustin (2008) measured methane isotherms for three U.S. coals of different coal rank at different temperatures. They found that the influence of depth variations (pressure and temperature) on the sorption capacity differs at different rank.

A “static” calculation was used to estimate the sorption capacity of a coal of a given rank as a function of depth in a time-invariant pressure and temperature field. To estimate the sorption capacity of coals from the USCB, the linear relationship between Langmuir sorption capacity and temperature for moisture equilibrated coal was used to recalculate sorption isotherms for pressures and temperatures for a depth interval down to 2000 m (*Fig. 4.17a-f*). Sorption measurements on this coal at different temperatures did not reveal a relationship between the Langmuir pressure P_L and temperature. Parameter used for these calculations are listed in *Table 4.2*. These calculations show, that, assuming present-day maturity, the sorption capacity of moisture-equilibrated coal from Prokop seam would increase with depth (10.1 MPa/km, 35K/km) until it reaches a maximum of 0.35 mmol/g (daf) at 1090 m depth, followed by a constant decline to 0.18 mmol/g (daf) at 2000 m. For moisture contents less than equilibrium moisture, the maximum would be higher and reached at shallower depth (0.49 mmol/g at 940 m for average hygroscopic moisture, 0.68 mmol/g at 660 m for dry coal). At low temperature gradients, the influence of the increasing pressure is the dominant factor on sorption capacity, and thus, higher temperature gradients result in a stronger decline of sorption capacity at depth >1000 m and also shift the maximum towards shallower depth.

A significantly higher pressure gradient of 15.1 MPa/km would increase the overall sorption capacity compared to a more realistic gradient of 10.1 MPa/km. At the higher pressure gradient, the maximum in sorption capacity (0.39 mmol/g, daf at 950 m) is reached at a shallower depth than with the lower pressure gradient (0.35 mmol/g, daf at 1090 m) (*Fig. 4.17c*).

The effect of rank was tentatively taken into account by assuming that the maturity increases with the trend observed for coal from Paskov mine ($n_L = 0.2289 \cdot VR + 0.3674$). Then the sorption capacity at 0.6% VR would be 7% lower than the sorption capacity at 0.96% (coal from Prokop seam used in the present measurements) and the sorption capacity at 2% VR and

3% VR would be 34% and 48% higher, respectively (*Fig. 4.17e*). The calculation of the sorption capacity trends with increasing depth provides an estimate of the range of sorption capacities that could be encountered in the USCB for coals of different rank. Assuming that the present coal rank was obtained in response to thermal stress at maximum burial of the coal seams, the uplift (erosion during Permian and Mesozoic times), caused an increase in sorption capacity until a depth shallower than 800 – 950 m was reached. This increase in sorption capacity would have resulted in undersaturation of coals, if no refilling of the sorptive storage capacity by gas from secondary generation or migration occurred. Further uplift above the depth of maximum sorption capacity would have caused a subsequent loss in sorption capacity. The calculated maximum of sorption capacity at a depth between 600 and 1000 m can be used to identify suitable coal seams for gas storage, such as carbon dioxide sequestration in coal seams.

Table 4.2 Parameter for 'static' estimation of sorption capacity (n_L) vs. depth trends

Pressure gradient	10.1 MPa/km, 15.1 MPa/km
Temperature gradient	15K/km - 35K/km
Temperature correlation	$n_L = -0.004 \cdot T + 0.752$ (T = 45°C – 65°C)
Moisture correlation	$n_L = -0.43 \cdot d + 1.13$ * $P_L = 4.2066 \cdot d + 1.4637$
Rank correlation	$n_L = 0.2289 \cdot VR + 0.3674$

* d=1 for moisture-equilibrated coal, d=0 for dry coal and d=0.53 ± 0.14 for "as received" coal

The calculated trends for the SW USCB were compared to results from the Ruhr Basin (RB) by Gaschnitz (2001). The sorption capacity trend calculated for a temperature gradient of 35K/km and a pressure gradient of 10.1 MPa/km for moisture-equilibrated coal was compared to the trend calculated from isotherm data of Gaschnitz (2001) on a vitrain sample (dry and moisture-equilibrated, VR 0.89%), using the same pressure and temperature gradients (*Fig. 4.17f*). Even though a direct comparison of sorption capacity trends derived from coal and isolated macerals might strictly not be valid, it shows that different sorption trends exist for different basins that are not only influenced by local p, T gradients and coal rank, but also depend on maceral composition and related differences in microporosity.

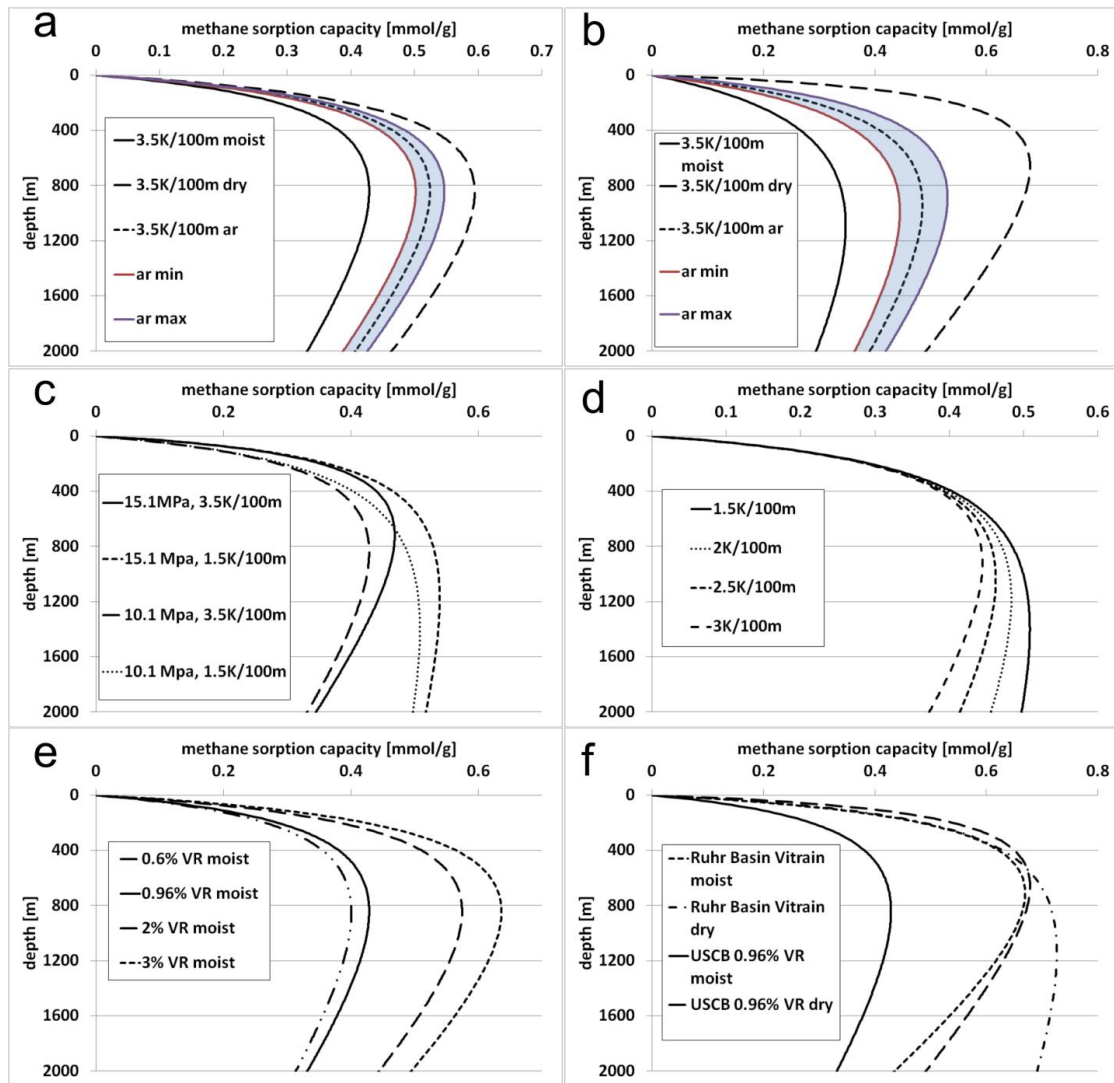


Fig. 4.17 Influence of different parameters on calculated sorption capacity depth trends.
 a: different moisture states with constant Langmuir pressure (VRr 0.96%, 35K/km, 10.1 MPa/km).
 b: different moisture states with Langmuir pressures calculated from weak correlation for all samples ($R^2 = 0.2$) (VRr 0.96%, 35K/km, 10.1 MPa/km).
 c: different pressure and temperature gradients (VR 0.96%, moisture equilibrated).
 d: different temperature gradients (VR 0.96%, moisture equilibrated, 10.1 MPa/km).
 e: different coal ranks (35K/km, 10.1 MPa/km, moisture equilibrated).
 f: comparison of sorption capacity-depth trends for coal from USCBA with trends calculated by Gaschnitz (2001) for vitrain isolated from German Ruhr Basin coal (VR 0.89%).

A “Dynamic model” was developed to follow the simultaneous evolution of rank, pressure and temperature throughout the entire burial history. In this model the sorption capacity was calculated for three of the main coal-bearing stratigraphic units (Poruba M., Saddle M. and Sucha M.) using depth information derived from the burial history of these units. A simplified burial history was assumed by Franců et al. (1999) for the USCBA. Based upon this approach, a 1-D model, calibrated on maturity and lithostratigraphic information from the Lazy 76 well was developed using PetroMod 11 software (Schlumberger, IES) (Fig. 4.18). The sorption capacity of coal for each formation was calculated using correlations derived in this study, as well as pore pressure, temperature and maturity (Easy%Ro) from the 1-D model. Additionally, sorption capacities were calculated for the same maturity, but with present-day pressure and temperature gradients of 10.1 MPa/km and 35K/km respectively. A comparison of

the ‘dynamic’ sorption capacity model with ‘static’ sorption capacity-depth calculations using correlations for different coal ranks and temperatures derived from sorption measurements of this study are given in Fig. 4.19.

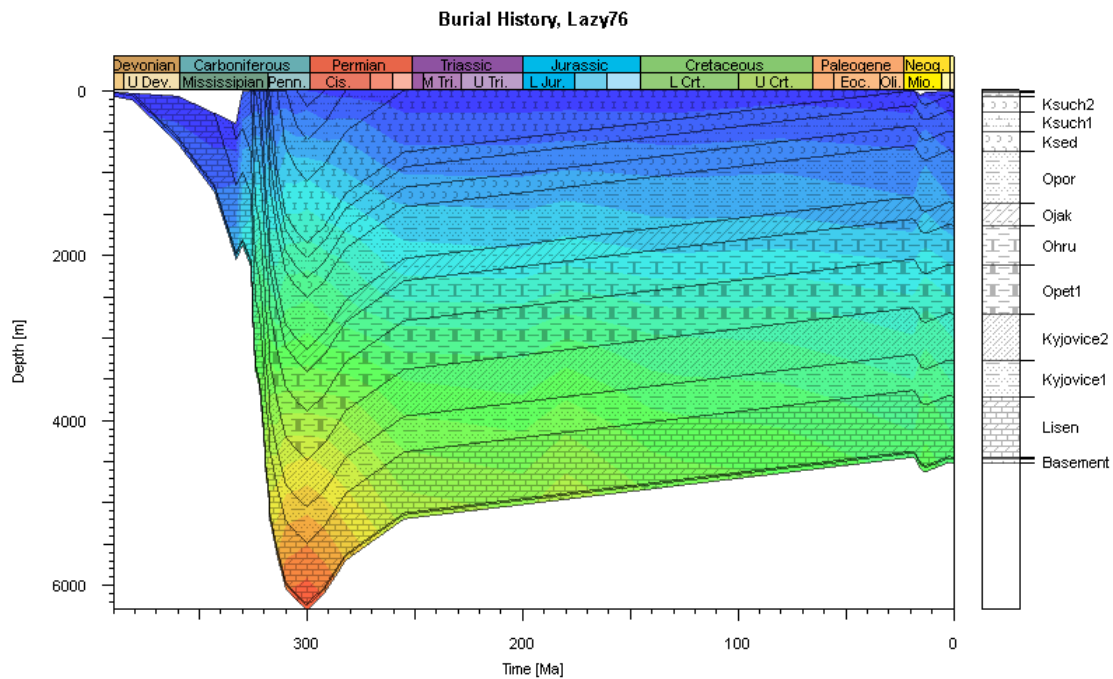


Fig. 4.18 Simplified burial history and 1-D model calibrated on data from Lazy 76 well.

This comparison shows that in the geologic past, when coal seams were at greater depth, the initial sorption capacity was significantly lower as if they would be buried to the same depth today. Figure 4.19 shows trajectories of the ‘dynamic’ paleo sorption capacity during uplift for three different coal bearing formations. These trajectories approach the sorption capacity that would be estimated from ‘static’ present-day pressure and temperature gradients in the late stage of uplift. The difference can be explained by higher paleo temperatures (higher paleo heat flow) (Fig. 4.20). Scatter in these paleo sorption capacity trajectories might be attributed to uncertainties in the simplified burial history. It should be noted that this simple model assumes a long period of erosion from early Permian to the Tertiary, which might not reflect the ‘true’ uplift history. However, detailed information on the uplift history of the basin was not available. Even though no re-initialization of the coalification process took place, uplift or re-burial events could have influenced the gas content of coal seams in the basin.

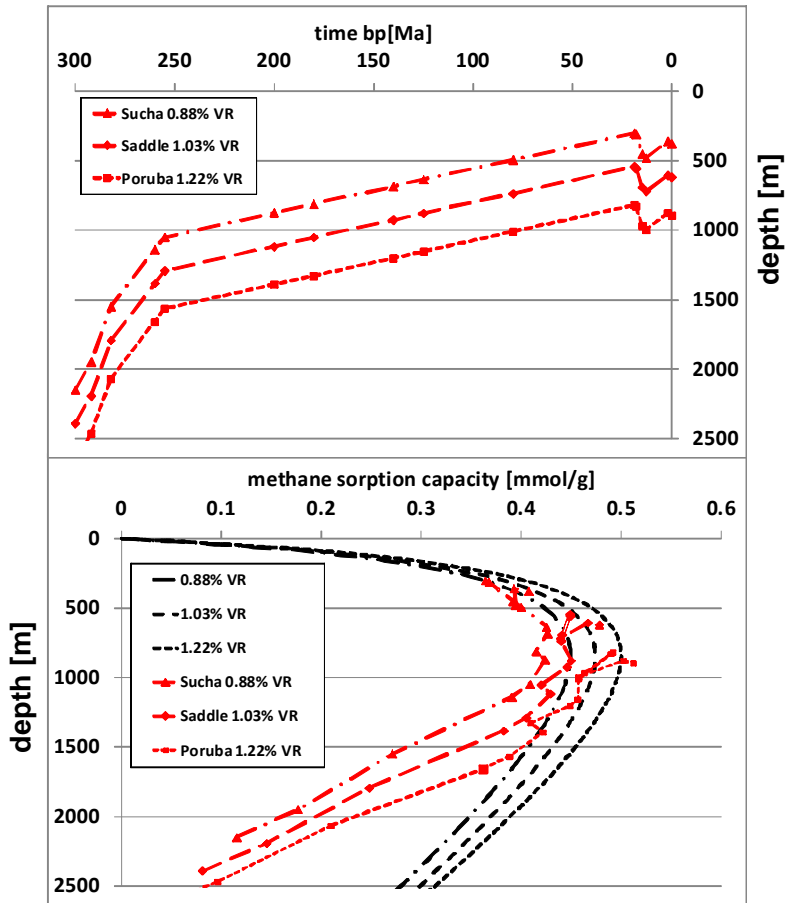


Fig. 4.19 Comparison of calculated sorption capacity depth trends for different stratigraphic units using depth data from burial history (top) data and pore pressure and temperature information from a 1-D model (Petromod). Black lines represent calculated trends using linear pressure (10.1 MPa/km) and temperature (35K/km) trends and depth information from the burial history. Red lines represent trajectories of sorption capacity during basin evolution (uplift).

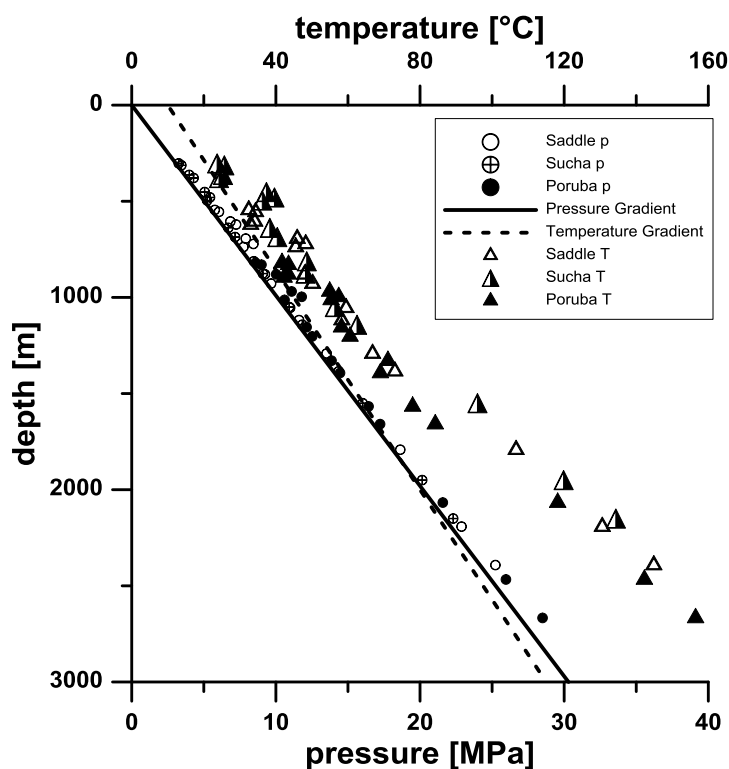


Fig. 4.20 Comparison of linear present-day pressure (p) (10.1 MPa/km) and temperature (T) (35K/km) gradients with paleo- pressure and temperature data from 1-D basin model.

4.8. Conclusions

In the Czech part of the Upper Silesian Basin, coal seams of bituminous rank (low volatile to high volatile bituminous) predominate. Different maturity parameter such as volatile matter yield, vitrinite reflectance and Rock-Eval T_{max} show good correlation, indicating that coal seams cover the mid to late oil window for type III kerogen (~1 to 1.8% VRr).

Methane sorption capacities of moisture-equilibrated coal are up to 47% lower as compared to sorption of “as-received” samples.

Comparison of methane sorption capacity (0.4 to 1 mmol/g) and present day gas contents (< 0.4 mmol/g) shows that most coal seams are undersaturated.

Methane sorption capacity shows a weak relation to coal rank and no significant correlation to maceral composition.

Methane sorption isotherms measured on a moisture-equilibrated coal at different temperatures (45, 55, 65°C), without changing the sample, revealed a linear decrease of sorption capacity of 0.1 cm³/g for every 1K temperature increase.

Carbon dioxide sorption capacity of coals is generally higher compared to methane sorption capacity. The average CO₂/CH₄ sorption ratio is higher for moisture-equilibrated coal and decreases with increasing coal rank and also with increasing experimental pressure.

Calculation of the ‘static’ methane sorption capacity variation with increasing depth, assuming a constant hydrostatic pressure gradient and a constant temperature gradient shows

that sorption capacity increases to a maximum value between 600 and 1000 m depth, followed by a constant decrease.

Relationships from experimental data and pressure and temperature information derived from a 1-D basin model can be used to model the 'dynamic' evolution of sorption capacity. During the basin history the initial sorption capacity of coal seams was significantly lower compared to the sorption capacity that would be estimated from 'static' present-day pressure and temperature gradients. Significant deviations for the earlier uplift stage result from higher paleo temperature gradients during basin evolution. To improve the applicability of sorption capacity – depth estimations, experimental data are required for temperatures > 70°C. The increase of sorption capacity during uplift alone is not sufficient to explain the gas undersaturation of most coal seams, indicating that a significant amount of gas, generated during coalification, was lost during times of uplift and erosion.

4.9. Acknowledgements

This study received financial support from the German Research Foundation (DFG) under grant KR1783/5-1 and from the Czech Science Foundation (GA_CR) under grant 205/07/J061. We thank two anonymous reviewers for their helpful contribution that improved the manuscript.

5. High-pressure methane and carbon dioxide sorption on coal and shale samples from the Paraná Basin, Brazil

High-pressure methane and carbon dioxide sorption on coal and shale samples from the Paraná Basin, Brazil

Philipp Weniger ^a, Wolfgang Kalkreuth ^b, Andreas Busch ^c, Bernhard M. Krooss ^a

^aInstitute of Geology and Geochemistry of Petroleum and Coal, RWTH Aachen University, Germany

^bInstituto de Geociências, UFRGS, Porto Alegre, Rio Grande do Sul, Brazil

^cShell International Exploration and Production B.V., Rijswijk, The Netherlands

5.1. Abstract

An experimental study has been conducted to assess the potential for coalbed methane production and carbon dioxide storage in coals, carbonaceous shales and source rocks in the Paraná Basin in Brazil. High pressure sorption tests with methane and carbon dioxide were performed on coal and carbonaceous shales from the Santa Terezinha Coalfield and samples from two principal petroleum source rocks. Measured excess sorption capacities ranged from 0.03 to 0.47 mmol/g for methane and 0.14 to 0.81 mmol/g for carbon dioxide, showing a decrease with decreasing organic matter content. Linear regression lines for methane sorption capacity vs. TOC extrapolated to approximately zero, whereas for carbon dioxide the intercept of the regression line indicated a residual sorption capacity of ~0.2 mmol/g on the mineral matter. Present-day gas contents of coals collected from the first CBM well in the Santa Terezinha Coalfield correspond to 13–38% of the measured maximum sorption capacities. Carbon dioxide sorption capacities exceed methane sorption capacities by a factor of 1.9 to 6.9 for these coals. Free sorption capacities of the under-saturated coals in combination with preferential sorption of carbon dioxide could favour CO₂-enhanced methane recovery and CO₂ storage in coals and shales of the study area. Based upon the calculated coal reserves, gas contents and measured sorption capacities, a total storage potential of 15.4 Gt CO₂ was estimated for an area of 20×40 km² in the Santa Terezinha coal field, assuming a combined CO₂ enhanced coalbed methane (ECBM) production and CO₂ storage operation. To fully evaluate the potential for carbon dioxide storage and coalbed methane production, further studies are required to assess producibility of methane and efficiency of long term CO₂ storage in the study area.

5.2. Introduction

Worldwide coalbed methane (CBM) resources are estimated to range between 2976 and 12649·10¹² scf (84.2–358.2 ·10¹² m³) (Murray, 1996). Conventional proven gas resources are in the order of 6533·10¹² scf (185·10¹² m³) (BP, 2009). Thus, CBM resources would correspond to 46% (minimum estimate) up to 193% (maximum estimate) of conventional gas resources (Holz et al., 2010). Presently CBM is being produced or under exploration in the USA, Canada, China, Australia, Germany and other countries. In Brazil the principal coal resources occur in the southern part of the Paraná Basin, associated with the Permian age Rio Bonito Formation. Earlier studies (Kalkreuth and Holz, 2000; Kalkreuth et al., 2003) have identified the Santa Terezinha Coalfield (Fig. 5.1), Rio Grande do Sul (RS), as the prime candidate for coalbed methane exploration in Brazil, based on coal distribution (coal thickness and lateral continuity of coal beds), size and depth of coal beds and coal rank, estimating a CBM gas in place (GIP) volume of 672·10⁹ scf (19·10⁹ m³) for this coalfield. In 2007 the first Brazilian CBM test well

(CBM-001-ST-RS) was drilled in the Santa Terezinha Coalfield (*Fig. 5.1*). Samples from 12 coal seams and carbonaceous shales were collected from a depth interval of 605 to 638 m using wire line core retrieval techniques, followed by canister desorption tests and coal quality analyses on 24 samples (Kalkreuth et al., 2008a,b). Total gas contents (desorbed gas, lost gas, and estimated residual gas) were found to range from 0.34 to 2.18 m³/t with an average value of 1 m³/t. Gas composition was determined on nine samples, indicating that methane constitutes >94 vol. % in all samples (Kalkreuth et al., 2008b), with minor contributions of hydrocarbon homologues (ethane, propane and butane), CO₂ and N₂. Stable carbon isotope values indicate a mixed (thermal/biogenic) origin of the methane (Kalkreuth et al., 2008b). Based on the average total desorbed gas volumes, and 3D modelling of the coal volume in a 20×40 km² area (Kalkreuth et al., 2008b), the total gas in place (GIP) associated with the coals and carbonaceous shales was estimated to amount to 194·10⁹ scf (5.5·10⁹ m³) CH₄. Only few studies have been published on the evaluation of the gas storage capacity of Brazilian coals. Soares et al. (2007) performed sorption experiments on dry coals from Santa Catarina State at sub-atmospheric pressures (<1 bar) and at a temperature of 30 °C. They report CO₂ storage capacities ranging between 0.089 and 0.186 mmol/g. In the present study, high-pressure sorption isotherms for methane (CH₄) and carbon dioxide (CO₂) were measured on seven samples (coals and carbonaceous shales) from the CBM-001-ST-RS well (*Table 5.1*) to evaluate the potential for coalbed methane (CBM) production, enhanced CBM recovery (CO₂-ECBM) and CO₂ sequestration in the Santa Terezinha Coalfield.



Fig. 5.1 Location of the Santa Terezinha coal field, state of Rio Grande do Sul, Brazil (Kalkreuth et al., 2008b).

It is known from earlier studies that moisture substantially reduces the sorption capacity of coals for methane (Joubert et al., 1973) and carbon dioxide (Krooss et al., 2002; Day et al., 2008b; Crosdale et al., 2008; Ozdemir and Schroeder, 2009). To evaluate the effect of moisture content on the sorption properties of Brazilian coals, methane and carbon dioxide sorption isotherms were measured on one selected coal (sample 07_166) first in the “as received” and then in the moisture-equilibrated state. In addition, this study includes measurements on five shale samples (Table 5.1) considered to be the principal petroleum source rocks of the Paraná Basin (Ponta Grossa Fm., Devonian; Irati Fm., Permian).

5.3. Geological setting

The Paraná Basin is a large intra-cratonic basin, located in southern Brazil, Paraguay, Uruguay and Argentina and covering an area of more than 1,400,000 km². Sediments and volcanic rocks of the basin range in age from Ordovician to Cretaceous (Zalán et al., 1990, 1991; Milani et al., 2007), with a cumulative thickness in excess of 7000 m in the depocentre. The samples analysed in this study come from the Permian Irati and Rio Bonito formations and from the Devonian Ponta Grossa Formation.

5.3.1. Irati Formation

According to Milani (1997) the Permo-Carboniferous sequence of the Paraná Basin was deposited during maximum flooding of the basin. The organic-rich bituminous shales, siltstones, sandstones and carbonates of the Permian Irati Formation occurs basinwide from the state of Rio Grande do Sul in the south, to the state of Mato Grosso in the north (a distance of approximately 2500 km). The Irati Formation varies in thickness from 10 to 50 m, with major bituminous shale development in Rio Grande do Sul (Padula, 1969), where cumulative shale thickness reaches up to 13.5 m. The bituminous shales of the Irati Formation are considered the principal petroleum source rocks of the basin (Milani and Zalán, 1999), with TOC contents between 8 and 13 wt.%, and TOC peaks in excess of 20 wt.%. Level of preservation of the organic matter (kerogen type I/II) was controlled by variations in the redox potential during deposition (Araújo et al., 2004).

5.3.2. Rio Bonito Formation

Coal deposits occur in the southern part of the Paraná basin in the Permian age Rio Bonito Formation, a fluvial to marine sand- and shale prone lithostratigraphic unit (Holz, 1998), where peat accumulated in coastal mires that formed in a back barrier/strand plain depositional system (Holz et al., 2000; Holz and Kalkreuth, 2004). In the Santa Terezinha Coalfield the cumulative coal thickness increases towards the north-east from ca. 4 m to more than 10 m, with individual coal seam thicknesses of up to 3 m (Kalkreuth and Holz, 2000). Coal rank, based on vitrinite reflectance values, also increases towards the north-east, from sub-bituminous to high volatile A bituminous. Local diabase intrusions have increased locally the thermal maturity of the coals to semi-anthracite and anthracite rank, with vitrinite reflectances of up to 5.46% VRr (Kalkreuth and Holz, 2000; Kalkreuth et al., 2008a,b).

Table 5.1 Sample list and results of proximate and petrographic analyses. For stratigraphic position of canister samples, see Fig. 5.2.

Sample #	Formation	Geol. Age	Sample Type	Seam interval, (Canister #)	Depth [m]	Total Gas Content [m ³ /t coal]*	V.M. [%] (V.M. % daf)	Ash Yield [wt.%]	TOC [wt.%]	VRr [%]	Moisture Content [wt.%, a.r.]	VIT, mmf [Vol%]	LIP, mmf [Vol%]	IN, mmf [Vol%]
08-154	Irati	Permian	shale	n.d.	n.d.	n.d.	n.d.	n.d.	1.62	n.d.	0.92	n.d.	n.d.	n.d.
08-168	Irati	Permian	shale	n.d.	n.d.	n.d.	n.d.	n.d.	24.21	n.d.	1.65	n.d.	n.d.	n.d.
08-170	Irati	Permian	shale	n.d.	n.d.	n.d.	n.d.	n.d.	11.66	n.d.	1.20	n.d.	n.d.	n.d.
07-114/	Rio Bonito	Permian	carb sh	L1, (2)	609.10	0.38	5.00 (79.37)	93.11	1.73	2.61	1.38	10.0	0.0	90.0
07-117-118/	Rio Bonito	Permian	carb sh	L2, (3)	610.30	1.04	9.94 (39.99)	67.21	21.09	1.51	1.33	42.0	0.5	57.5
07-153/	Rio Bonito	Permian	coal	C, (7)	618.24	1.69	19.73 (37.88)	35.8	n.d.	0.82	0.98	46.0	6.0	48.0
07-166/	Rio Bonito	Permian	coal	D, (11)	620.80	2.18	21.26 (43.19)	41.99	43.9	0.92	0.93	53.0	9.0	38.0
07-177/	Rio Bonito	Permian	carb sh	G, (20)	630.35	0.68	15.20 (42.26)	61.1	n.d.	1.62	0.89	20.0	6.0	74.0
07-186/	Rio Bonito	Permian	coal	H, (22)	636.47	1.03	22.72 (43.17)	44.9	n.d.	0.88	0.59	61.0	0.0	39.0
07-181/	Rio Bonito	Permian	carb sh	I, (24)	637.86	0.31	10.10 (52.80)	81.69	11.13	1.05	0.82	17.0	4.0	79.0
08-100	Ponta Grossa	Devonian	shale	n.d.	n.d.	n.d.	n.d.	n.d.	1.29	n.d.	3.26	n.d.	n.d.	n.d.
08-101	Ponta Grossa	Devonian	shale	n.d.	n.d.	n.d.	n.d.	n.d.	0.70	n.d.	1.01	n.d.	n.d.	n.d.

V.M. = volatile matter yield; TOC=total organic carbon; VRr[%]=mean vitrinite reflectance value, determined in random mode; a.r. = as received; daf=dry, ash-free; VIT=vitrinite; LIP=liptinite; IN=inertinite; mmf=mineral matter-free basis; Carb sh=carbonaceous shale, n.d. = not determined. * Includes measured desorbed gas, lost gas and estimated rest gas, from Kalkreuth et al (2008b).

Petrographic analysis of coal seams from the Santa Terezinha Coalfield indicated high inertinite contents, often exceeding 50%, and also high mineral matter contents (Araújo et al, 1995; Kalkreuth et al., 2006; Kalkreuth et al., 2008a,b) grading coal seams into carbonaceous shale. Recent sequence stratigraphic analysis (Kalkreuth et al., 2008a,b) identified five coal-bearing sequences (parasequences) in the Santa Terezinha Coalfield, with major coal development in parasequence 2.

5.3.3. Ponta Grossa Formation

Marine shale and sandstones of the Devonian Ponta Grossa Formation are widespread in the Paraná Basin (Zalán et al., 1990, 1991), reaching a maximum thickness of about 600 m (Neto, 1995). Black shales developed in the São Domingo Member of the Ponta Grossa Formation (Candido and Rostirolla, 2007) are considered important source rocks in the Paraná Basin (Milani and Zalán, 1999), with TOC contents ranging between 1.5 and 2.5 wt.%, occasionally reaching more than 4 wt.%. The organic matter is of kerogen type II and accumulated paleogeographically in an epicontinental sea depositional environment.

5.4. Samples

Seven coal and carbonaceous shale samples (*Table 5.1*) were obtained from the CBM pilot well CBM-001-ST-RS, drilled in early 2007 in the Santa Terezinha Coalfield, State of Rio Grande do Sul (RS), Brazil. The samples were collected from a depth interval between 605 and 638 m, using a wireline core retrieval technique. A stratigraphic overview of the CBM well as well as locations of sampled seam intervals is shown in (*Fig. 5.2*). Additionally, three oil shale samples of the Permian Irati Formation and two Devonian source rock samples of the Ponta Grossa Formation were investigated in this study. Excess sorption isotherms for CH₄ and CO₂ were measured in the “as received” moisture state, *i.e.* without drying. To assess the effect of moisture on sorption isotherms, methane and carbon dioxide sorption isotherms were measured both in the “as received” state and after moisture equilibration on one coal (sample 07_166).

5.4.1. Sample preparation

The grain size of coals controls gas diffusion (diffusivity) and sorption kinetics. On smaller particles, gas can diffuse faster to micropore sorption sites and the equilibration time will be shorter compared to larger particles. For sorption experiments coal samples are commonly pulverized to reduce the equilibration time. Grinding of coal and size fractionation (sieving) may cause compositional changes (Clove et al., 2002). Mineral matter tends to be enriched in the smaller size fractions (Spears and Booth, 2002) and maceral composition will also differ from the smallest fraction (inertinite enriched) to larger fractions (vitrinite enriched) (Clove et al., 2002). These compositional changes can also cause differences in sorption capacity (Busch et al., 2004). To avoid any compositional fractionation, the entire sample material was powdered to <0.2 mm. Proximate analysis and sorption measurements were carried out on sub-samples, acquired using a sample divider (homogenizer) from the powdered samples. The equilibrium moisture content was established according to ASTM D1412 (1999) with the exception that instead of -16 mesh sieve fractions, pulverized samples (<0.2 mm) were used and samples were moisture-equilibrated under vacuum.

5.5. Methods and experimental procedures

5.5.1. Coal characterisation

Proximate analyses of the coal samples were carried out according to DIN 51700: “Testing of solid fuels”. The analysis comprised thermo-gravimetric determination of the “as received” (hygroscopic) moisture content (DIN 51718) and ash yield (DIN 51719). All analyses were performed in triplicate on powdered sub-samples (1 g, <0.2 mm grain size). Optical petrographic characterization was performed on grain mounts and polished blocks according to common petrographical procedures (*e.g.* Bustin et al., 1989) at the Instituto de Geociencias Laboratories, Porto Alegre, Brazil. The characterization comprised vitrinite reflectance measurements (VRr%) and maceral group analysis (point counting). Total organic carbon (TOC) contents were determined in duplicate with a multiphase carbon analyser RC-412 (LECO, USA). Sample quantities of the carbonaceous shale were in the range of 50 mg, with grain sizes <0.2 mm.

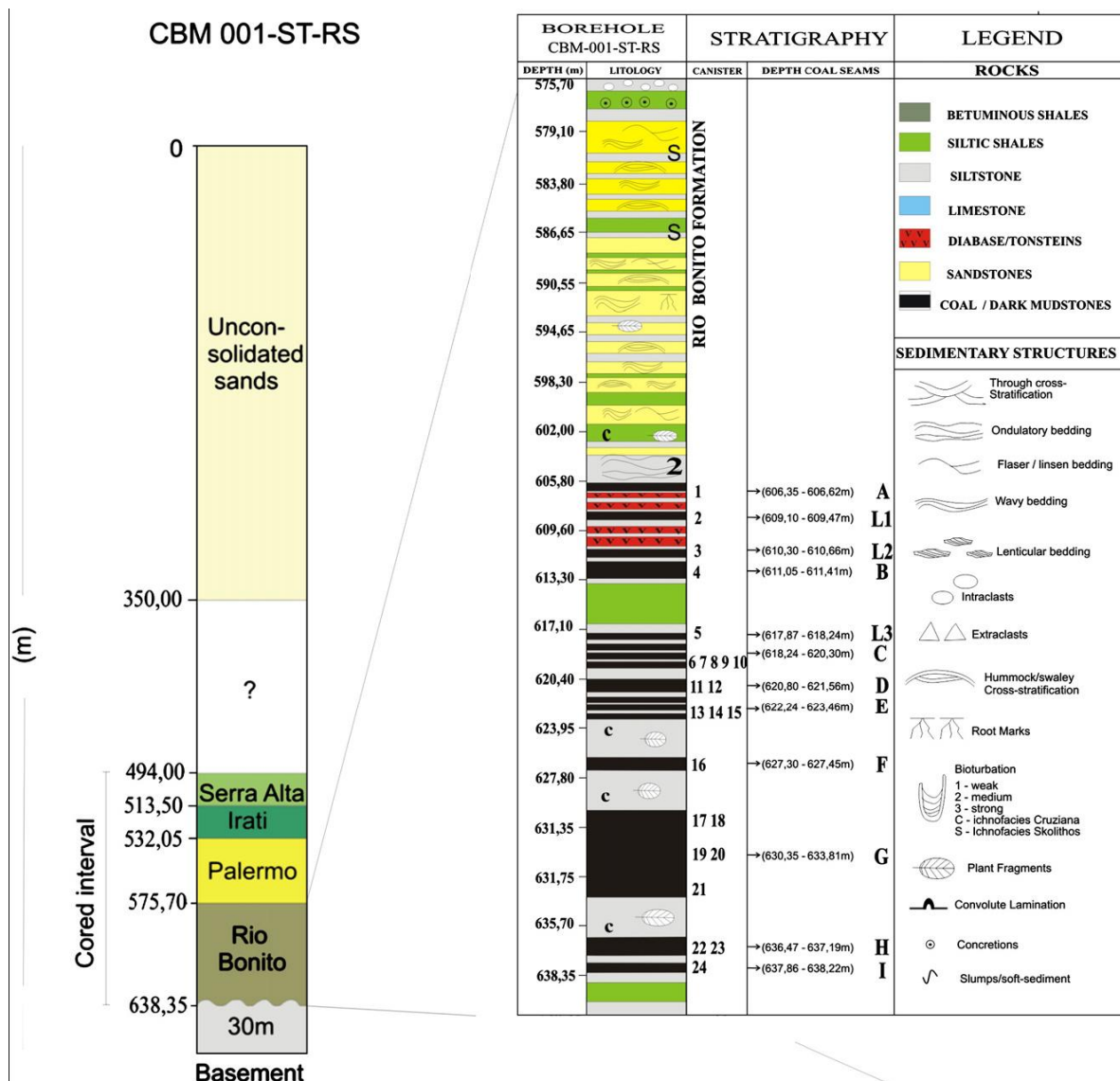


Fig. 5.2 Stratigraphic profile of the CBM-001-ST-RS well and position of canister samples analysed by Kalkreuth et al. (2008b). Sorption experiments of the present study were carried out on samples from canisters 2, 3, 7, 11, 20, 22 and 24.

5.5.2. High-pressure sorption isotherms

5.5.2.1. Experimental setup and conduction of sorption experiments

Methane and carbon dioxide excess sorption isotherms were determined using the manometric method described by Krooss et al. (2002), Busch et al. (2004), Siemons and Busch (2007) and Gensterblum et al. (2009). The experimental setup (Fig. 5.3) consists of a stainless-steel sample cell (~14 cm³ for CH₄ and ~8.5 cm³ for CO₂), a set of actuator-driven valves, and a pressure transducer (max. pressure 17 MPa for CH₄ and 25 MPa for CO₂), with a precision of 0.05% of the full-scale value. The volume between valve 1 and valve 2, including the void volume of the pressure transducer, is used as reference volume (~2 cm³ for CH₄ and ~1.1 for CO₂) and determined by helium (He) expansion in a calibration run. The sample cells are equipped with 2- μ m filters to prevent coal or mineral particles from entering the valves. The

entire experimental device is placed in a temperature-controlled oven. Sorption measurements in this study were conducted by the following procedure:

1. Samples were degassed by evacuation for 15 min at 1 mPa.
2. After moisture equilibration, samples were transferred immediately into the sorption cell. The evacuation time was reduced to 5– 10 min to avoid moisture loss.
3. Leak test was conducted using He at 10 MPa for 2 h to assure thermal equilibration of samples and a helium leakage rate of less than 5 mbar/h (<500 Pa/h).
4. Void volume determination by helium expansion. Void volume was calculated using the average value of 10 pressure steps ranging from 1 to 10 MPa with a standard deviation <0.05%. In addition the void volume determination provided the sample volume, which was used to calculate sample skeletal density.
5. Sorption measurement with CH₄ and CO₂ up to 17 and 25 MPa, respectively.

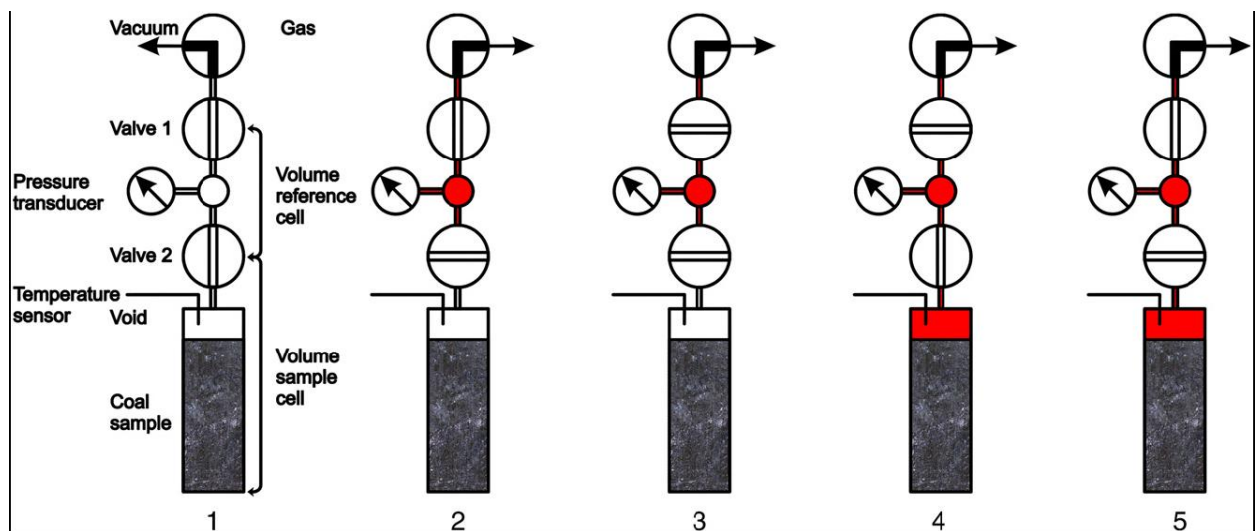


Fig. 5.3 Schematic flow diagram for the manometric method for gas sorption measurements: (1) evacuation of the whole system (2) filling of the reference cell (3) closure of valve 1 and thermal equilibration, (4) valve 2 is opened and gas transferred into the sample cell; start of the sorption process (5) after pressure equilibration, closure of valve 2 and refilling of the reference cell. Steps 3 to 5 are repeated until the maximum system pressure is reached (after Simons and Busch, 2007).

5.5.2.2. Parameterization of experimental sorption isotherms

The experimental methane sorption isotherms as well as carbon dioxide sorption isotherms measured at 35 °C were fitted by the (2- parameter) Langmuir function (1):

$$n_{\text{ads}} = n_L \cdot p / (P_L + p) \quad (1)$$

Here n_{ads} (mmol/g) denotes the adsorbed amount of substance at pressure p (MPa). P_L (MPa) is the Langmuir pressure, corresponding to the pressure at which half of the (“monolayer”) sorption sites are occupied and n_L (mmol/g) is the “Langmuir amount of substance” (corresponding to the “Langmuir volume”), denoting the amount adsorbed at full occupation of the Langmuir monolayer. Because the Langmuir sorption model is a limiting model for low pressures, its application to high-pressure sorption isotherms is strictly not justified. In many instances it represents, however, a reasonable approximation of the measured excess sorption isotherms and can thus be used as a fitting function. Some of the sorption isotherms reported here have characteristic features that cannot be represented by the simple Langmuir model. Here a modified Langmuir model, taking explicitly into account the volume of the adsorbed phase was used to approximate the measured data. This function is given by (2):

$$n_{\text{ads}} = n_L \cdot p / (P_L + p) \cdot (1 - (\rho_{\text{free}}/\rho_{\text{adsorbed}})) \quad (2)$$

It contains an additional adjustable parameter, the density of the adsorbed phase (ρ_{adsorbed}). Carbon dioxide isotherms were approximated by Eq. (2) by adjusting n_L , P_L and ρ_{adsorbed} in a least-squares fit. For comparison of CO₂ and CH₄ isotherms, methane isotherms were also approximated by Eq. (2), using a sorbed phase density value of 421 kg/m³ (Arri et al., 1992) and adjusting n_L and P_L . However, approximation of methane isotherms using Eq. (1) usually yields a better fit of experimental data compared to approximation using Eq. (2), which might indicate that the 'real' sorbed phase density differs from the assumed sorbed phase density.

5.5.2.3. Evaluation of sorption experiments

The equations of state (EOS) for CO₂ and CH₄ developed by Span and Wagner (1996) and Setzmann and Wagner (1991), respectively, were used in the evaluation of the manometric sorption experiments. The EOS provided the specific density of the free gas phase under the experimental pressure and temperature conditions. The amount of gas transferred from the reference to the sample cell was calculated from the density of the gas phase and the corresponding void volumes. Helium densities used for the assessment of the void volume of the measuring cell were calculated by a van der Waals equation of state after Michels and Wouters (1941). The total experimental error for adsorption measurements is less than 10% n_{ads} for carbon dioxide isotherms and less than 3% n_{ads} for methane isotherms at the final experimental pressure. Further information on the accuracy of the manometric sorption setup used for this study, as well as a thorough evaluation of possible errors and pitfalls has been published recently by Li et al. (2010) and Gensterblum et al. (2009).

5.6. Results and discussion

5.6.1. Proximate analysis

The results of the proximate analyses ("as received" moisture content and ash yield) are summarized in Table 5.1. Moisture contents of coal and carbonaceous shale samples from the CBM well range between 0.6% and 1.4%, and from 0.9% to 3.3% for the shale samples from the Irati and Ponta Grossa formations. Comparison of moisture contents measured in Brazil, shortly after retrieval of samples from the CBM well, with "as received" moisture contents measured ca. 1.5 years later in the RWTH laboratory, Aachen, revealed an average moisture loss of 0.3 wt.% (Fig. 5.4). Ash yields for the CBM well samples, reported on a dry basis, are generally high, ranging from 36% to more than 90%. This indicates that coal seams are grading into carbonaceous shales. A comparison of ash yields determined at Universidade Federal do Rio Grande do Sul, (UFRGS) and at RWTH Aachen University, revealed no significant differences.

5.6.2. TOC contents

TOC values for the two samples from Ponta Grossa Formation were 0.7% and 1.3% while the Irati oil shale had TOC contents extending from 2.3 to 26.3%. The TOC values of the samples from the Rio Bonito Formation ranged from 1.7% to 43.9%.

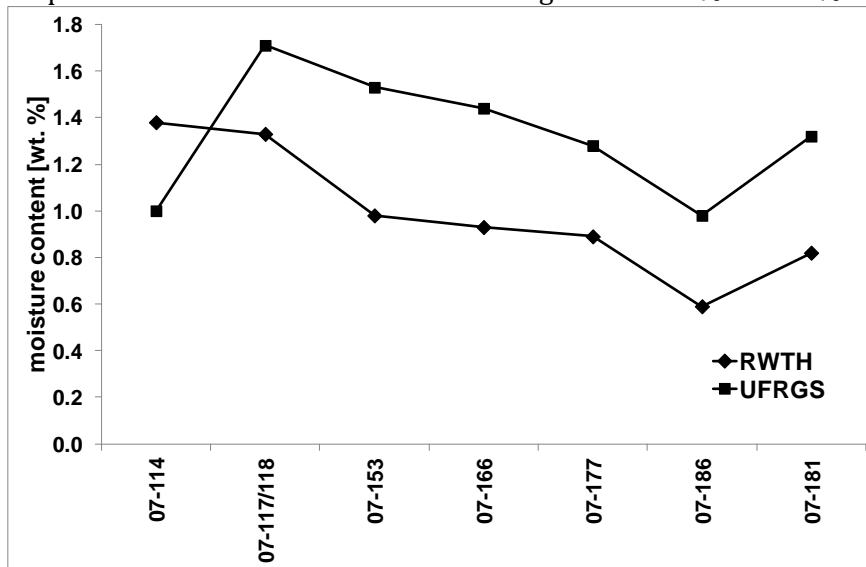


Fig. 5.4 Comparison of moisture content determined after sample acquisition in Brazil (UFRGS) and later before sorption tests in Germany (RWTH) indicating drying of powdered coal samples.

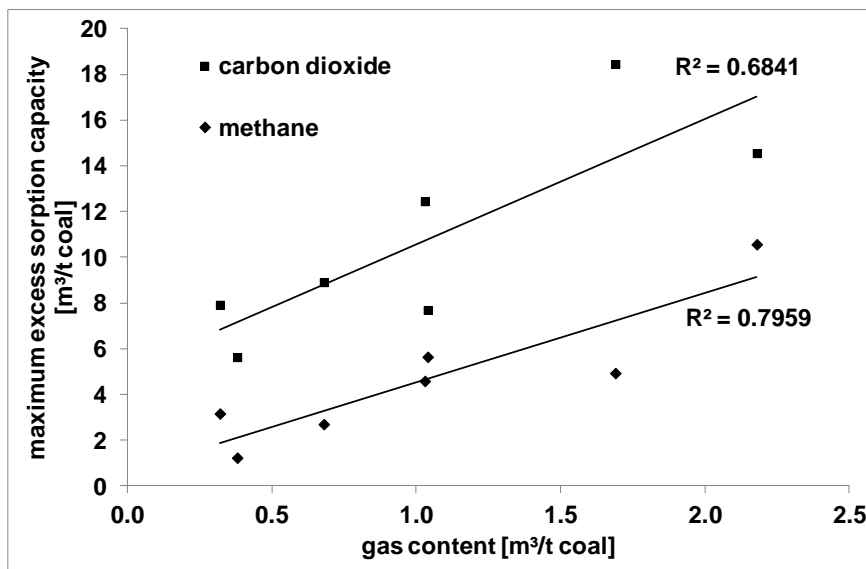


Fig. 5.5 Correlation of excess sorption capacity with gas content of coal and carbonaceous shale from CBM-001-ST-RS well.

5.6.3. Coal petrography

5.6.3.1. Vitrinite reflectance

Coals from the Rio Bonito Formation in the Santa Terezinha Coalfield are of high volatile bituminous rank (Kalkreuth et al., 2003) and have reached anthracite rank locally, where the

coal seams were thermally altered by diabase intrusions. The measured vitrinite reflectance values for the coals and carbonaceous shales from the CBM well range between 0.8% and 2.6%, with coals in contact with igneous intrusions (intervals L and G) showing the highest vitrinite reflectance.

5.6.3.2. Maceral group analysis

The maceral compositions of the Rio Bonito samples show large variations (*Table 5.1*). Inertinite contents are generally high and range from 38% to 90% with an average value of 61%. Most coals with high vitrinite reflectance (>1%) also show high inertinite contents (>50%). Liptinite is absent in coal seams from intervals L and H and reaches its highest value of 9% in interval D. Vitrinite content varies between 10% in interval L1 and 61% in interval H.

5.6.4. Gas contents

The coalbed gas contents of different intervals of the Rio Bonito CBM well have been reported previously by Kalkreuth et al. (2008b), based on temperature and pressure controlled gas (canister) desorption values. Gas contents range between 0.3 and 2.1 m³/t coal with the highest values in intervals C and D at a depth of ~620 m. Coal samples with less than 1% vitrinite reflectance show the highest gas contents. However, no clear correlation of gas content with maturity is observed. A slight correlation of gas content with increasing sorption capacity was observed for methane. This trend is less expressed for carbon dioxide (*Fig. 5.5*).

5.6.5. Results of gas sorption experiments

Most gas sorption isotherms in this study were measured at 45 °C up to pressures of 17 MPa for methane and up to 25 MPa for carbon dioxide. For three samples (07_153, 07_177, and 07_186) isotherms were measured at 35 °C. This temperature is only slightly above the critical temperature of CO₂ (31.1 °C) where the CO₂ density is very sensitive to temperature variations. Sorption isotherms for CO₂ in this temperature range therefore carry an inherent risk of inaccuracy due to even slight errors in temperature measurements. Maximum values of the measured excess sorption capacities and the Langmuir parameters (n_L and P_L for CH₄ and n_L , P_L and ρ_{adsorbed} for CO₂), obtained from approximation of the experimental data are listed in *Table 5.2*. Results of sorption measurements are reported in units of mmol/g, and in mmol/g dry, ash-free coal (daf). Conversion of the adsorbed amount of substance to gas volumes (Std. m³/t coal, daf) was performed using the standard conditions for gases (IUPAC, 1997).

5.6.5.1. Methane sorption isotherms

The methane sorption isotherms, measured on coal and carbonaceous shale samples from the Rio Bonito Formation of the CBM-001-ST-RS well are shown in *Fig. 5.6* (45 °C isotherms) and *Fig. 5.7* (35 °C isotherms). Sorption capacities for these samples range between 0.07 and 0.57 mmol/g (0.38 to 1.02 mmol/g coal, daf). Normalization of sorption isotherms to the dry ash-free basis shows that the first three samples have a significantly lower sorption capacity. This is unexpected because these isotherms were measured at a lower temperature (35 °C) than the other samples (45 °C). The reason for the lower sorption capacity is most likely a difference in moisture content. As described in chapter 5.1, coal samples lost a significant amount of water before sorption tests. It is very likely that samples measured at 45 °C lost additional moisture until they were measured. However, because most sample material was consumed, isotherms measured at 35 °C could not be re-measured at 45 °C and the moisture loss could not be quantified. For better comparison, isotherms measured at 35 °C have been excluded in the further data interpretation. The experimental isotherms were fitted by the Langmuir function (*Eq. (1)*) and the 3-parameter function (*Eq. (2)*), shown in the diagrams. The Langmuir parameters n_L and P_L for the individual sorption isotherms are listed in *Appendix IV*,

Table 2. Methane sorption isotherms, measured on the Permian and Devonian carbonaceous shales are shown in *Fig. 5.8*. As expected, the shale samples show lower methane sorption capacities (between 0.04 and 0.37 mmol/g) than coals. Normalized to TOC content, sorption capacities of the shale samples are, however, significantly higher than those of the coal samples on a daf basis (1.5 to 11.5 mmol/g, TOC). For shale samples with low TOC contents (<3%) (*e.g.* samples 08_100, 08_101 and 08_154), the bulk excess sorption values are also low and bear a relatively large error. Uncertainties in the assessment of low TOC values increase the experimental error. In consequence, the TOC-normalization of the sorption isotherms is likely to overestimate the methane sorption capacity of these samples (values in brackets in *Table 2*). The gas contents of coals from the CBM-001-ST-RS well are lower than their CH₄ sorption capacity (excess sorption), i.e. the coals are under-saturated in methane. Assuming a hydrostatic pressure gradient of 10MPa/km, the reservoir pressure in the depth interval under consideration should range between 6.1 and 6.4 MPa. Sorption capacities for the mean reservoir pressure (6.25 MPa) calculated from the Langmuir fits range between 7.7 and 16.5 m³/t coal. The actual methane contents of the coal seams, determined by canister desorption, thus represent between 13% and 38% of the sorption capacity.

5.6.5.2. Carbon dioxide sorption isotherms

Carbon dioxide excess sorption isotherms measured at 45 °C on coal and carbonaceous shale samples from well CBM-001-ST-RS are shown in *Fig. 5.9*, and another set of isotherms measured at 35 °C in *Fig. 5.10*. While the 45 °C isotherms were determined up to pressures of more than 20 MPa, the 35 °C isotherms were recorded only up to a pressure of ~7 MPa. *Fig. 5.11* shows 45 °C CO₂ sorption isotherms measured for the Permian (Irati) and Devonian (Ponta Grossa) shales. The CO₂ isotherms at 45 °C typically exhibit a maximum in the 8 to 10 MPa pressure range and then show a continuous decline. The maximum is related to the steep increase in the specific density of supercritical CO₂ in the corresponding pressure range (cf. Gensterblum et al., 2009). Maximum excess sorption capacities for CO₂, measured in this pressure interval, range from 0.25 - 0.81 mmol/g (5.6 - 18.5 m³/t) for coals and carbonaceous shales and from 0.14 - 0.54 mmol/g (3.2 - 12.2 m³/t) for the shales from the Irati and Ponta Grossa formations. The measured CO₂ isotherms were approximated by the excess sorption function given in *Eq. (2)*. The three parameters n_L , P_L and ρ_{adsorbed} , adjusted by a least-squares optimization procedure, for the individual isotherms are listed in *Table 2*. Some of the CO₂ isotherms for the shale samples (*Fig. 5.11*) show a pronounced maximum with a steep decline in the pressure range between 9 and 11 MPa. These isotherms could not be satisfactorily approximated by the 3-parameter fitting function. Isotherms with similar shapes were obtained by Busch et al. (2008) for CO₂ sorption on the Australian Muderong shale and on pure clay minerals, such as illite, montmorillonite and kaolinite.

5.6.6. Effect of mineral matter content (ash yield) on gas sorption

Coal seams from the Santa Terezinha Coalfield are known to have high mineral matter and inertinite contents as reported by Araújo et al. (1995) and more recently by Kalkreuth et al. (2006, 2008a,b). It has been suggested that the high-ash yields of coals from the Rio Bonito Formation are related to the occurrence of diamictites (Begossi and Della Fávera, 2002). X-ray diffraction analysis on coal samples from the CBM-001-ST-RS well revealed that the mineral matter is mostly composed of quartz, kaolinite and mica, with minor contributions of pyrite, ankerite, calcite, dolomite, albite and alunite (Kalkreuth et al., 2008b). Using the ash yield as a proxy for the mineral matter content, *Fig. 5.12* shows an essentially linear decrease of the maximum sorption capacity of methane and carbon dioxide with increasing mineral matter content for the coals and carbonaceous shales from the CBM-001-ST-RS well. The regression line for methane indicates that the sorption capacity is close to zero for ash yields approaching 100%, i.e. an organic matter content of zero. This supports the predominant role of organic matter in methane sorption in coals and carbonaceous sediments and is in agreement with

findings reported, for instance, for Australian Bowen Basin coals (Laxminarayana and Crosdale, 1999) and coals from British Columbia (Clarkson and Bustin, 2000). According to the regression in Fig. 5.12, the maximum sorption capacity for methane in the CBM-001- ST-RS well samples decreases by 0.009 mmol/g for each 1% increase in ash yield. This is somewhat lower than the value of 0.38 cm³/g (0.017 mmol/g) reported by Laxminarayana and Crosdale (1999), which is likely to reflect differences in the type (maceral composition) and maturity of the organic matter.

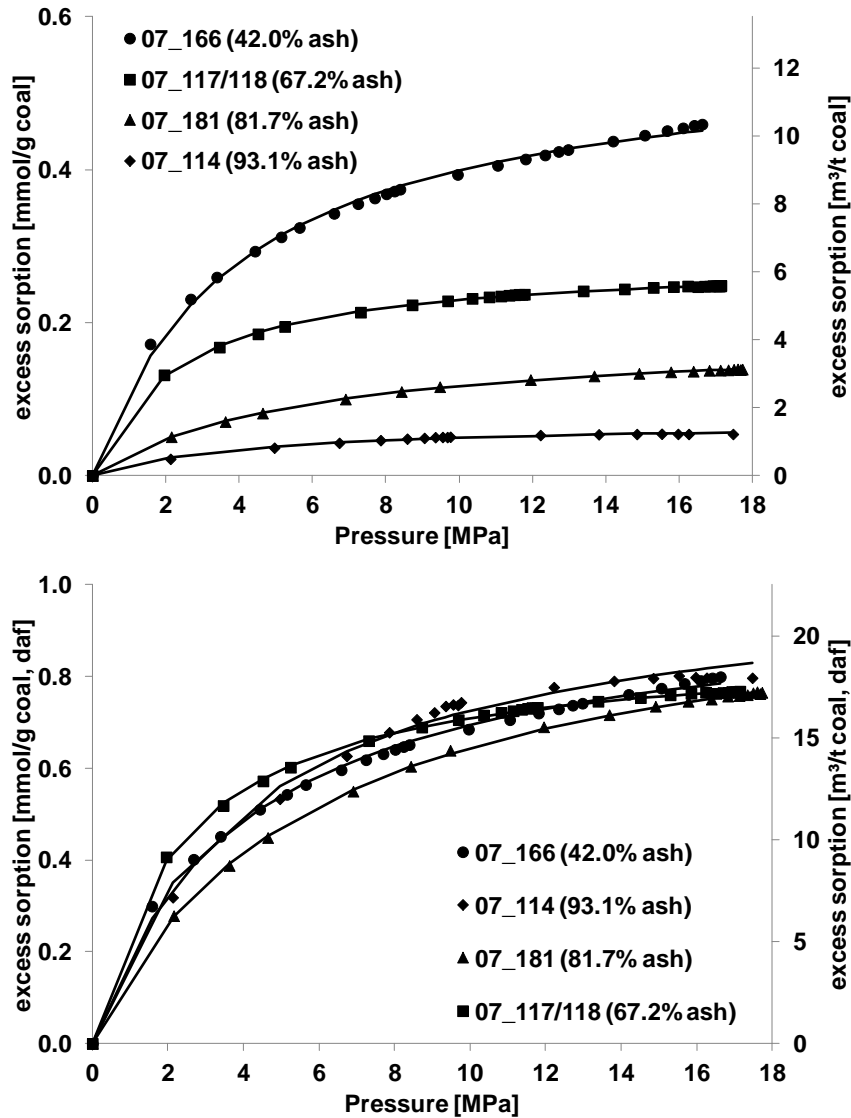


Fig. 5.6 Methane sorption isotherms (45 °C) with Langmuir approximations (solid lines) for coal and carbonaceous shale samples from the Permian Rio Bonito Formation of CBM well 001-ST-RS on a raw basis (top) and dry, ash-free basis (bottom).

The maximum sorption capacity of carbon dioxide for the CBM- 001-ST-RS well samples decreases by 0.008 mmol/g for each 1% increase in ash yield. The regression shows that at ash yields approaching 100%, i.e. organic carbon contents approaching zero, the samples still exhibit a considerable CO₂ sorption capacity (approximately 0.183 mmol/g) which can be attributed to the mineral matter. Fig. 5.13 shows maximum excess sorption capacities of methane and carbon dioxide for coal and shale samples from the CBM-001-ST-RS well and

Permian (Irati) and Devonian (Ponta Grossa) formations as a function of organic carbon contents (TOC). The following linear regression functions were obtained:

$$\text{CH}_4(\text{mmol/g}) = 0.009 \cdot \text{TOC}(\%) + 0.026$$

$$\text{CO}_2(\text{mmol/g}) = 0.008 \cdot \text{TOC}(\%) + 0.183$$

As stated above, the regression function for CO₂ indicates that the mineral matter exhibits a significant sorption capacity (0.183 mmol/g) for this gas. This finding is in general agreement with results reported by Nuttall et al. (2005), who evaluated the potential for carbon dioxide sequestration and enhanced natural gas production of Devonian black shales in Kentucky. These workers find a linear increase of CO₂ sorption capacity at 400 psia (2.75 MPa) with TOC content described by the regression function:

$$\text{CO}_2(\text{scf/ton}) = 7.9 \cdot \text{TOC}(\%) + 20.7 \quad (\text{CO}_2 \text{ pressure} = 400 \text{psia})$$

Expressed in metric units and amounts of substance this yields:

$$\text{CO}_2(\text{mmol/g}) = 0.009 \cdot \text{TOC}(\%) + 0.025 \quad (\text{CO}_2 \text{ pressure} = 2.75 \text{MPa})$$

This regression was obtained for a much lower CO₂ pressure than the pressure levels corresponding to the maximum excess sorption (8– 10 MPa) considered in the present study. However, even when taking this into account, the mineral matter in the Devonian black shales of Kentucky appears to have a significantly lower CO₂ sorption capacity than the sample sequences from the Paraná Basin investigated here. The difference in CO₂ sorption capacity is most likely related to differences in mineralogical composition. *Table 3 (Appendix IV)* shows a comparison of X-ray diffraction mineralogy for Santa Terezinha coal samples reported by Kalkreuth et al. (2006) and for Ohio shale samples (Huron Formation) reported by Nuttall et al. (2005).

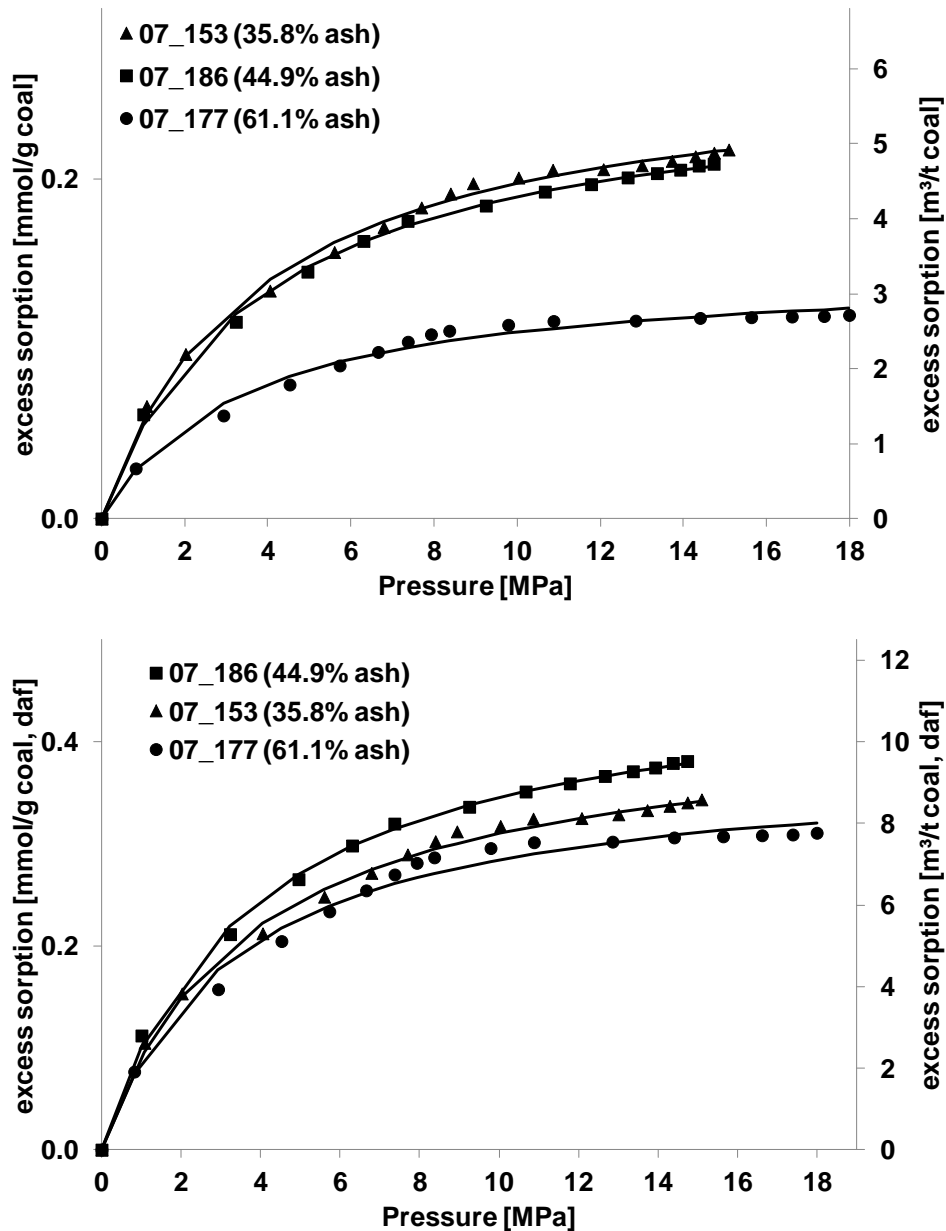


Fig. 5.7 Methane sorption isotherms (35 °C) with Langmuir approximations (solid lines) for coal and carbonaceous shale samples from the Permian Rio Bonito Formation of CBM-001- ST-RS well on a raw basis (top) and dry, ash-free basis (bottom).

Evidently, shales and some pure clay minerals exhibit a significant sorption capacity for CO₂. Busch et al. (2008) reported CO₂ sorption capacities for the Muderong shale and pure clay minerals (kaolinite, montmorillonite and illite), ranging from 0.1 mmol/g to 1.2 mmol/g for “as received” samples. The higher kaolinite and carbonate (calcite, ankerite and siderite) contents of coal samples explain the larger CO₂ sorption capacity of Brazilian coal samples. The Ohio shale has larger illite and mica contents as well as higher amounts of chlorite, plagioclase pyrite and quartz. Illite is reported to have a higher CO₂ sorption capacity compared to kaolinite (Busch et al., 2008). However, the sum of kaolinite and illite content is higher for the coal samples as compared to the Ohio shale. The higher carbonate content of the coals could also contribute to higher CO₂ sorption capacities through carbonate dissolution. However, this assumption is based on few literature data of coal samples. To better understand the variation of CO₂ sorption capacity of mineral matter, a more thorough mineralogical characterization of Santa Terezinha coal samples and shale samples in combination with isotherm measurements is

required. Particularly for high-ash coals and carbonaceous shales carbon dioxide adsorption on the mineral matter cannot be neglected and therefore normalization to a dry, ash-free basis is not appropriate.

5.6.7. Effect of moisture on sorption isotherms

It is well known that the moisture content of a coal significantly influences its methane sorption capacity (Joubert et al., 1973; Yalcin and Durucan, 1991; Crosdale et al., 2008; Day et al., 2008a). To investigate the effect of moisture, in addition to the measurements on the “as received” sample, methane and CO₂ sorption isotherms were measured on one coal (sample 07_166) in the moisture-equilibrated state (Figs. 5.14 and 5.15). The equilibrium moisture content of this sample was 2.44 wt.%, while the hygroscopic (“as-received”) moisture content was 0.98 wt.%. The methane sorption capacity of the moisture-equilibrated coal sample is significantly lower (0.30 mmol/g; 0.53 mmol/g, daf) than the sorption capacity of the “as received” sample (0.57 mmol/g; 0.99 mmol/g, daf). This corresponds to a reduction by 45%. For carbon dioxide the maximum excess sorption of the moisture equilibrated sample was 0.28 mmol/g, which is 56% lower than for the “as received” coal (0.64 mmol/g). This indicates a stronger competition for sorption sites (*e.g.* with functional oxygen groups) between water and CO₂ than for methane, which is in contrast to observations by Day et al. (2008a), who found that water saturation caused a stronger reduction of sorption capacity for methane than for carbon dioxide for a high volatile bituminous Australian coal (Hunter Valley, Australia, VR_{max}=0.8%). The authors suspect that clusters of water molecules attach to pore-surfaces with polar sites, which then can become inaccessible for other adsorbates. CO₂ is considered to be able to adsorb on top of the polar water clusters, whereas CH₄ is limited to hydrophobic sorption sites and thus, the reduction of methane sorption capacity would be greater than the reduction of CO₂ sorption capacity. This effect diminished for a high rank coal (Illawara, Australia, R_{max}=1.4%) with fewer polar sorption sites. Day et al. (2008a) also argue that the smaller kinetic diameter of CO₂, compared to CH₄ would allow carbon dioxide to enter some of the blocked pores, which methane could not access. The observation in the present study, that moisture equilibration results in a stronger reduction of CO₂ sorption capacity as compared to methane is based on only one sample; further investigations are needed to examine this effect in more detail.

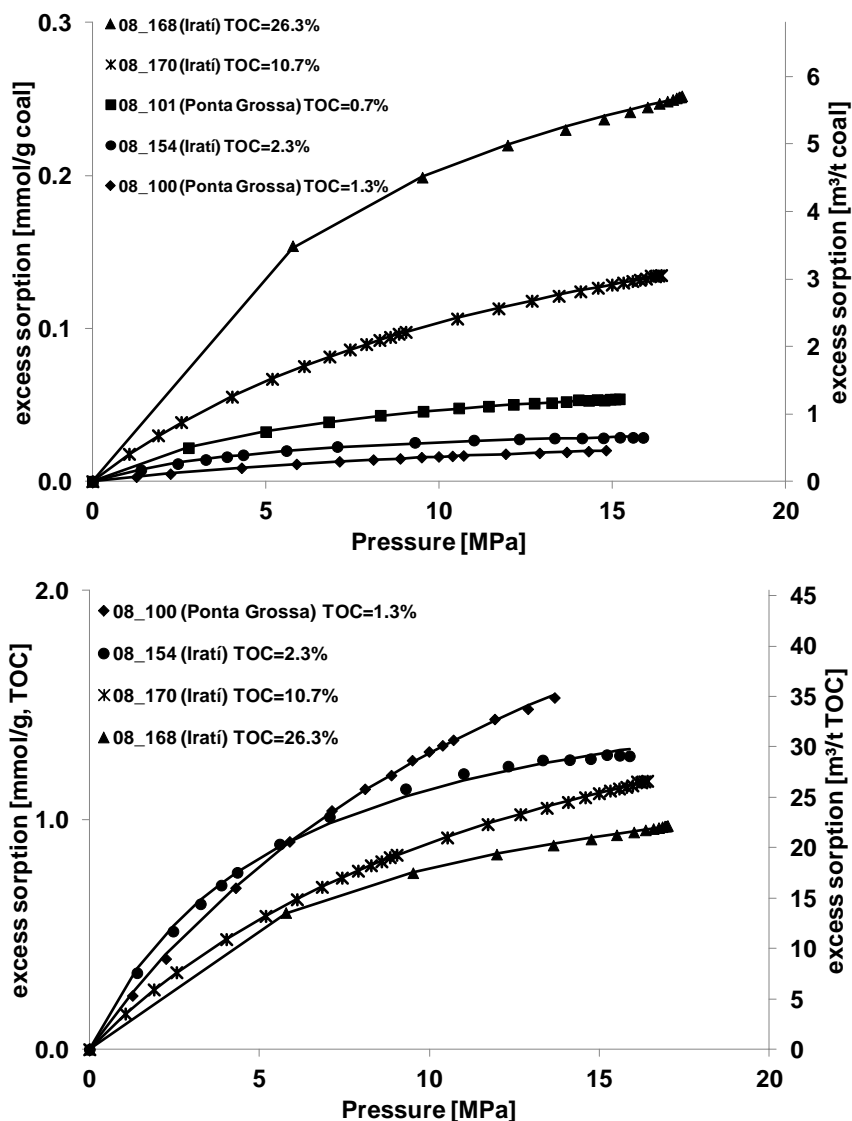


Fig. 5.8 Methane sorption isotherms with Langmuir approximations (solid lines) for Permian (Irati) and Devonian (Ponta Grossa) shale samples on a raw basis (top) and TOC basis (bottom, sample 08_101 with TOC<1% not included).

5.6.8. Effect of coal maceral composition on sorption isotherms

The effect of maceral composition on methane and carbon dioxide sorption on coals is attributed to differences in microporosity of the macerals. Vitrinite is predominantly microporous, whereas inertinite is rather meso- to macroporous (Lamberson and Bustin, 1993). Some authors report a significant influence of maceral composition on sorption capacities (*e.g.* Lamberson and Bustin, 1993; Mastalerz et al., 2004; Chalmers and Bustin, 2007), whereas others could not observe such a relationship (*e.g.* Krooss et al., 2002; Faiz et al., 2007; Day et al., 2008b). To compare the effect of coal composition on sorption, isotherms have to be normalized to a dry ash-free basis. Lamberson and Bustin (1993) report increasing methane sorption with increasing vitrinite content on medium-volatile coals from British Columbia. Chalmers and Bustin (2007) report higher methane sorption capacity for liptinite-rich coals with low microporosity, where methane is held as solution gas. Mastalerz et al. (2004) observed a relationship between maceral composition of coals from Indiana (high volatile bituminous C) and CO₂ sorption capacity, measured at 2.8 MPa (400 psi) and 17 °C (62 °F). They found increasing CO₂ sorption capacities for coals with higher vitrinite content and suggest that

telocollinite content may be of greatest influence on CO₂ sorption capacity of all macerals. Coals with higher liptinite content showed lower CO₂ sorption capacities. No correlation between methane or carbon dioxide sorption capacity and petrographic composition of coal was observed for coals and carbonaceous shale samples analysed in the present study (*Fig. 5.16*). As mentioned in section 5.6, the normalization of carbon dioxide sorption isotherms, measured on high-ash coals, to the dry, ash-free basis is prone to overestimation of sorption capacity, which could mask a correlation of CO₂ sorption capacity with maceral composition. Laxminarayana and Crosdale (1999) found that the influence of maceral composition on gas adsorption decreases with increasing rank. The high rank of some coals analysed in this study (high volatile A bituminous–anthracite) might explain why no correlation with maceral composition was observed.

5.6.1. Effect of maturity on sorption isotherms

Previous studies report that methane sorption capacity decreases with increasing rank to a minimum in the medium-volatile bituminous range, followed by an increase with increasing rank (Yalcin and Durucan, 1991; Faiz et al., 2007). This effect has also been observed for carbon dioxide sorption capacity (Busch et al., 2003; Day et al., 2008b). With increasing thermal maturity from mediumvolatile bituminous to anthracite rank, the microporosity of coal increases (Bustin and Clarkson, 1998; Prinz and Littke, 2005; Chalmers and Bustin, 2007). Since most of the physical adsorption takes place in the micropore structure of coal (Yalcin and Durucan, 1991), the increase in microporosity with increasing rank is also considered to cause an increase in sorption capacity from medium volatile bituminous coal to anthracite. In the present study no correlation was found between methane or carbon dioxide sorption and maturity (*Fig. 5.17*).

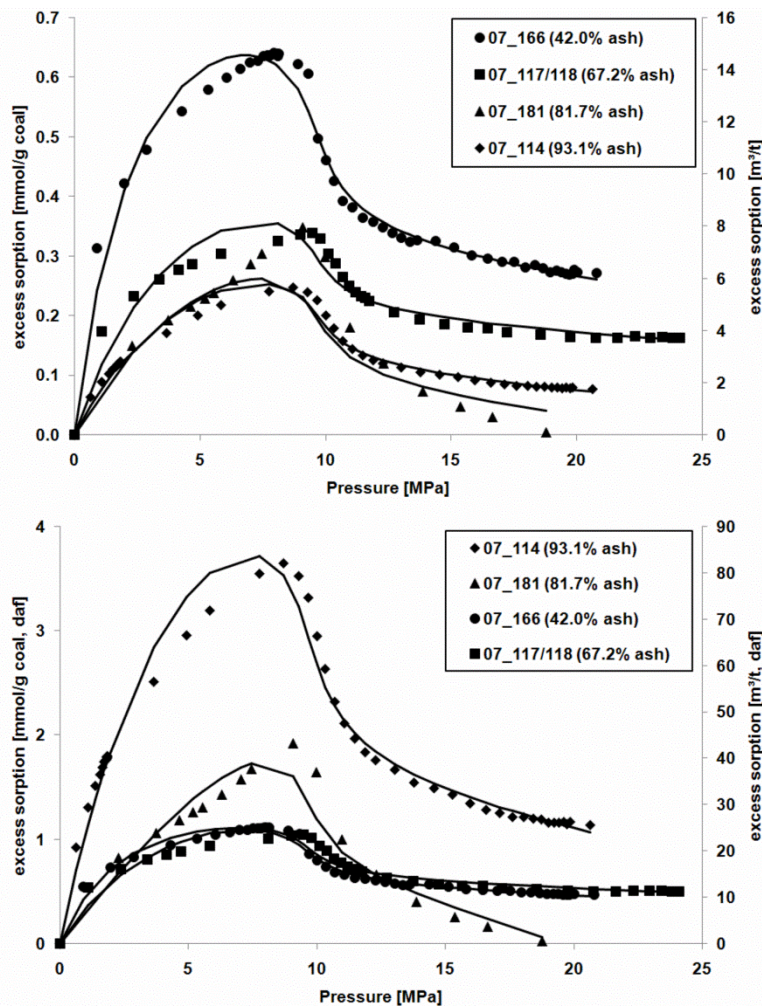


Fig. 5.9 Carbon dioxide sorption isotherms for coal and carbonaceous shale samples from well CBM-001-ST-RS on a raw basis (top) and dry, ash-free basis (bottom), measured at 45 °C.

5.6.2. Evaluation of potential for carbon dioxide sequestration and enhanced coalbed methane (CO₂-ECBM) and shale gas recovery (CO₂-ESG)

Sorption capacities for CO₂ on coals and shales are generally higher than for CH₄. Sorption capacities of samples from the CBM-001-ST-RS well (¹n_i) for an average reservoir pressure of 6.25 MPa, range between 0.29 and 0.73 mmol/g (6.66–16.63 m³/t) for carbon dioxide and between 0.04 and 0.34 mmol/g (0.95–7.72 m³/t) for methane. The sorption capacity ratios (V_LCO₂/V_LCH₄ at 6.25 MPa) range between 2.0 and 7.0 (average 3.6). Ratios of maximum excess sorption amounts (n_{max}CO₂/n_{max}CH₄) range between 1.4 and 4.6 for the coal and carbonaceous shale samples from the CBM well. For the Permian (Irati) and Devonian (Ponta Grossa) shales these ratios range between 2.1 and 10. Results from the present study suggest that coal seams in the Santa Terezinha Coalfield are generally under-saturated in methane, which means that the current gas content is lower than the measured sorption capacity. The free sorption capacity, not occupied by methane, could possibly be used for storage of carbon dioxide. Depending on the economical and market situation the methane present in the coals could be produced prior to CO₂ injection. Simultaneous injection of CO₂ for ECBM is considered less promising because the produced gas would have a low calorific value due to co-production of injected CO₂ (cf. van Bergen et al., 2008, 2009). In a first approach to estimate the effective CO₂ storage capacity of a CBM reservoir, a calculation similar to the

assessment of producible gas in place (PGIP) from initial gas in place (IGIP) (Eq. 3) can be applied (van Bergen et al., 2001):

$$PGIP = RF \cdot C \cdot IGIP \quad (3)$$

Here the producible part of the gas in place is estimated using a recovery factor (RF) and estimating a completion factor (C). The recovery factor represents the amount of gas that can technically be produced by reducing the reservoir pressure through water production. The completion factor (C) represents an estimation of the part of coal seams that can be accessed by drilling operations.¹

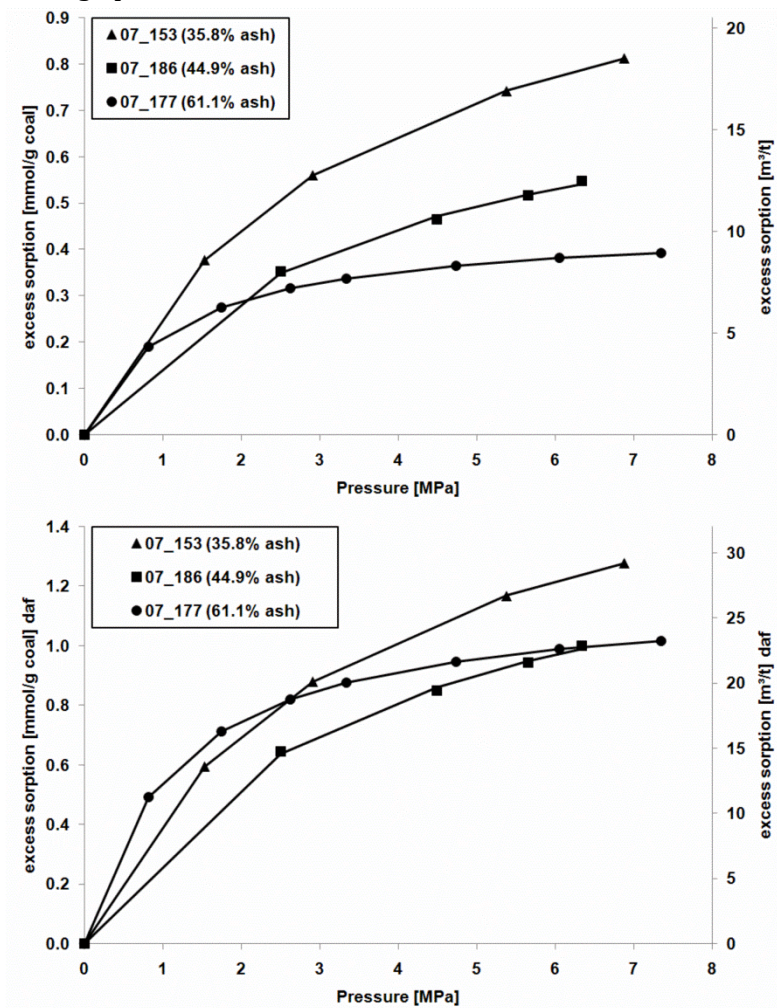


Fig. 5.10 Carbon dioxide sorption isotherms for coal and carbonaceous shale samples from CBM well 001-ST-RS on a raw basis (top) and dry, ash-free basis (bottom), measured at 35 °C. Solid lines represent Langmuir fit.

Hendriks et al. (2004) estimated the global carbon dioxide storage potential in various underground reservoirs. For the CO₂ storage capacity (SCO₂) in coal basins during ECBM operations they used the following equation:

$$SCO_2 = PGIP \cdot ER \cdot \rho_{CO_2} \quad (4)$$

PGIP = producible gas in place (standard conditions) [m³]

¹ In mmol/g rock; not daf-normalized

ER = exchange ratio [-]

ρ_{CO_2} = CO₂ density at standard conditions [1.977 kg/m³].

The amount of producible gas in place (PGIP) is estimated according to:

$$PGIP = A \cdot TH \cdot \rho_{coal} \cdot GC \cdot RF \cdot CF \quad (5)$$

A = area of the coal basin [m²]

TH = cumulative thickness of coal seams [m]

ρ_{coal} = coal density [t/m³]

GC = gas content [m³/t]

RF = recovery factor [-]

CF = completion factor [-].

In Eq. (5) the initial gas in place is calculated by multiplying the total mass of coal ($A \cdot TH \cdot \rho_{coal}$) by the average gas content (GC). Hendriks et al. (2004) conservatively assumed that only 10% of the total area of a coal basin can be used for CO₂ storage and thus they used a completion factor of 0.1. The recovery factor usually ranges between 20% and 60% (van Bergen et al., 2001). For the case of CO₂ sequestration, the recovery factor represents the storage efficiency. It was conservatively assumed to be 40% by Hendriks et al. (2004).

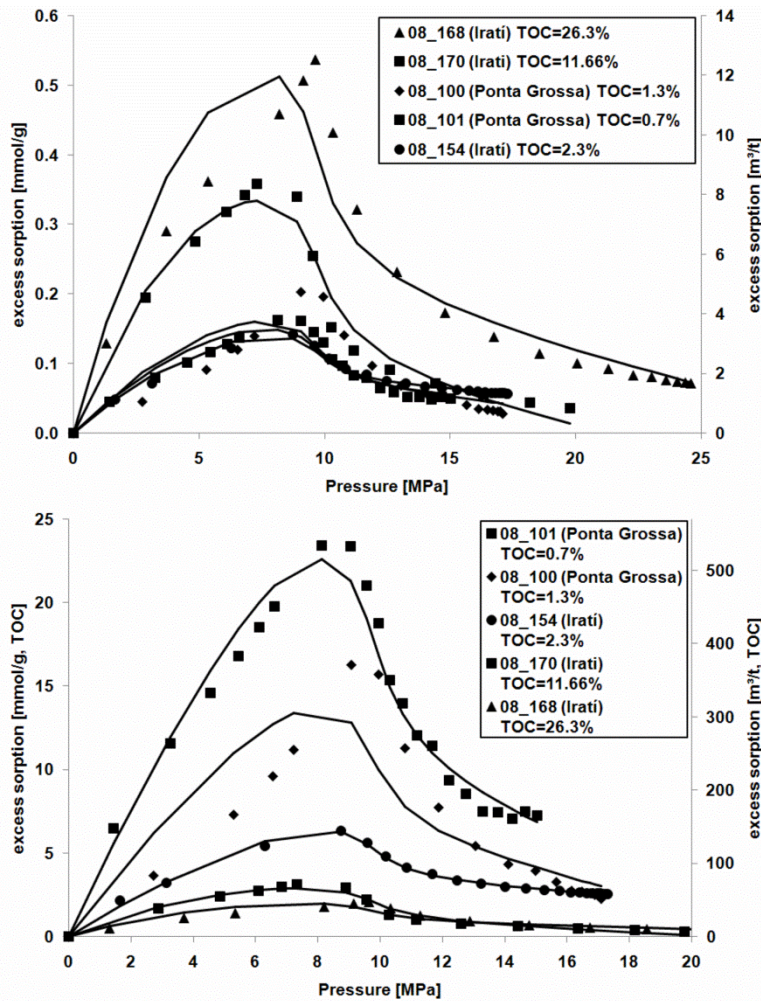


Fig. 5.11 Carbon dioxide sorption isotherms for Permian (Iratí) and Devonian (Ponta Grossa) shale samples on a raw basis (top) and TOC basis (bottom), measured at 45 °C.

To estimate the CO₂ storage capacity of the study area in the Santa Terezinha Coalfield, we used Eq. (5), assuming the same recovery factor and completion factor used by Hendriks et

al. (2004). Based upon 3D geological modelling for a study area of approx. 20×40 km in the Santa Terezinha Coalfield, Kalkreuth et al. (2008b) calculated the total mass of coal in the coal-bearing sequence to be in the order of $5.46 \cdot 10^9$ t. The average gas content of this area is $1 \text{ m}^3/\text{t}$ (Kalkreuth et al., 2008b). From sorption isotherm measurements for CO_2 and CH_4 , an average exchange ratio of 3.6 was calculated.

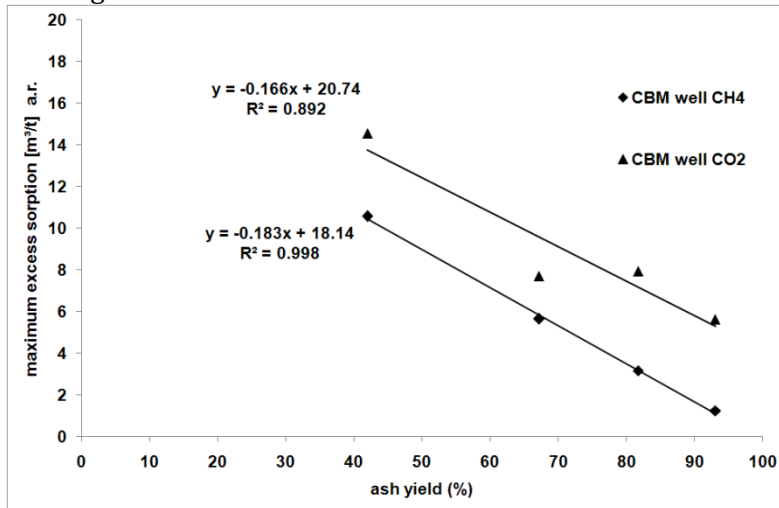


Fig. 5.12 Maximum excess sorption capacities (45 °C) of methane and carbon dioxide as a function of ash yield for coals and carbonaceous shales from CBM well 001-ST-RS.

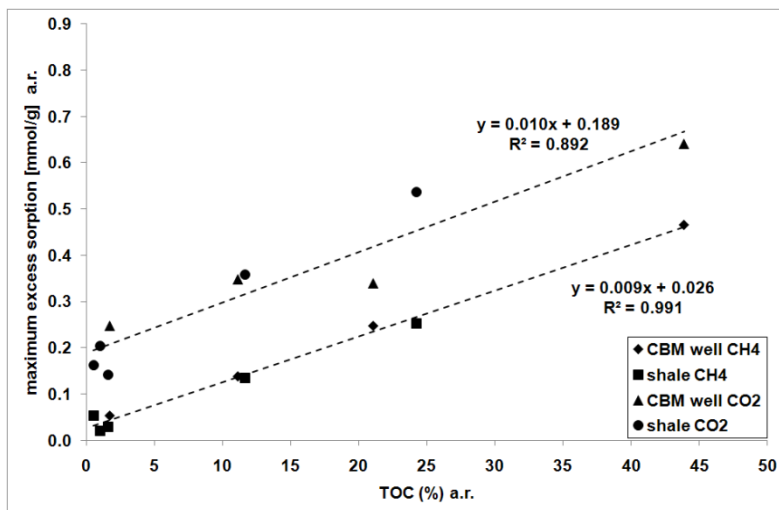


Fig. 5.13 Maximum excess sorption capacities for methane and carbon dioxide (8–12 MPa pressure range, 45 °C) vs. TOC contents of coal and shale samples from CBM-001-ST-RS well and Permian (Irati) and Devonian (Ponta Grossa) shale samples.

The CO_2 storage capacity for a $20 \times 40 \text{ km}^2$ area in the Santa Terezinha Coalfield has been estimated using Eq. (5). For the case of replacing sorbed methane by CO_2 injection, the storage potential of the study area would then amount to 1.55 Gt. For a mean reservoir pressure of 6.25 MPa, the average sorptive storage capacity for CO_2 is 0.43 mmol/g ($9.86 \text{ m}^3/\text{t}$). Considering carbon dioxide sequestration only, e.g. keeping the gas currently stored in the coal ($1 \text{ m}^3/\text{t}$) in place, the remaining “free” CO_2 sorption capacity of $8.86 \text{ m}^3/\text{t}$ could be used for CO_2 storage. Assuming a recovery factor of 40%, the above calculation then yields a total CO_2 storage capacity of 13.8 Gt in the coals of the study area. In a combined CBM production and CO_2 storage operation, a mass of 15.4 Gt CO_2 could theoretically be stored in the study area of the Santa Terezinha Coalfield as defined by Kalkreuth et al. (2008b). To refine this very simplistic calculation of the CO_2 storage potential of the Santa Terezinha Coalfield, additional factors

affecting CBM production (*e.g.* water saturation), injection (*e.g.* permeability) and storage (presence and integrity of sealing formations) as well as potential environmental safety and health problems associated with CO₂-ECBM need to be considered (Bachu, 2007; White et al., 2005).

5.7. Conclusions

To evaluate the sorptive storage capacity of the Paraná Basin in Brazil, methane and carbon dioxide sorption experiments were performed on coal and carbonaceous shale samples from a CBM test well, drilled in 2007 in the Santa Terezinha Coalfield. Additionally, storage capacities were determined on samples of the two major petroleum source rocks of the basin: the Devonian Ponta Grossa Formation and the Permian Irati Formation. Experiments were performed on powdered samples at pressures up to 25 MPa and temperatures of 35 °C and 45 °C. The present study reports the first comprehensive set of high-pressure sorption data for methane and carbon dioxide for coals, carbonaceous shales and petroleum source rocks of the Paraná Basin, Brazil. On a raw mass basis (“as received”, *i.e.* not dry, ash-free normalized), the Langmuir sorption capacities of methane on coal and carbonaceous shale from the CBM well ranged between 0.05 and 0.47 mmol/g. For the shale source rocks they were lower, ranging between 0.04 and 0.37 mmol/g. For carbon dioxide the maximum excess sorption, reached in the 8–12 MPa interval, ranged between 0.25 and 0.81 mmol/g for coal and carbonaceous shale samples, and between 0.14 and 0.54 mmol/g for shale source rocks. Normalized to dry, ash-free mass, methane sorption capacities of shales exceeded those of coal and carbonaceous shale. Methane and carbon dioxide sorption capacities of coal and shales correlated with the organic carbon content (TOC). For carbon dioxide the linear regression showed a non-zero intercept, indicating a significant sorption capacity of the mineral matter. This was not the case for methane.

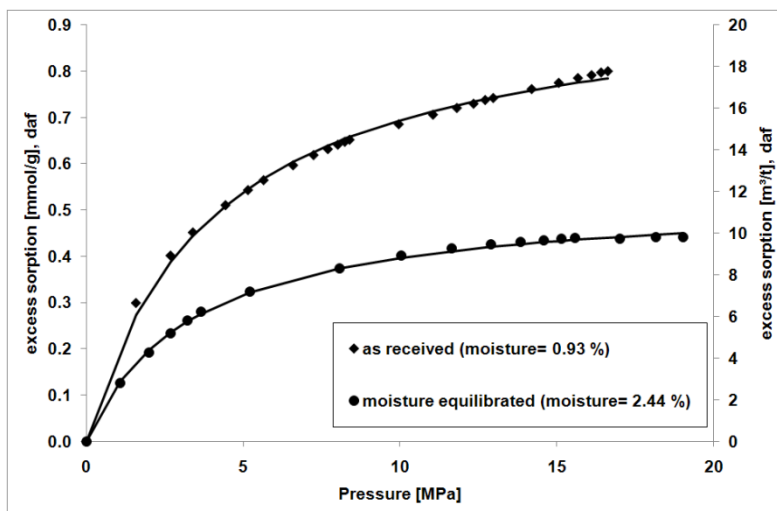


Fig. 5.14 Effect of moisture on methane sorption for coal sample 07_166. At equilibrium moisture (2.44%) the sorption capacity is 45% lower as compared to the “as received” coal (moisture content: 0.93%). Solid lines represent Langmuir fit.

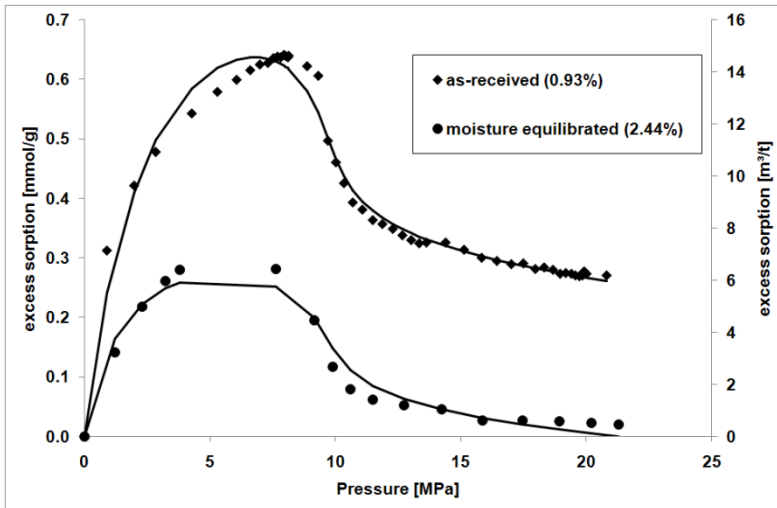


Fig. 5.15 Effect of moisture on carbon dioxide sorption for coal sample 07_166 from CBM well ST-RS-001. At equilibrium moisture (2.44%) the sorption capacity is 56% lower as compared to the “as received” coal (moisture content: 0.93%). Solid lines represent 3-parameter fit.

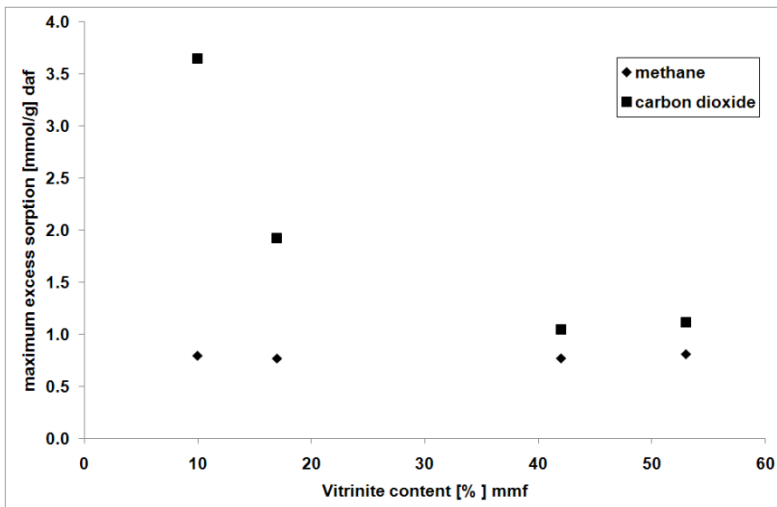


Fig. 5.16 Maximum excess sorption of capacity of methane and carbon dioxide vs. vitrinite content for coal samples from well CBM-001-ST-RS.

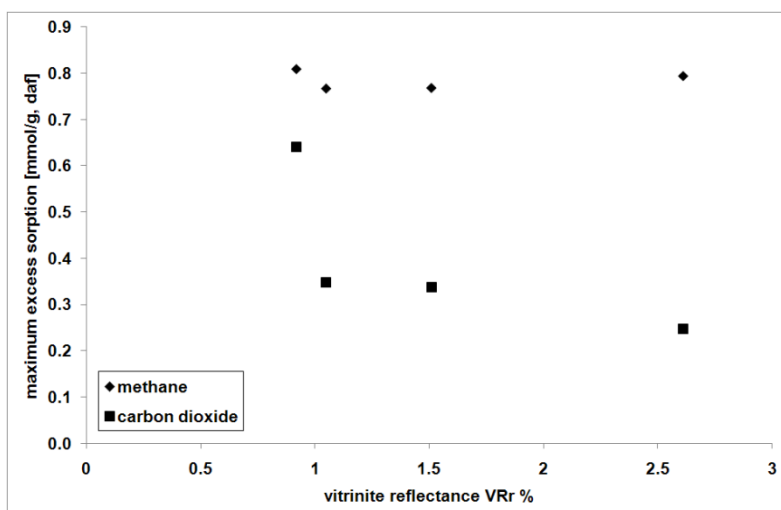


Fig. 5.17 Maximum excess sorption of capacity of methane and carbon dioxide vs. vitrinite reflectance for coals from well CBM-001-ST-RS.

The present-day gas content of coals analysed from the first CBM well in the Santa Terezinha Coalfield, as determined from canister desorption, amounts to 13–38% of the methane sorption capacity measured on “as-received” samples. Experiments on one coal sample from seam interval D (collected from a depth of 620.8 m) after moisture equilibration showed that its sorption capacity was reduced by 46% for methane and by 56% for CO₂ as compared to the “as received” state. No correlation between sorption capacity and coal composition or thermal maturity was observed. Carbon dioxide sorption capacity was higher than methane sorption capacity for all samples. The CO₂/CH₄ sorption capacity ratio was larger for coal and carbonaceous shales (1.9–6.9) than for source rock shale samples (1.4–4.5). Sorption capacities calculated for reservoir conditions indicated that theoretically an amount of 13.8 Gt carbon dioxide can be stored in coal seams of the study area. This amount would increase to 15.4 Gt, if all methane were produced from coal seams prior to carbon dioxide injection. In a further step, geological factors such as permeability, presence and integrity of sealing formations and economic factors such as depth and number of wells, costs for transport and injection of CO₂, that influence carbon dioxide storage, need to be evaluated to provide a more realistic view on the feasibility of carbon dioxide storage in the Santa Terezinha Coalfield.

5.8. Acknowledgements

This study received financial support from El Paso/ANEEL and Petrobras. Two anonymous reviewers provided helpful comments and suggestions.

6. Final Discussion and Outlook

6.1. Origin and composition of coal-related gas

Numerous gas samples from mine faces as well as desorbed from coals of the Upper Silesian Coal Basin were analyzed during the present study. Results of chapter 2 showed that microbial gas is associated with coal seams of the Pennsylvanian Karviná Formation, whereas thermogenic gas is associated with coal seams of the Mississippian Ostrava Formation, confirming results from earlier studies in the USCB. Apart from this general pattern, no correlation between gas composition and stratigraphy or coal rank was observed. Analyses of gas samples taken during desorption experiments, did not reveal any influence of sorption / desorption processes on gas composition. The composition of coal-related gases desorbed from drilling cores of a CBM well in the Santa Terezinha coalfield, Brazil, indicates a mixture of gases from thermogenic and microbial sources (*Fig. 6.1*).

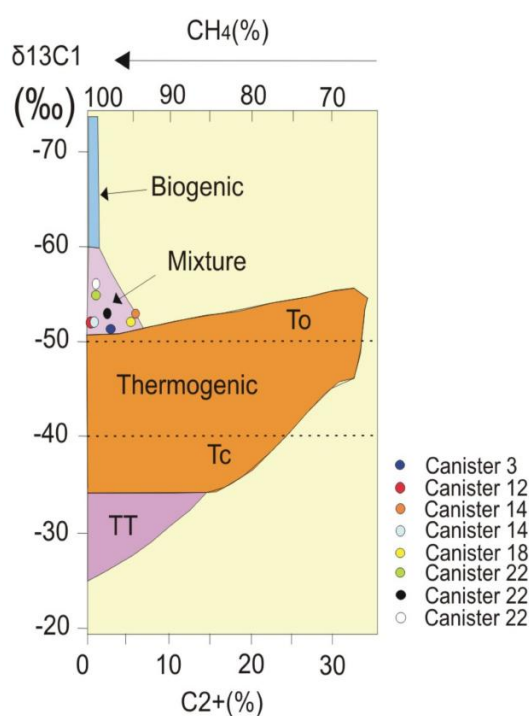


Fig. 6.1 Composition of gas from canister desorption of samples from the CBM well, drilled in the Santa Terezinha coalfield, Brazil (from Kalkreuth et al., 2011 (submitted); modified from Schoell, 1983). To = gas associated with oil, Tc = condensate, TT = dry gas.

Difficulties associated with the sampling procedure that arose during the study of coal-related gas in the USCB showed that additional measurements using an improved method are required to confirm that sorption / desorption processes do not significantly alter the geochemical and stable isotopic signature of coal related gases.

For effective microbial gas generation, temperatures lower than 80 – 100°C are required and consequently, microbial methanogenesis could only start after coal seams were uplifted and reservoir temperatures finally dropped below this temperature threshold. For the Karviná Formation, paleotemperatures ultimately dropped below 100°C in early Permian, while reservoir temperatures of coal seams of the Ostrava Formation were less favourable (*Fig. 6.2*). Coal from the Petrkovice and lower Hrusov Member reached temperatures > 80 – 90°C during

Miocene (Carpathian overthrust), resulting in paleopasteurization. Thermogenic gas generation, however, was not reinitiated during this reburial.

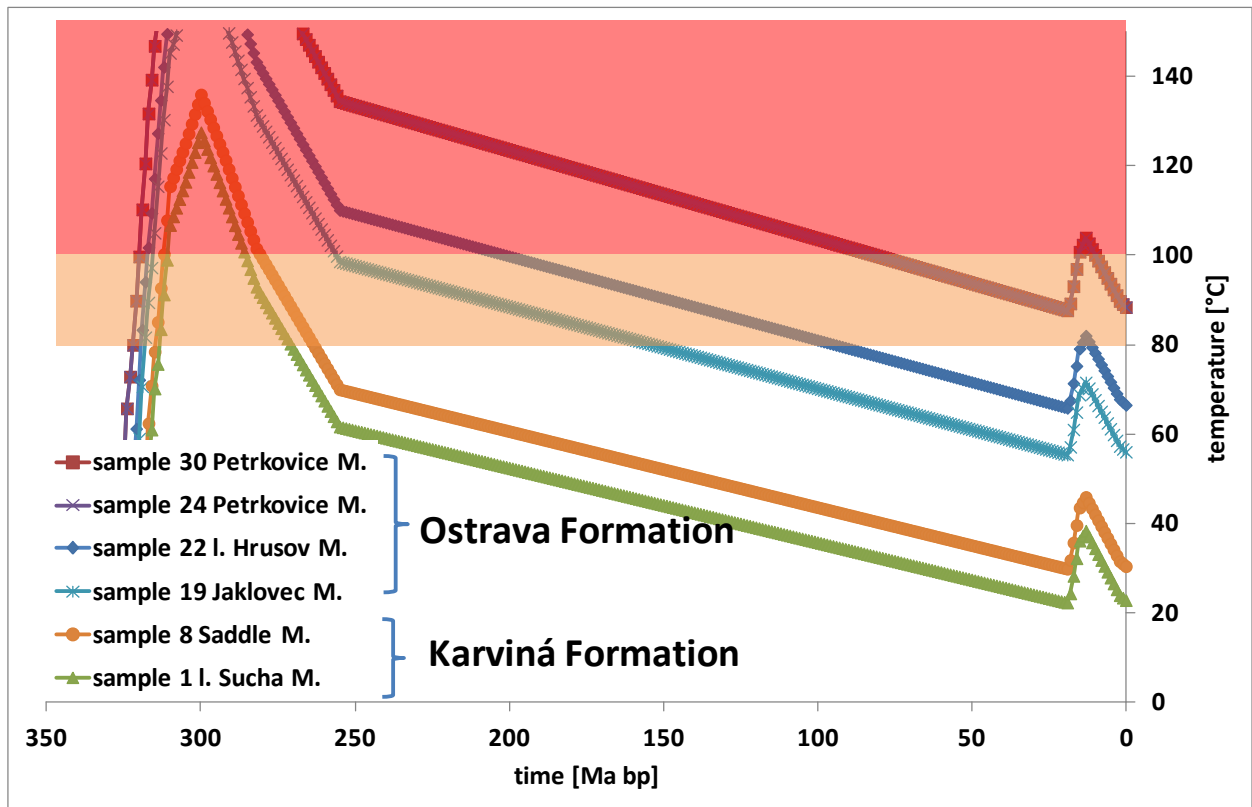


Fig. 6.2 Temperature history of coal-bearing formations in the USCBA showing that temperature conditions in the Ostrava Formations were less favourable for microbial methanogenesis than for sediments of the Karviná Formation.

From this information it can be concluded that, while all coal seams still have enough gas generation potential, temperature conditions were more favourable for microbial gas generation in coals of the Karviná Formation than for the Ostrava Formation.

Recent studies on microbial gas generation in coal seams in Poland (Kotarba and Pluta, 2009) and the Illinois Basin, USA (Strapoc et al., 2007) linked the timing of meteoric water percolation into coal-bearing sediments to microbial gas generation. On the one hand, meteoric waters dilute basinal brines and introduce nutrients for microbial activity and on the other hand, methanogenic microbes can be transported with percolating meteoric waters into coal beds. Kotarba and Pluta (2009) discuss that meteoric waters percolated into coal bearing sediments in the USCBA during early Jurassic and until the Miocene. These waters might have introduced microbes and nutrients enabling microbial gas generation until the marine transgression during the Miocene, and the associated increase in salinity impeded microbial activity. This is most likely also the case for coal bearing sediments of the Karviná Formation in the Czech part of the basin. Without detailed hydrogeologic information, *e.g.* composition of formation waters and occurrence and timing of meteoric water percolation, the exact origin and timing of microbial gas generation remains speculative. Differences in overburden sediments, *e.g.* permeable molasse sediments above the Karviná Formation compared to lower permeable flysch nappes of the Carpathian overthrust above parts of the Ostrava Formation might have favored percolation of meteoric water and microbial gas generation in the Karviná Formation.

Results from this study demonstrate that integration of experimental data on reaction kinetics and sorptive storage capacity into numerical basin modelling provides a useful tool for the reconstruction of gas generation history and the evolution of gas storage capacity. This information can improve the understanding of the distribution of different gases and gas mixtures in sedimentary basins.

6.2. Gas generation

Results of pyrolysis experiments and reaction kinetic modelling in the present study showed that coal seams of the USCB have generated significant amounts of thermogenic gas during late Carboniferous between 320 and 290 Ma at temperatures <210°C. At the time of gas generation the amount of generated gas exceeded the sorption capacity, *e.g.* 0.15 mmol/g (3.4 m³/t) at 292 Ma for coal from the Saddle Member. At present day, coals still have significant methane generation potential and also 'free' sorptive storage capacity. On the one hand, this remaining generation capacity can allow microbial gas generation from the coal organic matter, if the required conditions (temperature, nutrients) are met and methanogens are present in these sediments. The 'free' sorption capacity of these coals on the other hand would allow storage of a significant amount of microbially generated gas before expulsion and migration to the surface would occur.

6.3. Gas storage capacity

A large number of high-pressure sorption isotherms for methane and CO₂ on coal samples from the USCB was recorded under controlled temperature conditions and defined moisture state. These were used to establish functions that, in combination with pressure and temperature information from a 1-D basin model, could be used to model the dynamic evolution of the sorption capacity of coal seams in the study area over geologic time. These algorithms are useful complements to the reconstruction of gas generation history based on reaction kinetics and migration modelling. To improve the applicability of these calculations, experimental isotherms are required for temperatures >70°C. The increase of sorption capacity during uplift alone is not sufficient to explain the gas under-saturation of most coal seams, indicating that a significant amount of gas, generated during coalification, was lost during times of uplift and erosion.

Investigations of the sorption capacity and its controlling factors reported in chapters 4 and 5 indicate a significant correlation between coal rank and sorption capacity. Combination of these results with information from numerous analyses of coals from other European coal basins that were performed in our laboratory supports the control of coal rank on methane sorption capacity (*Fig. 6.3*).

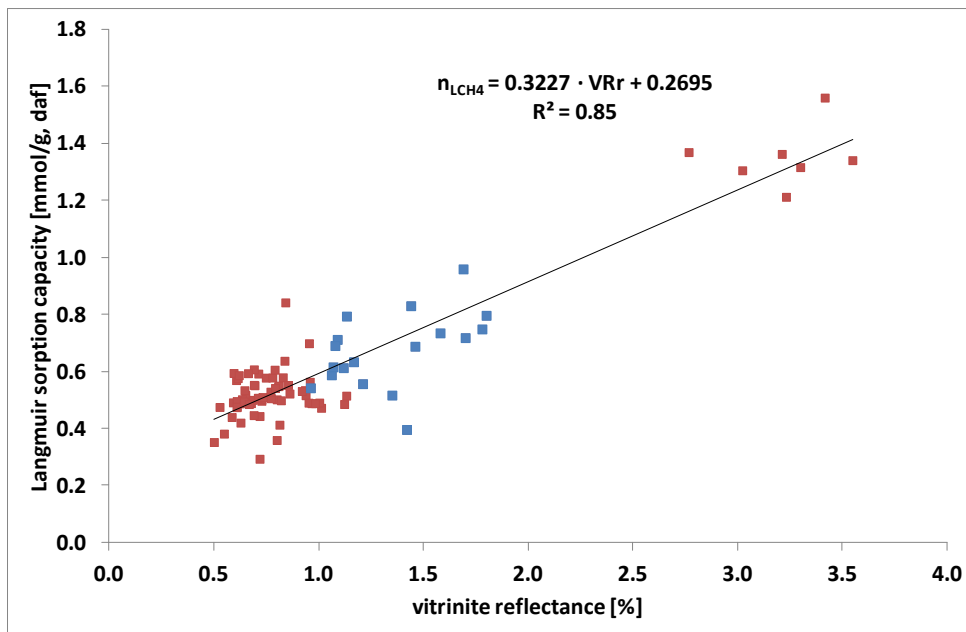


Fig. 6.3 Relationship between methane sorption capacity (n_L) and coal rank for Carboniferous coals from different European basins (blue squares represent samples from the USCB analysed in the present study).

Especially the variation of hygroscopic moisture and equilibrium moisture with increasing coal rank becomes more obvious, when considering a large rank interval from sub-bituminous coal to anthracite stage (Fig. 6.4). The hygroscopic moisture decreases with increasing coal rank between sub-bituminous and high volatile bituminous rank. With further increase in coal rank, the hygroscopic moisture shows a small increase, but generally stays below 4 wt.%. The equilibrium moisture of coal (moisture holding capacity), is reported to correlate with the 'in-situ' bed moisture of coal seams (Alpern et al., 1989). In contrast to the hygroscopic moisture, the equilibrium moisture shows a more significant increase in the high rank range (Fig. 6.4). These observations are in line with results from previous studies (Teichmüller and Teichmüller, 1979; Prinz et al., 2004; Levy et al., 1997; Day et al., 2008a).

The change in moisture content with increasing coal rank is believed to be related to the amount of functional oxygen groups and the formation of water clusters (Joubert et al., 1974; Prinz and Littke, 2005; Day et al., 2008a). The loss of oxygen groups and changes in the pore space during coalification result in a decrease in porosity and micropore volume towards medium volatile bituminous rank. Structural changes above 1.5% VRr lead to an increase in microporosity and micropore volume accessible for water, which results in a gradual increase of moisture in the high-rank range (Prinz and Littke, 2005).

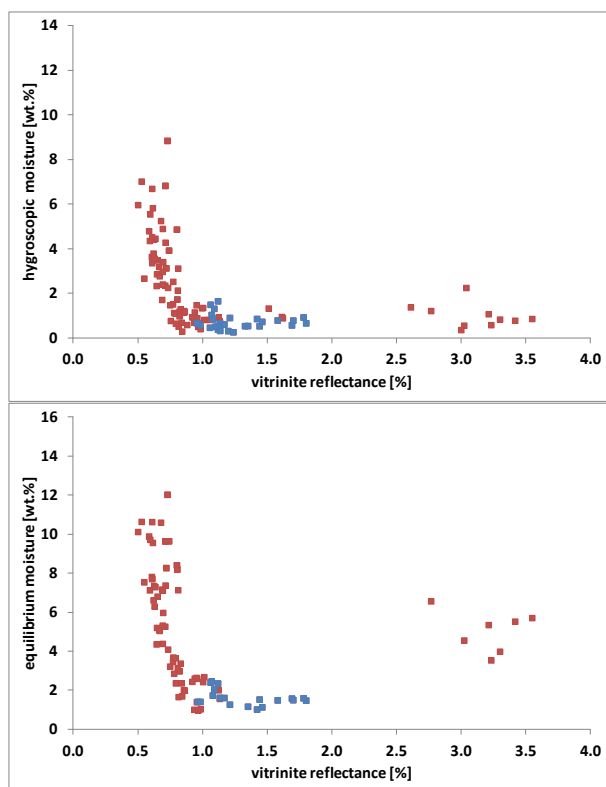


Fig. 6.4 Variation of “as-received” (hygroscopic) moisture (left) and equilibrium moisture (right) with coal rank for Carboniferous coals from different European basins (blue squares represent samples from the USCB analysed in the present study).

6.4. Comparison of sorption capacity of coals from the Upper Silesian Coal Basin and the Paraná Basin

The Permian Paraná Basin coals were deposited under different paleoenvironmental conditions than the Central European Carboniferous coals. Carboniferous coals of the northern hemisphere (Euramerica), such as those from the USCB, were deposited in a paralic environment under tropical conditions, whereas Permian coals of the southern hemisphere (Gondwana) were deposited under different (colder) paleoclimatic and depositional conditions (Diessel, 1992; DiMichele et al., 2009). The differences in plant organic matter affect the maceral composition and the geochemistry of such coals, *e.g.* liptinite from Gondwana coal can be different from liptinite from Euramerican coal. However, the geochemical composition of coal organic matter was not analyzed in detail in the present study. Despite a likely difference in organic matter composition, no correlation was observed between maceral composition and sorption capacity for coal from the USCB and the Paraná Basin. Both coals show a similar negative correlation between sorption capacity and ash yield (mineral matter content), indicating that the diluting effect of inorganic matter is the controlling factor for sorption capacity. Comparison of the rank dependence observed for coal from the USCB with results from the Paraná Basin shows that no or only a weak rank correlation exists for the Brazilian coal (Fig. 6.5). This could be related to differences in the coalification process for these coals. While coalification for the European coals was controlled by slow heating during burial ($T < 300^{\circ}\text{C}$), the high rank of some of the Brazilian coals was induced by volcanic activity and thus by exposure to high temperatures for a relatively short period of time. The increasing sorption capacity of bituminous coals with increasing coal rank is related to an increase in micropore volume, associated with changes during coalifications (Prinz et al., 2005). The lack of correlation between coal rank and sorption capacity for Brazilian coals could indicate that the coalification

process for these coals did not increase the micropore volume, or that micropores are ‘plugged’, *e.g.* by generated bitumen. Further investigations are required to create a statistically more significant dataset and to improve the understanding of different coalification processes on gas sorption capacity.

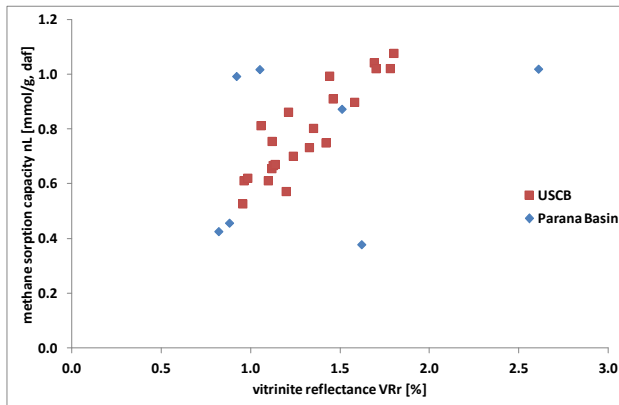


Fig. 6.5 Comparison of the influence of coal rank (vitrinite reflectance) on methane sorption capacity for coal from the Upper Silesian Coal Basin with coal from the Paraná Basin.

6.5. Outlook and Recommendation

In the present study a wide range of analyses were performed to investigate the gas composition, gas generation processes as well as the gas storage potential and influence factors of coal and reservoir properties on gas storage. Results of these investigations showed that some questions still remain open. The main questions that are still not satisfactorily answered are:

1. To what extent was the isotopic composition of coal related gas influenced by migration processes? Can light methane be the result of migration rather than of a different generation process?
2. What is the amount of gas generated by present day microbial gas generation from coal seams and what are the generation rates? Can microbial gas generated from coal seams be considered as a “regenerative energy source”?
3. How exactly did basin evolution influence the gas storage capacity of coal seams in the USCB? When and for how long was gas expelled from coal seams and lost to the atmosphere during the period of erosion and uplift?
4. How does the influence of coal rank on sorption capacity of gas or water change over the entire coalification range in the USCB?
5. Is the influence of coal rank and coal composition on gas sorption capacity different for Gondwana coals than for Euramerican coals?
6. What is the shale gas potential of organic-rich shales in the Upper Silesian Coal Basin in Czech Republic?
7. What is the environmental impact of exploration and production of coalbed methane and shale gas?

These principal questions are now briefly discussed and additional studies or measures to improve the understanding of these issues are recommended.

6.6. Gas composition and generation

Geochemical and stable isotopic analyses performed in the present study showed, that sampling procedures need to be improved in order to assess the influence of sorption/desorption processes on gas composition. Recent studies recommend purging coal samples with inert gas (Argon) during sampling, to avoid contamination with air that may result in oxidation and alteration of the gas composition during canister desorption experiments (Jin et al., 2010). Additional analyses and canister desorption experiments using such an improved method are required to evaluate the influence of sorption/desorption processes on the gas composition. Stable isotope analyses of coal-related gas can significantly be improved by including hydrogen isotope composition, especially to differentiate between different processes of microbial gas generation, as shown in recent studies on gas generated from coal and organic rich shales (Golding et al., 2010; Osborne and McIntosh, 2010; Strapoc et al., 2007, 2008, 2010). Additionally, the analysis of gas associated with the Oligocene Menilite Formation is required to evaluate whether thermogenic gas in coal seams of the USCB is mixed with gas from this source

6.7. Microbial gas

While several recent studies found evidence of active microbial gas generation in coal seams and abandoned coal mines (Hendry, 2006; Krüger et al., 2008; Faiz and Hendry, 2009; Penner et al., 2010), a quantitative assessment of microbial gas generation rates is still missing. Such a quantitative assessment of methanogenesis has been performed recently in laboratory experiments using methanogens extracted from recent lake sediments and peat swamps (Metje and Frenzel, 2007; Metje, 2006; Schwarz et al., 2008; Schwarz, 2007). Until the amount and the rate of microbial gas generation in present day coal seams is known, it remains speculative, whether microbial gas in coal seams represents a regenerative energy source. A possible enhancement of microbial gas generation from coal, *e.g.* by addition of nutrients or injection of more efficient microbial communities into coal seams is subject of current research projects, *e.g.* by CSIRO, Australia. Results of this research might show whether present day microbial gas generation in coal seams can yield commercial amounts of methane.

6.8. Basin history of the USCB

Pyrolysis experiments of coals of the Upper Silesian Coal Basin in the present study allowed estimation of the residual thermogenic gas generation potential of coal seams at a rank range between 1.0 and 1.7% VRr. To evaluate the amount of gas that was generated during the basin history, pyrolysis experiments of low-rank coals (<0.6% VRr) are required. Additionally, information on the basin evolution of the USCB, especially for the uplift phase between Permian and Tertiary, has to be improved. Apatite fission-track analysis provides information on timing and amount of uplift, which may be used to improve the reconstruction of the uplift history of a basin. Fission-track analysis has been successfully applied to reconstruct the uplift history of the northern Ruhr Basin (Karg et al., 2005) and could also be applied to improve basin history reconstruction of the USCB.

6.9. Influence of coal rank on sorptive gas storage capacity

From analyses of a large set of coal samples in the present study, correlations between coal properties and gas storage capacity could be derived. However, not the entire range of coalification in the study area could be covered. Additional measurements on low-rank coals (<1% VRr) as well as on coals of semi-anthracite and anthracite rank are required to improve

the assessment of gas storage capacity of coals for the entire basin. The influence of changes associated with coalification on gas and water sorption capacity could further be studied by characterization of the microporosity of coals, *e.g.* by low temperature adsorption of CO₂ or nitrogen (BET).

6.10. Comparison of European coals and Gondwana coals

The comparison of coal from the USCB and the Brazilian Paraná basin indicates differences in the influence of controlling parameters, such as coal rank, on gas storage capacity and gas generation potential. However, in the present study only few coals from Brazil were analyzed and studies on the CBM potential of coal in the Paraná basin are rare. Results from CBM exploration activities that are currently under way in southern Brazil could shed more light on controlling factors for CBM generation and storage, allowing a better comparison with other coal basins.

6.11. Shale gas

It has long been known that bituminous shales, *e.g.* from the Upper Carboniferous of the Ruhr Basin in Germany, have a significant potential as source rocks for thermogenic methane (Teichmüller et al., 1970). Even though shales contain a lower percentage of organic matter than coal, the significantly higher thickness and extension of shale formations may result in comparable or even higher yields of thermogenic gas. Recent technological developments have improved the production of shale gas and, as a consequence, exploration activities for shale gas or combined CBM and shale gas exploration are now under way in European basins. The analytical and experimental methods developed and applied in the present study for the evaluation of the potential for CBM in the USCB and in Brazil can also be adopted for the characterization of organic-rich shales to evaluate the shale gas potential of sediments in the USCB.

6.12. Environmental impact of coalbed methane and shale gas exploration

Recent studies investigated and discussed the environmental impact of shale gas and CBM exploration and production in the US. Especially a potential influence of reservoir stimulation techniques, such as hydraulic fracturing, on ground water quality is under debate (USEPA, 2004). A recent study by Osborn et al. (2011) reports that shale gas production in Pennsylvania and New York was associated with a significant increase in methane concentrations in drinking water. Contamination of drinking water and methane emissions to the surface that could reach explosive concentrations can pose a serious threat to the environment and the population. As a consequence of environmental concerns associated with unconventional gas exploration and production, several European countries put a moratorium on shale gas and CBM drilling and the use of hydraulic fracturing. Whether shale gas and CBM exploration and production activities in Europe are associated with environmental pollution remains speculative. Furthermore, the background emission of methane from unconventional reservoirs into aquifers and / or the atmosphere is only poorly understood. Detailed and independent monitoring studies of background methane concentrations and methane emissions, as well as water quality, before and during gas exploration and production activities are required to ensure the safety and sustainability of gas production from these unconventional resources. Furthermore, these studies should result in guidelines for the regulation and monitoring of gas drilling activities and finally improve the public acceptance and confidence in this technology.

7. References

- Alpern, B., Lemos de Sousa, M.J., Flores, D., 2002. Documented international enquiry on solid sedimentary fossil fuels; coal: definitions, classifications, reserves-resources, and energy potential. *International Journal of Coal Geology* 50, 3-41.
- Araújo, C.V., Corrêa da Silva, Z.C., Rodrigues, R., 1995. Petrographic and geochemical study of coals from Santa Terezinha Coalfield, Rio Grande do Sul, Brazil. *Revista Latino-Americana de Geoquímica Orogênica* 1, 28-45.
- Araújo, L.M., Rodrigues, R., dos Santos Scherer, C., 2004. Interrelação entre a fábrica sedimentar, o conteúdo orgânico e o potencial redox do ambiente deposicional, deduzida das litofácies de rampa distal das seqüências deposicionais da Formação Irati, Permiano da bacia do Paraná. *Boletim Geociências Petrobras* 12 (2), 429-434.
- Arets, L.A.G., Maas, W., Muysken, P.J., Stuffken, J., Wijffels, F.C.M., 1962. Het voórkomen van mijngas en de strijd tegen te hoge concentraties bij de staatsmijnen in Limburg. *Geologie en Mijnbouw* 41, 39- 86.
- Arri, L.E., Yee, D., Morgan, W.D., Jeansonne, M.W., 1992. Modeling coalbed methane production with binary gas sorption. SPE 24363, SPE Rocky Mountain Regional Meeting, 18-21 May 1992, Casper, Wyoming.
- ASTM D1412-1999 Standard Test Method for Equilibrium Moisture of Coal at 96 to 97 Percent Relative Humidity and 30 °C. ASTM International, West Conshohocken, PA.
- Bachu, S., 2007. Carbon dioxide storage capacity in uneconomic coal beds in Alberta, Canada: methodology, potential and site identification. *International Journal of Greenhouse Gas Control* 1, 374-385.
- Bae, J-S. and Bhatia, S.K., 2006. High-pressure adsorption of methane and carbon dioxide on coal. *Energy & Fuels* 20, 2599-2607.
- Barker-Read, G.R. and Radchenko, S.A., 1989. The relationship between the pore structure of coal and gas-dynamic behaviour of coal seams. *Mining Science and Technology* 8, 109-131.
- Barker, C.E. and Dallegge, T., 2006. Secondary gas emissions during desorption, Marathon Grassim Oskoloff-1 Well, Cook Inlet Basin, Alaska: implications for resource assessment. *Bulletin of Canadian Petroleum Geology* 54, 273-291.
- Begossi, R., Della Fávera, J.C., 2002. Catastrophic floods as possible cause of organic matter accumulation giving rise to coal, Paraná Basin, Brazil. *International Journal of Coal Geology* 52, 83-89.
- Bernard, B.; Brooks, J.; Sackett, W., 1976. Natural gas seepage in the Gulf of Mexico. *Earth and Planetary Science Letters* 31, 48-54.
- Berner, U. and Faber, E., 1996. Empirical carbon isotope/maturity relationships for gases from algal kerogens and terrigenous organic matter, based on dry, open-system pyrolysis. *Organic Geochemistry* 24, 947-955.

- Bertrand, P., 1984. Geochemical and petrographic characterization of humic coals considered as possible oil source rocks. *Organic Geochemistry* 6, 481-488.
- Boreham, C.J., Horsefield, B., Schenk, H.J., 1999. Predicting the quantities of oil and gas generation from Australian Permian coals, Bowen Basin using pyrolytic methods. *Marine and Petroleum Geology* 16, 165-188.
- Bostick, N.H. and Daws, T.A., 1994. Relationships between data from Rock-Eval pyrolysis and proximate, ultimate, petrographic, and physical analyses of 142 diverse U.S. coal samples. *Organic Geochemistry* 21, 35-49.
- BP, 2009. Statistical Review of World Energy. Internet Access, Date: 09.12.2009.
- BP 2011. BP Energy outlook 2030. London, January 2011. www.bp.com Internet access 18.12.2011.
- Busch, A., Gensterblum, Y., Krooss, B.M., 2003. Methane and CO₂ sorption and desorption measurements on dry Argonne premium coals: pure components and mixtures. *International Journal of Coal Geology* 55, 205-224.
- Busch, A., Gensterblum, Y., Krooss, B.M., Littke, R., 2004. Methane and carbon dioxide adsorption/diffusion experiments on coal: an upscaling- and modelling approach. *International Journal of Coal Geology* 60, 151-168.
- Busch, A., Alles, S., Gensterblum, Y., Prinz, D., Dewhurst, D.N., Raven, M.D., Stanjek, H., Krooss, B.M., 2008. Carbon dioxide storage potential of shales. *International Journal of Greenhouse Gas Control* 2, 297-308.
- Busch, A. and Gensterblum, Y., 2011. CBM and CO₂-ECBM related sorption processes in coal: A review. *International Journal of Coal Geology* 87, 49-71.
- Bustin, R., Cameron, A., Grieve, D., Kalkreuth, W., 1989. Coal petrology—its principles, methods and applications, Geological Association of Canada, Short Course Notes 3, Victoria, British Columbia, third edition. . May 8-10, 273 pp.
- Bustin, R.M., Clarkson, C.R., 1998. Geological controls on coalbed methane reservoir capacity and gas content. *International Journal of Coal Geology* 38, 3-26.
- Bustin, A.M. and Bustin, R.M., 2008. Coal reservoir saturation: Impact of temperature and pressure. *AAPG Bulletin* 92, 77-86.
- Bůžek F., Franců J., Boháček Z. 1999a. Geochemistry of coal bed methane in the Upper Silesian Basin, Czech Republic. Extended abstracts of the 19th Int. Conference on Organic geochemistry, TÜBITAK Marmara Res. Center, Gebze, 517-518.
- Bůžek, F.; Holub, V.; Bohciek, Z.; Franců, J., 1999b. Carbon isotope composition of methane emissions in the Czech Republic - preliminary results. Trace elements, enviromental impacts of coal mining and combustion *Vestnik Ceskeho geologickeho ustavu* 74, 2, 1999 (in Czech with English abstract).

- Candido, A., Rostirolla, S., 2007. Análise de fácies e revisão da estratigrafia de seqüências da Formação Ponta Grossa, Bacia do Parná – ênfase nos arenitos de Membro Tibagi. *Boletim Geociencias Petrobras* 15 (1), 45–62.
- Cervik, J. 1969. Behavior of coal-gas reservoirs. U.S. Bureau of Mines Technical Progress Report 10. 10p.
- Chalmers, G.R.L., Bustin, R.M., 2007. On the effects of petrographic composition on coalbed methane sorption. *International Journal of Coal Geology* 69, 288–304.
- Clarkson, C.R., Bustin, R.M., 2000. Binary gas adsorption/desorption isotherms: effect of moisture and coal composition upon carbon dioxide selectivity over methane. *International Journal of Coal Geology* 42, 241–271.
- Cloke, M., Lester, E., Belghazi, A., 2002. Characterisation of the properties of size fractions from ten world coals and their chars produced in a drop-tube furnace. *Fuel* 81, 699–708.
- Colombo, U.; Gazzarrini, F.; Gonfiantini, R.; Kneuper, G.; Teichmüller, M.; Teichmüller, R., 1966. Carbon isotope study on methane from German coal deposits, *Advances in Organic Geochemistry*, 1966, pp. 1–26.
- Coppens, P.L., 1967. Synthèse des propriétés chimiques et physiques des houilles — es houilles belges. Report of the Institut National de l'Industrie Charbonnière, publ. by Inichar.
- Cornford, C., 2011. Natural petroleum fractionation – what do we really mean. *International Meeting on Organic Geochemistry IMOG 2011*, 18 – 23 September, Interlaken, Switzerland, P-095, abstract.
- Cramer, B., Krooss, B.M., Littke, R., 1998. Modelling isotope fractionation during primary cracking of natural gas: a reaction kinetic approach. *Chemical Geology* 149, 235-250.
- Cramer, B., Faber, E., Gerling, P., Krooss, B.M. 2001. Reaction kinetics of stable carbon isotopes in natural gas - Insights from dry, open system pyrolysis experiments. *Energy & Fuels*, v. 15, p. 517-532.
- Crosdale, P., 2002. Controls on Methane Sorption Capacity of Indian Coals. *AAPG Bulletin* 86. 201-212.
- Crosdale, P., Moore, T., Mares, T., 2008. Influence of moisture content and temperature on methane adsorption isotherm analysis for coals from a low-rank, biogenically sourced gas reservoir. *International Journal of Coal Geology* 76, 166–174.
- Day, S., Sakurovs, R., Weir, S., 2008a. Supercritical gas sorption on moist coals. *International Journal of Coal Geology* 74, 203–214.
- Day, S., Duffy, G., Sakurovs, R., Weir, S., 2008b. Effect of coal properties on CO₂ sorption capacity under supercritical conditions. *International Journal of Greenhouse Gas Control* 2, 342–352.
- Denneberg, T., 1998. Untersuchungen zum Methan-Adsorptionsvermögen von Steinkohlen unterschiedlicher Reife aus dem Ruhrgebiet. Diplomarbeit (unpublished), RWTH-Aachen.

- Diessel, C.F.K., (1992). Coal-bearing depositional systems. Springer, Berlin, 721 pp.
- DiMichele, W.A., Montanez, I.P., Poulsen, C.J., Tabor, N.J., 2009. Climate and vegetational regime shifts in the late Paleozoic ice age earth. *Geobiology* 7, 200-226.
- DIN 51700 Testing of solid fuels—generalities and index of methods of tests. 2003. Beuth Verlag, Berlin.
- DIN 51718 Testing of solid fuels—solid mineral fuels—determination of the water content and the moisture of analysis sample. 2002. Beuth Verlag, Berlin.
- DIN 51719 Testing of solid fuels—determination of ash content. 1997. Beuth Verlag, Berlin.
- Dopita, M. and Kumpera, O., 1993, Geology of the Ostrava-Karviná coalfield, Upper Silesian Basin, Czech Republic, and its influence on mining. *International Journal of Coal Geology*, 23, 291-321.
- Dopita M. et al. 1997. Geology of the Czech part of the Upper Silesian Basin (in Czech). – Ministry of Environmental Protection CR. Praha. 278 p.
- EIA, 2007. U.S. Coalbed methane - past, present and future. King, B. and Long, G. US Energy Information Administration, November 2007. (www.eia.gov/oil_gas/rpd/cbmusa2.pdf, Internet access 18.12.2011.)
- Espitalie J., Laporte J. L., Madec M., Marquis F., Leplat P., Paulet J. and Boutefeu A. 1977. Methode rapide de caracterisation des roches meres, de leur potential petrolier et de leur degre d'evolution. *Rev. Inst. Fr. Per.* 32, 23-42.
- Ettinger, I. L., Lidin, G. D., Dmitrev, A. M., Zhupakhina, E. A., 1958. Systematic Handbook for the Determination of the Methane Content of Coal Seams from the Seam Pressure of the Gas and the Methane Capacity of the Coal; U.S. Bureau of Mines Translation No. 1505/National Board Translation No. A.1606/SEH: Moscow, 1958.
- Faber, E., 1987. Zur Isotopengeochemie gasförmiger Kohlenwasserstoffe. *Erdöl Erdgas Kohle* 103, 210-218.
- Faiz, M., Saghafi, A., Sherwood, N., Wang, I., 2007. The influence of petrographic properties and burial history on coal seam methane reservoir characterisation, Sydney Basin, Australia. *International Journal of Coal Geology* 70, 193–208.
- Faiz, M. and Hendry, P., 2009. Microbial activity in Australian CBM reservoirs. Search and Discovery Article #80033 (2009) Adapted from oral presentation at AAPG Annual Convention, San Antonio, TX, April 20-23, 2008.
- Franců J., Radke M., Schaefer R.G., Poelchau H.S., Čáslavský J., Boháček Z., 1996. Oil-oil and oil-source rock correlation in the northern Vienna basin and adjacent Flysch Zone. In: *Oil and Gas in Alpidic Thrustbelts and Basins of Central and Eastern Europe*. G. Wessely and W. Liebl, eds, EAPG Spec. Publ. No. 5, Geological Society Publishing House, Bath, pp. 343-354.
- Franců J., Franců E., Bezuško P. 1999. Model of burial and thermal history compaction, coalification and gas generation in the Upper Silesian basin - examples from boreholes

Štramberk and Tyra. Documenta Geonica 1999, PERES Publishers, 45-48. ISBN 80-902465-6-7

- Franců E., Franců J., Kalvoda J., Poelchau H.S., Otava J. 2002. Burial and uplift history of the Palaeozoic Flysch in the Variscan foreland basin (SE Bohemian Massif, Czech Republic) In: Bertotti G., Schulmann K., Cloetingh S., eds.: Continental collision and the tectono-sedimentary evolution of forelands. European Geophysical Society - Stephan Mueller Special Publication Series, 1, 259-278.
- Franců, J. , Bůžek, F. , Hemza, P. , Francu, E., 2007. Isotopic and geochemical evidence of gas producing microbial ecosystems in coal seams and gobs in the SW Upper Silesian basin, Czechia. *Geochimica et Cosmochimica Acta*, 71 (15): Suppl. 1, s. A291. Elsevier. Oxford.
- Fuex, A., 1980. Experimental evidence against an appreciable isotopic fractionation of methane during migration. In: *Advances in Organic Geochemistry, 1979* (eds. Douglas, A.G., Maxwell, J.R.) pp. 725-732, Pergamon, Oxford.
- Galimov, E.M., 1988. Sources and mechanisms of formation of gaseous hydrocarbons in sedimentary rocks. *Chemical Geology* 71, 77-95.
- Galimov, E.M., 2006. Isotope organic geochemistry. *Organic Geochemistry* 37, 1200-1262.
- Gaschnitz, R., 2001. Gasgenese und Gasspeicherung im flözführenden Oberkarbon des Ruhr-Beckens. *Berichte des Forschungszentrums Jülich*, 3859, pp 342. (PhD Thesis).
- Gaschnitz, R., Krooss, B.M., Gerling, P., Faber, E., Littke, R., 2001. On-line pyrolysis-GC-IRMS: isotope fractionation of thermally generated gases from coals. *Fuel* 80, 2139-2153.
- Gensterblum, Y., van Hemert, P., Billemont, P., Charrière, D., Li, D., Busch, A., Krooss, B. M., De Weireld, G., Wolf, K.-H.A.A., 2009. European Inter-laboratory comparison of high pressure CO₂ sorption isotherms. Phase I: activated carbon. *Carbon* 47, 2958-2969.
- Gensterblum, Y., van Hemert, P., Billemont, P., Battistutta, E., Busch, A., Krooss, B.M., De Weireld, G., Wolf, K.-H.A.A., 2010. European Inter-Laboratory Comparison of High Pressure CO₂ Sorption Isotherms II: Natural Coals. *International Journal of Coal Geology*, 84, 115-124.
- Golding, S.D., Uysal, I.T., Boreham, C.J., Kirste, D., Baublys, K.A., Esterle, J.S., 2010. Adsorption and mineral trapping dominate CO₂ storage in coal systems. In: 10th Conference on Greenhouse Gas Control Technologies (GHGT), Amsterdam, The Netherlands. 19-23 September, 2010.
- Hanbaba, P. and Jüntgen, H., 1969. Zur Übertragbarkeit von Laboratoriums-Untersuchungen auf geochemische Prozesse der Gasbildung aus Steinkohle und über den Einfluß von Sauerstoff auf die Gasbildung. *Advances in Organic Geochemistry*, 459-471.
- Heim, S., Jurisch, S.A., Krooss, B.M., Weniger, P., Littke, R., 2012. Systematics of pyrolytic N₂ and CH₄ release from peat and coals of different thermal maturity. *International Journal of Coal Geology* 89, 84-94.
- Hemza, P., Sivek, M., Jirásek, J., 2009. Factors influencing the methane content of coal beds of the Czech part of the Upper Silesian Coal Basin, Czech Republic. *Int. J. Coal Geol.* 79, 29-39.

- Hendriks, C., Graus, W., van Bergen, F., 2004. Global carbon dioxide storage potential and costs. Ecofys-report EEP-02001. 59 pp. <http://www.ecofys.com/com/publications/documents/GlobalCarbonDioxideStorage.pdf>, Internet Access, Date: 06.12.2009.
- Hendry, P., 2006. Extremophiles: There's more to life. *Environmental Chemistry* 3, 75–76.
- Hildenbrand, A., Krooss, B.M., Busch, A., Gaschnitz, R., 2006. Evolution of methane sorption capacity of coal seams as a function of burial history – a case study from Campine Basin, NE Belgium. *International Journal of Coal Geology* 66, 179-203.
- Holz, M., 1998. The Eo-Permian coal seams of the Paraná basin in southernmost Brazil: an analysis of the depositional conditions using sequence stratigraphy concepts. *International Journal of Coal Geology* 36, 141–163.
- Holz, M., Vieira, P., Kalkreuth, W., 2000. The Early Permian coal-bearing succession of the Paraná basin in southernmost Brazil: depositional model and sequence stratigraphy. *Revista Brasileira de Geociências* 30, 420–422.
- Holz, M., Kalkreuth, W., 2004. Sequence stratigraphy and coal petrology applied to the Early Permian coal-bearing Rio Bonito Formation, Paraná Basin, Brazil. In: Pashin, J., Gastaldo, R. (Eds.), *Sequence Stratigraphy, Paleoclimate, and Tectonics of Coal-Bearing Strata*, AAPG Studies in Geology, pp. 147–167.
- Holz, M., Kalkreuth, W., Alves Rolim, S., 2010. Extension of the Paraná Basin to offshore Brazil: implications for coalbed methane evaluation. *Journal of Marine Petroleum Geology* 27, 1119–1132.
- IEA, 2010. *World energy outlook 2010*. International Energy Agency, London 2010. (www.iea.org/weo/docs/weo2010/weo2010_london_nov9.pdf, Internet access 18.12.2011.)
- IPCC, 2005. *IPCC Special Report on Carbon Dioxide Capture and Storage*. Prepared by Working Group III of the Intergovernmental Panel on Climate Change. Metz, B., O. Davidson, H. C. de Coninck, M. Loos, and L. A. Meyer (eds.). Cambridge University Press, Cambridge, United Kingdom and New York, NY, USA, 442 pp.
- IUPAC. *Compendium of Chemical Terminology*, 2nd ed. (the “Gold Book”). Compiled by A. D. McNaught and A. Wilkinson, 1997. Blackwell Scientific Publications, Oxford.
- Jenden, P.D. and Kaplan, I.R., 1986. Comparison of microbial gases from the Middle American Trench and Scripps Submarine Canyon: Implications for the origin of natural gas. *Applied Geochemistry* 1, 631-646.
- Jin, H.; Schimmelmann, A.; Mastalerz, M.; Pope, J.; Moore, T.A., 2010. Coalbed gas desorption in canisters: Consumption of trapped atmospheric oxygen and implications for measured gas quality. *International Journal of Coal Geology* 81, 64-72
- Joubert, J., Grein, C.T., Bienstock, D., 1973. Sorption of methane in moist coal. *Fuel* 52, 181–185.
- Joubert, J.I., Grein, C.T., Bienstock, D., 1974. Effect of moisture on the methane capacity of American coals. *Fuel* 53, 186-191.

- Jüntgen, H. and Karweil, J., 1966. Gasbildung und Gasspeicherung in Steinkohlenflozen, Teil 1 und 2. *Erdöl und Kohle*, 19, 339-344.
- Jüntgen, H. and Klein, J., 1975. Formation of natural gas from coaly sediments. *Erdöl Kohle, Erdgas, Petrochemie* 19, 251-258.
- Kalkreuth, W., Holz, M., 2000. The coalbed methane potential of the Santa Terezinha Coalfield, Rio Grande do Sul, Brazil. *Revista Brasileira de Geociencias* 30, 342–345.
- Kalkreuth, W., Holz, M., Kern, M., Burger, H., Schauf, A., Prissang, R., Lemos de Sousa, M., Rodriguez, C., 2003. The Coalbed Methane Potential of the Paraná Basin. 2o Congresso Brasileiro de P&T em Petróleo & Gás, Rio de Janeiro, June 15–18, 2003, CD ROM, pp. 1–6.
- Kalkreuth, W., Holz, M., Kern, M., Machado, G., Mexias, A., Silva, M., Willett, J., Finkelmann, R., Burger, H., 2006. Petrology and chemistry of Permian coals from the Paraná Basin: 1. Santa Terezinha, Leão-Butia and Candiota Coalfields, Rio Grande do Sul, Brazil. *International Journal of Coal Geology* 68, 79–116.
- Kalkreuth, W., Levandowsky, J., Holz, M., Busch, A., Krooss, B., 2008a. Preliminary results of high-pressure CH₄ and CO₂ sorption tests on Permian age coals from the Paraná Basin, Brazil. *International Conference on Coal and Organic Petrology, ICCP-TSOP*, Oviedo Spain, Sept. 21–27, 2008, Program and Abstracts, p. 56.
- Kalkreuth, W., Holz, M., Casagrande, J., Cruz, R., Oliveira, T., Kern, M., Levandowski, J., Rolim, S., 2008b. O Potencial de Coalbed Methane (CBM) na jazida da Santa Terezinha – modelagem 3D e avaliação do poço de exploração CBM001-ST-RS. *Revista Brasileira de Geociencias* 38 (2), 1–17.
- Kalkreuth, W., Holz, M., Levandowski, J., Kern, M., Casagrande, J., Weniger, P., Busch, A., Krooss, B.M. (2011 submitted) The Coalbed Methane (CBM) Potential and CO₂ Storage Capacity of the Santa Terezinha Coalfield, Paraná Basin, Brazil. *AAPG Bulletin* (submitted in 2011).
- Karg, H., Carter, A., Brix, M., Littke, R., 2005. Late- and post-Variscan cooling and exhumation history of the northern Rhinish massif and the southern Ruhr Basin: new constraints from fission-track analysis. *International Journal of Earth Sciences* 94, 180-192.
- Karweil, J., 1969. Aktuelle Problem der Geochemie der Kohle; in *Advances In Geochemistry* (1968); Schenk, E.A. and Havernaar, I., Editors, Oxford Press, pp. 59-84.
- Kandarachevová, J., Sedláčková, L., Hýlová, L., Jirásek, J., Sivek, M., 2009. Lateral development of coalification in the Czech part of the Upper Silesian Coal Basin and its connection with gas deposits. *International Journal of Coal Geology*, 78 , 225-232.
- Kedzior, S., 2009. Accumulation of coal-bed methane in the south-west part of the Upper Silesian Coal Basin (southern Poland). *International Journal of Coal Geology* 80, 20-34.
- Kiessell, F.N., C.M. McCulloch, and C.H. Elder, 1973. "The Direct Method of Determining Methane Content of Coalbeds for Ventilation Design", U.S. Bureau of Mines, Report of Investigations 7767, 17 p.

- Killops, S.D., Funnell, R.H., Suggate, R.P., Sykes, R., Peters, K.E., Walters, C., Woolhouse, A.D., Weston, R.J., Boudou, J.-P. 1998. Predicting generation and expulsion of paraffinic oil from vitrinite-rich coals. *Organic Geochemistry* 29, 1-21.
- Kim, A.G., 1977. Estimating methane content of bituminous coalbeds from adsorption data. U.S. Department of the Interior, Bureau of Mines, Report of Investigations 8245, 22 p.
- Köster, J.; Rospondek, M.; Schouten, S.; Kotarba, M.; Zubrzycki, A.; Sinninghe Damste, J.S., 1998. Biomarker geochemistry of a foreland basin: the Oligocene Menilite Formation in the Flysch Carpathians of Southeast Poland. *Organic Geochemistry* 29, 649-669
- Kotarba, M., 2001. Composition and origin of coalbed gases in the Upper Silesian and Lublin basins, Poland. *Organic Geochemistry*, 32, 163-180.
- Kotarba, M.J., Clayton, J.L., Rice, D. D., Wagner, M., 2002. Assessment of hydrocarbon source rock potential of Polish bituminous coals and carbonaceous shales. *Chemical Geology* 184, 11-35.
- Kotarba, M.J. and Pluta, I., 2009. Origin of natural waters and gases within the Upper Carboniferous coal-bearing and autochthonous Miocene strata in South-Western part of the Upper Silesian Coal Basin, Poland. *Applied Geochemistry*, 24, 876-889.
- Krejčí O., Franců J., Poelchau H.S., Müller P., Stráník Z., 1996. Tectonic evolution and oil and gas generation model in the contact area of the North European Platform with the West Carpathians. In: *Oil and Gas in Alpidic Thrustbelts and Basins of Central and Eastern Europe*. G. Wessely and W. Liebl, eds, EAPG Spec Publ. No. 5, Geological Society Publishing House, Bath, pp. 177-186.
- Krooss, B.M., Leythaeuser, D., Lillack, H., 1993. Nitrogen-rich natural gases – qualitative and quantitative aspects of natural gas accumulation in reservoirs. *Erdöl und Kohle – Erdgas – Petrochemie* 46, 271-276.
- Krooss, B.M., Littke, R., Müller, B., Frielingsdorf, J., Schwochau, K., Idiz, E.F., 1995. Generation of nitrogen and methane from sedimentary organic matter: implications on the dynamics of natural gas accumulations. *Chemical Geology* 126, 291-318.
- Krooss, B.M., van Bergen, F., Gensterblum, Y., Siemons, N., Pagnier, H.J.M., David, P., 2002. High-pressure methane and carbon dioxide adsorption on dry and moisture-equilibrated Pennsylvanian coals. *International Journal of Coal Geology* 51, 69-92.
- Krooss, B.M., Friberg, L., Gensterblum, Y., Hollenstein, J., Prinz, D., Littke, R., 2005. Investigation of the pyrolytic liberation of molecular nitrogen from Palaeozoic sedimentary rocks. *Int. J. Earth Sci. (Geol. Rundschau)* 94, 1023-1038.
- Krüger, M., Beckmann, S., Engelen, B., Thielemann, T., Cramer, B., Schippers, A., Cypionka, H., 2008. Microbial methane formation from hard coal and timber in an abandoned coal mine. *Geomicrobiology Journal* 25, 315-321.
- Lamberson, M.N., Bustin, R.M., 1993. Coalbed methane characteristics of Gates Formation coals, Northeast British Columbia: effect of maceral composition. *American Association of Petroleum Geologists Bulletin* 77, 2062-2076.

- Lasaga, A.C. and Kirkpatrick, R.J. (Eds.), 1981. Kinetics of geochemical processes. Mineralogical Society of America, pp. 398.
- Laxminarayana, C., Crosdale, P., 1999. Role of coal type and rank on methane sorption characteristics of Bowen Basin, Australia coals. *International Journal of Coal Geology* 40, 309–325.
- Laxminarayana, C. and Crosdale, P., 2002. Controls on methane sorption capacity of Indian coals. *AAPG Bulletin* 86, 201-212.
- Levine, J.R., 1993. Coalification: The evolution of coal as source rock and reservoir rock for oil and gas. In: Law, B.E. and Rice, D.D., Editors, 1993. *Hydrocarbons from Coal AAPG Studies in Geology* vol. 38, pp. 39–77.
- Levy, J.H., Day, S.J., Killingley, J.S., 1997. Methane capacities of Bowen Basin coals related to coal properties. *Fuel* 76, 813-819.
- Li, D., Liu, Q., Weniger, P., Gensterblum, Y., Busch, A., Krooss, B.M., 2010. High-pressure sorption isotherms and sorption kinetics of CH₄ and CO₂ on coals. *Fuel* 89, 569–580.
- Littke, R. and Ten Haven, H.L., 1989. Palaeoecologic trends and petroleum potential of Upper carboniferous coal seams of western Germany as revealed by their petrographic and organic geochemical characteristics. *International Journal of Coal Geology* 13, 529-574.
- Littke, R., Krooss, B.M., Idiz, E., Frielingsdorf, J., 1995. Molecular nitrogen in natural gas accumulations; generation from sedimentary organic matter at high temperatures. *AAPG Bulletin* 79, 410-430.
- Martinec P., Dopita M., Bezuško P., Nováková D., Hettenberger V., Lukšová J. 1999. Bilance slojového metanu v historii české části hornoslezské pánve. - *MS Archív ČGÚ*, 83 p.
- Martinec, P. and Schejbalova, B., 2004. History and environmental impact of mining in the Ostrava-Karvina coal field (Upper Silesian coal basin, Czech Republic). *Geologica Belgica*, v. 7, p. 215–223.
- Martinec, P., Jirásek, J., Kožušníková, A., and Sivek, M. Editors, *Atlas of Coal — the Czech Part of the Upper Silesian Basin*, Anagram, Ostrava (2005) (in Czech with English summary).
- Mastalerz, M., Gluskoter, H., Rupp, J., 2004. Carbon dioxide and methane sorption in high volatile bituminous coals from Indiana, USA. *International Journal of Coal Geology* 60, 43–55.
- Mastalerz, M., Solano-Acosta, W., Schimmelmann, A., Drobniak, A., 2009. Effects of coal storage in air on physical and chemical properties of coal and on gas adsorption. *International Journal of Coal Geology* 79, 167-174.
- McCants, C.Y., Spafford, S., Stevens, S.H., 2001, Five-Spot Production Pilot on Tight Spacing: Rapid Evaluation of a Coalbed Methane Block in the Upper Silesian Coal Basin, Poland. *International Coalbed Methane Symposium*, University of Alabama, Tuscaloosa, (2001), p. 193-204.
- McLennan, J.D., P.S. Schafer and T.J. Pratt, 1995. A Guide to Determining Coalbed Gas Content. Gas Research Institute, Topical Report, GRI-94/0396.

- Meissner, F.F., 1984. Cretaceous and Lower Tertiary Coals tain Area: in Hydrocarbon Source Rocks of the Greater as Sources for Gas Accumulations in the Rocky Mountain Region. Woodward, I.; Meissner, F.F. and Clayton, J.L., Editors, Rocky Mountain Association of Geologists, 1984, Symposium, pp. 401-431.
- Menčík, E., Adamová, M., Dvořák, J., Dudek, A., Jetel, J., Jurková, A., Hanzlíková, E., et al., 1983. Geologie Moravskoslezských Beskyd a Podbeskydské pahorkatiny. Ústř. úst. geol. 1–304. (inCzech with English summary).
- Metje, M., 2006. Terminale Prozesse des anaeroben Abbaus in sauren Torfmooren der Subarktis und des südlichen Boreals. PhD Thesis, Max-Planck Institute for terrestrial microbiology, Marburg/Lahn. 185 p.
- Metje, M. and Frenzel, P., 2007. Methanogenesis and methanogenic pathways in a peat from subarctic permafrost. *Environmental Microbiology* 9, 954-964.
- Michels, G., Wouters, H., 1941. 6th. edition. Landolt-Börnstein (1971). Zahlenwerte und Funktionen aus Physik, Chemie, Astronomie Geophysik und Technik, Vol. 2. Springer (in German), p. 14. part 1.
- Milani, E.J., 1997. Evolucao tectono-estratigrafica da Baca do Parana e seu relacionamento com a geodinamica fanerozoica do Gondwana sul-ocidental: Porto Alegre, Rio Grande do Sul Federal University, unpub. PhD thesis, 225 p.
- Milani, E., Zalán, P., 1999. An outline of the geology and petroleum systems of the Paleozoic interior basins of South America. Episodes. *Journal of International Geoscience* 22 (3), 199–205.
- Milani, E.J., Melo, J.H.G., Souza, P.A., Fernandes, L.A., França, A.B., 2007. Bacia do Paraná. *Boletim de Geociências da Petrobrás*. Rio de Janeiro 15 (2), 265–287.
- Murray, D., 1996. Coal bed methane in the U.S.A.: analogues for worldwide development. In: Gayer, R., Harris, I. (Eds.), *Coal Bed Methane and Coal Geology*, pp. 1–12. Geological Society Special Publication No. 109, London.
- Neto, E., 1995. Source rock generative potential of Upper Devonian shales (Ponta Grossa Formation), Paraná Basin, Brazil. *American Association of Petroleum Geologists Bulletin* 79, 85 Abstract.
- Nuttall, B.C., Eble, C.F., Drahovzal, J.A., Bustin, R.M., 2005. Analysis of Devonian black shales in Kentucky for potential carbon dioxide sequestration and enhanced natural gas production. Report Kentucky Geological Survey/University of Kentucky (DE-FC26-02NT41442).
- OPEC, 2011. World oil outlook 2011. OPEC Secretariat, Vienna, Austria. www.opec.org. ISBN 978-3-9502722-2-2
- Osborne, S.G. and McIntosh, J.C., 2010. Chemical and isotopic tracers of the contribution of microbial gas in Devonian organic-rich shales and reservoir sandstones, northern Appalachian Basin. *Applied Geochemistry* 25, 456 – 471.

- Osborne, S.G., Vengosh, A., Warner, N.R., Jackson, R.B., 2011. Methane contamination of drinking water accompanying gas-well drilling and hydraulic fracturing. *PNAS* 108, 8172-8176.
- Ozdemir, E., Schroeder, K., 2009. Effect of moisture on adsorption isotherms and adsorption capacities of CO₂ on coals. *Energy and Fuels* 23, 2821–2831.
- Padula, V., 1969. Oil shale of Permian Iratí Formation. *American Association of Petroleum Geologists Bulletin* 53 (3), 591–602.
- Penner, T.J., Foght, J.M., Budwill, K., 2010. Microbial diversity of western Canadian subsurface coal beds and methanogenic coal enrichment cultures. *International Journal of Coal Geology* 82, 81-93.
- Pepper, A.S. and Corvi, P.J., 1995. Simple kinetic models of petroleum formation. Part I: oil and gas generation from kerogen. *Marine and Petroleum Geology* 12, 291-319.
- Petersen, H.-I., 2002. A re-consideration of the 'oil window' for humic coal and kerogen type III source rocks. *Journal of Petroleum Geology* 25, 407-432.
- Polanyi, M. and Wigner, E., 1928. Über die Interferenz von Eigenschwingungen als Ursache von Energieschwankungen und chemischer Umsetzungen. *Zeitschrift für physikalische Chemie A*, 139, 439.
- Prinz, D., Pyckhout-Hintzen, W., Littke, R., 2004. Development of the meso- and macroporous structure of coals with rank as analysed with small angle neutron scattering and adsorption experiments. *Fuel* 83, 547-556.
- Prinz, D. and Littke, R., 2005. Development of the micro- and ultramicroporous structure of coals with rank as deduced from the accessibility to water. *Fuel* 84, 1645–1652.
- Prinzhofer, A. and Pernaton, E., 1997. Isotopically light methane in natural gas: bacterial imprint or diffusive fractionation? *Chemical Geology* 142, 193-200.
- Reeves, S., Gonzalez, R., Gasem, K.A.M., Fitzgerald, J.E., Pan, Z., Sudibandriyo, M., Robinson, R.L., 2005. Measurement and prediction of single- and multi component methane, carbon dioxide and nitrogen isotherms for U.S. coals. *International Coalbed Methane Symposium*, Paper 0527, Tuscaloosa, Alabama, May 16-20, 2005.
- Rice, D.D. and Claypool, G.E., 1981. Generation, accumulation, and resource potential of biogenic gas. *AAPG Bulletin*, 65, 5-25.
- Rice, D., Law, B. and Clayton, C., 1993. Coalbed Gas – An Underdeveloped Resource. In: *The Future of Energy Gases*, USGS Professional Paper 1570. Editor: Howell D.G., pp 389 – 404.
- Rice, D.D., 1993. Composition and origins of coalbed gas. In: Law, B.E., Rice, D.D. (Eds.), *Hydrocarbons from coal*. AAPG Studies in Geology 38, 159-184.
- Ruppel, T.C., Grein, C.T., Bienstock, D., 1974. Adsorption of methane on dry coal at elevated pressure. *Fuel* 53, 152-162.

- Ruthven, D.M. 2008. Fundamentals of adsorption equilibrium and kinetics in microporous solids. In: *Molecular Sieves 7 (Adsorption and Diffusion)*, Editors: Karge, H.G., Weitkamp, J. pp 1-43.
- Ryan, B.D., 1992. An equation for estimation of maximum coalbed-methane resource potential. BC Ministry of Energy, Mines and Petroleum Resources, Geological Fieldwork 1991, Paper 1992-1, pp.393-396.
- Schenck, H.J., Horsfield, B., Krooss, B.M., Schaefer, R.G., Schwochau, K., 1997. Kinetics of petroleum formation and cracking. In: Welte, D.H., Horsfield, B., Baker, D.R. (Eds.), *Petroleum and Basin Evolution*. Springer Verlag, Berlin, pp. 231-269.
- Schimmelmann, A., Sessions, A.L., Mastalerz, M., 2006. Hydrogen isotopic (D/H) composition of organic matter during diagenesis and thermal maturation. *Annual Review of Earth and Planetary Sciences* 34, 501-533.
- Schoell M. 1980. The hydrogen and carbon isotopic composition of methane from natural gases of various origins. - *Geochim. Cosmochim. Acta* 44, 649-661.
- Schoell, M., 1983. Genetic characterization of natural gases. *AAPG bulletin* 67, 2225-2238.
- Schoell, M., 1988. Multiple origins of methane in the earth. *Chemical Geology* 71, 1-10.
- Schwarz, J., 2007. Identifizierung aktiver mikrobieller Populationen mit Hilfe stabiler Isotope. PhD Thesis, Max-Planck institute for terrestrial microbiology, Marburg/Lahn. 204 p.
- Schwarz, J.I., Eckert, W., Conrad, R., 2008. Response of the methanogenic microbial community of a profundal lake sediment (Lake Kinneret, Israel) to algal deposition. *Limnol. Oceanogr.* 53, 113-121.
- Setzmann, U., Wagner, W., 1991. A new equation of state and tables of thermodynamic properties for methane covering the range from the melting line to 625 K at pressures up to 1000 MPa. *Journal of Physical and Chemical Reference Data* 20, 1061-1155.
- Shen, D. and Bülow, M., 2000. Comparison of different techniques for measuring isosteric heat of adsorption. *Adsorption*, 6, 275-286.
- Sherwood-Lollar, B., Ballantine, C., Nions, R., 1997. The fate of mantle-derived carbon in a continental sedimentary basin: Integration of C/He relationships and stable isotopic signatures. *Geochimica et Cosmochimica Acta* 61, 2295-2307.
- Siemons, N., Busch, A., 2007. Measurement and interpretation of supercritical CO₂ adsorption on various coals. *International Journal of Coal Geology* 69, 229-242.
- Sircar, S., 1985. Excess properties and thermodynamics of multicomponent gas adsorption. *J. Chem. Soc., Faraday Trans. 1*, 81, 1527-1540.
- Sivek, M., Dopita, M., Krul, M., Čáslavský, M., Jirásek, J., 2003. Atlas of Chemical-Technological Properties of Coals in the Czech Part of the Upper Silesian Basin, In: *Transactions of the VSB – Technical University of Ostrava* 2003, vol. XLIX, Mining and Geological Series, Monograph 11

- Sivek, M., Čáslavský, M., Jirásek, J., 2008. Applicability of the Hilt's law to the Czech part of the Upper Silesian Coal Basin (Czech Republic). *Int. J. Coal Geol.* 73, 185–195.
- Smith, D.M. and Williams, F.L., 1987. Adsorption and diffusion in Western United States coals. In: Volborth, A., Editor, *Coal Science and Chemistry*, 1987. Elsevier, Amsterdam, pp. 381-403.
- Smith, J.W. and Pallasser, R., 1996. Microbial origin of Australian coalbed methane. *AAPG Bulletin* 80, 891-897.
- Soares, J.L., Oberziner, A.B., José, H.J., Rodrigues, A.E., Moreira, R.F., 2007. Carbon dioxide adsorption in Brazilian coals. *Energy and Fuels* 21, 209–215.
- Somers, J.M. and Schulz, H.L. 2008. Thermal oxidation of coal mine ventilation air methane. 12th U.S. North American Mine Ventilation Symposium 2008, Wallace. ISBN 978-0-615-20009-5. 6p.
- Span, R., Wagner, W., 1996. A new equation of state for carbon dioxide covering the fluid region from the triple-point temperature to 1100 K at pressures up to 800 MPa. *Journal of Physical and Chemical Reference Data* 25 (6), 1509–1596.
- Spears, D.A. and Booth, C.A., 2002. The composition of size-fractionated pulverised coal and the trace element associations. *Fuel* 81, 683–690.
- Stahl, W., 1977. Carbon and nitrogen isotopes in hydrocarbon research and exploration. *Chemical Geology*, 20, 121-149.
- Stöttner, T. 2003. Methanreduktion durch Gasabsaugung und -verwertung auf dem Anthrazitbergwerk Ibbenbüren. 1. Symposium "Ressourcen und Umwelt" 4. 4. 2003, Institut für Bergbau der TU Bergakademie Freiberg. (<http://www.bergbau.tu-freiberg.de/bergbau/symposium/Stoettner.pdf>)
- Strapoc, D., Schimmelmann, A., Mastalerz, M., 2006. Carbon isotopic fractionation of CH₄ and CO₂ during canister desorption of coal. *Organic Geochemistry* 37, 152-164.
- Strapoc, D., Mastalerz, M., Eble, C., Schimmelmann, A., 2007. Characterization of the origin of coalbed gases in the southeastern Illinois Basin by compound-specific carbon and hydrogen stable isotope ratios. *Organic Geochemistry* 38, 267 – 287.
- Strapoc, D., Picardal, F.W., Turich, C., Schaperdoth, I., Macalady, J.L., Lipp, J.S., Lin, Y-S., Ertefai, T.F., Schubotz, F., Hinrichs, K-U., Mastalerz, M., Schimmelmann, A., 2008. Methane-producing microbial community in coal bed of the Illinois Basin. *Applied and Environmental Microbiology*, Apr. 2008, 2424 – 2432.
- Strapoc, D., Mastalerz, M., Schimmelmann, A., Drobnik, A., Hasenmueller, N.R., 2010. Geochemical constraints on the origin and volume of gas in the New Albany Shale (Devonian – Mississippian), eastern Illinois Basin. *AAPG Bulletin* 94, 1713 – 1740.
- Strapoc, D., Mastalerz, M., Dawson, K., Macalady, J., Callaghan, A.V., Wawrik, B., Turich, C., Asgby, M., 2011. Biogeochemistry of coal-bed methane. *Annual Review of Earth and Planetary Science* 39, 617-656.

- Sudibandriyo, M., Pan, Z., Fitzgerald, J.E., Robinson, R.L., Gasem, K.A.M., 2003. Adsorption of methane, nitrogen, carbon dioxide, and their binary mixtures on dry activated carbon at 318.2 K and pressures up to 13.6 MPa. *Langmuir* 16, 5323 – 5331.
- Sykes, R. and Snowdon, L.R., 2002. Guidelines for assessing the petroleum potential of coaly source rocks using Rock-Eval pyrolysis. *Organic Geochemistry* 33, 1445-1455.
- Tang, Y.; Perry, J.K.; Jenden, P.D.; Schoell, M., 2000. Mathematical modeling of stable carbon isotope ratios in natural gases. *Geochimica et Cosmochimica Acta* 64, 2673-2687.
- Taylor, G.H., Teichmüller, M., Davies, A., Diessel, C.F.K., Littke, R., Robert, P. 1998. *Organic Petrology*. Gebrueder Borntraeger, Berlin-Stuttgart, 704 pp.
- Teichmüller, R.; Teichmüller, M.; Colombo, U.; Gazzarrini, F.; Gonfiantini, R.; Kneuper, G. (1970). Das Kohlenstoff-Isotopen-Verhältnis im Methan von Grubengas und Flözgas und seine Abhängigkeit von den geologischen Verhältnissen. *Geologische Mitteilungen*, 9, 181-206.
- Teichmüller M. and Teichmüller, R. 1979. Diagenesis of Coal (Coalification). In: Larsen G. and Chilingar, G. V. (Eds), *Diagenesis of Sediments and Sedimentary Rocks*, Elsevier, Amsterdam, pp. 207-246.
- Teichmüller, M. and Durand, B. 1983. Fluorescence microscopical rank studies on liptinites and vitrinites in peat and coals, and comparison with results of the Rock-Eval pyrolysis. *Int. J. Coal Geol.* 2, 197-230.
- Thauer, R.K., 1990. Energy metabolism of methanogenic bacteria. *Biochimica et Biophysica Acta* 1018, 256-259.
- Thauer, R.K., 1998. Biochemistry of methanogenesis: a tribute to Marjory Stephenson. *Microbiology* 144, 2377-2406.
- Thielemann, T. 2000. Der Methanhaushalt über kohleführenden Sedimentbecken: Das Ruhrbecken und die Niederrheinische Bucht. Methanbildung, -migration und -austausch mit der Atmosphäre: Berichte des Forschungszentrums Jülich, Nr. 3792, thesis, 350 p.
- Thielemann, T., Krooss, B.M., Littke, R. and Welte, D.H. 2001. Does coal mining induce methane emissions through the lithosphere/atmosphere boundary in the Ruhr Basin, Germany? *Journal of geochemical exploration*, v. 74, p. 219-231.
- Thielemann T., Cramer B., Schippers A. 2004. Coalbed methane in the Ruhr Basin, Germany: a renewable energy resource? - *Advances in Organic Geochemistry 2003. Proceedings of the 21st International Meeting on Organic Geochemistry* 35, 11-12, 1537-1549.
- Tissot, B.P. and Welte, D.H., 1984. *Petroleum formation and occurrence*, 2nd edition. Springer Verlag, Berlin.
- Ungerer, P. and Pelet, R., 1987. Extrapolation of the kinetics of oil and gas formation from laboratory experiments to sedimentary basins. *Nature* 327, 52-54.
- Ungerer, P., 1990. State of the art of research in kinetic modelling of oil formation and expulsion. *Organic Geochemistry* 16. 1-25.

- USEPA, 2004. Evaluation of impacts to underground sources of drinking water by hydraulic fracturing of coalbed methane reservoirs. EPA 816-R-04-003. 463pp.
- USEPA, 2005. Coalbed Methane Outreach Program – Czech Republic, U.S. Environmental Protection Agency, 2005.
- USEPA, 2006. Global Anthropogenic non-CO₂ Greenhouse Gas Emissions: 1990-2020. EPA-430-R-06-003, United States Environment Protection Agency, Climate Change Division, Washington, DC, 274 pp.
- van Bergen, F., Pagnier, H.J.M., Krooss, B.M., van der Meer, L.G.H., 2001. CO₂- sequestration in the Netherlands: inventory of the potential for the combination of subsurface carbon dioxide disposal with enhanced coalbed methane production. In: Williams, D., Durie, R., McMullan, P., Paulson, C., Smith, A. (Eds.), Proceedings of the 5th International Conference on Greenhouse Gas Control Technologies. CSIRO Publishing, Collingwood, VIC, Australia, pp. 555–560.
- van Bergen, F., Krzystolik, P., van Wageningen, N., Pagnier, H., Skiba, J., Winterhaegen, P., Kobiela, Z., 2008. Production of gas from coal seams in the Upper Silesian coal basin in Poland in the post-injection period of an ECBM pilot site. *International Journal of Coal Geology* 77, 175–187.
- van Bergen, F., Winterhaegen, P., Pagnier, H., Krzystolik, P., Jura, B., Skiba, J., van Wageningen, N., 2009. Assessment of CO₂ storage performance of the enhanced coalbed methane pilot site in Kaniow. *Energy Procedia* 1, 3407–3414.
- van Heek K. H. and Jüntgen, H., 1968. Bestimmung der reaktionskinetischen Parameter aus nichtisothermen Messungen. *Ber. Bunsenges. Phys. Chem.* 72, 1223–1231.
- van Krevelen, D.W., 1961. *Coal*. Elsevier, Amsterdam.
- van Krevelen, D.W., 1993. *Coal: Typology - Physics - Chemistry - Constitution (Coal Science & Technology)*. 3rd edition, Elsevier.
- Waples, D.W., 1980. Time and temperature in petroleum formation: Application of Lopatin's method to oil exploration. *AAPG Bulletin* 64, 916-926.
- Weniger, P., Kalkreuth, W., Busch, A., Krooss, B.M., 2010. High-pressure methane and carbon dioxide sorption on coal and shale samples from the Paraná Basin, Brazil. *International Journal of Coal Geology* 84, 190-205.
- Weniger, P., Franců, J., Littke, R., Busch, A., Krooss, B.M., 2011a. Evaluation of thermal maturity and sorptive gas storage characteristic of bituminous coal from the Ostrava-Karvina Coal District, Upper Silesian Basin, Czech Republic. *DGMK/ÖGEW Frühjahrstagung 2011, Fachbereich Aufsuchung und Gewinnung, Celle, 11.-12. April 2011*. 9 p. ISBN 978-3-941721-16-6.
- Weniger, P., Krooss, B.M., Franců, J., Bůzek, F., Littke, R., 2011b. Geochemical and stable carbon isotopic composition of coal related gases from the SW Upper Silesian Coal Basin, Czech Republic. *Organic Geochemistry* 53, 153 - 165.

- Weniger, P., Franců, J., Hemza, P., Krooss, B.M., 2012. Investigations on the methane and carbon dioxide sorption capacity of coals from the SW Upper Silesian Coal Basin, Czech Republic. *International Journal of Coal Geology* 93, 23 – 39.
- White, C.M., Smith, D.H., Jones, K.L., Goodman, A.L., Jikich, S.A., LaCount, R.B., DuBose, S. B., Ozdemir, E., Morsi, B.I., Schroeder, K.T., 2005. Sequestration of carbon dioxide in coal with enhanced coalbed methane recovery—a review. *Energy and Fuels* 19, 659–724.
- Whiticar, M.J., Faber, E., Schoell, M., 1986. Biogenic methane formation in marine and fresh water environment, CO₂ reduction vs. acetate fermentation - Isotopic evidence. *Geochimica et Cosmochimica Acta* 50, 693-709.
- Whiticar M.J. 1990. A geochemical perspective of natural gas and atmospheric methane. - *Organic Geochemistry* 16, 531–547.
- Whiticar, M.J., 1994. Correlation of natural gases with their sources. In L.B. Magoon & W.G. Dow, *The petroleum system – from source to trap* (pp. 261-283), AAPG Memoir 60
- Whiticar, M.J., 1996. Stable isotope geochemistry of coals, humic kerogens and related natural gases. *International Journal of Coal Geology* 32, 191-215.
- Whiticar, M.J., 1999. Carbon and hydrogen isotope systematic of bacterial formation and oxidation of methane. *Chemical Geology* 161, 291-314.
- Wycherley, H.; Fleet, A.; Shaw, H., 1999. Some observations on the origins of large volumes of carbon dioxide accumulations in sedimentary basins. *Marine and Petroleum Geology* 16, 489-494.
- Yalcin, E., Durucan, S., 1991. Methane capacities of Zonguldak coals and the factors affecting methane adsorption. *Mining Science and Technology* 13, 215–222.
- Yee, D., Seidle, J.P., Hanson, W.B., 1993. Gas sorption on coal and measurement of gas content. In: Law, B.E. and Rice, D.D., Editors, 1993. *Hydrocarbons from Coal AAPG Studies in Geology* vol. 38, pp. 203–218.
- Zalán, P.V., Wolff, S., Conceição, J.C., Marques, A., Astolfi, M.A., Vieira, I.S., Appi, V.T., Zanotto, O.A., 1990. Bacia do Paraná. In: Raja Gabaglia, G.P., Milani, E.J. (Eds.), *Origem e Evolução das Bacias Sedimentares: Rio de Janeiro, Petrobras*, pp. 135–168.
- Zalán, P.V., Wolff, S., Astolfi, M., Vieira, I., Conceição, J., Appi, V., Neto, E., Cerqueira, J., Marques, A., 1991. The Paraná Basin, Brazil. in: Leighton, M., Kolata, D., Oltz, D., Eidel, J. eds. *Interior Cratonic Basins. American Association of Petroleum Geologists Memoir* 51, 681–708.
- Zhang, T. and Krooss, B.M., 2001. Experimental investigation on the carbon isotopic fractionation of methane during gas migration by diffusion through sedimentary rocks at elevated temperature and pressure. *Geochimica et Cosmochimica Acta* 65, 2723-2742.

Appendix I Geochemical and stable carbon isotopic composition of coal related gases from the SW Upper Silesian Coal Basin, Czech Republic

Table 1 gas samples from cross-measure boreholes

mine	sea m	stratigraphy	time	$\delta^{15}\text{O}_2$	$\delta^{13}\text{CH}_4$	$^1\text{O}_2$	$^1\text{N}_2$	He	H ₂	CO ₂	Ar	N ₂	CH ₄	C ₂ H ₆	C ₃ H ₈	i-C ₄ H ₁₀	C ₄ H ₁₀	2-m-C ₄ H ₁₀	C ₅ H ₁₂	sum i-C ₆ H ₁₄	C ₆ H ₁₄	C ₇ H ₁₆	C1/(C2+C3)	C1/(C2+)	
			days	‰ vs VPDB	‰ vs VPDB	%	%	ppm	ppm	%	%	%	%	ppm	ppm	ppm	ppm	ppm	ppm	ppm	ppm	ppm	ppm	ppm	ppm
Paskov	84	Petrkovice M	0	-12.8	-27.1	16.2	60.23	0	0	0.8	3.1	0	90.8	49450	3117	142	126	11	7	4	21	4	17	17	
Paskov	84	Petrkovice M	12	2.8	-35.5	0.72	7.55	40	101	0.4	0.1	5.06	92.29	19692	1060	47	41	4	2	1	4	1	43	43	
Paskov	84	Petrkovice M	21	-9.8	-23.5	15.72	61.91	0	0	3.2	2.9	12.98	79.38	3667	682	43	38	6	3	2	9	2	53	53	
Paskov	84	Petrkovice M	23	-1	-38.9	7.29	35.15	45	31	3.3	0.7	12.19	82.48	8580	591	31	27	4	2	1	5	1	60	60	
Paskov	84	Petrkovice M	28	3.5	-36.3	12	46.41	0	0	1.7	1.3	3.86	91.76	5278	584	26	25	2	2	1	5	1	72	71	
ČSM S	504	Saddle M	0	-22	-66.2	5.37	43.88	13	0	5.5	0.7	31.99	61.78	173	2	1	1	1	0	0	3	0	2640	2568	
ČSM S	504	Saddle M	8	-24.4	-63	4.21	38.94	0	0	2.7	0.6	29.02	67.63	145	2	1	0	1	0	0	4	1	3692	3560	
ČSM S	504	Saddle M	12	-23.3	-62.8	3.81	37.05	0	0	1.2	0.6	27.88	70.31	285	59	7	7	2	1	0	2	0	1729	1644	
ČSM N	643	Sucha M	0	-8.7	-59.9	7.35	71.59	0	0	8.2	1.4	67.72	22.64	110	4	1	2	0	0	0	0	0	1319	1297	
ČSM N	643	Sucha M	2	-10	-65.4	6.3	67.95	0	0	7.5	1.2	63.33	27.95	146	5	1	3	1	1	0	0	0	1313	1277	
ČSM N	643	Sucha M	11	-12.9	-66.9	13.88	67.09	0	0	7.4	2.4	44.66	45.52	70	4	0	3	1	1	0	0	0	2188	2125	
ČSM N	643	Sucha M	14	-13.1	-63.8	15.94	70.99	0	0	6.2	3.6	46.97	43.19	56	4	1	3	2	3	7	8	3	1865	1659	
ČSM N	643	Sucha M	25	-14.1	-67.6	10.67	64.37	0	0	7.2	1.6	49.63	41.49	112	5	1	4	1	1	0	0	0	1797	1736	

Table 2 gas samples from canister desorption

mine_well_ canister_ sample	stratigr aphy	Desorpt ion time	Sea m #	VRr	depth min	depth max	lost gas	des. gas	res. gas	total gas	$\delta^{13}\text{C}$ - CO ₂	$\delta^{13}\text{C}$ - CH ₄	O ₂	N ₂	He	H ₂	N ₂	CO ₂	Ar	CH ₄	C ₂ H ₆	C ₃ H ₈	i+n- C ₄ H ₁₀	C1/(C2 +C3)	C1/(C2 +)	
d			%	m	m	m ³ /t	m ³ /t	m ³ /t	m ³ /t		‰ vs VPDB	‰ vs VPDB	%	%	ppm	ppm	%	%	%	%	ppm	ppm	ppm			
ČSM_S1c1_2	Saddle	4.8	522	n.d.	175.4	175.85					-32.6	-61.84	7.51	63.9	279	0	56	1.97	1.3	41.06	111	1	0	3672	3672	
ČSM_S1c1_3	Saddle	8	522	n.d.	175.4	175.85	0.02	0.72	0.28	1.02	-42.1	-59.63	0.46	69.1	123	0	69	3.5	0.95	26.64	50	0	0	5304	5304	
ČSM_S1c2_2	Saddle	3.9	507	n.d.	190.5	191					-19.2	-53.31	12.42	59.9	460	0	33	2.3	2.03	62.67	188	1	0	3311	3304	
ČSM_S1c2_3	Saddle	7	507	n.d.	190.5	191	0.03	1.59	0.28	1.9	-40.4	-52.23	0.3	71.4	193	304	71	4.28	1.03	23.33	83	1	0	2778	2771	
ČSM_S1c3_1	Saddle	0	504	1.12	194	194.5					-41.2	-50.62	9.42	79	1225	0	79	8.09	1.87	10.86	55	1	2	1957	1884	
ČSM_S1c3_2	Saddle	3.1	504	1.12	194	194.5					-38	-57.02	4.09	58.2	682	0	53	7	0.99	38.67	245	2	9	1563	1505	
ČSM_S1c3_3	Saddle	8.9	504	1.12	194	194.5	0.02	0.44	0.39	0.85	-41.2	-54.18	1.51	60.7	399	0	59	3.32	0.88	36.41	180	1	3	2010	1974	
ČSM_N2c1_1	Saddle	0	532	1.17	156.3	157					-16.2	-72	1.85	39.1	0	0	35	3.17	0	61.55	164	0	0	3747	3747	
ČSM_N2c1_2	Saddle	9.8	532	1.17	156.3	157					-19.6	-71.9	0.36	1.63	0	0	0	0.03	0	99.63	133	0	0	7467	7467	
ČSM_N2c1_3	Saddle	18	532	1.17	156.3	157					-17.1	-72.2	4.36	58.9	0	0	54	12.73	0	33.52	113	0	0	2956	2956	
ČSM_N2c1_4	Saddle	31.9	532	1.17	156.3	157	0.04	1.59	0.67	2.3	-22.2	-70.2	2.14	24.7	0	0	19	2.66	0	78.69	345	0	0	2281	2281	
ČSM_S3c1_1	Saddle	0	559	n.d.	85.55	86					-35.7	-54.3	10.2	51	0	0	25	2.43	0	72.44	377	0	0	1923	1923	
ČSM_S3c1_2	Saddle	11.1	559	n.d.	85.55	86					-26.7	-65.6	3.25	44.2	0	0	38	1.57	0	60.49	331	0	0	1829	1829	
ČSM_S3c2_1	Saddle	0	559	n.d.	163.5	164					-15.8	-66	5.63	57	0	0	49	3.96	0	46.97	245	0	0	1917	1917	
ČSM_S3c2_2	Saddle	32.4	559	n.d.	163.5	164					-17.9	-69	4.84	53.2	0	0	46	2.33	0	52.08	324	0	0	1608	1608	
ČSM_S3c2_3	Saddle	35.3	559	n.d.	163.5	164	0.02	1.08	0.53	1.63	-19.6		9.27	57.7	0	0	41	2.69	0	56.07	285	0	0	1969	1969	
ČSM_S4c1_1	-	-	-	n.d.	167.8	168.65					-23.14	-59.56	16.4	67.28	0	0	27	1.29	3.11	68.18	734	23	0	900	900	
Lazy_1c1_1	Poruba	2.3	465	n.d.	73.85	74.55					-14.86	-61.31	12.4	54.44	0	0	20	0.85	1.39	77.54	3350	318	46	211	209	
Lazy_1c1_2	Poruba	20.3	465	n.d.	73.85	74.55					-11.54	-48.01	16.19	54.24	0	0	0	0.23	0	98.94	8107	169	0	120	120	
Lazy_1c1_3	Poruba	27.3	465	n.d.	73.85	74.55					-17.06	-44.23	11.94	47.6	0	0	7	0.66	0	90.52	16743	115	0	54	54	
Lazy_1c1_4	Poruba	32.3	465	n.d.	73.85	74.55	0.04	2.57	0.37	2.98	-6.99	-64.58	7.03	34.93	0	0	13	0.21	0	86.69	75	75	0	5790	5790	
Lazy_1c2_1	Poruba	0.3	465	n.d.	255.88	256.75					-2.84	-55.11	16.39	63.82	0	0	12	0.02	0	87.82	222	222	0	1979	1979	
Lazy_1c2_2	Poruba	8.3	465	n.d.	255.88	256.75					-4.65	-54.71	8.77	39.41	0	0	12	0.07	0	87.63	7870	85	0	110	110	
Lazy_1c2_3	Poruba	15.3	465	n.d.	255.88	256.75					-3.62	-54.41	4.86	24.89	0	0	9	0.05	0	90.43	7187	65	0	125	125	
Lazy_1c2_4	Poruba	20.3	465	n.d.	255.88	256.75	0.11	3	0.44	3.54	-1.27	-55.36	3.73	22.39	0	0	10	0	0	89	6813	61	0	129	129	
Lazy_2c1_3	Saddle	5.8	504	n.d.	55	55.5	0.02	0.56	0.29	0.87	-26.2	-71.1	13.7	66.7	0	0	44	1.32	2.4	51.91	66	1	0	7685	7685	
Lazy_3c1_1	Saddle	0	504	0.96	56.65	57.15					-16.1	-64.3	5.25	46.5	0	0	36	1	0	63.15	4	0	0	158333	158333	
Lazy_3c1_2	Saddle	14.5	504	0.96	56.65	57.15	0.04	1.33	0.66	2.03	-19.4	-64.9	n.d.	n.d.	0	0	0	2	0	98.37	6	0	0	156667	156667	
Lazy_4c1_1	Saddle	0	504	n.d.	51	51.5					-19.8	-55.01	14.52	67.3	0	0	42	1.12	2.7	54.16	153	1	1	3533	3518	
Lazy_4c1_2	Saddle	10.4	504	n.d.	51	51.5	0.02	0.74	0.41	1.17	-49.6	-44.2	11.9	60.7	0	0	37	1.46	0	61.2	30	0	0	20615	20615	
Paskov_1c1_1	Petrko.	0	41	1.35	180.61	181.05					-22.8	-46.39	1.82	39.9	0	0	36	1.03	0.58	61.6	5547	38	4	110	110	
Paskov_1c1_2	Petrko.	9.4	41	1.35	180.61	181.05					-21.4	-39.6	9.59	47.6	0	0	22	0.9	0	77.4	34	0	0	22500	22500	
Paskov_1c1_3	Petrko.	30.3	41	1.35	180.61	181.05	0.06	3.37	0.44	3.86	-31.5	-46.3	n.d.	n.d.	0	0	0	1.18	0	98.82	49	0	0	20000	20000	
Paskov_2c1_1	-	-	-	n.d.	178.75	188					-17.19	-45.06	12.8	51.97	0	435	11	0.37	1.53	84.42	26482	1463	257	30	30	
Paskov_3c1_1	-	3.4	-	n.d.	17.2	18.2					-1.04	-42.21	4.02	15.98	0	0	1	1.39	0.23	96.55	5467	168	63	171	169	
Paskov_3c1_3	-	33.4	-	n.d.	17.2	18.2					-7.15	-48.95	6.32	29.39	0	0	8	0.1	0	90.8	7511	71	0	120	120	
Paskov_4c1_1	Petrko.	2.2	47	1.5	127.7	128.4					-7.32	-40.9	4	34.2	26	578	24	1	0.43	69.96	43863	3054	570	15	15	
Paskov_4c1_2	Petrko.	17.2	47	1.5	127.7	128.42					-2.36	-39.46	10.18	33.74	0	0	0	0.72	0	94.76	42678	2222	362	21	21	
Paskov_4c1_3	Petrko.	32.2	47	1.5	127.7	128.42	0.04	1.47	0.41	1.92	-2.95	-39.03	4.24	24.43	0	0	11	1.61	0	82.9	44281	2350	331	18	18	
Paskov_4c2_1	-	0.8	-	n.d.	269	270					-7.86	-35.8	8.98	48.08	0	0	25	0.41	0	72.08	20820	129	0	34	34	
Paskov_4c2_2	-	4.8	-	n.d.	269	270					-0.94	-36.77	6.08	28.2	0	0	8	0.58	0	89.16	24487	215	0	36	36	
Paskov_4c2_3	-	14.8	-	n.d.	269	270					-18.65	-42.78	4.02	23.34	0	0	10	0.89	0	86.79	19749	198	0	44	44	
Paskov_4c2_4	-	19.8	-	n.d.	269	270	0.04	1.53	0.42	1.99	-5.92	-36.96	4.21	25.12	0	0	12	1.06	0	84.05	30674	719	0	27	27	

Appendix II Pyrolytic gas generation from bituminous coals of the Upper Silesian Coal Basin, Czech Republic and the Paraná Basin, Brazil

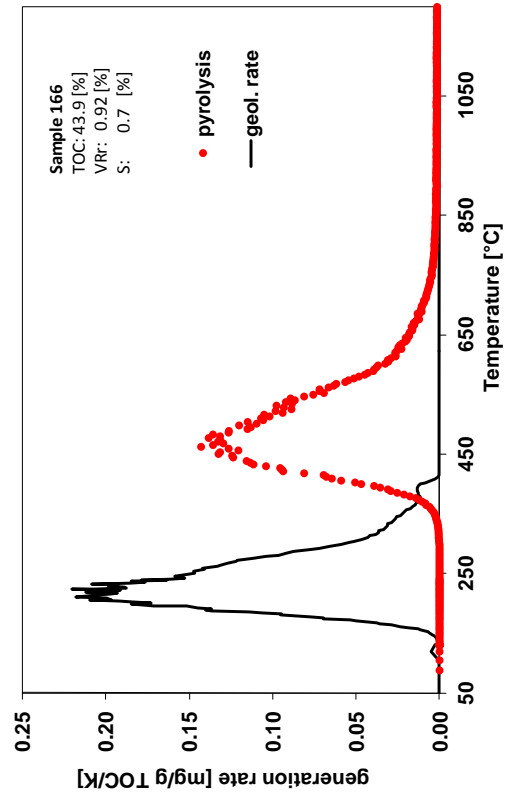
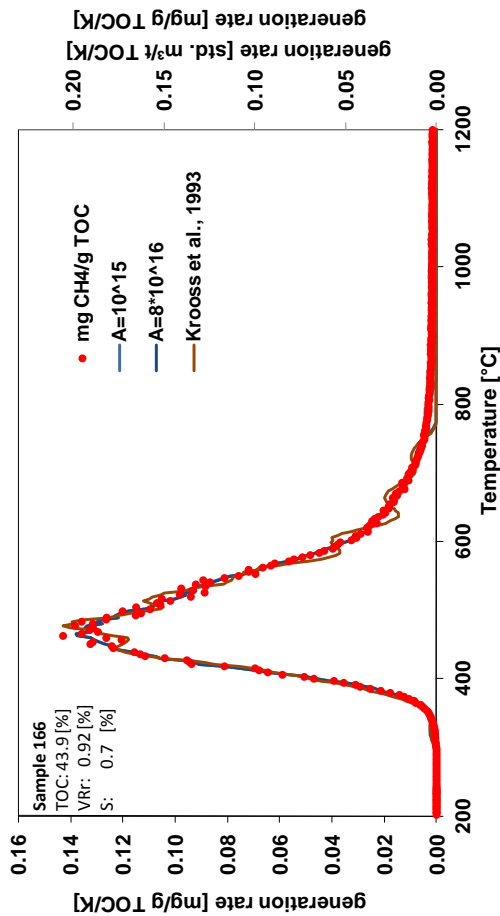
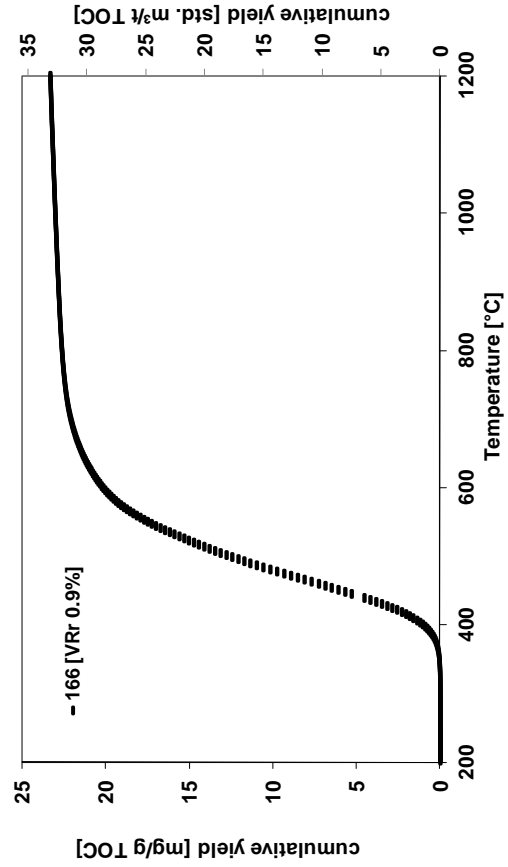
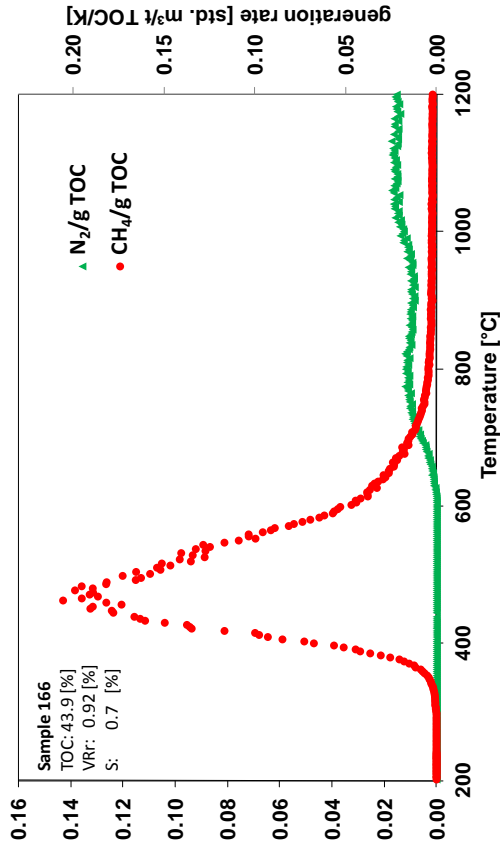
Appendix II Table 1 Results from Rock-Eval pyrolysis

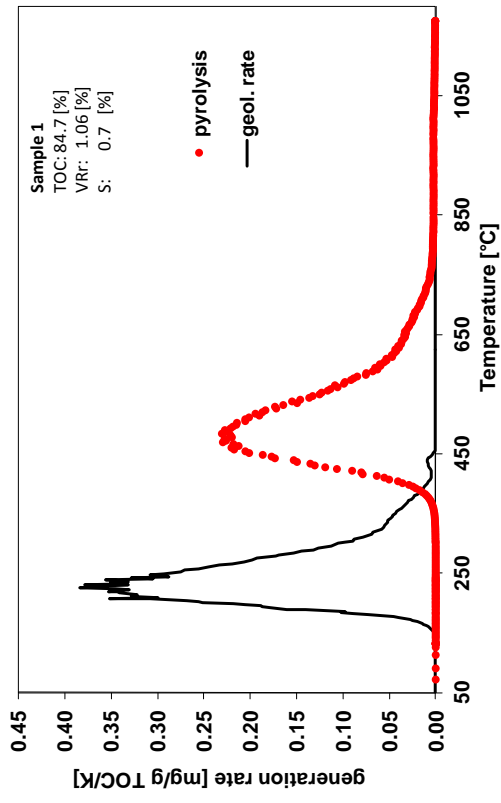
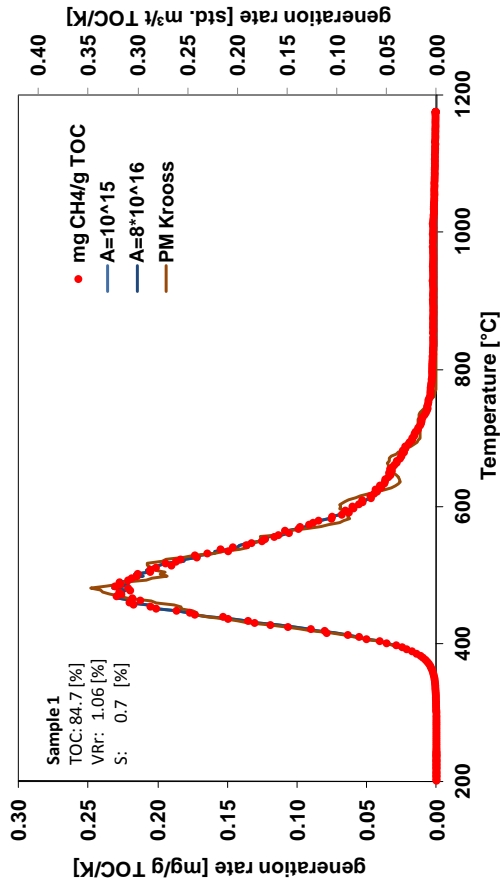
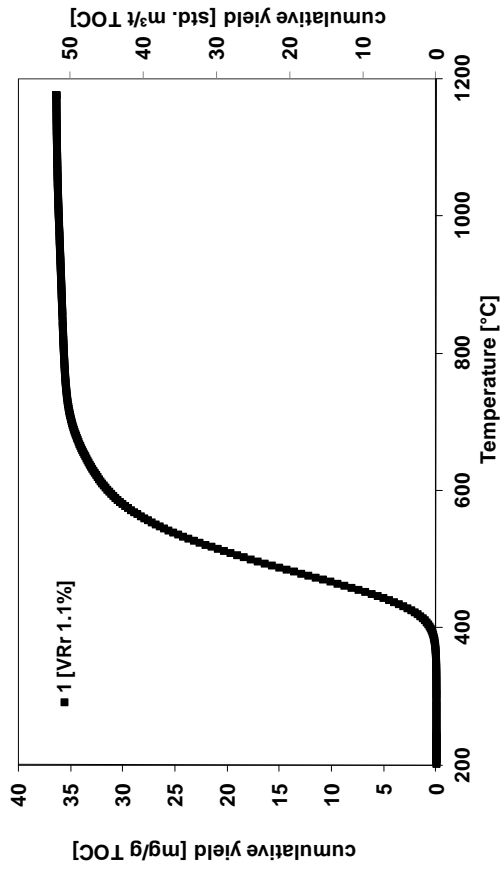
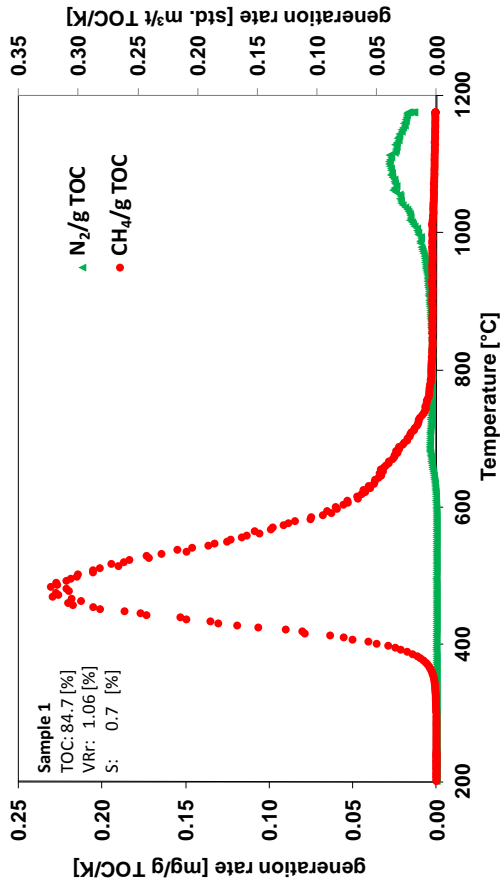
sample	mine	formation	TOC [%]	S1 [mg/g]	S2 [mg/g]	S3 [mg/g]	Tmax [°C]	HI	OI	BI	QI	TR
										[mg HC/g TOC]	[mg HC/g TOC]	
1	ČSM	Karviná	84.7	0.4	109.2	3.3	463	129	0.5	0	1.3	0
2	ČSM	Karviná	80.8	0.4	90.8	3.4	460	112	0.5	0.01	1.1	0
3	ČSM	Karviná	78	0.5	90.3	5.9	460	116	0.7	0.01	1.2	0.01
4	ČSM	Karviná	84.1	0.8	104.2	4.2	456	124	0.9	0.01	1.2	0.01
5	ČSM	Karviná	70.4	0.8	88.8	10.6	466	126	1.2	0.01	1.3	0.01
6	ČSM	Karviná	85.3	1.2	118	3	465	138	1.4	0.01	1.4	0.01
7	ČSM	Karviná	84.3	0.5	96.4	0.3	464	114	0.6	0.01	1.1	0.01
8.1	Lazy	Karviná	80.9	9.2	192.7	7.9	444	238	11.4	0.11	2.5	0.05
8.2	Lazy	Karviná	80.9	7	251.8	1.2	443	311	8.7	0.09	3.2	0.03
9	Lazy	u. Ostrava	41.6	4	77.8	1.2	452	187	9.5	0.1	2	0.05
10	Lazy	u. Ostrava	57.1	8.7	102.5	n.d.	459	180	15.2	0.15	1.9	0.08
11	Lazy	u. Ostrava	81.5	5.4	160.6	1.9	461	197	6.6	0.07	2	0.03
12	Lazy	u. Ostrava	78.9	11	181.3	0.1	452	230	13.9	0.14	2.4	0.06
13	Lazy	u. Ostrava	82.8	4.6	152.7	4.8	454	184	5.5	0.05	1.9	0.03
14	Lazy	u. Ostrava	37.1	3.4	44.8	1	474	121	9	0.09	1.3	0.07
15	Lazy	u. Ostrava	72.7	4.6	106.8	1.8	465	147	6.3	0.06	1.5	0.04
16	Lazy	u. Ostrava	85.2	9.5	209.8	4.6	457	246	11.2	0.11	2.6	0.04
17	Lazy	u. Ostrava	83.7	6	143.3	1.9	456	171	7.2	0.07	1.8	0.04
18	Lazy	u. Ostrava	5.8	1	6.7	1.7	465	114	17.8	0.18	1.3	0.14
19	Lazy	u. Ostrava	49.4	4.1	49.3	2.3	475	100	8.3	0.08	1.1	0.08
20	Lazy	u. Ostrava	12.1	1.6	9	0.6	468	74	13.2	0.13	0.9	0.15
21	Pskov	l. Ostrava	82.8	2.9	87.8	2.6	468	106	3.5	0.04	1.1	0.03
22	Pskov	l. Ostrava	73.1	9.8	101.5	3.3	456	139	13.3	0.13	1.5	0.09
23	Pskov	l. Ostrava	79	2.8	52.2	0.3	482	66	3.6	0.04	0.7	0.05
24	Pskov	l. Ostrava	83.5	1.9	47	3.4	483	56	2.3	0.02	0.6	0.04
25	Pskov	l. Ostrava	85.4	1.9	58.5	0.7	479	69	2.2	0.02	0.7	0.03
26	Pskov	l. Ostrava	83.5	2	58.4	1.8	480	70	2.4	0.02	0.7	0.03
27	Pskov	l. Ostrava	81.6	2.1	91.5	2.2	466	112	2.6	0.03	1.1	0.02
28	Pskov	l. Ostrava	83.3	1.5	82.9	1.6	470	100	1.8	0.02	1	0.02
29	Pskov	l. Ostrava	70.3	2	57.3	2.6	468	81	2.8	0.03	0.8	0.03
30	Pskov	l. Ostrava	78.4	3.5	103.3	3.3	458	132	4.4	0.04	1.4	0.03

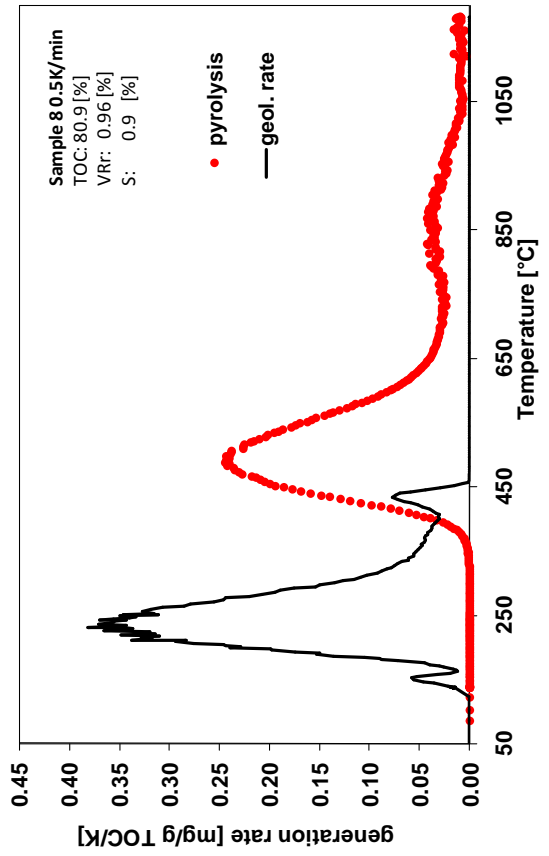
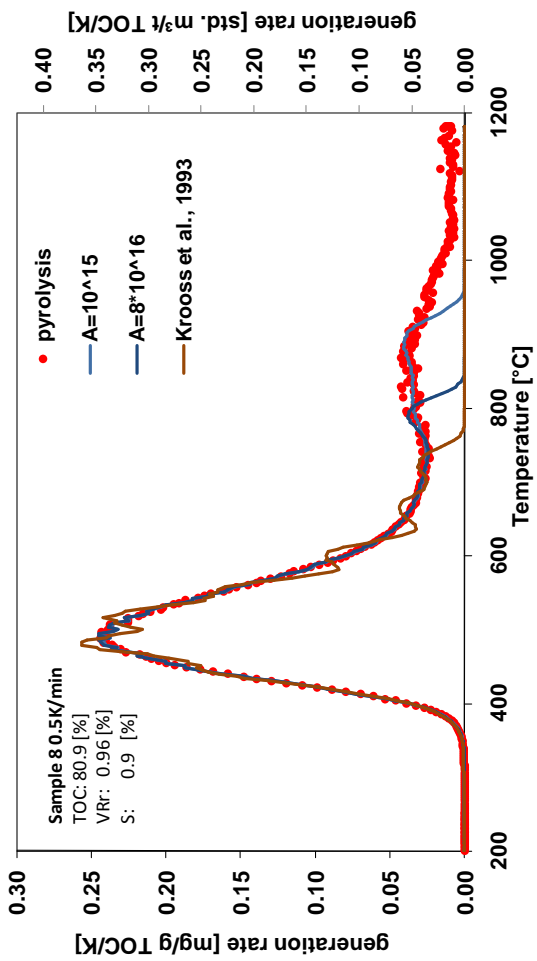
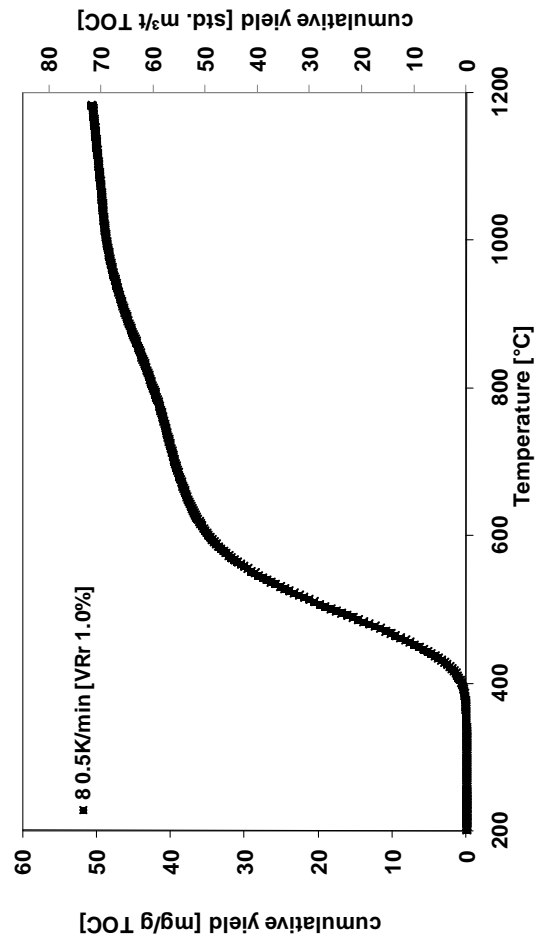
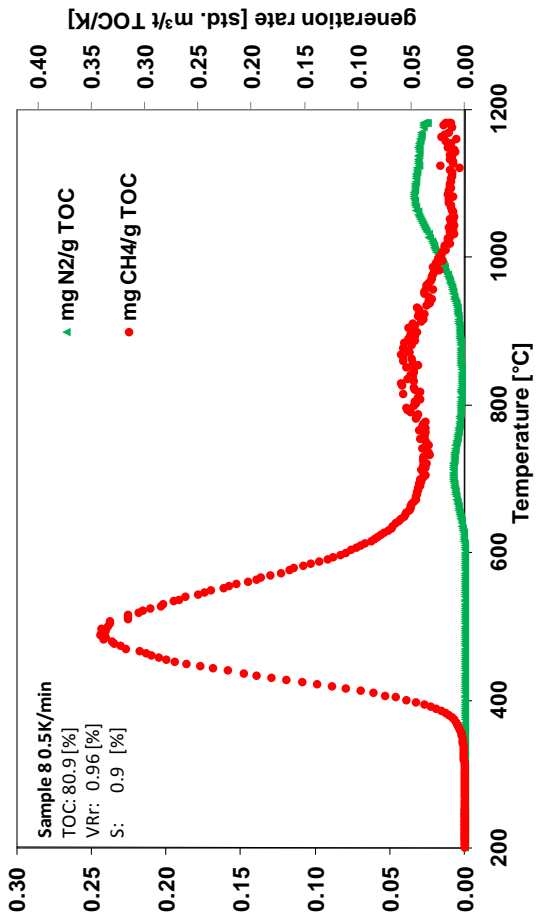
Appendix II Table 2 Results of mass balance calculations

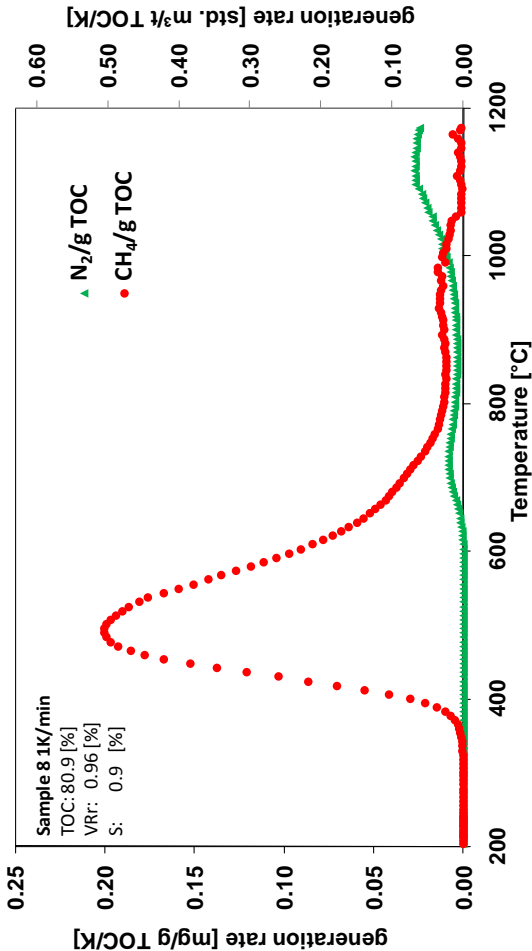
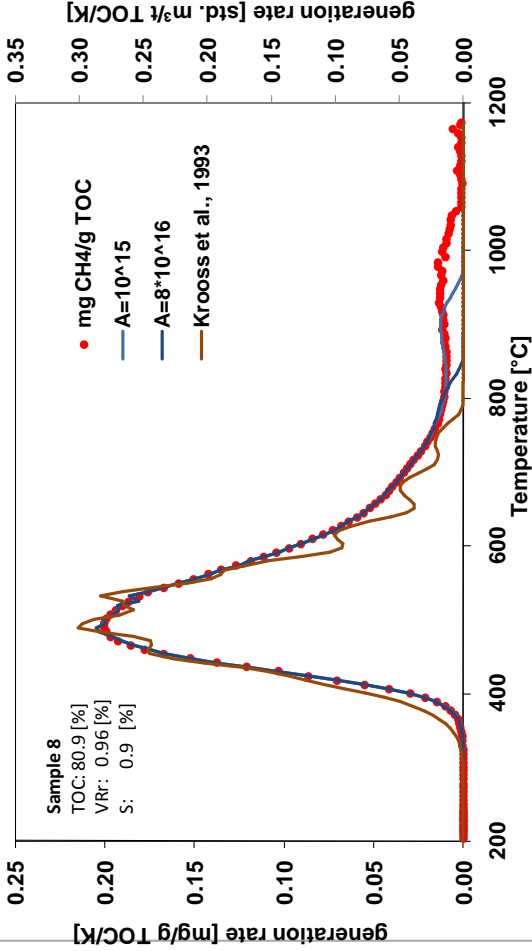
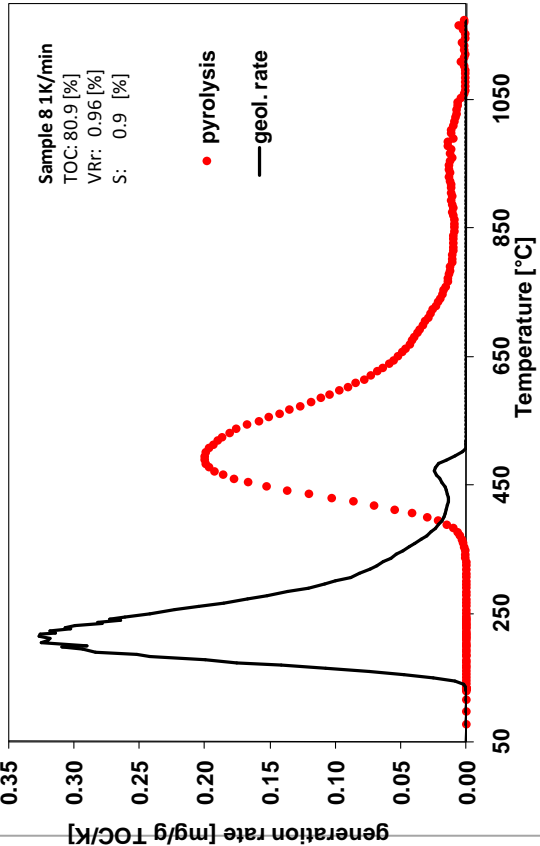
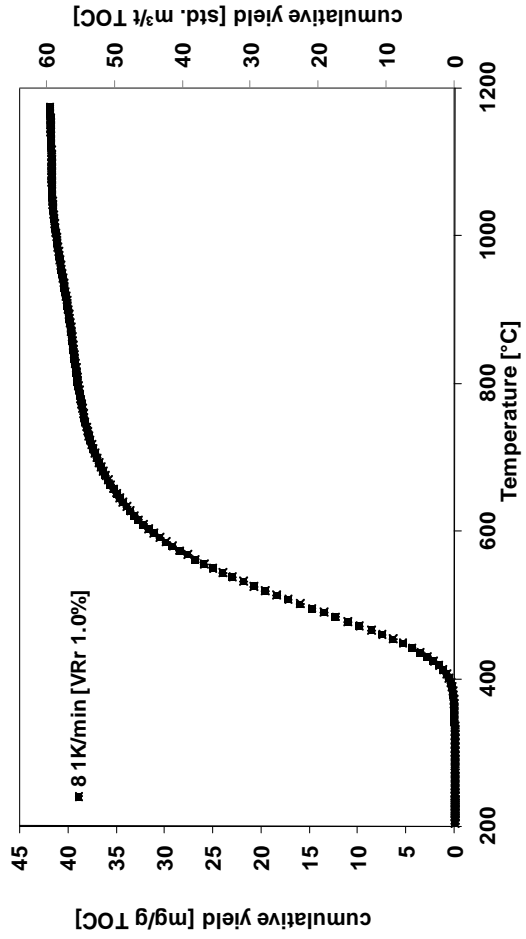
VRc	VM	C	O	H	N	C	O	H	H/C	O/C	$\Delta\text{CH}_4/\text{ncO}$	$\Delta\text{CO}_2/\text{ncO}$
%	wt. %	wt. %	wt. %	wt. %	wt. %	mol	mol	mol			$\text{m}^3\text{CH}_4/\text{tTOC}$	$\text{m}^3\text{CO}_2/\text{tTOC}$
0.57	45	74.00	19.07	5.45	1.48	6.16	1.19	5.40	0.88	0.19		
0.58	44	75.26	17.81	5.44	1.48	6.27	1.11	5.40	0.86	0.18	10.62	13.37
0.59	43	76.46	16.63	5.44	1.47	6.37	1.04	5.39	0.85	0.16	20.32	25.39
0.60	42	77.59	15.51	5.43	1.47	6.46	0.97	5.39	0.83	0.15	29.22	36.21
0.62	41	78.65	14.47	5.42	1.47	6.55	0.90	5.38	0.82	0.14	37.41	45.97
0.64	40	79.64	13.49	5.41	1.46	6.63	0.84	5.37	0.81	0.13	44.99	54.80
0.66	39	80.57	12.57	5.39	1.46	6.71	0.79	5.35	0.80	0.12	52.03	62.78
0.68	38	81.44	11.72	5.38	1.46	6.78	0.73	5.34	0.79	0.11	58.59	70.00
0.71	37	82.26	10.93	5.36	1.45	6.85	0.68	5.32	0.78	0.10	64.73	76.53
0.74	36	83.02	10.19	5.34	1.45	6.91	0.64	5.30	0.77	0.09	70.50	82.45
0.77	35	83.73	9.51	5.32	1.45	6.97	0.59	5.28	0.76	0.09	75.94	87.81
0.80	34	84.38	8.88	5.30	1.44	7.03	0.55	5.25	0.75	0.08	81.09	92.65
0.83	33	84.99	8.30	5.27	1.44	7.08	0.52	5.23	0.74	0.07	85.99	97.04
0.86	32	85.56	7.76	5.24	1.44	7.12	0.49	5.20	0.73	0.07	90.67	100.99
0.90	31	86.08	7.28	5.21	1.43	7.17	0.45	5.17	0.72	0.06	95.15	104.56
0.94	30	86.56	6.83	5.18	1.43	7.21	0.43	5.14	0.71	0.06	99.46	107.78
0.98	29	87.00	6.42	5.15	1.43	7.24	0.40	5.11	0.70	0.06	103.63	110.67
1.02	28	87.41	6.06	5.11	1.42	7.28	0.38	5.07	0.70	0.05	107.68	113.27
1.07	27	87.78	5.73	5.07	1.42	7.31	0.36	5.03	0.69	0.05	111.63	115.59
1.12	26	88.12	5.43	5.03	1.42	7.34	0.34	4.99	0.68	0.05	115.50	117.67
1.17	25	88.44	5.16	4.99	1.41	7.36	0.32	4.95	0.67	0.04	119.30	119.53
1.22	24	88.72	4.92	4.95	1.41	7.39	0.31	4.91	0.66	0.04	123.06	121.19
1.27	23	88.99	4.70	4.90	1.40	7.41	0.29	4.86	0.66	0.04	126.79	122.66
1.32	22	89.23	4.51	4.86	1.40	7.43	0.28	4.82	0.65	0.04	130.49	123.97
1.38	21	89.45	4.34	4.81	1.40	7.45	0.27	4.77	0.64	0.04	134.20	125.14
1.44	20	89.66	4.19	4.75	1.39	7.47	0.26	4.72	0.63	0.04	137.91	126.18
1.50	19	89.85	4.06	4.70	1.39	7.48	0.25	4.66	0.62	0.03	141.65	127.12
1.56	18	90.03	3.94	4.64	1.39	7.50	0.25	4.61	0.61	0.03	145.42	127.96
1.63	17	90.20	3.83	4.59	1.38	7.51	0.24	4.55	0.61	0.03	149.23	128.73
1.70	16	90.37	3.72	4.53	1.38	7.52	0.23	4.49	0.60	0.03	153.10	129.43
1.77	15	90.53	3.63	4.47	1.38	7.54	0.23	4.43	0.59	0.03	157.03	130.10
1.84	14	90.68	3.54	4.40	1.37	7.55	0.22	4.37	0.58	0.03	161.04	130.73
1.91	13	90.84	3.45	4.34	1.37	7.56	0.22	4.30	0.57	0.03	165.12	131.35
1.98	12	91.00	3.36	4.27	1.37	7.58	0.21	4.23	0.56	0.03	169.30	131.98
2.06	11	91.17	3.27	4.20	1.36	7.59	0.20	4.17	0.55	0.03	173.56	132.62
2.14	10	91.34	3.17	4.13	1.36	7.60	0.20	4.09	0.54	0.03	177.93	133.29
2.22	9	91.52	3.07	4.05	1.36	7.62	0.19	4.02	0.53	0.03	182.40	134.00
2.30	8	91.72	2.95	3.98	1.35	7.64	0.18	3.95	0.52	0.02	186.98	134.77
2.39	7	91.93	2.83	3.90	1.35	7.65	0.18	3.87	0.51	0.02	191.68	135.62
2.48	6	92.15	2.68	3.82	1.35	7.67	0.17	3.79	0.49	0.02	196.49	136.55

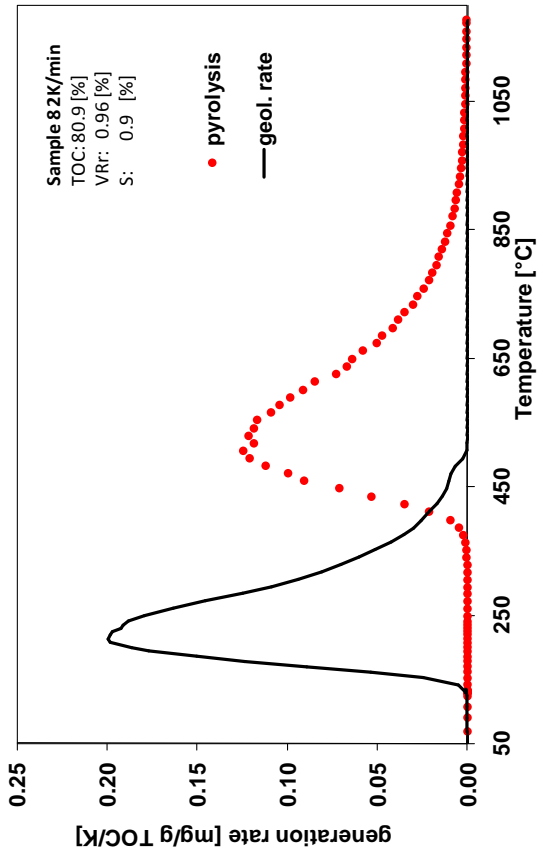
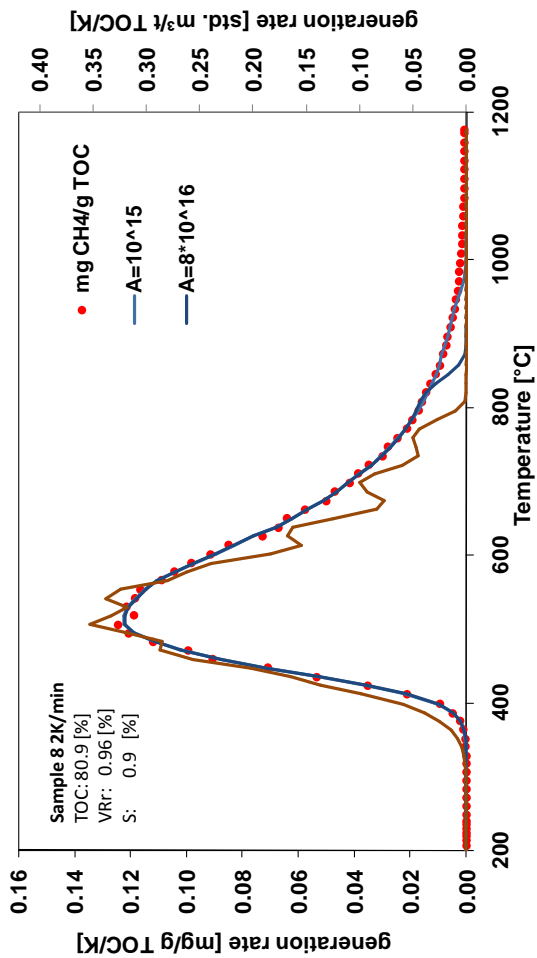
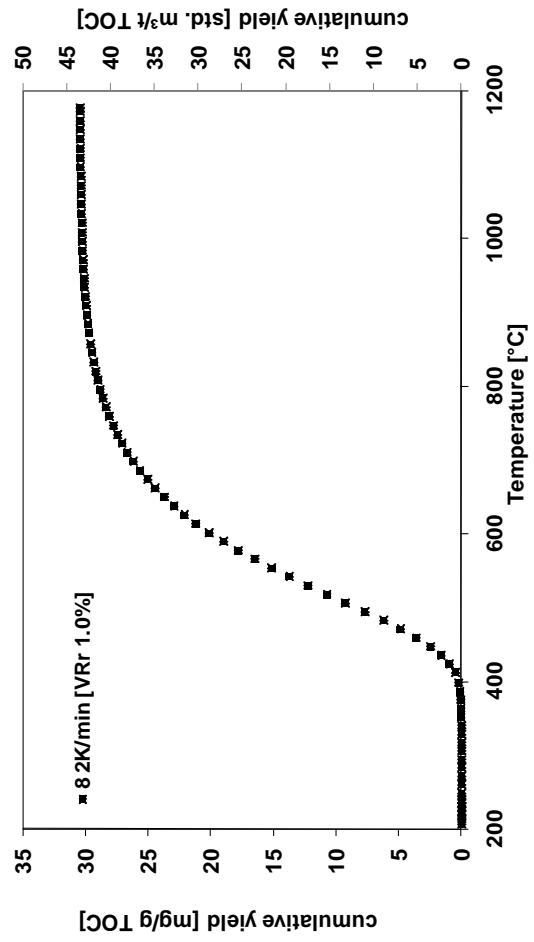
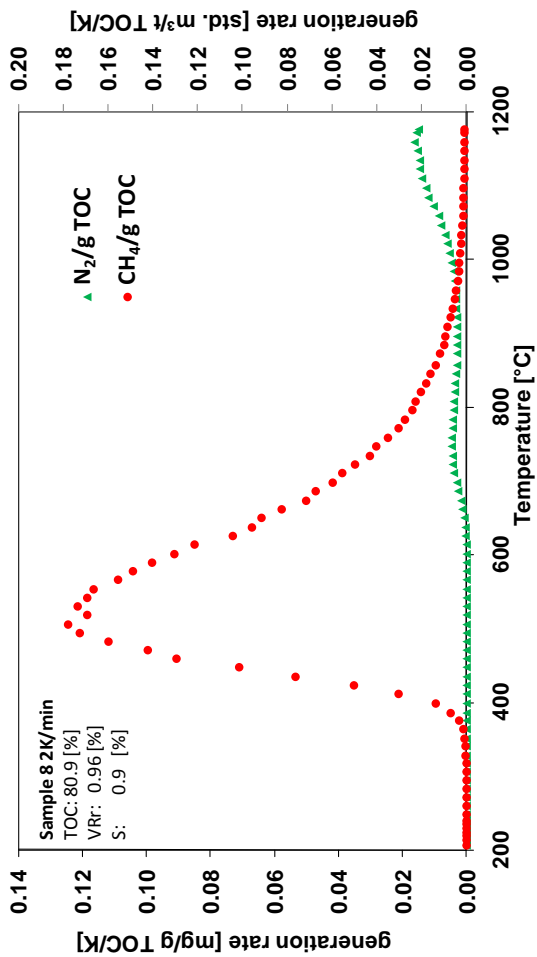
Appendix II Results of temperature-programmed open system pyrolysis

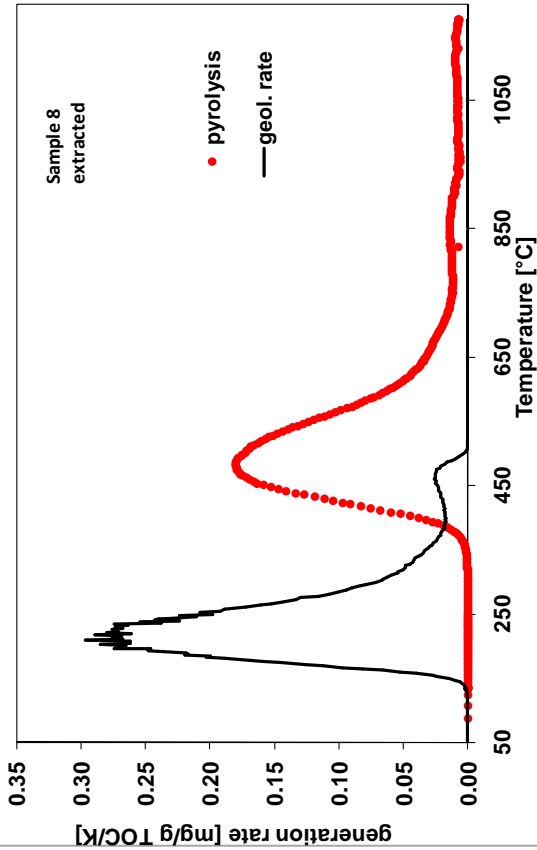
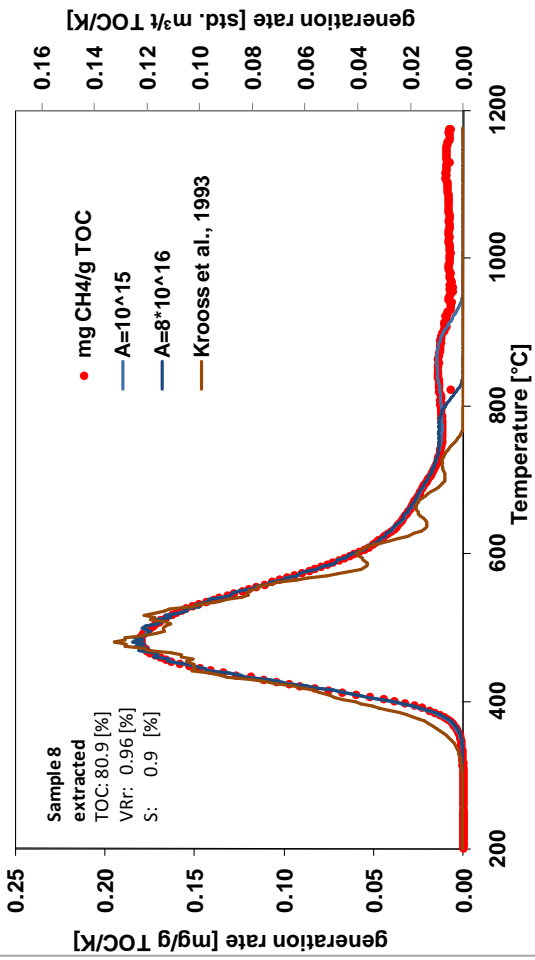
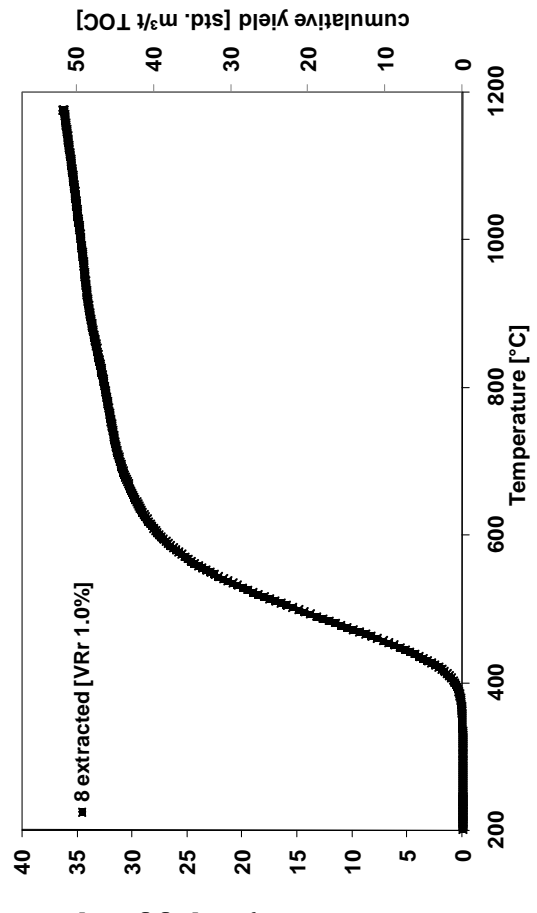
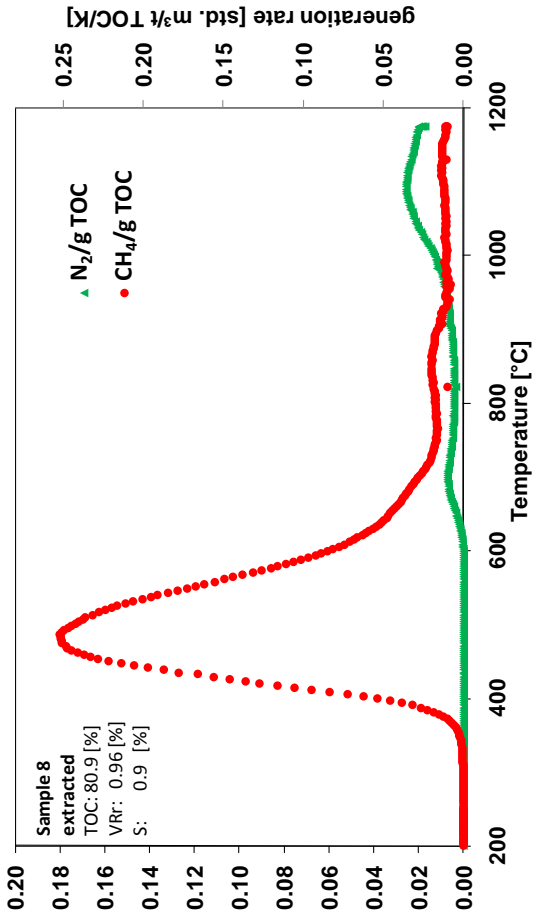


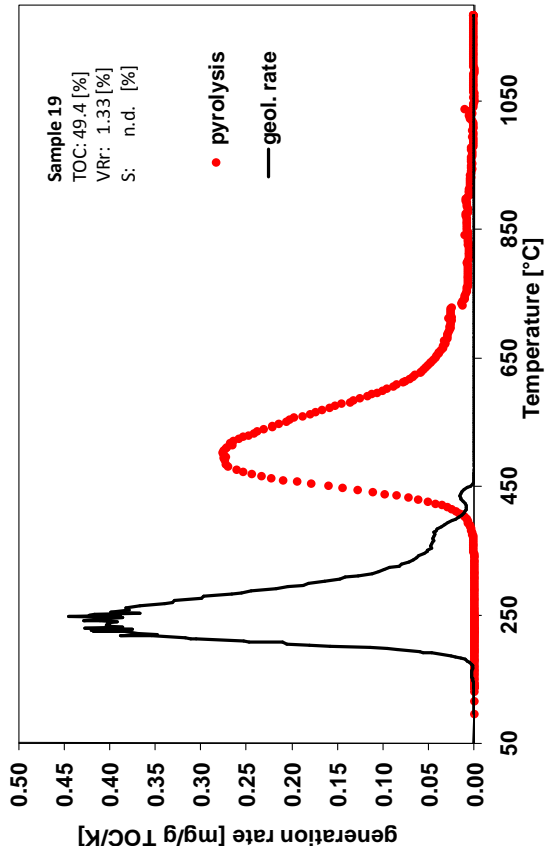
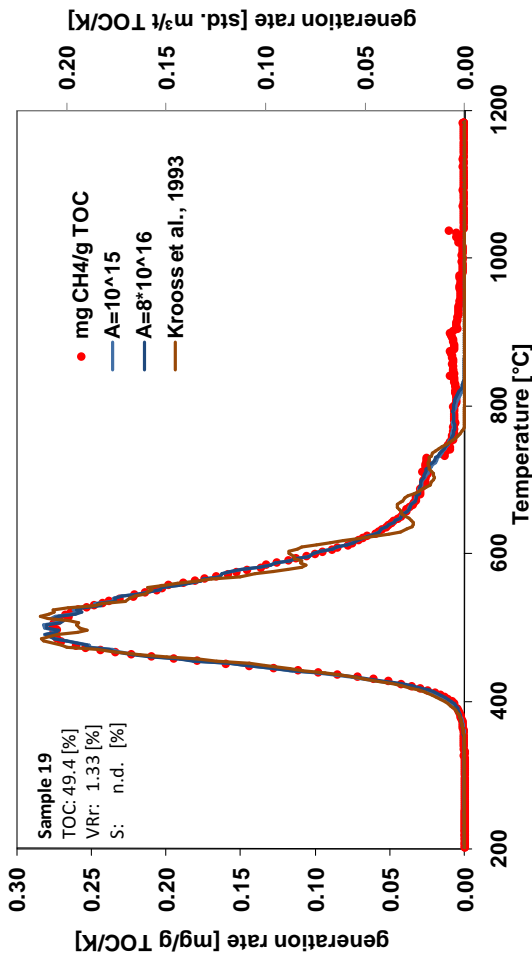
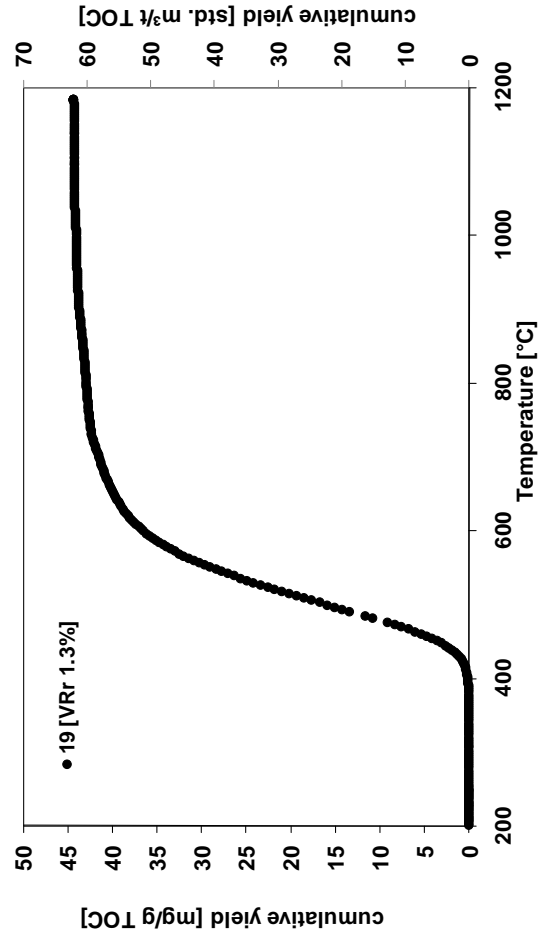
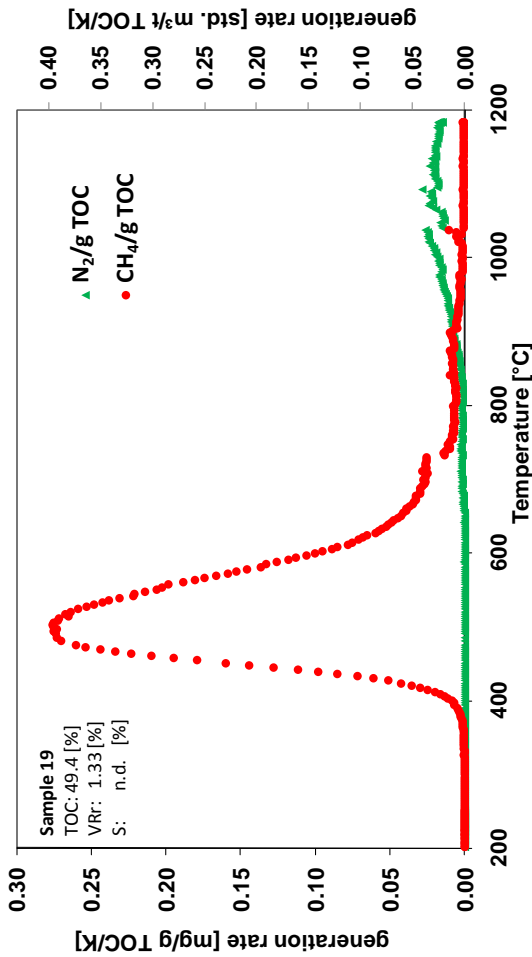


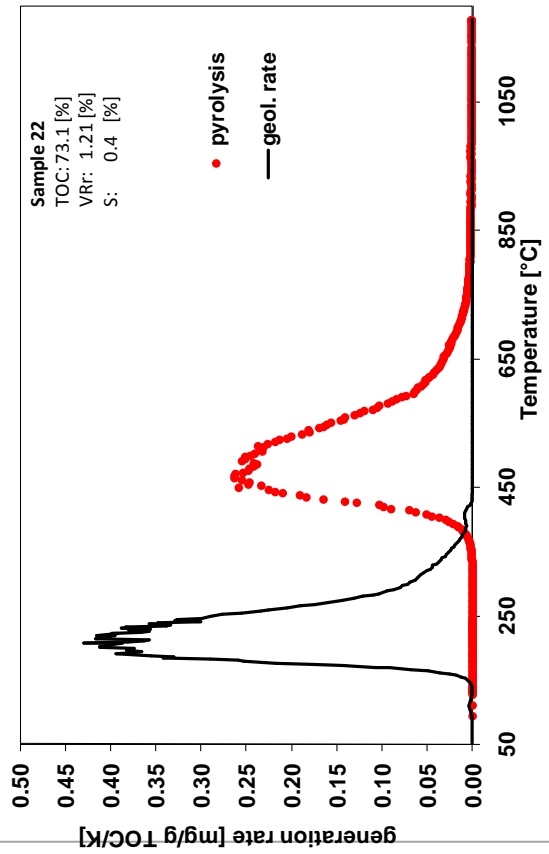
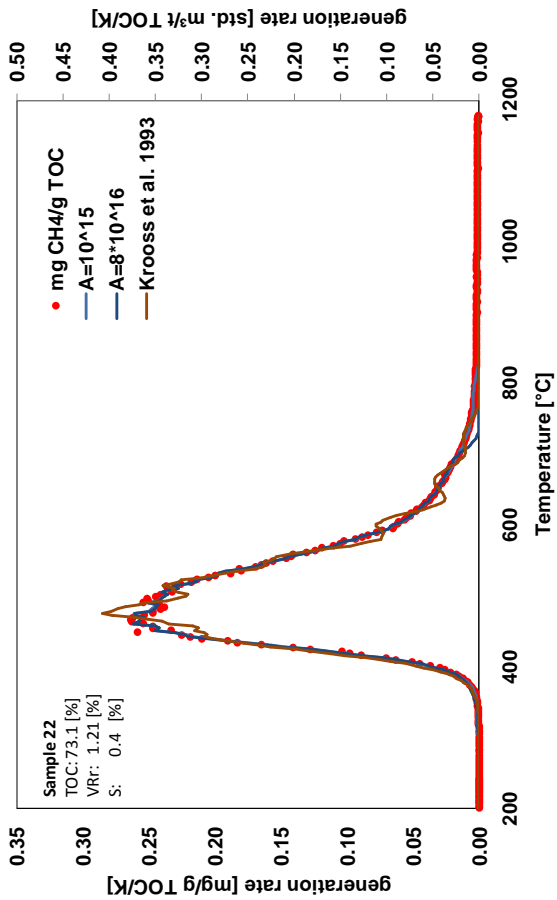
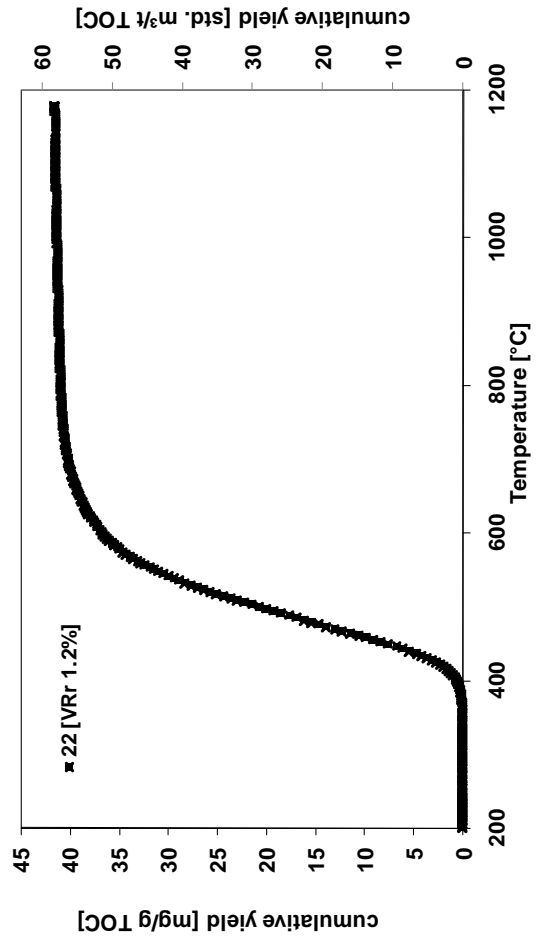
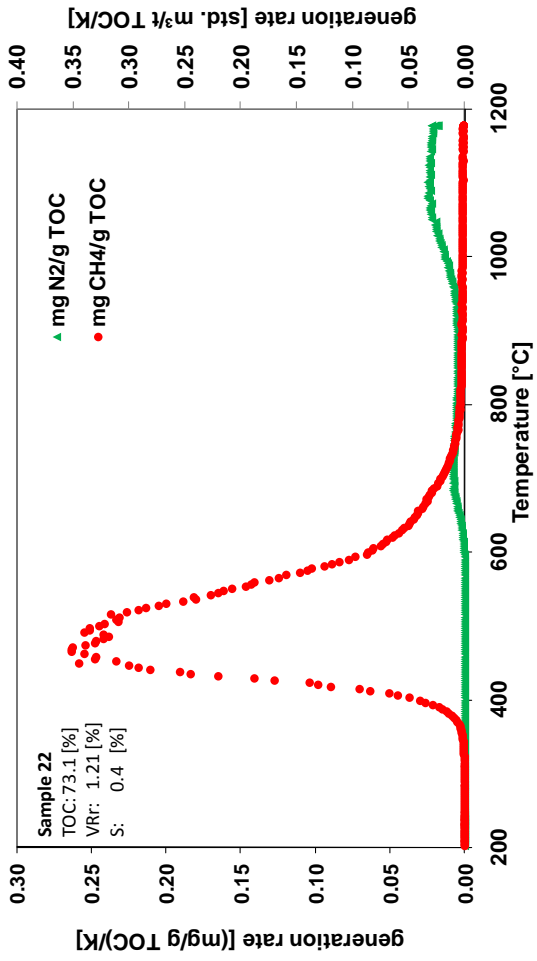


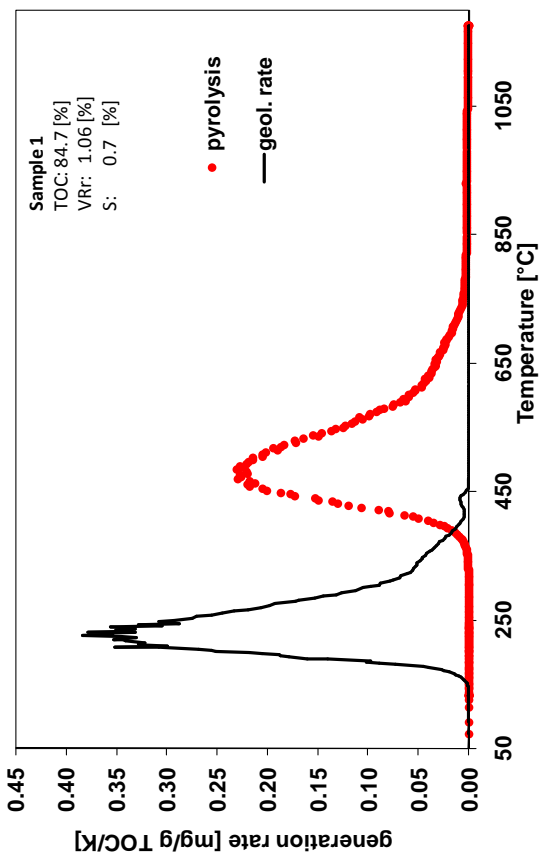
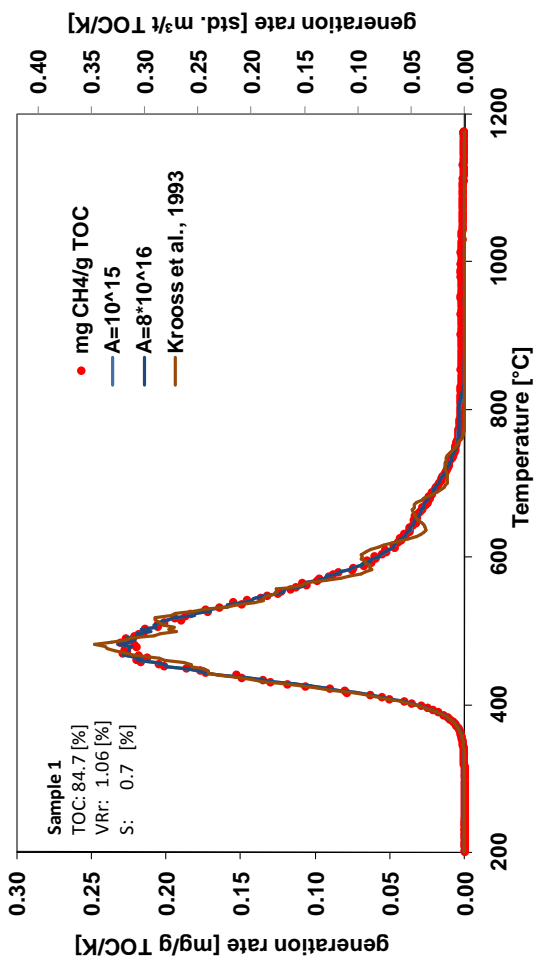
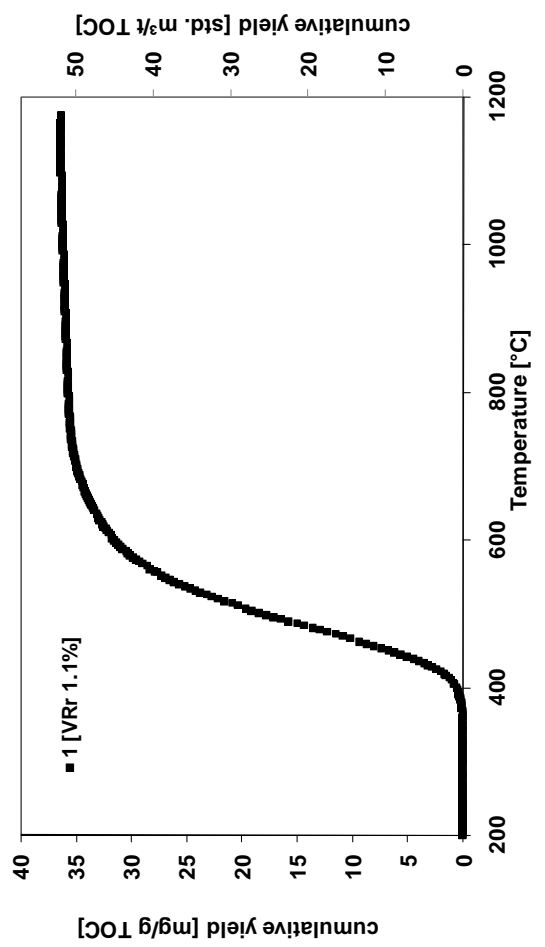
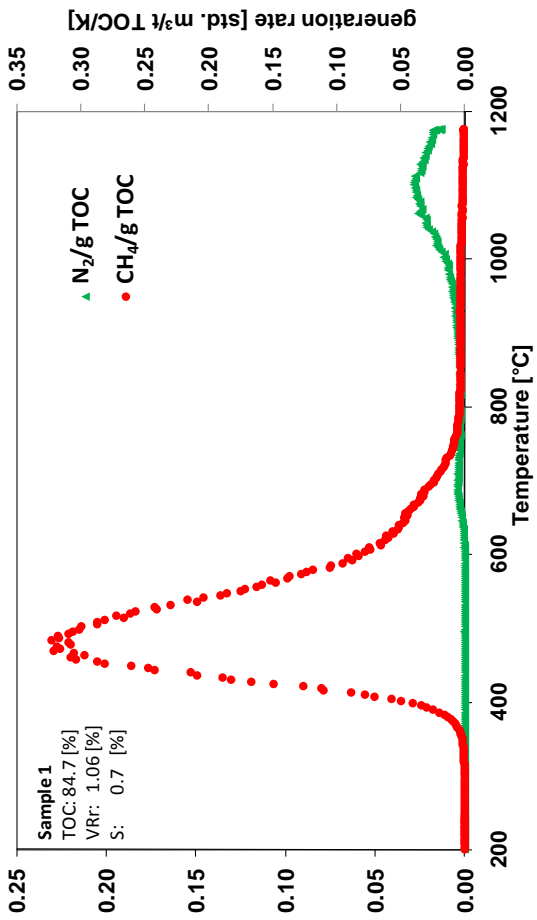


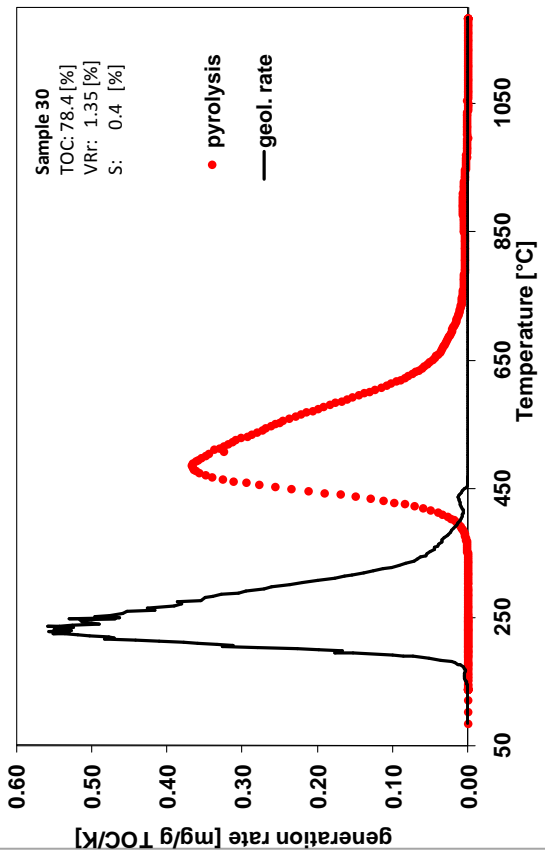
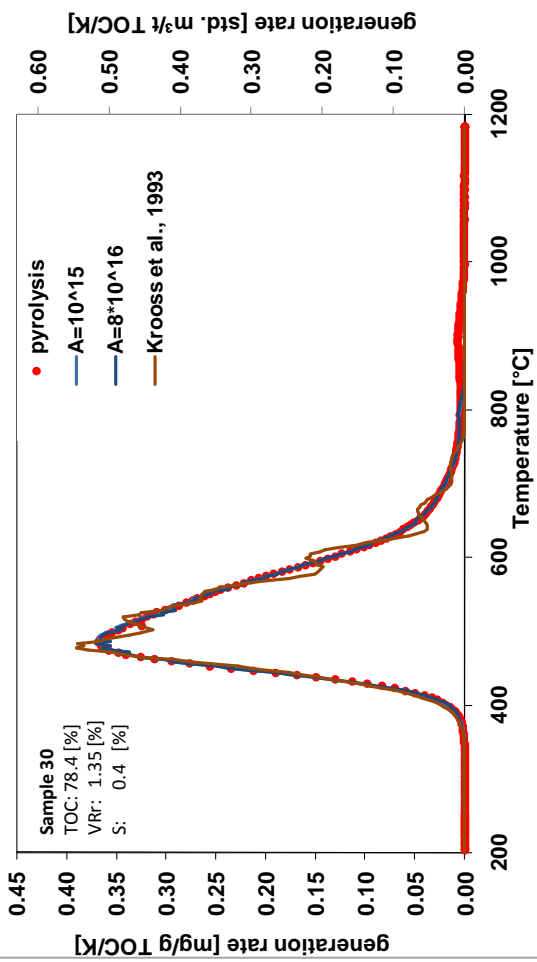
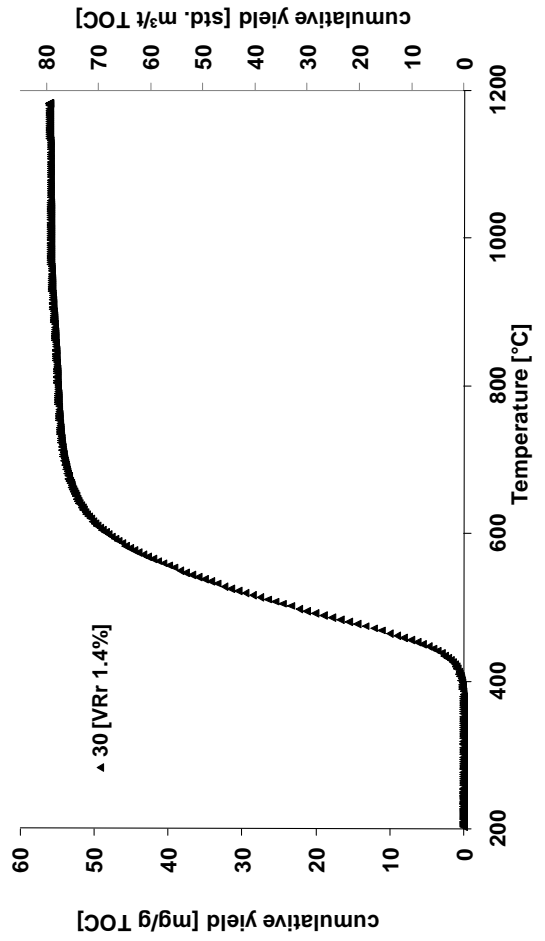
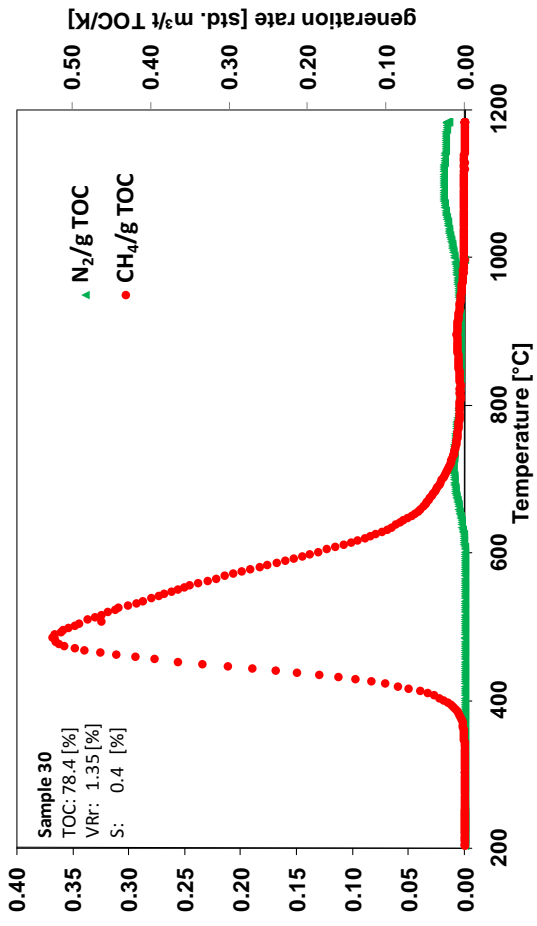












Appendix II Table 3 Temperature and maturity values derived from 1D basin modeling (PetroMod11) for different formations of the USCB. EASY%Ro values calculated after Sweeney and Burnham (1987). Sample number indicates coal samples that were analyzed from the respective geologic formation.

sample: 1			sample: 8			sample: 19			sample: 22			sample: 24			sample: 30		
seam:	648		seam:	504		seam:	386		seam:	112		seam:	82	41	seam:	82	41
Formation:	L. Sucha M.		Formation:	Saddle M.		Formation:	Jaklovec M.		Formation:	L. Hrušov M.		Formation:	Petrkovice M	Petrkovice M	Formation:	Petrkovice M	Petrkovice M
Time	Temperature	EASY%Ro	Time	Temperature	EASY%Ro	Time	Temperature	EASY%Ro	Time	Temperature	EASY%Ro	Time	Temperature	EASY%Ro	Time	Temperature	EASY%Ro
[Ma]	[°C]	[%Ro]	[Ma]	[°C]	[%Ro]	[Ma]	[°C]	[%Ro]	[Ma]	[°C]	[%Ro]	[Ma]	[°C]	[%Ro]	[Ma]	[°C]	[%Ro]
318	33	0.24	319	33	0.24	322	34	0.25	324	34	0.24	326	35	0.25			
317	44	0.28	318	47	0.30	320	59	0.33	322	50	0.32	325	51	0.31			
314	76	0.43	317	56	0.32	319	71	0.38	320	72	0.38	324	66	0.36			
310	107	0.63	314	85	0.48	318	82	0.43	319	83	0.44	322	80	0.44			
305	116	0.71	310	115	0.69	317	89	0.46	318	94	0.49	320	100	0.54			
300	128	0.80	305	125	0.77	314	115	0.68	317	101	0.53	319	110	0.60			
292	113	0.80	300	136	0.88	310	145	0.98	314	127	0.77	318	121	0.68			
282	93	0.80	292	121	0.89	305	155	1.18	310	157	1.17	317	127	0.71			
255	62	0.80	282	102	0.89	300	166	1.38	305	167	1.40	314	153	1.08			
19	22	0.80	255	70	0.89	292	152	1.40	300	178	1.64	310	183	1.67			
18	24	0.80	19	30	0.89	282	131	1.40	292	164	1.66	305	193	2.00			
15	36	0.80	18	32	0.89	255	99	1.40	282	143	1.66	300	204	2.31			
13	38	0.80	15	44	0.89	19	55	1.40	255	110	1.66	292	190	2.34			
2	24	0.80	13	46	0.89	18	57	1.40	19	66	1.66	282	169	2.35			
0	23	0.80	2	32	0.89	15	69	1.40	18	68	1.66	255	135	2.35			
			0	30	0.89	13	72	1.40	15	79	1.66	19	88	2.35			
						2	57	1.40	13	82	1.66	18	89	2.35			
						0	56	1.40	2	68	1.66	15	101	2.35			
									0	67	1.66	13	104	2.35			
												2	90	2.35			
												0	88	2.35			

Table 4 Results of temperature-programmed open system pyrolysis (continued)

2021.5	1009.9	0.0004	0.0029	2027.2	997.0	0.0011	0.0048	2015.0	1006.8	0.0061	0.0076
2027.7	1013.3	0.0004	0.0032	2033.4	999.8	0.0010	0.0047	2021.2	1009.8	0.0053	0.0080
2033.9	1016.4	0.0004	0.0030	2039.6	1002.8	0.0010	0.0051	2027.4	1013.0	0.0054	0.0082
2040.1	1019.8	0.0004	0.0035	2045.8	1006.2	0.0010	0.0050	2033.6	1015.8	0.0056	0.0085
2046.3	1023.0	0.0004	0.0032	2052.0	1009.0	0.0011	0.0057	2039.9	1018.7	0.0041	0.0087
2052.5	1026.3	0.0003	0.0033	2058.2	1012.2	0.0012	0.0061	2046.0	1021.6	0.0045	0.0090
2058.7	1029.6	0.0004	0.0032	2064.4	1015.0	0.0010	0.0063	2052.2	1025.0	0.0046	0.0094
2064.9	1033.0	0.0004	0.0035	2070.6	1017.9	0.0010	0.0070	2058.5	1027.7	0.0041	0.0097
2071.1	1036.3	0.0004	0.0035	2076.8	1021.2	0.0009	0.0068	2064.7	1030.8	0.0028	0.0099
2077.3	1039.8	0.0004	0.0036	2083.0	1024.7	0.0009	0.0068	2070.8	1034.1	0.0040	0.0103
2083.5	1042.8	0.0003	0.0032	2089.2	1027.5	0.0008	0.0070	2077.1	1037.0	0.0032	0.0107
2089.7	1046.4	0.0004	0.0036	2095.4	1030.5	0.0008	0.0073	2083.3	1039.7	0.0043	0.0110
2095.9	1049.7	0.0003	0.0033	2101.6	1033.6	0.0008	0.0076	2089.4	1042.9	0.0030	0.0113
2102.1	1052.9	0.0003	0.0031	2107.8	1036.8	0.0008	0.0081	2095.7	1046.1	0.0036	0.0116
2108.3	1056.1	0.0004	0.0036	2114.0	1040.1	0.0008	0.0088	2101.9	1049.1	0.0030	0.0119
2114.5	1059.6	0.0004	0.0037	2120.2	1043.0	0.0008	0.0092	2108.1	1051.7	0.0041	0.0121
2120.7	1063.1	0.0004	0.0035	2126.4	1046.1	0.0007	0.0093	2114.3	1055.1	0.0027	0.0124
2126.9	1066.7	0.0004	0.0036	2132.6	1049.3	0.0007	0.0095	2120.5	1057.8	0.0032	0.0126
2133.1	1069.9	0.0003	0.0034	2138.8	1053.2	0.0007	0.0094	2126.7	1061.3	0.0031	0.0128
2139.4	1073.2	0.0004	0.0033	2145.0	1055.6	0.0006	0.0096	2132.9	1063.6	0.0035	0.0132
2145.5	1076.5	0.0004	0.0035	2151.2	1058.5	0.0007	0.0105	2139.1	1067.2	0.0037	0.0132
2151.7	1079.7	0.0004	0.0033	2157.4	1061.7	0.0007	0.0113	2145.3	1070.5	0.0038	0.0135
2158.0	1083.6	0.0004	0.0033	2163.6	1064.9	0.0006	0.0110	2151.5	1072.8	0.0042	0.0136
2164.2	1087.1	0.0004	0.0035	2169.8	1067.9	0.0006	0.0104	2157.7	1075.8	0.0042	0.0136
2170.4	1090.1	0.0004	0.0036	2176.0	1071.2	0.0007	0.0108	2163.9	1079.3	0.0043	0.0137
2176.6	1093.4	0.0003	0.0034	2182.2	1074.2	0.0006	0.0110	2170.1	1082.0	0.0032	0.0138
2182.8	1096.8	0.0003	0.0033	2188.4	1077.3	0.0006	0.0110	2176.3	1084.8	0.0045	0.0138
2189.0	1100.3	0.0004	0.0036	2194.6	1080.3	0.0006	0.0115	2182.5	1087.8	0.0042	0.0138
2195.2	1103.8	0.0004	0.0034	2200.8	1083.9	0.0005	0.0119	2188.7	1090.7	0.0043	0.0136
2201.4	1107.0	0.0004	0.0036	2207.0	1086.8	0.0005	0.0116	2194.9	1094.2	0.0037	0.0136
2207.6	1111.3	0.0004	0.0037	2213.2	1090.7	0.0005	0.0119	2201.1	1096.8	0.0041	0.0135
2213.8	1114.2	0.0004	0.0037	2219.4	1093.5	0.0005	0.0119	2207.3	1099.9	0.0039	0.0136
2220.0	1117.5	0.0004	0.0035	2225.6	1096.6	0.0005	0.0122	2213.5	1102.8	0.0038	0.0134
2226.2	1120.8	0.0004	0.0037	2231.8	1100.0	0.0005	0.0124	2219.7	1106.0	0.0037	0.0134
2232.4	1124.1	0.0004	0.0033	2238.0	1103.5	0.0005	0.0124	2225.9	1109.0	0.0036	0.0132
2238.6	1127.8	0.0003	0.0033	2244.2	1106.2	0.0005	0.0121	2232.1	1111.7	0.0035	0.0131
2244.8	1131.4	0.0004	0.0038	2250.4	1109.5	0.0005	0.0118	2238.3	1114.9	0.0034	0.0131
2251.0	1134.4	0.0003	0.0032	2256.6	1112.9	0.0005	0.0123	2244.5	1117.6	0.0042	0.0130
2257.2	1138.0	0.0004	0.0032	2262.8	1116.0	0.0004	0.0109	2250.7	1120.8	0.0015	0.0129
2263.4	1141.3	0.0004	0.0036	2269.0	1118.9	0.0004	0.0106	2256.9	1123.8	0.0067	0.0125
2269.6	1145.8	0.0003	0.0032	2275.2	1121.8	0.0004	0.0106	2263.1	1126.4	0.0031	0.0128
2275.8	1149.5	0.0003	0.0032	2281.4	1124.7	0.0004	0.0104	2269.3	1130.3	0.0032	0.0127
2282.0	1152.7	0.0004	0.0035	2287.6	1128.1	0.0003	0.0108	2275.5	1133.1	0.0039	0.0127
2288.2	1156.2	0.0004	0.0035	2293.8	1131.2	0.0005	0.0103	2281.7	1136.2	0.0036	0.0127
2294.4	1160.4	0.0003	0.0032	2300.0	1134.3	0.0004	0.0099	2287.9	1138.9	0.0039	0.0125
2300.6	1164.2	0.0004	0.0035	2306.2	1137.5	0.0003	0.0101	2294.1	1142.0	0.0026	0.0124
2306.8	1167.5	0.0003	0.0032	2312.4	1140.3	0.0003	0.0097	2300.3	1145.0	0.0029	0.0124
2313.0	1171.2	0.0003	0.0030	2318.6	1143.7	0.0004	0.0097	2306.5	1147.8	0.0045	0.0126
2319.2	1174.6	0.0003	0.0033	2324.8	1146.9	0.0003	0.0091	2312.7	1151.2	0.0042	0.0124
2325.4	1178.3	0.0003	0.0034	2331.0	1149.8	0.0004	0.0091	2318.9	1154.1	0.0037	0.0124
2331.6	1181.8	0.0004	0.0034	2337.2	1152.8	0.0003	0.0087	2325.1	1157.0	0.0051	0.0121
2337.8	1185.3	0.0003	0.0031	2343.4	1155.7	0.0003	0.0082	2331.3	1160.5	0.0024	0.0121
2344.0	1189.1	0.0003	0.0033	2349.6	1159.1	0.0003	0.0085	2337.5	1163.1	0.0064	0.0119
2350.2	1192.6	0.0003	0.0034	2355.8	1162.1	0.0003	0.0080	2343.7	1166.4	0.0054	0.0118
2356.4	1195.9	0.0003	0.0035	2362.0	1164.9	0.0003	0.0080	2349.9	1169.3	0.0043	0.0117
2362.7	1199.4	0.0003	0.0033	2368.2	1168.0	0.0003	0.0078	2356.1	1173.3	0.0035	0.0114
2368.9	1202.9	0.0003	0.0031	2374.4	1171.2	0.0003	0.0077	2362.3	1176.4	0.0057	0.0112
2375.1	1206.4	0.0003	0.0031	2380.6	1173.7	0.0003	0.0076	2368.5	1179.4	0.0050	0.0112
2381.3	1209.8	0.0003	0.0034	2386.8	1175.1	0.0003	0.0075	2374.7	1181.2	0.0052	0.0110
				2393.0	1175.1	0.0002	0.0072	2380.9	1181.2	0.0036	0.0108
				2399.2	1175.1	0.0003	0.0069	2387.1	1181.3	0.0043	0.0105
				2405.4	1175.4	0.0002	0.0063	2393.3	1181.3	0.0041	0.0102
				2411.6	1175.0	0.0002	0.0060	2399.6	1181.6	0.0041	0.0102
				2417.8	1175.2	0.0002	0.0057				

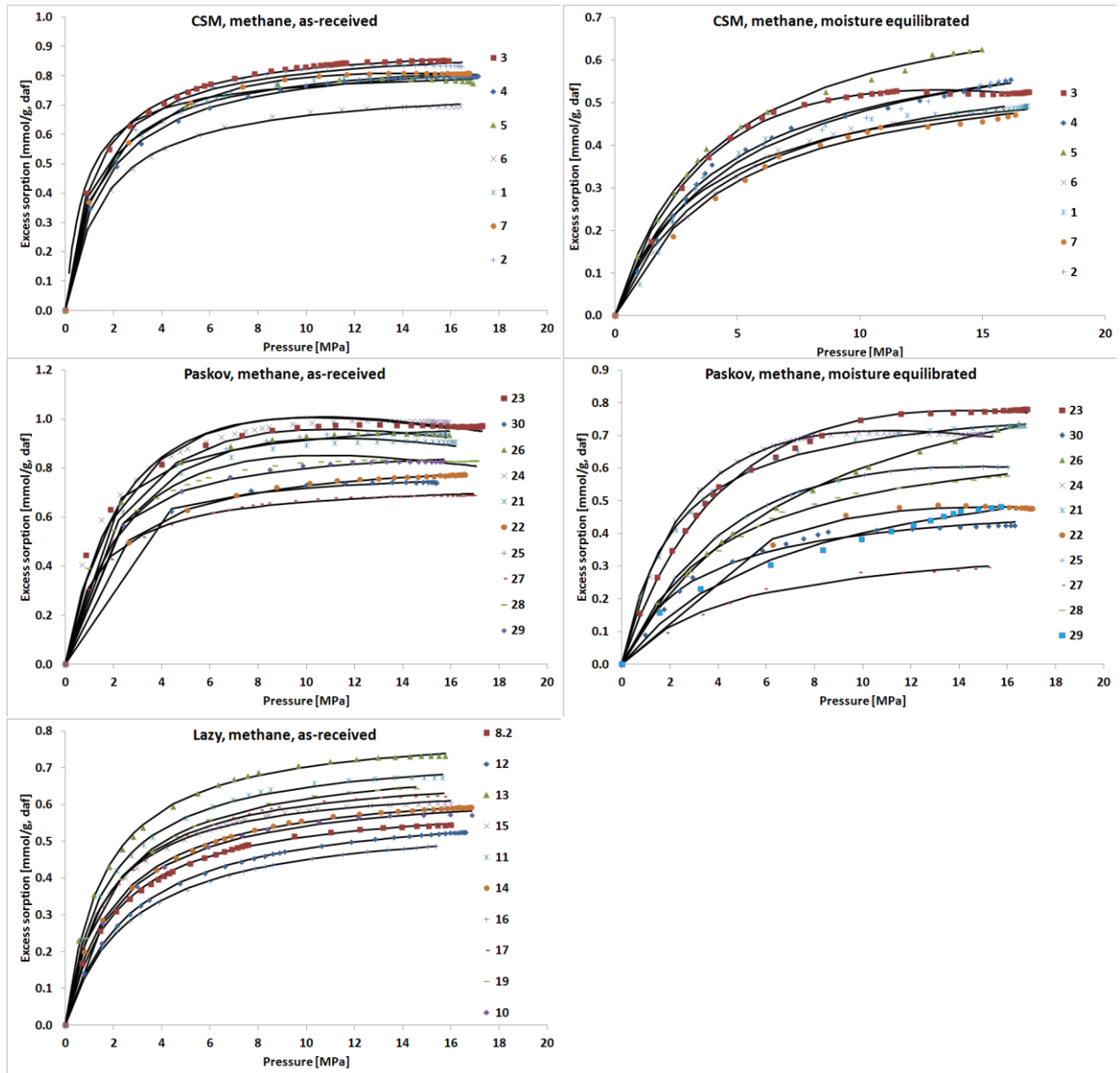
Table 5 Results of temperature-programmed open system pyrolysis (continued)

626.0	318.8	0.0001	0.0000	626.7	329.1	0.0000	0.0000	626.1	316.7	0.0001	0.0000	626.1	317.8	0.0001	0.0000	626.7	333.7	0.0001	0.0000
632.2	321.7	0.0002	0.0000	632.9	332.1	0.0001	0.0000	632.3	319.4	0.0001	0.0000	632.3	320.9	0.0001	0.0000	632.9	336.7	0.0001	0.0000
638.4	324.8	0.0002	0.0000	639.1	335.0	0.0001	0.0000	638.5	323.3	0.0001	0.0000	638.5	323.6	0.0001	0.0000	639.1	339.5	0.0002	0.0000
644.6	327.7	0.0002	0.0000	645.3	338.7	0.0001	0.0000	644.7	325.1	0.0001	0.0000	644.7	326.7	0.0001	0.0000	645.3	342.8	0.0002	0.0000
650.8	330.6	0.0003	0.0000	651.5	341.8	0.0001	0.0000	650.9	328.2	0.0002	0.0000	650.9	329.5	0.0001	0.0000	651.5	345.6	0.0002	0.0000
657.0	333.5	0.0002	0.0000	657.7	344.7	0.0001	0.0000	657.1	331.0	0.0002	0.0000	657.1	332.5	0.0001	0.0000	657.7	348.7	0.0002	0.0000
663.2	336.7	0.0004	0.0000	663.9	347.7	0.0002	0.0000	663.3	333.9	0.0002	0.0000	663.3	335.4	0.0001	0.0000	663.9	351.8	0.0003	0.0000
669.4	339.6	0.0004	0.0000	670.1	350.8	0.0002	0.0000	669.5	336.9	0.0002	0.0000	669.5	338.3	0.0002	0.0000	670.1	354.7	0.0003	0.0000
675.6	342.5	0.0005	0.0000	676.3	353.8	0.0002	0.0000	675.7	339.5	0.0002	0.0000	675.7	341.3	0.0002	0.0000	676.3	357.8	0.0004	0.0000
681.8	345.4	0.0005	0.0000	682.5	356.9	0.0002	0.0000	681.9	342.5	0.0003	0.0000	681.9	344.3	0.0002	0.0000	682.5	360.7	0.0005	0.0000
688.0	348.6	0.0007	0.0000	688.7	359.9	0.0002	0.0000	688.1	345.5	0.0004	0.0000	688.1	347.1	0.0003	0.0000	688.8	363.9	0.0006	0.0000
694.2	351.4	0.0008	0.0000	694.9	363.0	0.0003	0.0000	694.3	349.0	0.0005	0.0000	694.3	350.1	0.0003	0.0000	695.0	366.9	0.0008	0.0000
700.3	354.4	0.0010	0.0000	701.1	365.8	0.0004	0.0000	700.5	351.8	0.0006	0.0000	700.5	353.0	0.0003	0.0000	701.2	369.9	0.0009	0.0000
706.5	357.3	0.0012	0.0000	707.3	368.8	0.0004	0.0000	706.7	355.0	0.0006	0.0000	706.7	355.9	0.0004	0.0000	707.4	372.9	0.0011	0.0000
712.7	360.4	0.0014	0.0000	713.5	371.7	0.0004	0.0000	712.9	357.6	0.0008	0.0000	712.9	358.8	0.0004	0.0000	713.6	375.9	0.0014	0.0000
718.9	363.3	0.0018	0.0000	719.7	374.7	0.0006	0.0000	719.1	360.7	0.0010	0.0000	719.1	361.9	0.0005	0.0000	719.8	379.0	0.0017	0.0000
725.1	366.3	0.0022	0.0000	725.9	377.8	0.0006	0.0000	725.3	363.6	0.0011	0.0000	725.3	364.8	0.0006	0.0000	726.0	381.9	0.0021	0.0000
731.4	369.3	0.0026	0.0000	732.1	380.7	0.0007	0.0000	731.5	366.5	0.0014	0.0000	731.5	367.8	0.0007	0.0000	732.2	385.2	0.0027	0.0000
737.5	372.1	0.0031	0.0000	738.3	384.1	0.0009	0.0000	737.7	369.4	0.0017	0.0000	737.7	370.6	0.0007	0.0000	738.4	388.1	0.0033	0.0000
743.7	375.2	0.0038	0.0000	744.5	387.0	0.0011	0.0000	743.9	372.3	0.0021	0.0000	743.9	373.5	0.0009	0.0000	744.6	390.9	0.0039	0.0000
749.9	378.3	0.0046	0.0000	750.7	389.8	0.0012	0.0000	750.1	375.1	0.0025	0.0000	750.1	377.1	0.0011	0.0000	750.8	394.1	0.0049	0.0000
756.1	381.2	0.0056	0.0000	757.0	393.1	0.0017	0.0000	756.3	378.2	0.0031	0.0000	756.3	380.1	0.0012	0.0000	757.0	397.2	0.0060	0.0000
762.3	384.1	0.0068	0.0000	763.1	396.0	0.0018	0.0000	762.5	380.8	0.0037	0.0000	762.5	383.0	0.0015	0.0000	763.2	400.1	0.0074	0.0000
768.5	387.2	0.0082	0.0000	769.4	399.1	0.0022	0.0000	768.7	382.4	0.0044	0.0000	768.7	385.9	0.0017	0.0000	769.4	403.1	0.0090	0.0000
774.7	390.2	0.0098	0.0000	775.6	402.3	0.0028	0.0000	774.9	387.0	0.0054	0.0000	774.9	388.9	0.0021	0.0000	775.6	406.3	0.0109	0.0000
780.9	393.1	0.0117	0.0000	781.8	405.1	0.0033	0.0000	781.1	389.8	0.0062	0.0000	781.1	391.9	0.0025	0.0000	781.8	409.4	0.0131	0.0000
787.1	396.1	0.0139	0.0000	788.0	408.1	0.0040	0.0000	787.3	393.0	0.0078	0.0000	787.3	394.8	0.0029	0.0000	788.0	412.3	0.0158	0.0000
793.3	399.1	0.0164	0.0000	794.2	411.1	0.0049	0.0000	793.5	395.8	0.0094	0.0000	793.5	397.8	0.0035	0.0000	794.2	416.0	0.0197	0.0000
799.5	402.1	0.0190	0.0000	800.4	414.1	0.0061	0.0000	799.7	398.8	0.0108	0.0000	799.7	400.7	0.0042	0.0000	800.5	418.9	0.0235	0.0000
805.7	405.3	0.0221	0.0000	806.6	417.3	0.0074	0.0000	805.9	401.7	0.0134	0.0000	805.9	403.7	0.0050	0.0000	806.7	422.0	0.0278	0.0000
811.9	408.2	0.0254	0.0000	812.8	420.1	0.0089	0.0000	812.1	404.6	0.0163	0.0000	812.1	406.7	0.0059	0.0000	812.9	425.3	0.0327	0.0000
818.1	411.2	0.0288	0.0000	819.0	423.1	0.0106	0.0000	818.3	407.7	0.0182	0.0000	818.3	409.8	0.0070	0.0000	819.1	428.1	0.0385	0.0000
824.3	414.1	0.0321	0.0000	825.2	426.3	0.0127	0.0000	824.5	410.5	0.0228	0.0000	824.5	412.7	0.0085	0.0000	825.3	431.1	0.0443	0.0000
830.5	417.2	0.0354	0.0000	831.4	429.3	0.0152	0.0000	830.7	413.3	0.0254	0.0000	830.7	415.5	0.0102	0.0000	831.5	434.0	0.0510	0.0000
836.7	420.0	0.0388	0.0000	837.6	432.3	0.0179	0.0000	836.9	416.3	0.0323	0.0000	836.9	418.4	0.0121	0.0000	837.7	437.2	0.0586	0.0000
842.9	423.1	0.0413	0.0000	843.8	435.2	0.0210	0.0000	843.0	419.2	0.0353	0.0000	843.1	421.6	0.0144	0.0000	843.9	440.2	0.0663	0.0000
849.1	425.9	0.0443	0.0000	850.0	438.2	0.0242	0.0000	849.2	422.3	0.0373	0.0000	849.3	424.4	0.0172	0.0000	850.1	443.1	0.0746	0.0000
855.3	428.8	0.0473	0.0000	856.2	441.4	0.0277	0.0000	855.4	425.2	0.0400	0.0000	855.5	427.4	0.0204	0.0000	856.3	446.3	0.0831	0.0000
861.5	432.1	0.0505	0.0000	862.4	444.3	0.0317	0.0000	861.6	428.2	0.0509	0.0000	861.7	430.3	0.0242	0.0000	862.5	449.3	0.0919	0.0000
867.7	434.9	0.0540	0.0000	868.6	447.5	0.0358	0.0000	867.8	431.1	0.0595	0.0000	867.9	433.4	0.0285	0.0000	868.7	452.2	0.1003	0.0000
873.9	437.9	0.0569	0.0000	874.8	450.4	0.0396	0.0000	874.0	434.0	0.0661	0.0000	874.1	436.3	0.0336	0.0000	875.0	455.3	0.1086	0.0000
880.1	441.0	0.0600	0.0000	881.0	453.0	0.0444	0.0000	880.2	437.0	0.0736	0.0000	880.3	439.2	0.0389	0.0000	881.1	458.4	0.1155	0.0000
886.3	443.9	0.0635	0.0000	887.3	456.8	0.0482	0.0000	886.4	440.0	0.0758	0.0000	886.5	442.4	0.0449	0.0000	887.4	461.3	0.1221	0.0000
892.5	446.9	0.0669	0.0000	893.4	459.8	0.0519	0.0000	892.6	443.0	0.0787	0.0000	892.7	445.1	0.0516	0.0000	893.6	464.5	0.1276	0.0000
898.7	449.9	0.0675	0.0000	899.7	462.9	0.0552	0.0000	898.8	445.9	0.0811	0.0000	898.9	448.0	0.0580	0.0000	899.8	467.5	0.1333	0.0000
904.9	453.1	0.0694	0.0000	905.9	466.1	0.0579	0.0000	905.0	448.8	0.0832	0.0000	905.1	451.1	0.0650	0.0000	906.0	470.5	0.1366	0.0000
911.1	456.0	0.0707	0.0000	912.1	469.0	0.0604	0.0000	911.2	451.8	0.0840	0.0000	911.3	454.0	0.0720	0.0000	912.2	473.5	0.1402	0.0000
917.3	459.0	0.0720	0.0000	918.3	472.1	0.0629	0.0000	917.4	454.7	0.0891	0.0000	917.5	457.0	0.0785	0.0000	918.4	476.7	0.1420	0.0000
923.5	462.0	0.0732	0.0000	924.5	475.1	0.0644	0.0000	923.6	457.6	0.0890	0.0000	923.7	460.0	0.0845	0.0000	924.6	479.5	0.1431	0.0000
929.7	465.0	0.0744	0.0000	930.9	481.1	0.0668	0.0000	929.8	461.3	0.0917	0.0000	929.9	463.0	0.0905	0.0000	930.8	482.7	0.1437	0.0000
935.9	468.1	0.0752	0.0000	943.1	484.1	0.0675	0.0000	936.0	464.2	0.0948	0.0000	936.1	466.1	0.0960	0.0000	937.0	485.3	0.1442	0.0000
942.1	470.9	0.0754	0.0000	955.5	490.3	0.0677	0.0000	942.2	467.2	0.0950	0.0000	942.3	468.7	0.0998	0.0000	943.2	488.5	0.1436	0.0000
948.3	474.0	0.0762	0.0000	961.7	493.3	0.0681	0.0000	948.4	470.0	0.0946	0.0000	948.5	471.7	0.1045	0.0000	949.4	491.6	0.1415	0.0000
954.5	476.9	0.0763	0.0000	967.9	496.1	0.0676	0.0000	954.6	474.7	0.1014	0.0000	954.7	474.7	0.1074	0.0000	955.6	494.7	0.1404	0.0000
960.7	480.0	0.0765	0.0000	974.1	499.2	0.0680	0.0000	960.8	476.3	0.0892	0.0000	960.9	477.8	0.1094	0.0000	961.8	497.8	0.1388	0.0000
966.9	483.0	0.0765	0.0000	980.3	502.3	0.0684	0.0000	967.0	478.9	0.0889	0.0000	967.1	481.7	0.1113	0.0000	968.0	500.7	0.1366	0.0000
973.1	486.0	0.0767	0.0000	986.5	505.2	0.0681	0.0000	973.2	481.9	0.0871	0.0000	973.3	483.7	0.1129	0.0000	974.2	503.8	0.1370	0.0000
979.3	488.9	0.0762	0.0																

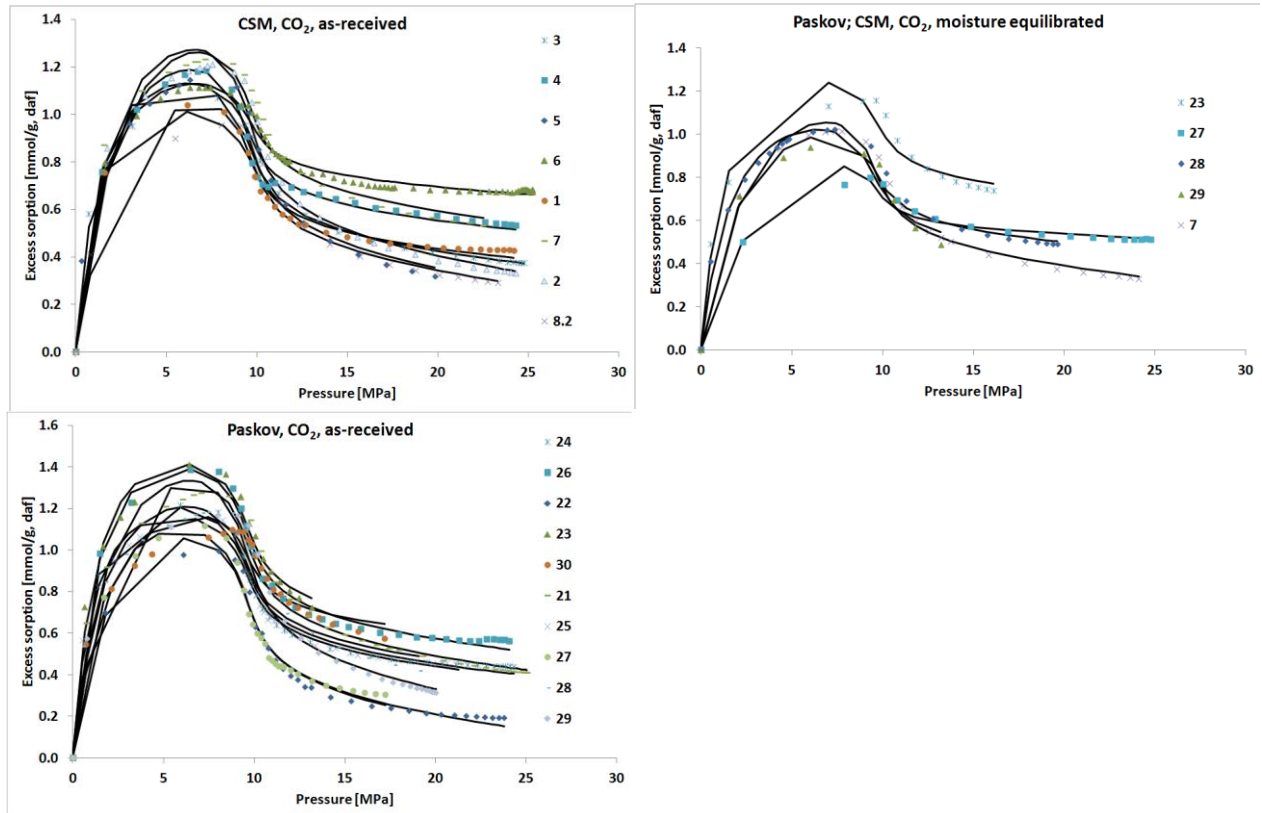
Table 5 Results of temperature-programmed open system pyrolysis (continued)

1326.5	656.5	0.0131	1340.1	677.6	0.0081	0.0003	1326.5	652.7	0.0113	0.0016	1326.7	655.1	0.0214	0.0024	1327.9	677.1	0.0115	0.0030	
1332.7	659.5	0.0127	0.0019	1346.3	680.2	0.0074	0.0003	1332.7	655.8	0.0112	0.0017	1332.9	658.1	0.0209	0.0026	1334.1	680.1	0.0111	0.0032
1338.9	662.4	0.0124	0.0020	1352.5	683.3	0.0074	0.0006	1338.9	658.8	0.0103	0.0017	1339.1	661.0	0.0202	0.0028	1340.3	683.2	0.0104	0.0033
1345.1	665.5	0.0120	0.0022	1358.7	686.9	0.0074	0.0006	1345.1	661.8	0.0099	0.0018	1345.3	664.1	0.0197	0.0030	1346.6	686.2	0.0100	0.0034
1351.3	668.4	0.0118	0.0023	1364.9	690.0	0.0071	0.0005	1351.3	664.9	0.0094	0.0019	1351.5	667.1	0.0192	0.0033	1352.7	689.2	0.0095	0.0035
1357.5	671.4	0.0115	0.0024	1371.1	693.0	0.0068	0.0004	1357.5	668.0	0.0090	0.0020	1357.7	670.3	0.0185	0.0034	1359.0	692.2	0.0091	0.0037
1363.7	674.4	0.0112	0.0026	1377.3	696.0	0.0066	0.0005	1363.7	671.0	0.0093	0.0023	1363.9	673.2	0.0178	0.0036	1365.2	695.1	0.0086	0.0037
1369.9	677.3	0.0108	0.0027	1383.5	699.1	0.0069	0.0004	1369.9	673.7	0.0086	0.0023	1370.1	676.2	0.0172	0.0038	1371.4	698.2	0.0081	0.0039
1376.1	680.4	0.0104	0.0027	1389.7	701.9	0.0065	0.0005	1376.1	676.8	0.0084	0.0025	1376.3	679.4	0.0164	0.0040	1377.6	701.2	0.0076	0.0039
1382.3	683.4	0.0102	0.0029	1395.9	704.9	0.0065	0.0005	1382.3	679.8	0.0080	0.0026	1382.5	682.4	0.0156	0.0041	1383.8	704.1	0.0071	0.0039
1388.5	686.6	0.0099	0.0029	1402.1	707.8	0.0062	0.0006	1388.5	683.1	0.0078	0.0027	1388.7	685.2	0.0149	0.0043	1390.0	707.2	0.0067	0.0039
1394.7	689.5	0.0095	0.0029	1408.3	710.9	0.0070	0.0007	1394.7	685.9	0.0075	0.0028	1394.9	688.3	0.0139	0.0044	1396.2	710.2	0.0063	0.0041
1400.9	692.6	0.0093	0.0030	1414.5	714.1	0.0063	0.0005	1400.9	688.8	0.0067	0.0026	1401.1	691.3	0.0132	0.0045	1402.4	713.1	0.0059	0.0040
1407.1	695.6	0.0089	0.0030	1420.7	716.9	0.0065	0.0005	1407.1	692.6	0.0064	0.0027	1407.3	694.3	0.0125	0.0047	1408.6	716.2	0.0056	0.0041
1413.3	698.5	0.0086	0.0030	1426.9	720.1	0.0065	0.0005	1413.3	695.7	0.0059	0.0026	1413.5	697.3	0.0119	0.0049	1414.8	719.3	0.0053	0.0040
1419.4	701.6	0.0082	0.0030	1433.1	723.1	0.0064	0.0006	1419.5	698.6	0.0058	0.0028	1419.7	700.3	0.0112	0.0050	1421.0	722.2	0.0049	0.0039
1425.6	704.6	0.0079	0.0030	1439.3	726.1	0.0064	0.0006	1425.7	701.5	0.0055	0.0028	1425.9	703.5	0.0107	0.0051	1427.2	725.2	0.0047	0.0040
1431.9	707.6	0.0077	0.0030	1445.5	729.2	0.0063	0.0006	1431.9	704.8	0.0052	0.0028	1432.1	706.5	0.0102	0.0052	1433.4	728.3	0.0043	0.0039
1438.0	710.5	0.0074	0.0029	1451.7	732.0	0.0034	0.0003	1438.1	707.8	0.0048	0.0028	1438.3	709.5	0.0095	0.0052	1439.6	731.4	0.0040	0.0038
1444.2	713.8	0.0070	0.0028	1457.9	735.1	0.0035	0.0003	1444.3	710.5	0.0046	0.0028	1444.5	712.5	0.0088	0.0052	1445.8	734.2	0.0038	0.0038
1450.4	716.5	0.0068	0.0028	1464.1	738.2	0.0031	0.0007	1450.5	713.5	0.0044	0.0027	1450.7	715.4	0.0083	0.0052	1452.0	737.3	0.0036	0.0037
1456.6	719.7	0.0065	0.0027	1470.3	741.0	0.0025	0.0006	1456.7	716.8	0.0041	0.0027	1456.9	718.5	0.0079	0.0054	1458.2	740.3	0.0033	0.0037
1462.8	722.6	0.0063	0.0027	1476.5	744.1	0.0025	0.0005	1462.9	719.8	0.0040	0.0028	1463.1	721.6	0.0073	0.0054	1464.4	743.4	0.0032	0.0036
1469.0	725.7	0.0061	0.0026	1482.7	747.1	0.0027	0.0006	1469.1	722.9	0.0037	0.0027	1469.3	725.2	0.0067	0.0054	1470.6	746.4	0.0031	0.0036
1475.2	728.8	0.0060	0.0026	1488.9	750.2	0.0024	0.0006	1475.4	725.8	0.0035	0.0028	1475.5	728.1	0.0062	0.0055	1476.8	749.3	0.0030	0.0035
1481.4	731.7	0.0058	0.0024	1495.2	753.3	0.0020	0.0004	1481.6	728.9	0.0033	0.0027	1481.7	731.3	0.0058	0.0055	1483.0	752.3	0.0028	0.0034
1487.6	734.6	0.0057	0.0024	1501.3	756.2	0.0022	0.0006	1487.8	732.0	0.0032	0.0027	1487.9	734.1	0.0053	0.0056	1489.2	755.4	0.0027	0.0034
1493.8	737.8	0.0056	0.0023	1507.6	759.1	0.0021	0.0006	1494.0	735.0	0.0029	0.0026	1494.1	737.4	0.0049	0.0055	1495.5	758.5	0.0026	0.0033
1500.0	740.7	0.0055	0.0023	1513.8	762.2	0.0017	0.0004	1500.2	738.0	0.0028	0.0026	1500.3	740.2	0.0045	0.0055	1501.6	761.4	0.0025	0.0032
1506.2	743.8	0.0054	0.0022	1519.9	765.3	0.0019	0.0004	1506.4	741.2	0.0026	0.0026	1506.5	743.1	0.0043	0.0055	1507.8	764.5	0.0024	0.0031
1512.4	746.8	0.0053	0.0022	1526.2	768.2	0.0017	0.0004	1512.6	743.9	0.0025	0.0026	1512.7	746.4	0.0038	0.0054	1514.1	768.1	0.0024	0.0030
1518.6	749.8	0.0051	0.0021	1532.4	771.0	0.0019	0.0004	1518.8	747.2	0.0024	0.0026	1518.9	749.4	0.0035	0.0054	1520.3	771.3	0.0023	0.0029
1524.8	752.7	0.0052	0.0021	1538.5	774.1	0.0017	0.0004	1525.0	750.3	0.0022	0.0025	1525.1	752.5	0.0033	0.0054	1526.5	774.1	0.0021	0.0030
1531.0	756.0	0.0051	0.0020	1544.8	777.3	0.0017	0.0004	1531.2	753.3	0.0022	0.0025	1531.3	755.4	0.0031	0.0054	1532.7	777.2	0.0021	0.0028
1537.2	758.9	0.0050	0.0020	1551.0	780.2	0.0018	0.0004	1537.4	756.3	0.0021	0.0025	1537.5	758.3	0.0029	0.0054	1538.9	780.2	0.0020	0.0028
1543.4	761.9	0.0050	0.0020	1557.1	783.1	0.0017	0.0005	1543.6	759.4	0.0020	0.0024	1543.7	761.5	0.0027	0.0054	1545.1	783.2	0.0020	0.0026
1549.6	765.0	0.0049	0.0020	1563.4	786.0	0.0017	0.0003	1549.8	762.5	0.0017	0.0022	1549.9	764.4	0.0025	0.0054	1551.3	786.2	0.0017	0.0022
1555.8	767.9	0.0050	0.0020	1569.6	789.2	0.0018	0.0005	1556.0	765.4	0.0016	0.0021	1556.1	767.3	0.0023	0.0054	1557.5	789.1	0.0018	0.0023
1562.0	771.1	0.0051	0.0019	1575.8	792.4	0.0018	0.0004	1562.2	768.6	0.0017	0.0023	1562.3	770.6	0.0023	0.0055	1563.7	792.1	0.0019	0.0024
1568.2	773.8	0.0050	0.0019	1582.0	795.1	0.0018	0.0005	1568.4	771.4	0.0016	0.0024	1568.5	773.7	0.0020	0.0053	1569.9	795.2	0.0018	0.0022
1574.4	777.0	0.0050	0.0019	1588.2	798.2	0.0019	0.0005	1574.6	774.3	0.0016	0.0023	1574.7	776.7	0.0019	0.0054	1576.1	798.1	0.0017	0.0020
1580.6	780.0	0.0052	0.0019	1594.4	801.3	0.0017	0.0005	1580.8	777.7	0.0014	0.0022	1580.9	779.8	0.0017	0.0052	1582.3	801.2	0.0017	0.0019
1586.8	783.1	0.0052	0.0020	1600.6	804.9	0.0018	0.0004	1587.0	780.7	0.0013	0.0021	1587.1	782.8	0.0016	0.0052	1588.5	804.2	0.0017	0.0020
1593.0	786.1	0.0051	0.0019	1606.8	808.7	0.0014	0.0004	1593.2	783.9	0.0013	0.0021	1593.3	785.7	0.0016	0.0052	1594.7	807.2	0.0017	0.0019
1599.2	789.0	0.0053	0.0019	1613.0	810.9	0.0015	0.0004	1599.4	786.8	0.0013	0.0021	1599.5	788.8	0.0015	0.0052	1600.9	810.1	0.0017	0.0019
1605.4	792.1	0.0052	0.0019	1619.2	813.8	0.0014	0.0003	1605.6	789.8	0.0012	0.0020	1605.7	791.8	0.0013	0.0050	1607.1	813.0	0.0017	0.0018
1611.6	795.2	0.0052	0.0018	1625.4	816.8	0.0016	0.0004	1611.8	793.1	0.0011	0.0020	1611.9	794.9	0.0012	0.0050	1613.3	816.2	0.0018	0.0019
1617.8	798.1	0.0053	0.0018	1631.6	819.8	0.0016	0.0003	1618.0	796.0	0.0012	0.0020	1618.1	798.0	0.0012	0.0050	1619.5	819.1	0.0016	0.0017
1624.0	801.1	0.0055	0.0018	1637.8	822.8	0.0014	0.0004	1624.2	798.9	0.0011	0.0021	1624.3	801.2	0.0012	0.0049	1625.7	822.3	0.0017	0.0017
1630.2	804.2	0.0053	0.0017	1644.0	826.0	0.0017	0.0005	1630.4	801.9	0.0010	0.0020	1630.5	804.1	0.0011	0.0049	1631.9	825.3	0.0017	0.0016
1636.4	807.2	0.0054	0.0018	1650.2	828.9	0.0015	0.0004	1636.6	805.2	0.0011	0.0019	1636.7	806.9	0.0011	0.0049	1638.1	828.0	0.0016	0.0016
1642.6	810.2	0.0052	0.0018	1656.4	831.9	0.0017	0.0005	1642.8	808.2	0.0010	0.0019	1642.9	810.0	0.0011	0.0049	1644.3	831.3	0.0017	0.0016
1648.8	813.1	0.0054	0.0017	1662.6	834.9	0.0018	0.0006	1649.0	812.0	0.0010	0.0019	1649.1	813.2	0.0010	0.0048	1650.6	834.3	0.0018	0.0016
1655.0	816.1	0.0055	0.0018	1668.8	837.9	0.0017	0.0006	1655.2	815.0	0.0009	0.0018	1655.3	816.2	0.0010	0.0047	1656.8	837.2	0.0018	0.0016
1661.2	819.0	0.0057	0.0018	1675.0	840.7	0.0025	0.0009	1661.4	818.0	0.0009	0.0018	1661.5	819.3	0.0009	0.0046	1663.0	840.2	0.0019	0.0017
1667.4	822.2	0.0031	0.0015	1681.2	843.9	0.0018	0.0007	1667.6	820.9	0.0009	0.0018	1667.7	822.4	0.0009	0.0046	1669.2	843.3	0.0019	0.0

Appendix III Investigations on the methane and carbon dioxide sorption capacity of coals from the SW Upper Silesian Coal Basin, Czech Republic



Appendix III Fig. 1 Methane sorption isotherms measured at 45°C.



Appendix III Fig. 2 Carbon dioxide sorption isotherms measured at 45°C.

Appendix III Table 1 Results of proximate and petrographic analysis

Sample #	Hygr. moisture [wt.%]	Equil. moisture [wt.%]	Ash [wt.%, dry]	Vol. matter [wt.%, daf]	Fixed carbon [wt.%, daf]	VRr [%]	Vitr. [vol.%, mmf]	Lipt. [vol.%, mmf]	Inert. [vol.%, mmf]	TOC [wt. %]	Rock-Eval T _{max} [°C]
1	1.5	2.4	1.5	26.0	74.0	1.1	72.0	6.2	21.7	84.7	463
2	1.3	2.0	7.4	25.8	74.2	1.1	65.6	5.2	29.2	80.8	460
3	1.0	2.5	10.2	25.4	74.6	1.1	51.8	9.7	38.5	78.0	460
4	0.8	1.7	4.1	25.2	74.8	1.1	83.7	11.4	4.8	84.1	456
5	0.7	1.6	18.5	25.8	74.2	1.1	81.8	0.9	17.3	70.4	466
6	0.6	1.6	3.4	23.3	76.7	1.2	76.5	9.1	14.4	85.3	465
7	1.7	2.4	3.0	25.1	74.9	1.1	75.1	5.8	19.1	84.3	464
8.1	0.7	1.4	2.9	32.2	67.8	1.0	n.d.	n.d.	n.d.	n.d.	n.d.
8.2	0.6	n.d.	3.3	35.3	64.7	1.0	48.4	23.4	28.2	80.9	443
9	0.7	n.d.	49.0	(37.1)	62.9	1.0	80.0	0.0	20.0	41.6	452
10	0.5	n.d.	32.0	29.3	70.7	1.1	89.0	0.0	11.0	57.1	459
11	0.4	n.d.	6.0	25.7	74.3	1.1	79.2	0.0	20.8	81.5	461
12	0.5	n.d.	4.2	27.9	72.1	1.1	77.8	2.6	19.6	78.9	452
13	0.5	n.d.	3.1	27.2	72.8	1.1	84.6	1.2	14.2	82.8	454
14	0.5	n.d.	54.6	(31.8)	68.2	1.1	98.3	0.0	1.7	37.1	474
15	0.3	n.d.	12.3	28.3	71.7	1.1	48.8	0.0	51.2	72.7	465
16	0.3	n.d.	2.4	25.0	75.0	1.2	95.6	0.2	4.2	85.2	457
17	0.3	n.d.	1.9	22.0	78.0	1.2	73.4	5.4	21.2	83.7	456
18	1.0	n.d.	89.8	(68.0)	32.0	1.2	n.d.	n.d.	n.d.	n.d.	n.d.
19	0.5	n.d.	41.1	26.3	73.7	1.3	80.8	0.0	19.2	49.4	475
20	0.3	n.d.	85.2	(38.6)	61.4	n.d.	n.d.	n.d.	n.d.	n.d.	n.d.
21	0.5	1.5	2.9	21.5	78.5	1.4	88.8	1.0	10.1	82.8	468
22	0.9	1.3	20.0	28.3	71.7	1.2	80.0	2.5	17.5	73.1	456
23	0.6	1.6	8.6	17.8	82.2	1.7	88.1	0.0	11.9	79.0	482
24	0.7	1.5	4.4	16.1	83.9	1.8	84.0	0.0	16.0	83.5	483
25	0.8	1.5	1.6	17.7	82.3	1.7	87.7	0.0	12.3	85.4	479
26	0.9	1.6	4.3	16.9	83.1	1.8	77.9	0.0	22.1	83.5	480
27	0.9	1.0	5.8	24.1	75.9	1.4	91.8	0.2	8.0	81.6	466
28	0.8	1.5	3.4	20.0	80.0	1.6	86.9	1.2	11.9	83.3	470
29	0.7	1.1	16.5	26.0	74.0	1.5	85.3	1.0	13.6	70.3	468
30	0.5	1.2	6.5	27.1	72.9	1.4	82.6	1.2	16.2	78.4	458

VRr=mean vitrinite reflectance (random); TOC=total organic carbon; ; n.d.= not determined; daf=dry, ash-free; mmf=mineral matter free; volatile matter values in brackets are from 'high-ash' samples

Appendix III Table 2 Results of high-pressure methane sorption experiments on “as received” coal samples at 45°C.

Sample #	n_{\max} raw [mmol/g]	P at n_{\max} [MPa]	n_L raw [mmol/g]	n_{\max} daf [mmol/g]	n_L daf [mmol/g]	P_L daf [MPa]	He density [g/cm ³]	V_{\max} daf [m ³ /t]	V_L daf [m ³ /t]
1	0.77	16.36	0.85	0.80	0.88	1.39	1.21	18.14	19.90
2	0.76	14.05	0.83	0.84	0.91	1.27	1.25	18.98	20.69
3	0.76	15.70	0.82	0.85	0.92	1.18	1.30	19.39	20.91
4	0.76	17.14	0.84	0.80	0.88	1.63	1.22	18.15	20.00
5	0.64	13.13	0.67	0.79	0.83	0.80	1.43	17.95	18.75
6	0.67	15.77	0.74	0.70	0.77	1.62	1.22	15.79	17.54
7	0.77	14.04	0.84	0.81	0.88	1.29	1.22	18.36	19.90
8.1	0.50	15.78	0.59	0.52	0.61	2.65	1.29	11.75	13.89
8.2	0.52	16.00	0.60	0.55	0.62	2.11	1.32	12.39	14.10
11	0.63	14.89	0.71	0.67	0.76	1.67	1.35	15.30	17.15
12	0.50	16.62	0.58	0.53	0.61	2.73	1.32	11.93	13.89
13	0.71	15.78	0.78	0.73	0.81	1.58	1.32	16.65	18.46
14	0.27	16.75	0.30	0.59	0.67	2.07	1.85	13.48	15.15
15	0.53	15.75	0.59	0.60	0.67	1.59	1.48	13.67	15.24
16	0.47	15.39	0.56	0.49	0.57	2.71	1.31	11.06	13.00
17	0.61	15.39	0.69	0.62	0.70	1.75	1.33	14.15	15.93
19	0.38	14.30	0.43	0.64	0.73	1.90	1.71	14.64	16.64
21	0.88	14.57	0.96	0.91	0.99	1.33	1.21	20.66	22.57
22	0.61	16.55	0.68	0.77	0.86	1.85	1.29	19.58	19.58
23	0.88	17.30	0.95	0.97	1.04	1.10	1.28	22.10	23.68
24	0.94	13.05	1.02	0.99	1.08	1.17	1.26	22.57	24.46
25	0.92	13.68	1.00	0.94	1.02	1.19	1.23	21.40	23.19
26	0.89	12.94	0.97	0.94	1.02	1.17	1.26	21.38	23.20
27	0.64	16.68	0.70	0.69	0.75	1.33	1.23	15.68	17.03
28	0.80	13.73	0.86	0.83	0.90	1.19	1.23	18.93	20.40
29	0.69	14.95	0.75	0.83	0.91	1.40	1.35	18.80	20.68
30	0.69	15.29	0.75	0.74	0.80	1.17	1.26	16.86	18.24

daf= dry, ash-free; n_{\max} =maximum measured excess sorption; n_L =Langmuir sorption capacity; P_L =Langmuir pressure; V_{\max} = volume of maximum measured excess sorption; V_L =volume of Langmuir sorption capacity

Appendix III Table 3 Results of high-pressure carbon dioxide sorption experiments on “as received” coal samples at 45°C.

Sample #	n_{\max} raw [mmol/g]	P at n_{\max} [MPa]	n_L (Eq.3) raw [mmol/g]	n_{\max} daf [mmol/g]	n_L (Eq.3) daf [mmol/g]	P_L (Eq.3) daf [MPa]	Density SP (Eq.3) [g/cm ³]	Density SP graph. [g/cm ³]	He density [g/cm ³]	V_{\max} daf [m ³ /t]	V_L (Eq.3) daf [m ³ /t]
1	1.01	6.15	1.34	1.04	1.38	1.23	1213	1256	1.44	23.64	31.28
2	1.11	7.56	2.09	1.21	2.29	3.44	1026	1034	1.25	27.49	51.93
3	0.95	7.85	1.43	1.07	1.60	1.44	1134	1107	1.47	24.31	36.42
4	1.13	7.21	1.50	1.19	1.58	1.48	1303	1490	1.34	26.98	35.92
5	0.97	7.27	1.59	1.20	1.96	2.55	1018	990	1.46	27.17	44.61
6	1.07	6.81	1.52	1.11	1.58	1.66	1551	1463	1.20	25.30	35.89
7	1.17	7.16	1.90	1.23	1.99	2.32	1218	1200	1.35	27.97	45.23
8.2	0.92	8.04	1.96	0.96	2.04	4.18	1018	1020	1.44	21.71	46.33
21	1.23	7.11	2.07	1.27	2.14	2.40	1094	1105	1.34	28.95	48.66
22	0.79	8.06	1.45	1.00	1.83	2.81	936	938	1.56	22.61	41.51
23	1.28	6.43	1.81	1.41	2.00	1.47	1223	1131	1.40	32.06	45.31
24	1.15	5.92	1.55	1.22	1.64	1.15	1150	1239	1.49	27.60	37.19
25	1.14	6.80	1.58	1.17	1.61	1.29	1146	1155	1.50	26.53	36.66
26	1.31	6.47	1.56	1.39	1.99	1.54	1179	1244	1.19	31.49	45.24
27	1.04	7.27	1.63	1.12	1.76	2.15	931	1029	1.20	25.40	40.01
28	1.14	7.43	1.77	1.19	1.84	2.01	1137	1018	1.35	26.95	41.90
29	0.93	9.70	2.01	1.12	2.42	3.41	968	965	1.50	25.46	54.99
30	1.02	8.79	1.73	1.10	1.86	2.57	1295	1156	1.39	24.94	42.16

daf= dry, ash-free; n_{\max} =maximum measured excess sorption; n_L =Langmuir sorption capacity; P_L =Langmuir pressure; V_{\max} = volume of maximum measured excess sorption; V_L =volume of Langmuir sorption capacity; Eq.3 = calculated from equation 3; SP=sorbed phase; graph=graphical estimation; P=pressure

Appendix III Table 4 Results of high-pressure methane sorption experiments on moisture equilibrated coal samples.

Sample #	n_{\max} raw [mmol/g]	P at n_{\max} [MPa]	n_L raw [mmol/g]	n_{\max} daf [mmol/g]	n_L daf [mmol/g]	P_L daf [MPa]	He density [g/cm ³]	V_{\max} daf [m ³ /t]	V_L daf [m ³ /t]
1	0.47	16.81	0.58	0.49	0.59	3.58	1.33	11.19	13.34
2	0.33	14.61	0.50	0.36	0.60	8.66	1.38	8.17	13.52
3	0.46	11.49	0.54	0.53	0.62	2.37	1.47	11.98	13.98
4	0.52	16.15	0.65	0.55	0.69	4.26	1.35	12.60	15.68
5	0.50	14.96	0.64	0.63	0.79	4.12	1.47	14.21	18.02
6	0.46	15.88	0.60	0.48	0.63	4.61	1.35	10.98	14.39
7	0.45	16.33	0.58	0.47	0.61	4.72	1.32	10.73	13.91
8.1	0.43	15.15	0.52	0.44	0.54	2.75	1.28	10.11	12.31
21	0.70	16.58	0.80	0.73	0.83	2.16	1.34	16.56	18.85
22	0.38	13.12	0.44	0.49	0.56	2.56	1.41	11.05	12.64
23	0.70	16.82	0.88	0.78	0.96	3.19	1.41	17.72	21.78
24	0.67	10.59	0.75	0.71	0.80	1.47	1.34	16.08	18.09
25	0.58	16.76	0.70	0.60	0.72	3.03	1.34	13.70	16.31
26	0.69	16.47	1.01	0.74	1.08	8.02	1.43	16.73	24.61
27	0.28	15.20	0.37	0.30	0.40	4.83	1.33	6.74	8.99
28	0.55	15.99	0.70	0.58	0.73	4.20	1.29	13.10	16.68
29	0.40	15.74	0.57	0.48	0.69	7.11	1.52	10.96	15.62
30	0.39	16.15	0.48	0.42	0.52	6.04	1.43	9.64	11.73

daf= dry, ash-free; n_{\max} =maximum measured excess sorption; n_L =Langmuir sorption capacity; P_L =Langmuir pressure; V_{\max} = volume of maximum measured excess sorption; V_L =volume of Langmuir sorption capacity; P=pressure

Appendix III Table 5 Results of high-pressure and carbon dioxide sorption experiments on moisture equilibrated coal samples.

Sample #	n_{\max} raw [mmol/g]	P at n_{\max} [MPa]	n_L (Eq.3) raw [mmol/g]	n_{\max} daf [mmol/g]	n_L (Eq.3) daf [mmol/g]	P_L (Eq.3) daf [MPa]	Density SP (Eq.3) [g/cm ³]	density SP graph. [g/cm ³]	He density [g/cm ³]	V_{\max} daf [m ³ /t]	V_L (Eq.3) daf [m ³ /t]
1	0.95	8.31	1.79	0.99	1.86	3.34	1104	945	1.34	22.46	42.21
7	0.96	7.76	1.87	1.01	1.96	3.77	1066	1106	1.35	23.03	44.53
23	1.05	9.64	1.59	1.16	1.75	1.64	1475	1319	1.43	26.30	39.63
27	0.78	9.34	1.67	0.80	1.70	5.20	1350	1469	1.36	18.16	38.71
28	0.98	7.39	1.46	1.02	1.53	1.99	1272	1190	1.35	23.23	34.68
29	0.77	6.04	1.38	0.94	1.67	2.96	1170	1015	1.54	21.30	37.98

daf= dry, ash-free; n_{\max} =maximum measured excess sorption; n_L =Langmuir sorption capacity; P_L =Langmuir pressure; V_{\max} = volume of maximum measured excess sorption; V_L =volume of Langmuir sorption capacity; Eq.3 = calculated from equation 3; SP=sorbed phase; graph=graphical estimation; P=pressure

Appendix III Table 6 Results of methane sorption experiments on “as received” coal samples at 20°C.

Sample #	n_{\max} raw [mmol/g]	P at n_{\max} [MPa]	n_L raw [mmol/g]	n_{\max} daf [mmol/g]	n_L daf [mmol/g]	P_L daf [MPa]	He density [g/cm ³]	V_{\max} daf [m ³ /t]	V_L daf [m ³ /t]
22	0.62	16.20	0.67	0.78	0.85	1.31	1.45	17.70	19.22
24	1.00	11.98	1.05	1.05	1.10	0.77	1.40	23.88	25.06
26	0.90	12.09	0.97	0.95	0.99	0.80	1.39	21.54	22.58

daf= dry, ash-free; n_{\max} =maximum measured excess sorption; n_L =Langmuir sorption capacity; P_L =Langmuir pressure; V_{\max} = volume of maximum measured excess sorption; V_L =volume of Langmuir sorption capacity; P=pressure

Appendix III Table 7 of carbon dioxide sorption experiments on “as received” coal samples at 20°C.

Sample #	n_{\max} raw [mmol/g]	P at n_{\max} [MPa]	n_L (Eq.3) raw [mmol/g]	n_{\max} daf [mmol/g]	n_L (Eq.3) daf [mmol/g]	P_L (Eq.3) daf [MPa]	Density SP (Eq.3) [g/cm ³]	He density [g/cm ³]	V_{\max} daf [m ³ /t]	V_L (Eq.3) daf [m ³ /t]
22	0.85	2.25	1.66	1.07	1.99	0.98	214	1.45	24.41	45.23
24	1.29	3.56	2.36	1.36	2.48	1.45	369	1.40	30.91	56.37
26	1.17	3.24	2.06	1.23	2.18	1.17	325	1.51	28.04	49.40

daf= dry, ash-free; n_{\max} =maximum measured excess sorption; n_L =Langmuir sorption capacity; P_L =Langmuir pressure; V_{\max} = volume of maximum measured excess sorption; V_L =volume of Langmuir sorption capacity; Eq.3 = calculated from equation 3; SP=sorbed phase; graph=graphical estimation; P=pressure

Appendix III Table 8 Results of high pressure methane sorption experiments on moisture equilibrated coal samples 8 at different temperatures

Temperature (°C)	n_{\max} raw [mmol/g]	P at n_{\max} [MPa]	n_L raw [mmol/g]	n_{\max} daf [mmol/g]	n_L daf [mmol/g]	P_L daf [MPa]	He density [g/cm ³]	V_{\max} daf [m ³ /t]	V_L daf [m ³ /t]
45	0.43	15.15	0.52	0.44	0.54	2.75	1.28	10.11	12.31
55	0.40	15.28	0.48	0.42	0.50	2.66	1.28	9.60	11.31
65	0.37	17.54	0.43	0.39	0.45	2.84	1.28	8.79	10.19

daf= dry, ash-free; n_{\max} =maximum measured excess sorption; n_L =Langmuir sorption capacity; P_L =Langmuir pressure; V_{\max} = volume of maximum measured excess sorption; V_L =volume of Langmuir sorption capacity; P=pressure

Appendix III Table 9 Experimental data (pressure, excess sorption) for high-pressure sorption isotherms.

Sample: 1				Sample: 1				Sample: 1				Sample: 2				Sample: 2				Sample: 2				Sample: 3											
Moisture: a.r.				Moisture: e.m.				Moisture: p.d.				Moisture: a.r.				Moisture: e.m.				Moisture: e.m. (2)				Moisture: a.r.				Moisture: a.r.							
Gas: CH4				Gas: CO2				Gas: CH4				Gas: CH4				Gas: CH4				Gas: CH4				Gas: CO2				Gas: CH4							
T (°C): 44.56				T (°C): 45.4				T (°C): 46.09				T (°C): 45.02				T (°C): 46.68				T (°C): 45.41				T (°C): 45.41				T (°C): 45.02				T (°C): 44.55			
P [MPa]	n_{ads} [mmol/g]	P [MPa]	n_{ads} [mmol/g]	P [MPa]	n_{ads} [mmol/g]	P [MPa]	n_{ads} [mmol/g]	P [MPa]	n_{ads} [mmol/g]	P [MPa]	n_{ads} [mmol/g]	P [MPa]	n_{ads} [mmol/g]	P [MPa]	n_{ads} [mmol/g]	P [MPa]	n_{ads} [mmol/g]	P [MPa]	n_{ads} [mmol/g]	P [MPa]	n_{ads} [mmol/g]	P [MPa]	n_{ads} [mmol/g]	P [MPa]	n_{ads} [mmol/g]	P [MPa]	n_{ads} [mmol/g]	P [MPa]	n_{ads} [mmol/g]						
0	0	0	0	0	0	0	0	0	0	0	0	0	0	0	0	0	0	0	0	0	0	0	0	0	0	0	0	0							
0.98	0.349	1.01	0.071	1.6	0.732	0.86	0.44	0.65	0.18	0.94	0.349	0.92	0.09	1.74	0.784	1.74	0.784	1.74	0.784	1.74	0.784	1.74	0.784	1.74	0.784	1.74	0.784	1.74	0.784						
2.12	0.5	1.77	0.143	6.15	1.01	2.13	0.69	2.29	0.35	2.92	0.564	2.7	0.099	3.84	0.985	3.84	0.985	3.84	0.985	3.84	0.985	3.84	0.985	3.84	0.985	3.84	0.985	3.84	0.985						
3.16	0.58	2.34	0.213	8.18	0.98	3.27	0.82	5.17	0.48	4.67	0.651	3.86	0.153	5.29	1.054	5.29	1.054	5.29	1.054	5.29	1.054	5.29	1.054	5.29	1.054	5.29	1.054	5.29	1.054						
4.03	0.628	2.86	0.259	9.05	0.902	4.1	0.88	7.52	0.53	6.13	0.696	4.78	0.189	6.23	1.081	6.23	1.081	6.23	1.081	6.23	1.081	6.23	1.081	6.23	1.081	6.23	1.081	6.23	1.081						
4.76	0.658	3.29	0.293	9.52	0.815	4.69	0.91	9.38	0.56	7.34	0.721	5.51	0.216	6.85	1.094	6.85	1.094	6.85	1.094	6.85	1.094	6.85	1.094	6.85	1.094	6.85	1.094	6.85	1.094						
5.36	0.679	3.64	0.318	9.88	0.716	5.1	0.93	10.87	0.57	8.33	0.736	6.07	0.236	7.27	1.101	7.27	1.101	7.27	1.101	7.27	1.101	7.27	1.101	7.27	1.101	7.27	1.101	7.27	1.101						
5.85	0.693	5.04	0.368	10.23	0.658	5.38	0.94	12.07	0.58	9.16	0.745	6.51	0.251	7.56	1.106	7.56	1.106	7.56	1.106	7.56	1.106	7.56	1.106	7.56	1.106	7.56	1.106	7.56	1.106						
6.25	0.704	6.13	0.4	10.59	0.629	8.31	0.95	13.03	0.58	9.83	0.751	6.85	0.264	8.75	1.078	8.75	1.078	8.75	1.078	8.75	1.078	8.75	1.078	8.75	1.078	8.75	1.078	8.75	1.078						
6.58	0.712	8.58	0.431	10.99	0.593	9.26	0.91	13.8	0.58	10.39	0.756	7.12	0.274	9.34	1.044	9.34	1.044	9.34	1.044	9.34	1.044	9.34	1.044	9.34	1.044	9.34	1.044	9.34	1.044						
6.85	0.718	10.47	0.445	11.42	0.563	9.73	0.87	14.42	0.59	10.85	0.758	7.33	0.283	10.25	0.961	10.25	0.961	10.25	0.961	10.25	0.961	10.25	0.961	10.25	0.961	10.25	0.961	10.25	0.961						
8.76	0.748	11.92	0.452	11.86	0.545	10.47	0.73	14.93	0.59	11.89	0.762	7.49	0.29	11.66	0.885	11.66	0.885	11.66	0.885	11.66	0.885	11.66	0.885	11.66	0.885	11.66	0.885	11.66	0.885						
10.3	0.762	13.06	0.455	12.3	0.522	11.45	0.62	15.33	0.59	12.75	0.764	7.62	0.296	12.77	0.853	12.77	0.853	12.77	0.853	12.77	0.853	12.77	0.853	12.77	0.853	12.77	0.853	12.77	0.853						
11.56	0.769	13.94	0.458	12.7	0.521	12.7	0.55	13.46	0.55	13.46	0.764	7.72	0.302	13.65	0.654	13.65	0.654	13.65	0.654	13.65	0.654	13.65	0.654	13.65	0.654	13.65	0.654	13.65	0.654						
12.59	0.772	14.63	0.46	13.82	0.487	14.05	0.5	14.05	0.5	14.05	0.764	7.8	0.306	14.34	0.48	14.34	0.48	14.34	0.48	14.34	0.48	14.34	0.48	14.34	0.48	14.34	0.48	14.34	0.48						
13.42	0.774	15.15	0.463	15	0.47	15.34	0.47	14.54	0.59	14.54	0.764	7.86	0.31	14.88	0.49	14.88	0.49	14.88	0.49	14.88	0.49	14.88	0.49	14.88	0.49	14.88	0.49	14.88	0.49						
14.1	0.774	15.54	0.464	16.2	0.45	16.48	0.44	14.95	0.59	14.95	0.763	7.92	0.314	15.32	0.5	15.32	0.5	15.32	0.5	15.32	0.5	15.32	0.5	15.32	0.5	15.32	0.5	15.32	0.5						
14.66	0.775	15.84	0.466	17.36	0.44	17.41	0.43	15.28	0.44	15.28	0.762	7.96	0.317	15.65	0.5	15.65	0.5	15.65	0.5	15.65	0.5	15.65	0.5	15.65	0.5	15.65	0.5	15.65	0.5						
15.11	0.774	16.08	0.467	18.45	0.44	18.15	0.42	15.56	0.42	15.56	0.762	9.66	0.309	15.92	0.5	15.92	0.5	15.92	0.5	15.92	0.5	15.92	0.5	15.92	0.5	15.92	0.5	15.92	0.5						
15.48	0.774	16.26	0.469	19.44	0.43	18.73	0.41	15.79	0.41	15.79	0.762	10.92	0.305	16.27	0.4	16.27	0.4	16.27	0.4	16.27	0.4	16.27	0.4	16.27	0.4	16.27	0.4	16.27	0.4						
15.77	0.775	16.41	0.469	20.33	0.43	19.15	0.4	15.98	0.4	15.98	0.762	11.87	0.304	16.37	0.4	16.37	0.4	16.37	0.4	16.37	0.4	16.37	0.4	16.37	0.4	16.37	0.4	16.37	0.4						
16.02	0.773	16.53	0.471	21.12	0.42	19.47	0.4	16.14	0.4	16.14	0.761	12.99	0.322	16.46	0.4	16.46	0.4	16.46	0.4	16.46	0.4	16.46	0.4	16.46	0.4	16.46	0.4	16.46	0.4						
16.21	0.774	16.62	0.471	21.8	0.42	19.7	0.4	16.27	0.4	16.27	0.761	13.92	0.321	16.59	0.32	16.59	0.32	16.59	0.32	16.59	0.32	16.59	0.32	16.59	0.32	16.59	0.32	16.59	0.32						
16.36	0.775	16.69	0.471	22.38	0.42	19.88	0.4	16.37	0.4	16.37	0.761	14.61	0.326	16.64	0.32	16.64	0.32	16.64	0.32	16.64	0.32	16.64	0.32	16.64	0.32	16.64	0.32	16.64	0.32						
16.49	0.774	16.73	0.472	22.88	0.42	20.01	0.4	16.46	0.4	16.46	0.761	15.19	0.32	16.66	0.32	16.66	0.32	16.66	0.32	16.66	0.32	16.66	0.32	16.66	0.32	16.66	0.32	16.66	0.32						
16.59	0.774	16.77	0.473	23.3	0.42	20.11	0.4	16.59	0.4	16.59	0.761	15.19	0.32	16.66	0.32	16.66	0.32	16.66	0.32	16.66	0.32	16.66	0.32	16.66	0.32	16.66	0.32	16.66	0.32						
		16.79	0.473	23.66	0.42	20.17	0.4	16.79	0.4	16.79	0.761	15.19	0.32	16.66	0.32	16.66	0.32	16.66	0.32	16.66	0.32	16.66	0.32	16.66	0.32	16.66	0.32	16.66	0.32						
		16.81	0.474	23.96	0.42	20.2	0.4	16.81	0.4	16.81	0.761	15.19	0.32	16.66	0.32	16.66	0.32	16.66	0.32	16.66	0.32	16.66	0.32	16.66	0.32	16.66	0.32	16.66	0.32						
				24.21	0.42			24.21	0.42	24.21	0.761																								

Sample: 8.1			Sample: 8.1			Sample: 8.1			Sample: 8.1			Sample: 8.1			Sample: 8.1			Sample: 8.1			Sample: 8.1			Sample: 8.2			Sample: 8.2			Sample: 10											
Moisture: p.d.			Moisture: e.m.			Moisture: e.m.			Moisture: dry			Moisture: e.m.			Moisture: e.m.			Moisture: a.r.			Moisture: a.r.			Moisture: a.r.			Moisture: a.r.			Moisture: a.r.			Moisture: a.r.								
Gas: CH4			Gas: CH4			Gas: CH4			Gas: CH4			Gas: CO2			Gas: CO2			Gas: CH4			Gas: CO2			Gas: CO2			Gas: CH4			Gas: CH4			Gas: CH4								
T (°C): 45.52			T (°C): 45.52			T (°C): 45.52			T (°C): 65.02			T (°C): 45.03			T (°C): 55.05			T (°C): 45.42			T (°C): 45.42			T (°C): 45.42			T (°C): 45.42			T (°C): 45.02											
P [MPa]			P [MPa]			P [MPa]			P [MPa]			P [MPa]			P [MPa]			P [MPa]			P [MPa]			P [MPa]			P [MPa]			P [MPa]			P [MPa]								
n _{h2s} [mmol/g]			n _{h2s} [mmol/g]			n _{h2s} [mmol/g]			n _{h2s} [mmol/g]			n _{h2s} [mmol/g]			n _{h2s} [mmol/g]			n _{h2s} [mmol/g]			n _{h2s} [mmol/g]			n _{h2s} [mmol/g]			n _{h2s} [mmol/g]			n _{h2s} [mmol/g]											
1.75	0.3	0	1.58	0.168	0	1.33	0.31	0	1.11	0.29	0	1.2	0.28	0	0.8	0.394	0	0.8	0.394	0	0.8	0.394	0	0.8	0.394	0	1.54	0.187	0	1.54	0.187	0	1.54	0.187	0						
3	0.41	0	3.01	0.247	0	2.68	0.41	0	2.46	0.42	0	2.64	0.39	0	5.49	0.864	0	5.49	0.864	0	5.49	0.864	0	5.49	0.864	0	2.97	0.255	0	2.97	0.255	0	2.97	0.255	0						
4.07	0.47	0	4.21	0.284	0	3.93	0.46	0	3.56	0.47	0	3.81	0.43	0	8.04	0.919	0	8.04	0.919	0	8.04	0.919	0	8.04	0.919	0	4.12	0.291	0	4.12	0.291	0	4.12	0.291	0	4.12	0.291	0			
4.93	0.5	0	6.11	0.332	0	4.85	0.49	0	4.37	0.5	0	4.67	0.45	0	9.13	0.916	0	9.13	0.916	0	9.13	0.916	0	9.13	0.916	0	5.93	0.328	0	5.93	0.328	0	5.93	0.328	0	5.93	0.328	0			
6.53	0.54	0	7.58	0.364	0	5.51	0.5	0	4.95	0.52	0	5.29	0.46	0	9.71	0.876	0	9.71	0.876	0	9.71	0.876	0	9.71	0.876	0	7.33	0.348	0	7.33	0.348	0	7.33	0.348	0	7.33	0.348	0			
7.77	0.56	0	8.74	0.374	0	6.99	0.52	0	6.19	0.53	0	6.65	0.47	0	10.31	0.761	0	10.31	0.761	0	10.31	0.761	0	10.31	0.761	0	8.4	0.36	0	8.4	0.36	0	8.4	0.36	0	8.4	0.36	0			
8.73	0.57	0	9.61	0.384	0	7.94	0.53	0	6.94	0.53	0	7.49	0.47	0	11.23	0.608	0	11.23	0.608	0	11.23	0.608	0	11.23	0.608	0	10.53	0.374	0	10.53	0.374	0	10.53	0.374	0	10.53	0.374	0			
10.56	0.59	0	10.26	0.394	0	8.58	0.54	0	7.43	0.52	0	8.06	0.46	0	12.5	0.51	0	12.5	0.51	0	12.5	0.51	0	12.5	0.51	0	12.18	0.382	0	12.18	0.382	0	12.18	0.382	0	12.18	0.382	0			
11.98	0.6	0	11.81	0.403	0	9.02	0.56	0	7.74	0.51	0	8.44	0.46	0	14.05	0.437	0	14.05	0.437	0	14.05	0.437	0	14.05	0.437	0	13.46	0.385	0	13.46	0.385	0	13.46	0.385	0	13.46	0.385	0			
13.09	0.61	0	12.95	0.402	0	9.33	0.57	0	7.96	0.51	0	8.7	0.45	0	15.71	0.387	0	15.71	0.387	0	15.71	0.387	0	15.71	0.387	0	14.87	0.386	0	14.87	0.386	0	14.87	0.386	0	14.87	0.386	0			
13.96	0.61	0	13.63	0.401	0	11.36	0.58	0	9.13	0.36	0	10.31	0.37	0	17.33	0.352	0	17.33	0.352	0	17.33	0.352	0	17.33	0.352	0	15.99	0.387	0	15.99	0.387	0	15.99	0.387	0	15.99	0.387	0			
14.65	0.61	0	14.5	0.397	0	12.92	0.58	0	9.78	0.21	0	11.41	0.32	0	18.79	0.331	0	18.79	0.331	0	18.79	0.331	0	18.79	0.331	0	16.87	0.386	0	16.87	0.386	0	16.87	0.386	0	16.87	0.386	0			
15.18	0.61	0	15.28	0.404	0	14.22	0.6	0	10.27	0.2	0	12.29	0.33	0	20.09	0.311	0	20.09	0.311	0	20.09	0.311	0	20.09	0.311	0	17.56	0.386	0	17.56	0.386	0	17.56	0.386	0	17.56	0.386	0			
15.6	0.61	0	15.94	0.386	0	15.5	0.61	0	10.78	0.23	0	13.18	0.34	0	21.15	0.303	0	21.15	0.303	0	21.15	0.303	0	21.15	0.303	0	18.1	0.385	0	18.1	0.385	0	18.1	0.385	0	18.1	0.385	0			
15.92	0.61	0	16.38	0.384	0	16.76	0.62	0	11.35	0.25	0	14.1	0.34	0	22.04	0.294	0	22.04	0.294	0	22.04	0.294	0	22.04	0.294	0	18.53	0.385	0	18.53	0.385	0	18.53	0.385	0	18.53	0.385	0			
16.17	0.61	0	16.38	0.384	0	20.71	0.62	0	13.51	0.25	0	15.76	0.24	0	23.32	0.281	0	23.32	0.281	0	23.32	0.281	0	23.32	0.281	0	19.12	0.385	0	19.12	0.385	0	19.12	0.385	0	19.12	0.385	0			
			24.19	0.62	0	22.55	0.62	0	14.68	0.25	0	20.06	0.33	0	24.72	0.281	0	24.72	0.281	0	24.72	0.281	0	24.72	0.281	0	21.06	0.378	0	21.06	0.378	0	21.06	0.378	0	21.06	0.378	0			
			25.58	0.63	0	24.19	0.62	0	16.71	0.24	0	21.23	0.33	0	25.58	0.63	0	25.58	0.63	0	25.58	0.63	0	25.58	0.63	0	22.48	0.373	0	22.48	0.373	0	22.48	0.373	0	22.48	0.373	0			
						17.51	0.24	0	17.51	0.24	0	17.51	0.24	0	11.02	0.505	0	11.02	0.505	0	11.02	0.505	0	11.02	0.505	0	23.63	0.368	0	23.63	0.368	0	23.63	0.368	0	23.63	0.368	0			
						18.18	0.23	0	18.18	0.23	0	18.18	0.23	0	12.23	0.512	0	12.23	0.512	0	12.23	0.512	0	12.23	0.512	0	24.56	0.364	0	24.56	0.364	0	24.56	0.364	0	24.56	0.364	0			
						19.65	0.23	0	19.65	0.23	0	19.65	0.23	0	13.19	0.516	0	13.19	0.516	0	13.19	0.516	0	13.19	0.516	0															
						20.89	0.22	0	20.89	0.22	0	20.89	0.22	0	13.97	0.518	0	13.97	0.518	0	13.97	0.518	0	13.97	0.518	0															
						21.9	0.22	0	21.9	0.22	0	21.9	0.22	0	14.58	0.521	0	14.58	0.521	0	14.58	0.521	0	14.58	0.521	0															
						22.72	0.22	0	22.72	0.22	0	22.72	0.22	0	15.07	0.522	0	15.07	0.522	0	15.07	0.522	0	15.07	0.522	0															
						23.33	0.22	0	23.33	0.22	0	23.33	0.22	0	15.46	0.522	0	15.46	0.522	0	15.46	0.522	0	15.46	0.522	0															
						23.82	0.21	0	23.82	0.21	0	23.82	0.21	0	15.77	0.523	0	15.77	0.523	0	15.77	0.523	0	15.77	0.523	0															
															16	0.525	0	16	0.525	0	16	0.525	0	16	0.525	0															

Sample: 11		Sample: 12		Sample: 13		Sample: 14		Sample: 15		Sample: 16		Sample: 17		Sample: 19		Sample: 21		Sample: 21		
Moisture: a.r.		Moisture: a.r.		Moisture: a.r.		Moisture: a.r.		Moisture: a.r.		Moisture: a.r.		Moisture: a.r.		Moisture: a.r.		Moisture: a.r.		Moisture: e.m.		
Gas: CH4	T (°C): 45.02	Gas: CH4	T (°C): 45.40	Gas: CH4	T (°C): 45.40	Gas: CH4	T (°C): 45.41	Gas: CH4	T (°C): 45.38	Gas: CH4	T (°C): 45.40	Gas: CH4	T (°C): 45.03	Gas: CH4	T (°C): 45.02	Gas: CH4	T (°C): 44.75	Gas: CH4	T (°C): 44.75	
P [MPa]	n _{ads} [mmol/g]	P [MPa]	n _{ads} [mmol/g]	P [MPa]	n _{ads} [mmol/g]	P [MPa]	n _{ads} [mmol/g]	P [MPa]	n _{ads} [mmol/g]	P [MPa]	n _{ads} [mmol/g]	P [MPa]	n _{ads} [mmol/g]	P [MPa]	n _{ads} [mmol/g]	P [MPa]	n _{ads} [mmol/g]	P [MPa]	n _{ads} [mmol/g]	
0	0	0	0	0	0	0	0	0	0	0	0	0	0	0	0	0	0	0	0	
0.67	0.216	0.77	0.135	0.54	0.221	0.78	0.09	0.6	0.175	0.76	0.131	0.7	0.209	0.85	0.139	2.39	0.601	0.74	0.194	
1.44	0.327	1.51	0.212	1.19	0.342	1.55	0.129	1.29	0.263	1.49	0.202	1.48	0.314	2.34	0.233	4.81	0.752	1.53	0.314	
2.16	0.392	2.15	0.258	1.81	0.414	2.76	0.169	1.93	0.316	2.12	0.246	2.18	0.375	3.59	0.277	6.89	0.817	2.25	0.392	
2.75	0.432	2.68	0.288	2.36	0.461	3.77	0.191	2.48	0.35	2.66	0.275	2.77	0.414	4.58	0.302	8.6	0.848	2.86	0.445	
3.23	0.459	3.12	0.309	2.82	0.494	4.59	0.205	2.94	0.373	3.11	0.295	3.24	0.44	5.35	0.317	10.01	0.863	3.35	0.482	
3.61	0.478	3.48	0.324	3.22	0.517	5.26	0.215	3.33	0.39	3.88	0.323	3.62	0.39	5.96	0.328	11.17	0.872	3.74	0.506	
5	0.527	4.76	0.366	4.46	0.573	5.8	0.221	4.21	0.42	5.06	0.358	5	0.506	8.43	0.354	12.13	0.875	5.26	0.565	
6.11	0.556	5.8	0.393	5.49	0.607	6.23	0.226	4.93	0.44	6.01	0.38	6.08	0.535	10.33	0.366	12.92	0.877	6.43	0.601	
6.95	0.574	6.63	0.411	6.33	0.629	6.58	0.23	5.51	0.454	6.77	0.396	6.92	0.552	11.8	0.372	13.58	0.878	7.31	0.625	
7.61	0.586	7.3	0.423	7.01	0.644	6.87	0.232	5.97	0.463	7.39	0.406	7.58	0.564	12.95	0.375	14.12	0.878	9.68	0.658	
8.12	0.594	7.83	0.432	7.56	0.654	7.85	0.24	6.35	0.471	7.89	0.414	8.1	0.572	13.84	0.377	14.57	0.878	11.45	0.674	
8.51	0.599	8.26	0.438	8.01	0.662	8.64	0.245	6.66	0.476	8.29	0.42	8.5	0.578	14.55	0.378	14.94	0.878	12.79	0.683	
10.33	0.615	8.61	0.443	9.66	0.681	9.27	0.249	6.91	0.483	8.61	0.424	8.81	0.582	14.3	0.378	15.24	0.877	13.79	0.688	
11.75	0.623	8.89	0.447	11	0.692	9.78	0.251	7.13	0.483	10.23	0.441	10.69	0.596	13.23	0.377	15.49	0.876	14.55	0.691	
12.84	0.627	9.11	0.45	12.08	0.698	11.12	0.257	7.3	0.486	11.5	0.452	12.01	0.602	11.93	0.374	15.7	0.876	15.12	0.693	
13.68	0.63	10.65	0.465	12.97	0.701	12.21	0.26	7.44	0.488	12.53	0.459	13.05	0.605	10.63	0.369	15.86	0.876	15.55	0.694	
14.36	0.63	11.87	0.475	13.7	0.704	13.09	0.262	8.31	0.497	13.36	0.465	13.86	0.607	9.42	0.362	16	0.876	15.87	0.694	
14.89	0.631	12.85	0.482	14.3	0.704	13.81	0.263	8.44	0.499	14.04	0.467	14.49	0.608	8.32	0.353	16.11	0.877	16.12	0.695	
15.31	0.631	13.64	0.486	14.78	0.705	14.4	0.264	9.11	0.505	14.59	0.47	15	0.609	7.34	0.344	16.2	0.876	16.31	0.696	
15.65	0.631	14.27	0.489	15.18	0.706	14.88	0.265	9.65	0.509	15.03	0.472	15.39	0.61			16.46	0.876	16.46	0.696	
		14.77	0.492	15.51	0.706	15.27	0.265	10.09	0.511	15.39	0.474	15.71	0.609			16.58	0.876	16.58	0.697	
		15.18	0.494	15.78	0.707	15.59	0.266	10.45	0.514							16.67	0.876	16.67	0.697	
		15.5	0.496			15.84	0.266	11.66	0.519							16.74	0.876	16.74	0.697	
		15.76	0.497			16.04	0.267	12.66	0.521											
		15.97	0.498			16.21	0.267	13.47	0.523											
		16.15	0.5			16.34	0.268	14.13	0.524											
		16.28	0.5			16.46	0.267	14.67	0.525											
		16.4	0.5			16.55	0.267	15.1	0.526											
		16.49	0.5			16.63	0.267	15.46	0.526											
		16.56	0.5			16.7	0.267	15.75	0.526											
		16.62	0.5			16.75	0.268	15.99	0.526											

Sample: 21					Sample: 22					Sample: 22					Sample: 22					Sample: 22					Sample: 22					Sample: 23					Sample: 23					Sample: 23					Sample: 23				
Moisture: a.r.					Moisture: a.r.					Moisture: e.m.					Moisture: a.r.					Moisture: a.r.					Moisture: a.r.					Moisture: e.m.					Moisture: p.d.					Moisture: a.r.									
Gas: CO2					Gas: CH4					Gas: CH4					Gas: CO2					Gas: CH4					Gas: CO2					Gas: CH4					Gas: CH4					Gas: CO2									
T (°C): 45.02					T (°C): 44.84					T (°C): 46.12					T (°C): 19.54					T (°C): 19.42					T (°C): 44.85					T (°C): 44.68					T (°C): 45.43					T (°C): 45.02									
P [MPa]					P [MPa]					P [MPa]					P [MPa]					P [MPa]					P [MPa]					P [MPa]					P [MPa]					P [MPa]					P [MPa]				
nads [mmol/g]					nads [mmol/g]					nads [mmol/g]					nads [mmol/g]					nads [mmol/g]					nads [mmol/g]					nads [mmol/g]					nads [mmol/g]					nads [mmol/g]									
0					0					0					0					0					0					0					0					0					0				
0.73	1.88	3.78	5.15	6.06	6.68	7.11	8.6	9.25	9.83	10.4	11.12	12	13.01	14.06	15.05	16.77	17.45	18.01	19.32	20.45	21.39	22.17	22.8	23.31	23.72	24.04	24.51	24.65	24.77	24.87	24.93																		
0.626	0.888	1.09	1.168	1.201	1.221	1.231	1.215	1.2	1.105	0.961	0.82	0.738	0.66	0.605	0.57	0.66	0.51	0.5	0.47	0.45	0.44	0.43	0.42	0.41	0.41	0.4	0.4	0.4	0.4	0.4																			
0	0	0	0	0	0	0	0	0	0	0	0	0	0	0	0	0	0	0	0	0	0	0	0	0	0	0	0	0	0	0	0																		
0.289	0.499	0.547	0.572	0.586	0.594	0.598	0.6	0.604	0.605	0.606	0.607	0.608	0.61	0.61	0.61	0.61	0.61	0.61	0.61	0.61	0.61	0.61	0.61	0.61	0.61	0.61	0.61	0.61	0.61	0.61	0.61																		
0.289	0.361	0.38	0.385	0.384	0.382	0.381	0.379	0.378	0.378	0.378	0.377	0.377	0.377	0.376	0.377	0.377	0.377	0.377	0.377	0.377	0.377	0.377	0.377	0.377	0.377	0.377	0.377	0.377	0.377	0.377	0.377																		
0.66	1.36	1.99	2.52	3.84	4.95	5.87	6.64	7.29	7.84	8.74	9.49	10.43	11.28	12.01	12.62	13.15	13.99	14.33	14.61	14.87	15.12	15.35	15.55	15.72	15.87	15.99	16.1	16.2	16.28	16.28	16.2																		
0	0	0	0	0	0	0	0	0	0	0	0	0	0	0	0	0	0	0	0	0	0	0	0	0	0	0	0	0	0	0	0																		
0.14	0.31	0.44	0.6	0.76	0.91	1.06	1.18	1.29	1.39	1.72	2.01	2.25	2.45	2.62	2.77	2.88	3.28	3.62	4.05	4.05	4.05	4.05	4.05	4.05	4.05	4.05	4.05	4.05	4.05	4.05	4.05																		
0.19	0.33	0.48	0.59	0.66	0.71	0.75	0.77	0.79	0.8	0.83	0.85	0.85	0.85	0.85	0.85	0.84	0.8	0.76	0.66	0.66	0.66	0.66	0.66	0.66	0.66	0.66	0.66	0.66	0.66	0.66	0.66																		
0.554	0.777	0.79	0.756	0.714	0.633	0.5	0.476	0.419	0.373	0.342	0.314	0.298	0.273	0.27	0.23	0.22	0.2	0.19	0.18	0.18	0.18	0.18	0.18	0.18	0.18	0.18	0.18	0.18	0.18	0.18	0.18																		
0	0	0	0	0	0	0	0	0	0	0	0	0	0	0	0	0	0	0	0	0	0	0	0	0	0	0	0	0	0	0	0																		
0.74	1.46	2.09	2.63	3.08	3.46	3.77	4.02	5.35	6.38	7.18	7.81	8.3	8.68	8.98	9.22	9.41	9.55	9.65	9.73	9.84	9.88	9.88	9.88	9.88	9.88	9.88	9.88	9.88	9.88	9.88	9.88																		
0.141	0.24	0.313	0.368	0.41	0.442	0.468	0.488	0.536	0.57	0.595	0.615	0.629	0.641	0.65	0.657	0.663	0.668	0.671	0.674	0.677	0.679	0.682	0.683	0.684	0.689	0.691	0.691	0.691	0.691	0.691																			
0	0	0	0	0	0	0	0	0	0	0	0	0	0	0	0	0	0	0	0	0	0	0	0	0	0	0	0	0	0	0	0																		
0.65	1.67	2.63	3.42	4.86	6.43	7.7	8.69	10.07	11.14	12.45	13.46	14.24	14.85	15.32	15.68	15.97	16.2	16.37	16.5	16.61	16.69	16.81	16.85	16.87	16.89	16.89	16.89	16.89	16.89	16.89	16.89																		
0.661	0.926	1.053	1.119	1.282	1.241	1.144	1.026	0.97	0.871	0.816	0.769	0.731	0.701	0.703	0.698	0.696	0.695	0.693	0.692	0.691	0.691	0.691	0.691	0.691	0.691	0.691	0.691	0.691	0.691	0.691	0.691																		

Sample: 23			Sample: 24			Sample: 24			Sample: 24			Sample: 24			Sample: 24			Sample: 25			Sample: 25			Sample: 25			
Moisture: e.m.			Moisture: a.r.			Moisture: e.m.			Moisture: a.r.			Moisture: a.r.			Moisture: a.r.			Moisture: e.m.			Moisture: a.r.			Moisture: e.m.			
Gas: CO2	T (°C): 45.5	$\rho_{\text{H}_2\text{O}}$ [mmol/g]	Gas: CH4	T (°C): 44.66	$\rho_{\text{H}_2\text{O}}$ [mmol/g]	Gas: CH4	T (°C): 45.63	$\rho_{\text{H}_2\text{O}}$ [mmol/g]	Gas: CO2	T (°C): 44.97	$\rho_{\text{H}_2\text{O}}$ [mmol/g]	Gas: CH4	T (°C): 19.54	$\rho_{\text{H}_2\text{O}}$ [mmol/g]	Gas: CO2	T (°C): 44.84	$\rho_{\text{H}_2\text{O}}$ [mmol/g]	Gas: CH4	T (°C): 43.94	$\rho_{\text{H}_2\text{O}}$ [mmol/g]	Gas: CH4	T (°C): 46.08	$\rho_{\text{H}_2\text{O}}$ [mmol/g]	Gas: CO2	T (°C): 44.94	$\rho_{\text{H}_2\text{O}}$ [mmol/g]	
P [MPa]	0	0	P [MPa]	0	0	P [MPa]	0	0	P [MPa]	0	0	P [MPa]	0	0	P [MPa]	0	0	P [MPa]	0	0	0	P [MPa]	0	0	P [MPa]	0	0
0.52	0.446	0.386	0.69	1.16	0.252	1.16	0.252	0.64	0.48	1.4	0.833	2.21	0.629	2.59	0.268	2.21	0.629	2.59	0.268	2.59	0.268	2.2	0.26	0.52	0.553	6.8	1.141
1.54	0.708	0.56	1.5	2.23	0.415	2.23	0.415	1.46	0.66	5.92	1.154	4.62	0.792	4.46	0.384	4.62	0.792	4.46	0.384	4.46	0.384	3.94	0.37	1.43	0.805	8.25	1.119
7.03	1.027	0.656	2.26	3.2	0.503	3.2	0.503	2.9	0.81	8.03	1.124	6.66	0.859	5.7	0.452	6.66	0.859	5.7	0.452	5.7	0.452	5.17	0.43	2.32	0.929	8.96	1.048
8.92	1.047	0.717	2.93	4.06	0.554	4.06	0.554	4.14	0.88	8.96	1.029	8.34	0.891	6.52	0.496	8.34	0.891	6.52	0.496	6.52	0.496	6.02	0.47	3.08	1	9.37	0.95
9.64	1.052	0.757	3.5	4.78	0.586	4.78	0.586	5.19	0.92	9.45	0.921	9.72	0.907	7.06	0.528	9.72	0.907	7.06	0.528	7.06	0.528	6.62	0.49	3.7	1.04	9.66	0.866
10.18	0.988	0.786	3.99	5.38	0.607	5.38	0.607	6.07	0.94	9.8	0.817	10.85	0.915	7.42	0.552	10.85	0.915	7.42	0.552	7.42	0.552	7.04	0.51	6.8	1.141	9.9	0.807
10.83	0.883	0.807	4.4	5.87	0.621	5.87	0.621	6.81	0.96	10.13	0.743	11.78	0.919	7.65	0.571	11.78	0.919	7.65	0.571	7.65	0.571	7.34	0.53	8.25	1.119	10.12	0.768
11.6	0.811	0.823	4.75	6.28	0.63	6.28	0.63	7.42	0.97	10.48	0.682	12.54	0.92	9.23	0.595	12.54	0.92	9.23	0.595	9.23	0.595	8.98	0.54	8.96	1.048	10.34	0.715
12.45	0.764	0.835	5.05	6.61	0.637	6.61	0.637	7.94	0.98	10.85	0.647	13.17	0.92	10.23	0.613	13.17	0.92	10.23	0.613	10.23	0.613	10.07	0.55	9.37	0.95	10.54	0.687
13.28	0.732	0.862	5.83	6.88	0.642	6.88	0.642	8.38	0.98	11.25	0.609	13.68	0.92	10.88	0.628	13.68	0.92	10.88	0.628	10.88	0.628	11.16	0.55	9.66	0.866	10.74	0.649
14.06	0.71	0.88	6.47	7.11	0.646	7.11	0.646	8.75	0.99	11.67	0.585	14.11	0.919	12.15	0.56	14.11	0.919	12.15	0.56	12.15	0.56	12.83	0.56	10.34	0.715	9.9	0.807
14.74	0.693	0.892	7.01	7.29	0.649	7.29	0.649	9.63	0.99	12.09	0.562	14.46	0.919	12.56	0.56	14.46	0.919	12.56	0.56	12.56	0.56	14.1	0.57	10.54	0.687	10.74	0.649
15.29	0.685	0.902	7.44	7.44	0.651	7.44	0.651	10.38	0.99	13.08	0.53	14.75	0.919	2.66	1.27	14.75	0.919	2.66	1.27	14.75	0.919	14.99	0.57	10.54	0.687	10.74	0.649
15.76	0.677	0.909	7.84	7.57	0.653	7.57	0.653	11	1	14.18	0.499	15.18	0.919	3.16	1.29	14.98	0.919	3.16	1.29	14.98	0.919	15.6	0.57	10.74	0.649	10.74	0.649
16.12	0.672	0.914	8.16	7.68	0.654	7.68	0.654	11.53	0.914	15.32	0.48	15.32	0.919	3.56	1.29	15.18	0.919	3.56	1.29	15.18	0.919	15.67	0.58	11.83	0.6	10.74	0.649
		0.918	8.43	7.77	0.655	7.77	0.655	11.98	1	16.46	0.47	15.34	0.918	3.88	1.28	15.34	0.918	3.88	1.28	15.34	0.918	16.03	0.57	10.92	0.66	10.92	0.66
		0.929	9.42	7.84	0.656	7.84	0.656	12.36	0.99	17.56	0.45	15.46	0.918	4.14	1.27	15.46	0.918	4.14	1.27	15.46	0.918	16.32	0.58	11.09	0.64	11.09	0.64
		0.935	10.23	7.91	0.657	7.91	0.657	12.68	0.99	18.59	0.44	15.57	0.918	4.34	1.25	15.57	0.918	4.34	1.25	15.57	0.918	16.53	0.58	11.24	0.63	11.24	0.63
		0.939	11.14	7.98	0.661	7.98	0.661	13.08	0.99	19.53	0.44	15.65	0.918	4.5	1.23	15.65	0.918	4.5	1.23	15.65	0.918	16.67	0.58	11.83	0.6	11.83	0.6
		0.942	11.9	8.11	0.664	8.11	0.664	13.41	0.99	20.37	0.43	15.71	0.918	15.71	0.918	15.71	0.918	15.71	0.918	15.71	0.918	16.76	0.58	12.56	0.57	12.56	0.57
		0.943	12.52	8.16	0.665	8.16	0.665	13.69	0.99	21.12	0.43	15.76	0.919	15.76	0.919	15.76	0.919	15.76	0.919	15.76	0.919	16.76	0.58	13.37	0.53	13.37	0.53
		0.944	13.05	8.21	0.666	8.21	0.666	13.94	0.99	21.76	0.43	15.79	0.919	15.79	0.919	15.79	0.919	15.79	0.919	15.79	0.919	16.76	0.58	14.49	0.52	14.49	0.52
		0.943	13.48	8.26	0.667	8.26	0.667	14.15	0.99	22.33	0.42	15.82	0.919	15.82	0.919	15.82	0.919	15.82	0.919	15.82	0.919	16.76	0.58	15.69	0.48	15.69	0.48
		0.943	13.85	8.31	0.666	8.31	0.666	14.32	0.98	22.81	0.42											16.84	0.47	16.84	0.47		
		0.941	14.15	8.34	0.666	8.34	0.666	14.48	0.99	23.22	0.42											17.94	0.46	17.94	0.46		
		0.94	14.62	8.37	0.666	8.37	0.666	14.73	0.99	23.87	0.42											18.93	0.45	18.93	0.45		
		0.941	14.8	8.39	0.666	8.39	0.666	14.83	0.99	24.12	0.42											19.85	0.44	19.85	0.44		
		0.941	15.06	8.41	0.665	8.41	0.665	14.91	0.99	24.33	0.42											20.62	0.45	20.62	0.45		
		0.941	15.17	8.42	0.664	8.42	0.664	14.99	0.98													21.31	0.45	21.31	0.45		
		0.94	15.26	8.43	0.663	8.43	0.663	15.06	0.98																		
		0.939	15.33	8.44	0.663	8.44	0.663	15.3	0.98																		
		0.94	15.4	8.45	0.662	8.45	0.662	15.4	0.98																		
		0.94	15.56	8.46	0.663	8.46	0.663	15.47	0.99																		
		0.94	15.67	8.47	0.662	8.47	0.662	15.55	0.98																		
		0.939	15.76	8.48	0.662	8.48	0.662	15.6	0.99																		
		0.938	15.84	8.49	0.663	8.49	0.663	15.65	0.98																		

Sample: 26			Sample: 26			Sample: 26			Sample: 26			Sample: 26			Sample: 27			Sample: 27			Sample: 27		
Moisture: a.r.	Moisture: e.m.	Moisture: p.d.	Moisture: a.r.	Moisture: a.r.	Moisture: a.r.	Moisture: a.r.	Moisture: e.m.	Moisture: a.r.	Moisture: e.m.	Moisture: a.r.	Moisture: e.m.	Moisture: a.r.	Moisture: a.r.	Moisture: a.r.	Moisture: e.m.	Moisture: a.r.	Moisture: a.r.	Moisture: e.m.	Moisture: a.r.	Moisture: e.m.	Moisture: a.r.		
Gas: CH4	Gas: CH4	Gas: CH4	Gas: CH4	Gas: CO2	Gas: CO2	Gas: CH4	Gas: CH4	Gas: CO2	Gas: CH4	Gas: CH4	Gas: CH4	Gas: CO2	Gas: CO2	Gas: CO2	Gas: CO2	Gas: CO2	Gas: CO2	Gas: CO2	Gas: CO2	Gas: CO2	Gas: CO2		
T (°C): 19.39	T (°C): 46.08	T (°C): 45.12	T (°C): 19.42	T (°C): 45.02	T (°C): 44.7	T (°C): 45.37	T (°C): 44.83	T (°C): 45.02	T (°C): 44.7	T (°C): 44.7	T (°C): 45.37	T (°C): 44.83	T (°C): 44.83	T (°C): 44.83	T (°C): 45.02	T (°C): 44.83	T (°C): 44.83	T (°C): 45.02	T (°C): 44.83	T (°C): 44.83	T (°C): 45.02		
n _{ads} [mmol/g]	n _{ads} [mmol/g]	n _{ads} [mmol/g]	n _{ads} [mmol/g]	n _{ads} [mmol/g]	n _{ads} [mmol/g]	n _{ads} [mmol/g]	n _{ads} [mmol/g]	n _{ads} [mmol/g]	n _{ads} [mmol/g]	n _{ads} [mmol/g]	n _{ads} [mmol/g]	n _{ads} [mmol/g]	n _{ads} [mmol/g]	n _{ads} [mmol/g]	n _{ads} [mmol/g]	n _{ads} [mmol/g]	n _{ads} [mmol/g]	n _{ads} [mmol/g]	n _{ads} [mmol/g]	n _{ads} [mmol/g]	n _{ads} [mmol/g]		
P [MPa]	P [MPa]	P [MPa]	P [MPa]	P [MPa]	P [MPa]	P [MPa]	P [MPa]	P [MPa]	P [MPa]	P [MPa]	P [MPa]	P [MPa]	P [MPa]	P [MPa]	P [MPa]	P [MPa]	P [MPa]	P [MPa]	P [MPa]	P [MPa]	P [MPa]		
0.44	1.77	0.86	0.27	1.49	0.9	1.85	1.7	1.49	0.9	0.286	3.3	0	0	0	0	0	0	0	0	0	0	0	
0.44	3.15	2.06	0.44	3.22	1.89	3.3	1.49	3.22	1.89	0.399	4.42	0	0	0	0	0	0	0	0	0	0	0	
1	4.27	3.21	0.68	6.47	3.22	4.21	0.44	6.47	3.22	0.485	5.94	3.45	3.45	3.45	3.45	3.45	3.45	3.45	3.45	3.45	3.45	3.45	
1.54	5.16	4.21	0.95	8.05	4.35	5.01	0.68	8.05	4.35	0.532	5.94	4.73	4.73	4.73	4.73	4.73	4.73	4.73	4.73	4.73	4.73	4.73	
2.02	5.84	5.01	1.22	8.83	5.3	5.84	0.95	8.83	5.3	0.56	5.94	7.27	7.27	7.27	7.27	7.27	7.27	7.27	7.27	7.27	7.27	7.27	
3.24	6.37	6.53	1.47	9.27	6.09	6.37	1.22	9.27	6.09	0.578	9.87	8.47	8.47	8.47	8.47	8.47	8.47	8.47	8.47	8.47	8.47	8.47	
4.27	6.77	7.73	1.69	9.57	6.74	6.77	1.47	9.57	6.74	0.59	11.61	9.07	9.07	9.07	9.07	9.07	9.07	9.07	9.07	9.07	9.07	9.07	
5.14	8.11	8.11	1.89	10.47	7.28	8.11	1.69	10.47	7.28	0.6	12.91	9.71	9.71	9.71	9.71	9.71	9.71	9.71	9.71	9.71	9.71	9.71	
5.87	8.11	9.75	1.89	10.98	8.11	9.75	1.89	10.98	8.11	0.615	15.2	10.38	10.38	10.38	10.38	10.38	10.38	10.38	10.38	10.38	10.38	10.38	
6.48	9.09	11.32	2.05	11.58	8.11	11.32	2.05	11.58	8.11	0.624	15.2	10.38	10.38	10.38	10.38	10.38	10.38	10.38	10.38	10.38	10.38	10.38	
6.99	9.82	12.56	2.37	12.26	10.47	12.56	2.37	12.26	10.47	0.63	15.2	10.38	10.38	10.38	10.38	10.38	10.38	10.38	10.38	10.38	10.38	10.38	
7.42	11.62	13.52	2.64	12.26	10.98	13.52	2.64	12.26	10.98	0.634	15.2	10.38	10.38	10.38	10.38	10.38	10.38	10.38	10.38	10.38	10.38	10.38	
7.77	12.95	14.28	2.86	12.26	11.58	14.28	2.86	12.26	11.58	0.638	15.2	10.38	10.38	10.38	10.38	10.38	10.38	10.38	10.38	10.38	10.38	10.38	
9.1	13.95	14.88	3.24	12.26	12.26	14.88	3.24	12.26	12.26	0.641	15.2	10.38	10.38	10.38	10.38	10.38	10.38	10.38	10.38	10.38	10.38	10.38	
10.28	14.71	15.34	3.56	13.75	13	15.34	3.56	13.75	13	0.641	15.2	10.38	10.38	10.38	10.38	10.38	10.38	10.38	10.38	10.38	10.38	10.38	
11.27	15.27	15.71	3.81	13.75	13.75	15.71	3.81	13.75	13.75	0.641	15.2	10.38	10.38	10.38	10.38	10.38	10.38	10.38	10.38	10.38	10.38	10.38	
12.09	15.71	15.99	4.02	15.21	14.49	15.99	4.02	15.21	14.49	0.641	15.2	10.38	10.38	10.38	10.38	10.38	10.38	10.38	10.38	10.38	10.38	10.38	
12.79	15.71	16.22	4.19	15.21	15.87	16.22	4.19	15.21	15.87	0.641	15.2	10.38	10.38	10.38	10.38	10.38	10.38	10.38	10.38	10.38	10.38	10.38	
13.4	16.22	16.22	4.32	15.21	16.22	16.22	4.32	15.21	16.22	0.641	15.2	10.38	10.38	10.38	10.38	10.38	10.38	10.38	10.38	10.38	10.38	10.38	
13.92	16.22	16.22	4.54	16.96	16.96	16.22	4.54	16.96	16.96	0.641	15.2	10.38	10.38	10.38	10.38	10.38	10.38	10.38	10.38	10.38	10.38	10.38	
14.37	16.22	16.22	4.71	17.99	17.99	16.22	4.71	17.99	17.99	0.641	15.2	10.38	10.38	10.38	10.38	10.38	10.38	10.38	10.38	10.38	10.38	10.38	
14.76	16.22	16.22	4.84	18.95	18.95	16.22	4.84	18.95	18.95	0.641	15.2	10.38	10.38	10.38	10.38	10.38	10.38	10.38	10.38	10.38	10.38	10.38	
15.09	16.22	16.22	5.02	19.82	19.82	16.22	5.02	19.82	19.82	0.641	15.2	10.38	10.38	10.38	10.38	10.38	10.38	10.38	10.38	10.38	10.38	10.38	
15.37	16.22	16.22	5.02	20.6	20.6	16.22	5.02	20.6	20.6	0.641	15.2	10.38	10.38	10.38	10.38	10.38	10.38	10.38	10.38	10.38	10.38	10.38	
15.62	16.22	16.22	5.2	21.29	21.29	16.22	5.2	21.29	21.29	0.641	15.2	10.38	10.38	10.38	10.38	10.38	10.38	10.38	10.38	10.38	10.38	10.38	
15.84	16.22	16.22	5.2	21.9	21.9	16.22	5.2	21.9	21.9	0.641	15.2	10.38	10.38	10.38	10.38	10.38	10.38	10.38	10.38	10.38	10.38	10.38	
16.04	16.22	16.22	5.2	22.42	22.42	16.22	5.2	22.42	22.42	0.641	15.2	10.38	10.38	10.38	10.38	10.38	10.38	10.38	10.38	10.38	10.38	10.38	
16.2	16.22	16.22	5.2	22.84	22.84	16.22	5.2	22.84	22.84	0.641	15.2	10.38	10.38	10.38	10.38	10.38	10.38	10.38	10.38	10.38	10.38	10.38	
16.34	16.22	16.22	5.2	23.23	23.23	16.22	5.2	23.23	23.23	0.641	15.2	10.38	10.38	10.38	10.38	10.38	10.38	10.38	10.38	10.38	10.38	10.38	
16.46	16.22	16.22	5.2	23.56	23.56	16.22	5.2	23.56	23.56	0.641	15.2	10.38	10.38	10.38	10.38	10.38	10.38	10.38	10.38	10.38	10.38	10.38	
16.57	16.22	16.22	5.2	23.84	23.84	16.22	5.2	23.84	23.84	0.641	15.2	10.38	10.38	10.38	10.38	10.38	10.38	10.38	10.38	10.38	10.38	10.38	
16.66	16.22	16.22	5.2	24.09	24.09	16.22	5.2	24.09	24.09	0.641	15.2	10.38	10.38	10.38	10.38	10.38	10.38	10.38	10.38	10.38	10.38	10.38	

Appendix IV High-pressure methane and carbon dioxide sorption on coal and shale samples from the Paraná Basin, Brazil

Appendix IV Table 1 Results of high-pressure methane and carbon dioxide sorption experiments measured at 45 °C.

sample number	CH ₄ isotherms			Langmuir parameter				
	n _{max} CH ₄ [mmol/g]	n _{max} CH ₄ [mmol/g, daf]	V _{max} CH ₄ [m ³ /t, daf]	n _L CH ₄ [mmol/g]	n _L CH ₄ [mmol/g, daf]	P _L [MPa]	V _L [m ³ /t] at 6.25 MPa (reservoir pressure)	helium density [g/cm ³]
07_114	0.05	0.79	17.94	0.07	1.02	4.09	0.95	2.32
07_117/118	0.25	0.77	17.49	0.28	0.87	2.31	4.68	2.29
07_153 ^a	0.22	0.34	7.72	0.27	0.43	3.73	3.85	1.84
07_166	0.47	0.81	18.4	0.57	0.99	4.23	7.72	1.66
07_166 ^b	0.25	0.44	9.99	0.3	0.53	3.35	4.06	1.7
07_177 ^a	0.12	0.31	7.04	0.15	0.38	3.34	2.15	2.07
07_186 ^a	0.2	0.37	8.4	0.25	0.46	3.47	3.65	1.83
07_181	0.14	0.77	17.49	0.18	1.02	5.79	2.18	2.04
08_100	0.02	1.63 ^c	-36.98	0.04	3.37 ^c	16.09	n.d.	2.59
08_101	0.05	7.78 ^c	-194.79	0.08	11.45 ^c	7.09	n.d.	2.46
08_168	0.25	1.02 ^c	5.73	0.37	1.52 ^c	8.39	n.d.	1.9
08_170	0.13	1.27 ^c	-26.58	0.25	2.36 ^c	14.16	n.d.	2.25
08_154	0.03	1.28 ^c	-33.55	0.04	1.77 ^c	5.65	n.d.	2.72

Appendix IV Table 1 continued

sample number	CO ₂ isotherms					Langmuir parameter				
	n _{max} CO ₂ [mmol/g]	Pressure at n _{max} [MPa]	V _{max} CO ₂ [m ³ /t]	n _{max} CO ₂ / n _{max} CH ₄	n _L CO ₂ [mmol/g]	P _L CO ₂ [MPa]	ρ _{sorbate} [g/cm ³]	V _L [m ³ /t] at 6.25 MPa (reservoir pressure)	V _{CCO₂} /V _{LCH₄} at 6.25 MPa	helium density [g/cm ³]
07_114	0.25	8.7	5.63	4.58	0.69	8.43	960	6.66	7	2.81
07_117/118	0.34	9.47	7.69	1.36	0.8	6.19	1133	9.14	2	2.46
07_153 ^a	0.81	6.88	18.45	3.4	1.91	3.4	n.d.	n.d.	n.d.	1.72
07_166	0.64	7.94	14.56	1.38	1.11	3.18	1129	16.63	2.2	1.88
07_166 ^b	0.28	7.65	6.38	1.12	0.43	1.87	825	6.47	1.59	1.69
07_177 ^a	0.39	7.35	8.91	3.3	1.18	1.14	n.d.	n.d.	n.d.	1.93
07_186 ^a	0.55	6.34	12.45	2.71	1.54	3.56	n.d.	n.d.	n.d.	1.66
07_181	0.35	9.08	7.92	2.51	0.9	12.01	862	6.99	3.2	2.02
08_100	0.2	9.083	4.62	10.01	0.78	20	882	n.d.	n.d.	2.23
08_101	0.16	8.13	3.68	3	0.69	19.03	902	n.d.	n.d.	2.71
08_168	0.54	9.63	12.21	2.13	2.02	15	907	n.d.	n.d.	1.88
08_170	0.359	7.32	8.15	2.76	1.25	13.43	823	n.d.	n.d.	2.27
08_154	0.14	8.73	3.22	4.93	0.65	19.9	960	n.d.	n.d.	2.72

^a Measured at 35 °C. ^b Moisture equilibrated. ^c [mmol/g TOC]; n_L=Langmuir sorption; P_L=Langmuir pressure; n_{max}=maximum excess sorption; n.d. = not determined.

Appendix IV Table 2 Semi-quantitative and quantitative X-ray mineralogy.

Santa Terezinha Coal Kalkreuth et al., (2006)			
seaminterval	I	D	G
Quartz	40%	45%	30%
Kaolinite	30%	T	60%
Siderite	15%	R	R
Calcite	T	15%	n.d.
Ankerite	n.d.	15%	n.d.
Illite	M	M	10%
Pyrite	n.d.	M	n.d.
Feldspar	T	T	T
Dolomite	n.d.	T	n.d.
Sphalerite	T	R	R
Bassanite	n.d.	T	T
Apatite	T	R	T
Rutile	R	n.d.	T
Hematite	T	R	n.d.

Ohio Shale Nuttall et al., (2005)			
formation	Lower Huron	Middle Huron	Upper Huron
Quartz	48%	47%	51%
Kaolinite	1.30%	2.50%	2.30%
Barite	1.10%	0.60%	0.70%
Calcite	0.30%	1.10%	0.30%
Gypsum	0.30%	0.30%	0.50%
Illite+Mica	25%	29%	25%
Pyrite	8.60%	6.20%	5.40%
Feldspar (Plagioclase)	5.40%	7.00%	7.50%
Fe-Dolomite	5.40%	1.30%	4.40%
Chlorite	4.10%	5.00%	3.10%

T=trace amount≤5%, M=minor amount N5≤10%, R=rejected, n.d. =not detected.

Appendix IV Table 3 Experimental data for methane sorption isotherms

166			166			181			117-118			114		
sample	a.r.	CH4	excess sorption [mmol/g]	sample	e.m.	CH4	excess sorption [mmol/g]	sample	a.r.	CH4	excess sorption [mmol/g]	sample	a.r.	CH4
moisture state	43.92	43.92	43.92	moisture state	45.02	45.02	45.02	moisture state	44.60	44.60	44.60	moisture state	45.02	45.02
gas	gas	gas	gas	gas	gas	gas	gas	gas	gas	gas	gas	gas	gas	gas
temperature	temperature	temperature	temperature	temperature	temperature	temperature	temperature	temperature	temperature	temperature	temperature	temperature	temperature	temperature
pressure [MPa]	0.00	0.00	0.00	pressure [MPa]	0.00	0.00	0.00	pressure [MPa]	0.00	0.00	0.00	pressure [MPa]	0.00	0.00
0.00	0.00	0.00	0.00	0.00	0.00	0.00	0.00	0.00	0.00	0.00	0.00	0.00	0.00	0.00
1.58	0.172	1.08	0.072	2.15	0.051	1.96	0.132	1.96	1.96	1.96	0.132	2.13	2.13	0.022
2.68	0.231	1.98	0.109	3.62	0.070	3.46	0.168	3.46	3.46	3.46	0.168	4.96	4.96	0.036
3.39	0.259	2.68	0.132	4.64	0.082	4.52	0.185	4.52	4.52	4.52	0.185	6.73	6.73	0.043
4.43	0.293	3.22	0.147	6.90	0.100	5.25	0.195	5.25	5.25	5.25	0.195	7.86	7.86	0.046
5.15	0.312	3.65	0.158	8.43	0.110	7.31	0.214	7.31	7.31	7.31	0.214	8.58	8.58	0.048
5.65	0.324	5.21	0.183	9.47	0.116	8.72	0.223	8.72	8.72	8.72	0.223	9.05	9.05	0.049
6.59	0.343	8.05	0.212	11.95	0.125	9.69	0.228	9.69	9.69	9.69	0.228	9.35	9.35	0.050
7.24	0.355	10.03	0.227	13.68	0.130	10.36	0.232	10.36	10.36	10.36	0.232	9.55	9.55	0.050
7.70	0.363	11.64	0.236	14.91	0.134	10.82	0.233	10.82	10.82	10.82	0.233	9.68	9.68	0.050
8.01	0.368	12.88	0.241	15.77	0.135	11.14	0.235	11.14	11.14	11.14	0.235	9.76	9.76	0.051
8.24	0.372	13.83	0.243	16.39	0.136	11.36	0.236	11.36	11.36	11.36	0.236	12.22	12.22	0.053
8.39	0.374	14.56	0.246	16.82	0.137	11.52	0.236	11.52	11.52	11.52	0.236	13.81	13.81	0.054
9.96	0.394	15.13	0.248	17.12	0.138	11.64	0.237	11.64	11.64	11.64	0.237	14.85	14.85	0.054
11.05	0.406	15.57	0.249	17.34	0.138	11.72	0.237	11.72	11.72	11.72	0.237	15.53	15.53	0.054
11.81	0.414	17.01	0.248	17.49	0.139	11.78	0.237	11.78	11.78	11.78	0.237	15.97	15.97	0.054
12.34	0.419	18.13	0.250	17.60	0.139	13.39	0.241	13.39	13.39	13.39	0.241	16.26	16.26	0.054
12.71	0.424	19.01	0.250	17.67	0.138	14.51	0.244	14.51	14.51	14.51	0.244	17.47	17.47	0.054
12.97	0.426	20.33	0.249	17.73	0.139	15.30	0.246	15.30	15.30	15.30	0.246			
14.20	0.437	21.36	0.248			15.85	0.247	15.85	15.85	15.85	0.247			
15.06	0.445	22.17	0.248			16.23	0.248	16.23	16.23	16.23	0.248			
15.67	0.451	22.80	0.248			16.51	0.247	16.51	16.51	16.51	0.247			
16.11	0.455	23.29	0.248			16.70	0.248	16.70	16.70	16.70	0.248			
16.41	0.458	23.66	0.247			16.83	0.248	16.83	16.83	16.83	0.248			
16.63	0.459	23.95	0.248			16.93	0.248	16.93	16.93	16.93	0.248			
		24.17	0.247			17.00	0.248	17.00	17.00	17.00	0.248			
						17.05	0.248	17.05	17.05	17.05	0.248			
						17.09	0.248	17.09	17.09	17.09	0.248			
						17.11	0.248	17.11	17.11	17.11	0.248			
						17.13	0.248	17.13	17.13	17.13	0.248			
						17.14	0.248	17.14	17.14	17.14	0.248			

Curriculum vitae

Philipp Weniger

Diplom Geologe

Date of birth: 13.12.1976

Place of birth: Osterode am Harz

Education

1997 Abitur, Fachgymnasium für Technik an den Berufsbildenden Schulen II, Göttingen

1999 – 2007 Tertiary education at RWTH Aachen University in Geology Diplom (MSc)

Title of mapping thesis: “Stratigraphie und Strukturgeologie der variszischen Überschiebungsfront südöstlich von Aachen”.

Title of Diplom (MSc) thesis: “Organic geochemical and compound specific stable carbon isotope analysis of saturated carboxylic acids, extracted from Late Paleozoic coals”.

2007-2012

PhD thesis:

„Thermal and microbial gas generation, accumulation and dissipation in coal basins: role of sorptive storage capacity evolution”

Research exchange:

July 2006: Electron microscopy and XRD analysis on fly ash and soil samples at IGME Athens, Greece as part of the IKYDA program. Investigation of fly-ash related soil pollution in the Ptolemaida Basin, Greece.

October 2009: Development and application of experimental methods (mercury porosimetry, helium pycnometry, true triaxial stress permeameter) to evaluate compressibility and permeability of bituminous coals at the University of Queensland, Brisbane, Australia. Go8 / DAAD project: „New experimental methods for the investigation of gas sorption and transport processes in coal seams”.

Awards

Best Student Paper Award at the International Conference On Coal and Organic Petrology ICCP – TSOP - 2008 - Oviedo, SPAIN